BIO-INSPIRED NONHEME IRON CATALYSIS FOR OLEFIN OXIDATION – LIGAND DESIGN AND MECHANISTIC STUDIES

A DISSERTATION
SUBMITTED TO THE FACULTY OF THE GRADUATE SCHOOL
OF THE UNIVERSITY OF MINNESOTA
BY

YAN FENG

IN PARTIAL FULFILLMENT OF THE REQUIREMENTS
FOR THE DEGREE OF
DOCTOR OF PHILOSOPHY

PROFESSOR LAWRENCE QUE, JR., ADVISER

AUGUST, 2011

ACKNOWLEDGEMENTS

I would like to thank Prof. Lawrence Que for guiding me through the last six years. Without his guidance and support, it would be impossible to successfully finish my graduate research projects. And these projects could not have been completed without technical supports from many people. Specifically, Mr. Gregory Rohde of the Que group solved several crystal structures for me, which were essential for catalyst characterization. Dr. Lei Yang from Prof. Tolman's lab taught me FT/IR techniques and Dr. Letitia Yao of the NMR lab greatly facilitated the NMR characterization of my catalysts in solution. In addition, Dr. Samistha Chakrabarty from Prof. Lipscomb's lab helped me quite a bit in the identification of the naphthalene oxidation product by HPLC.

I would also like to thank Drs. Paul Oldenburg and Ruben Mas-Ballesté for helping me adjust into this lab smoothly when I joined the Que group. My special thanks are given to Drs. Jason England and Chunyen Ke, who initiated two of my projects. I also feel grateful to Dr. Genqiang Xue and Dr. Matthew Cranswick for their valuable suggestions and advice in research and my life.

Last but not least, I would like to thank my wife and my parents who have been always supportive along the way.

DEDICATION

This dissertation is dedicated to my wife, Ru Yan.

ABSTRACT

Olefin *cis*-dihydroxylation is an important chemical transformation for the synthesis of both natural products and pharmaceuticals that typically involves the use of osmium reagents. Unfortunately, osmium has some unavoidable drawbacks due to its high toxicity and low earth abundance. However, Nature has evolved a family of enzymes called Rieske dioxygenases to degrade polyaromatic molecules that can accomplish this transformation using an iron active site. This active site consists of a mononuclear iron center coordinated by two histidines and one aspartate in a facial array. Intrigued by the biological systems and the need to replace toxic and precious osmium reagents, I have designed and developed novel synthetic bio-inspired iron catalysts for C=C *cis*-dihydroxylation. The central theme of my thesis is to determine how ligands affect the electronic and structural properties of the iron catalysts. To achieve this goal, I have investigated two ligand families: facial tridentate NNO ligands and tetradentate tripodal N4 ligands. The NNO ligands are structurally more related to the enzymatic active sites but only a few complexes are catalytically active. A series of newly designed and structurally related ligands has been synthesized and their reactivities have been compared. Mechanistic results point to a novel active oxidant (Chapters 2 and 3). On the other hand, a comparison of two pairs of catalysts supported by closely related N4 ligands demonstrate the importance of available *cis*-sites on the

metal center to carry out *cis*-dihydroxylation (Chapters 4 and 5). Lastly, the first example of naphthalene *cis*-dihydroxylation by a synthetic iron catalyst, mimicking the action of naphthalene 1,2-dioxygenase, is described (Chapter 6).

TABLE OF CONTENTS

LIST OF TABLES

LIST OF FIGURES

LIST OF SCHEMES

LIST OF EQUATIONS

CHAPTER 1

Olefin oxygenation in biological and synthetic systems

1.1 Introduction

Nature has evolved many enzymes that can activate dioxygen from the air to catalyze various kinds of important oxidative reactions. Many of the enzymes contain metal(s) in their active sites.[1] Among metalloenzymes, iron containing dioxygen activating enzymes are a huge family, which is divided into two sub-families: heme and nonheme.[2-4] In both cases, the metal center interacts with dioxygen, generating the active oxidant responsible for product oxidation through a series of intermediates.

Oxidative reactions constitute a huge branch in chemistry both on an industrial and a laboratory scale. Of particular interest is olefin oxygenation, especially olefin epoxidation and olefin *cis*-dihydroxylation. Epoxides are important building blocks in organic synthesis and industry. Epoxidation typically involves peracetic acid as oxidant, which generates acid waste, or it uses precious metals as catalysts.[5] On the other hand, olefin *cis*-dihydroxylation is typically catalyzed by osmium compounds,[6] but alternative methodology is needed due to the toxicity and high cost of osmium.

The current synthetic methodologies for these transformations have their own drawbacks, so it is interesting to consider the use of enzymatic methodology because of its high efficiency and low waste. However, enzymes are tailored for only a limited range of substrates, and thus they are not practical for general reactions.

Alternatively, the increasing understanding of the iron containing dioxygen activating enzymes has thus inspired efforts to design synthetic iron catalysts that mimic the action of these enzymes and develop more environmentally friendly alternatives for olefin epoxidation and *cis*-dihydroxylation. This chapter will introduce nonheme

monoiron enzymes and bio-inspired iron catalysts in olefin epoxidation and *cis*-dihydroxylation.

1.2 Nonheme monoiron oxygen activating enzymes

Nonheme iron enzymes are a huge family of metalloenzymes that can perform a variety of metabolically important reactions. A number of nonheme iron enzymes catalyze oxidation reactions utilizing dioxygen as oxidant.[3] These enzymes usually contain monoiron[4,7] or diiron active centers.[8] Nonheme monoiron oxygen activating enzymes are of particular interest. At the active center, the mononuclear iron is often coordinated by two histidines residues and a carboxylate, which is a recurring binding motif called the 2-His-1-carboxylate facial triad.[9,10] However, a new binding motif came from the crystal structure of apocarotenoid-15,15'–oxygenase (ACO),[11] whose active site consists of a mononuclear iron center coordinated to four histidines. This section will focus on these two different binding environments in the active site.

1.2.1 Enzymatic systems that contain the 2-His-1-carboxylate facial triad in their active sites

Although mononuclear nonheme iron oxygenases catalyze a variety of transformations,[4] they unequivocally demonstrate a common structural motif. This motif consists of three endogenous protein ligands arranged at the vertices of one triangular face of an octahedron, which anchor the iron to the enzyme (Figure 1.1). It has been coined the '2-His-1-carboxylate facial triad'.[9,10,12,13] The metal centers of the nonheme monoiron enzymes have three coordination sites opposite the 2-His-1-carboxylate facial

triad available for binding exogenous ligands such as O_2, substrate, and/or cofactor that provide protein with the flexibility with which to tune the reactivity of the iron(II) center.

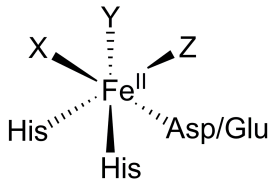

Figure 1.1 Nonheme monoiron center coordinated by the 2-His-1-carboxylate facial triad. X, Y and Z represent labile ligands or vacant sites.

A general mechanism is shown in Scheme 1.1 for dioxygen activating mononuclear nonheme iron(II) enzymes containing a 2-His-1-carboxylate motif. It starts with the iron(II) center that is coordinated to the facial triad on one face of its octahedral coordination sphere, with three readily displaceable solvent ligands. One labile ligand dissociates after the binding of substrate, which opens the site for the dioxygen binding. O_2 is then reduced, after which O-O bond is cleaved to form high-valent iron-oxo species that is responsible for attacking the prime substrate and transforming it into product. This sub-section will use two families of nonheme monoiron oxygenases as examples.

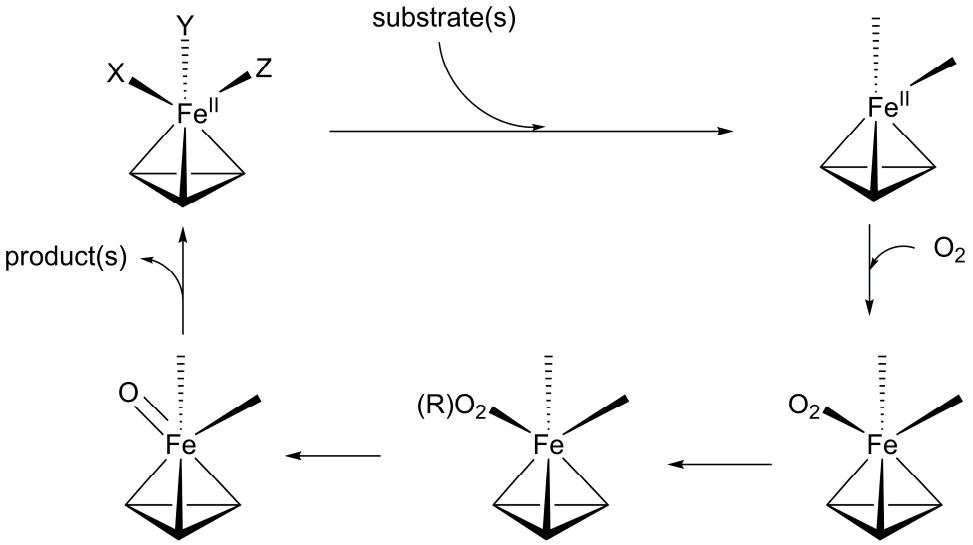

Scheme 1.1 A general mechanistic pathway catalyzed by nonheme monoiron oxygenases containing 2-His-1-carboxylate facial triad.

α-Keto-acid-dependent dioxygenases. The *α*-keto acid dependent enzymes are a class of nonheme monoiron enzymes that activate dioxygen.[4] They can catalyze a variety of metabolically important reactions, including oxygen sensing in cells, DNA and RNA repair, the biosynthesis of collagen, and the demethylation of histones.[14-16] These enzymes require an *α*-keto acid as a cosubstrate. Their primary function is hydroxylation, where dioxygen is activated and both oxygen atoms are incorporated into products, with one oxygen atom incorporated into the hydroxylated substrate and the other involved in the oxidative decarboxylation of the coordinated *α*-keto acid (Scheme 1.2).

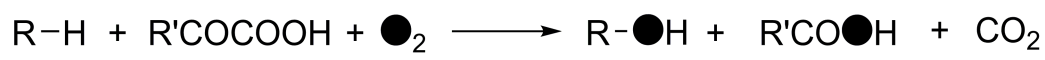

Scheme 1.2 Hydroxylation reaction catalyzed by α-keto acid enzymes.

A general mechanism has been proposed for these enzymes based on spectroscopic and reactivity studies (Scheme 1.3).[4,17-20] It involves a high-spin iron(IV) oxo intermediate that is responsible for substrate oxidation.[21-24] In the first step, the α-keto acid binds to the iron(II) center bidentately, replacing two water molecules and leaving a singly available site to activate dioxygen. Then the substrate enters the active site, causing the dissociation of the third water molecule, and allowing the coordination of dioxygen. An Fe(III)-coordinated superoxide radical is formed, which then attacks the α carbon of the α-keto acid. O-O bond cleavage forms a high valent Fe(IV)=O intermediate. This intermediate is responsible for the hydroxylation. Dissociation of the hydroxylated substrate and the carboxylic acid regenerates the iron(II) resting state.

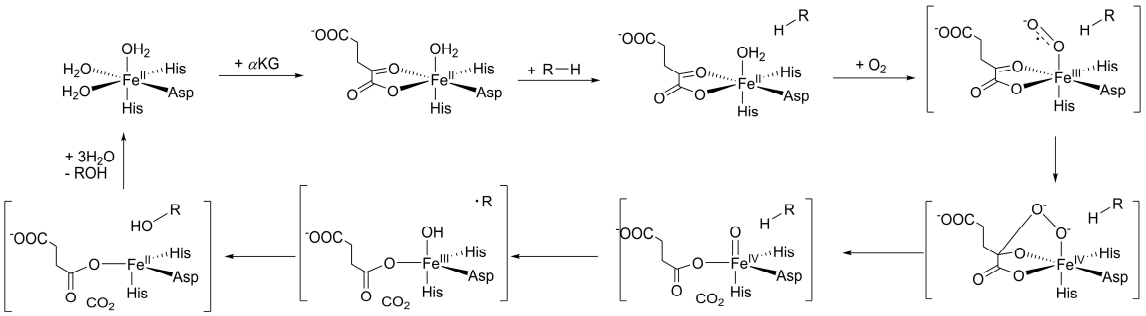

Scheme 1.3 A general mechanism of α-keto acid-dependent dioxygenases.

Rieske dioxygenases. Rieske dioxygenases are a family of nonheme iron

dioxygenases containing the iron-sulfur cluster. They catalyze the *cis*-dihydroxylation of arene substrates, the first step of many bacterial degradation pathways.[4,25] The known Rieske oxygenases largely function in the catabolism of hydrocarbons and substituted aromatic compounds, both of natural and anthropogenic origin; thus they are of great importance in bioremediation.[26-28] In the course of catalysis, both atoms of O_2 are incorporated into the *cis*-diol product.[29-33] Since the first X-ray crystal structure of a Rieske dioxygenase became available for naphthalene 1,2-dioxygenase,[34] more crystallographic structures of Rieske dioxygenases have been solved.[35,36] However, naphthalene 1,2-dioxygenase (NDO) is the best studied member of this family of enzymes, which catalyzes the oxidation of naphthalene yielding *cis*-1R, 2S-dihydroxy-1,2-dihydronaphthalene (Scheme 1.4).

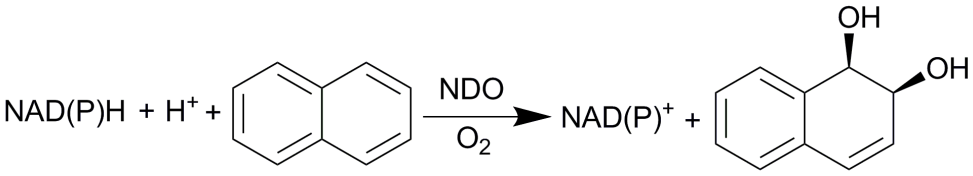

Scheme 1.4 Naphthalene oxidation by naphthalene 1,2-dioxygenase (NDO).

From the crystal structure, the mononuclear iron center of NDO is coordinated to two histidine residues (His208 and His213) and a bidentate aspartate (Asp362) (Figure 1.2),[34,37] occupying four sites of the metal center in a variation of the 2-His-1-carboxylate facial triad.[9] A water molecule occupies a fifth coordination site, and there is an asparagine residue 3.7 Å from the iron in the vicinity of the sixth coordination site.[34]

Incubation of the crystal of the fully reduced enzyme with substrate and O_2 at low temperature results in an O_2-adduct of NDO, the first example for a nonheme iron enzyme.[38] The two similar Fe-O bonds (2.2 and 2.3 Å) and the O-O bond length(1.4 Å) suggest a side-on bound dioxygen moiety, probably an Fe(III)-(hydro)peroxo species.

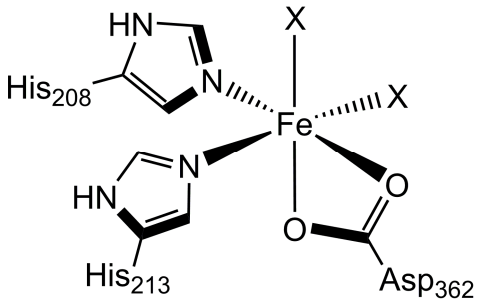

Figure 1.2 Naphthalene 1,2-dioxygenase (NDO) active site.

Extensive mechanistic studies have been carried out for NDO. MCD studies indicate that the oxidation state of the Rieske cluster and the binding of substrate both affect the coordination geometry of the iron active center.[39] Both reduction of the Rieske center and the binding of the substrate are required for O_2 activation, a self-protective mechanism to avoid unwanted oxidative species. Single turnover experiments on NDO suggested that the reaction starts from the Fe(III)-OO(H).[40,41] The study of another Rieske dioxygenase,[42] benzoate 1,2-dioxygenase, also showed that the fully oxidized enzyme and hydrogen peroxide can *cis*-dihydroxylate benzoate in stoichiometric yield, eliminating the possibility that the ferrous state is the starting species. Monooxygenase reactions of NDO implies the possible involvement of high valent species (Scheme 1.5),[43] while computational calculations suggest that this species is not energetically

feasible.[44]

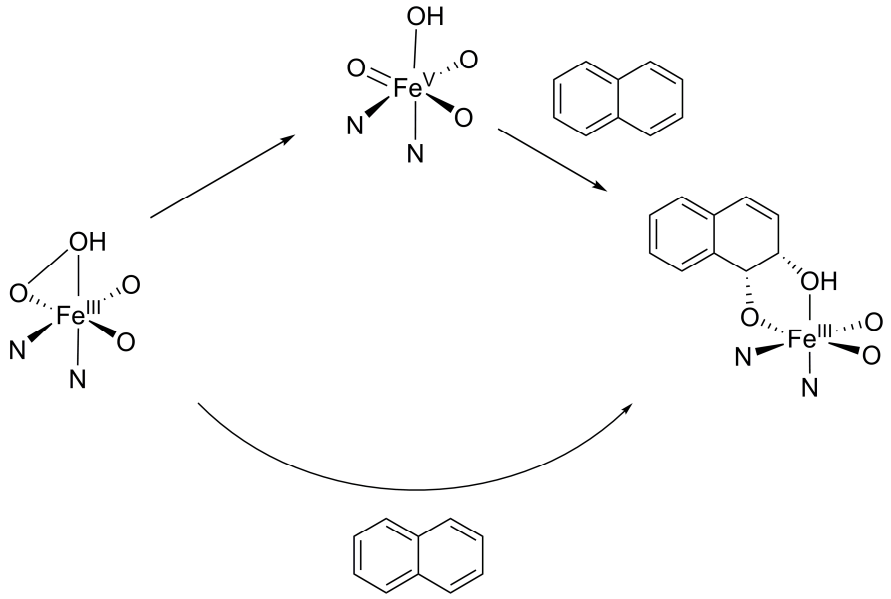

Scheme 1.5 Proposed mechanisms for naphthalene oxidation catalyzed by NDO.

1.2.2 Enzymatic systems that contain 4 Histidines in the active site

Carotenoid oxygenase. Carotenoids are isoprenoid compounds present in the membranes of all phototrophic as well as many heterotrophic organisms. They can be oxidatively cleaved to smaller compounds called apo-carotenoids. For example, retinal (vitamin A), is an apo-carotenoid, which is indispendable for growth, embryonal development, and visual function. Most apo-carotenoids are not synthesized from smaller molecules, but rather result from the oxidative cleavage of larger isoprenoids and subsequent modification in a process termed 'oxidative remodeling'.[45-47] The cleavage reaction is catalyzed by a family of related enzymes, which convert specific substrate double bonds to the corresponding aldehydes or ketones. The individual family

members differ in their substrate preference and the position of the cleaved double bond, giving rise to a remarkable number of products starting from a limited number of carotenoid substrate molecules.[48]

The only crystal structure of this family of enzymes is of apocarotenoid-15,15'–oxygenase (ACO),[11] which catalyzes the reaction shown in Figure 1.3. Based on the crystallographic data, the active site contains an octahedral ferrous center coordinated by four histidines and one water molecule, leaving a position unoccupied (Figure 1.4). This coordination environment (4-His and no carboxylate) is quite unusual among iron nonheme oxygenases that often contain 2-His-1-carboxylate facial triad.[9]

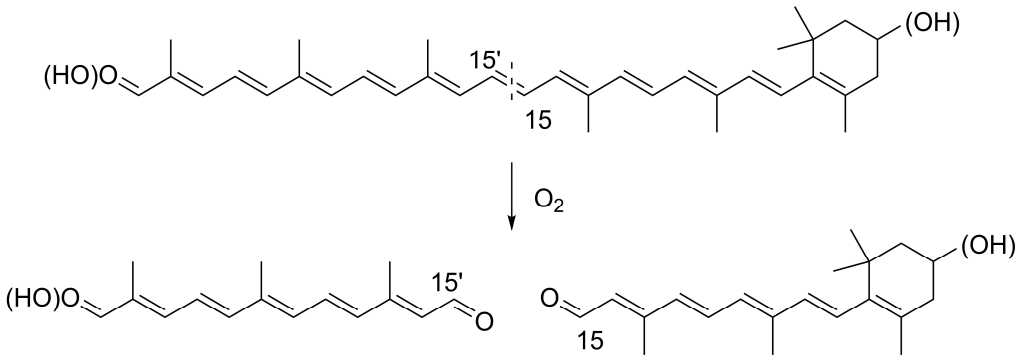

Figure 1.3 Carotenoid cleavage reaction catalyzed by ACO.

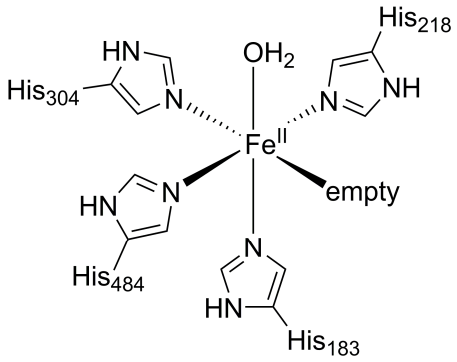

Figure 1.4 Active site of apocarotenoid-15,15'–oxygenase (ACO).

Since the resulting aldehyde product readily exchanges oxygen atom with water, no experiment is 100% conclusive about the oxygen incorporation from water. There are two proposed mechanisms, monooxygenase and dioxygenase pathways.[48] In the first case, the scissile double bond is first epoxidized by activated dioxygen and the epoxide is then opened by water molecule. Subsequently, the resulting vicinal diol is cleaved, leading to the incorporation of one oxygen atom from dioxygen and another one from a water molecule into the products (Scheme 1.6, left branch). On the other hand, dioxygen binds to the double bond forming a dioxetane intermediate, which subsequently decays to the products (Scheme 1.6, right branch). Computational calculation favors the dioxetane mechanism, while the other pathway cannot be ruled out.[49]

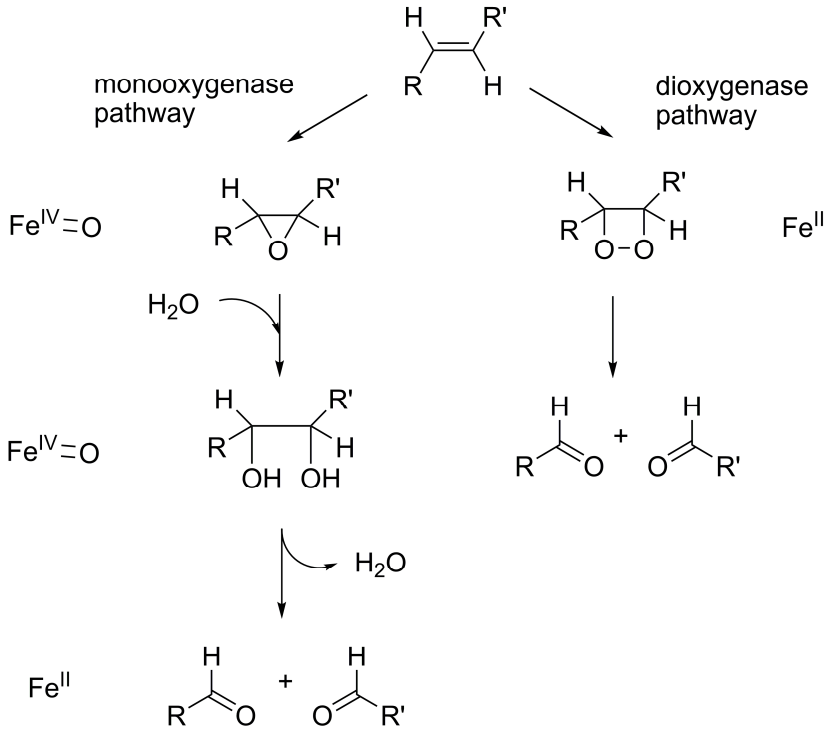

Scheme 1.6 Two mechanisms proposed for carotenoid oxygenases.

1.3 Synthetic nonheme iron olefin oxidation catalysts

1.3.1 Olefin epoxidation

Olefin epoxidation is an important chemical transformation in both the academic world and chemical industry. This transformation builds two C-O bonds in one step and the subsequent epoxide ring can be easily opened to make other chemicals. Nature utilizes iron containing enzymes to accomplish this transformation.[4,8] So in recent years, people have become more interested in using iron complexes as catalysts in olefin epoxidation reactions, because iron is of low cost and benign to the environment. The terminal oxidant is the other important factor that determines the value of the catalytic reaction. Molecular dioxygen and hydrogen peroxide stand out among available oxidants

from the viewpoint of cost and byproduct. In this part, we will focus on the iron-catalyzed olefin epoxidation with hydrogen peroxide or dioxygen as oxidant.

Beller and his coworkers have made great progress in the field of bio-mimetic iron-catalyzed olefin epoxidation. His system does not require pre-formed, but relies on the iron catalyst forming in situ. The first generation of this system consists of iron trichloride hexahydrate, pyridine-2,6-dicarboxylic acid (H_2pydic) and an organic amine.[50-56] Iron trichloride hexahydrate is the best behaved iron salt in this system. It is interesting that catalytic capability involving anhydrous iron trichloride is not as good as hydrate iron salts. Selected examples are listed in Table 1.1. This is a convenient and efficient method. *trans*-Stilbene is transformed into epoxide in as high as 97% yield (Table 1.1, entry 1). In addition, the generally considered difficult substrate, styrene, is also converted in high yield (Table 1.1, entry 2). This system is useful for different olefins by varying organic amine. When using derivatives of benzyl amine, excellent yield is obtained for aliphatic olefins (Table 1.1, entry 3 and 4). More importantly, this system can catalyze asymmetric epoxidation when the chiral amine is used, although with lower yield (Table 1.1, entry 5).

Table 1.1 Selected results of epoxidation catalyzed by the first generation of Beller's system[a]

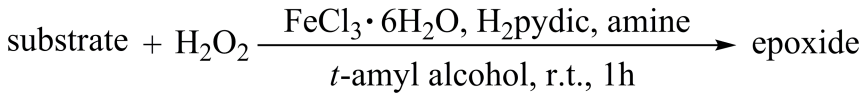

Entry	Substrate	Amine	Yield	ee
1	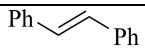		97	-
2			93	-
3	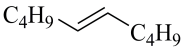	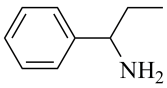	96	-
4		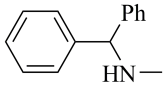	89	-
5[b]	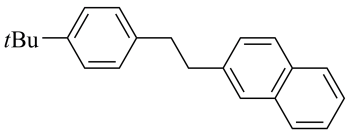	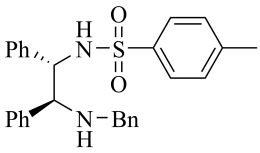	40	97

[a]Reaction conditions: 5 mol% $FeCl_3 \cdot 6H_2O$, 5 mol% H_2pydic, 10-12 mol% amine, 2 equiv H_2O_2. [b]4 equiv H_2O_2, 10 mol% $FeCl_3 \cdot 6H_2O$, 10 mol% H_2pydic, 24 mol% amine, 10°C.

Later, Beller and his coworkers realized that H_2pydic was not necessary if imidazole or its derivatives is used as base and developed their second generation.[57-60] The more moderate base, imidazole, has the same effect as the combination of the acid and a stronger base. Selected results are listed in Table 1.2. The second generation catalytic

system shows good to excellent yield for both aromatic and aliphatic olefins (Table 1.2, entry 1-4). The big breakthrough is that, when a sacrificial reductant is used, olefin can be oxidized by dioxygen of air. Even though it is costly to include a sacrificial reductant, this system shows exciting results that dioxygen can be used in catalytic epoxidation catalyzed by an iron complex. Mechanistic studies for this system were carried out by spectroscopy and well-defined iron complexes, but mechanism is not definite yet. A radical is possibly involved in the system.

Table 1.2 Selected results of epoxidation catalyzed by the second generation of Beller's system[a]

substrate $\xrightarrow[t\text{-amyl alcohol, r.t.}]{FeCl_3 \cdot 6H_2O,\ \text{imidazole derivative}}$ epoxide

Entry	Substrate	Oxidant	Imidazole derivative	Other additive	Yield
1	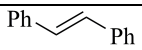	3 equiv H_2O_2	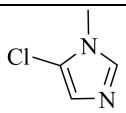	-	87
2		3 equiv H_2O_2	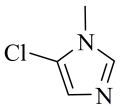	-	70
3[b]		3 equiv H_2O_2	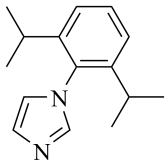	-	65
4[b]	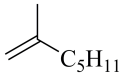	3 equiv H_2O_2	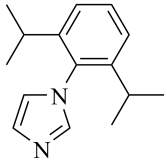	-	53
5[c]	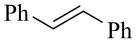	O_2 (Air)	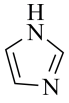	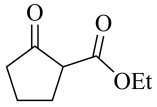	92

[a]Reaction conditions: 5 mol% $FeCl_3 \cdot 6H_2O$, 15 mol% imidazole derivative. [b]10 mol% imidazole derivative. [c]1 equiv imidazole, 3 equiv sacrificial reductant.

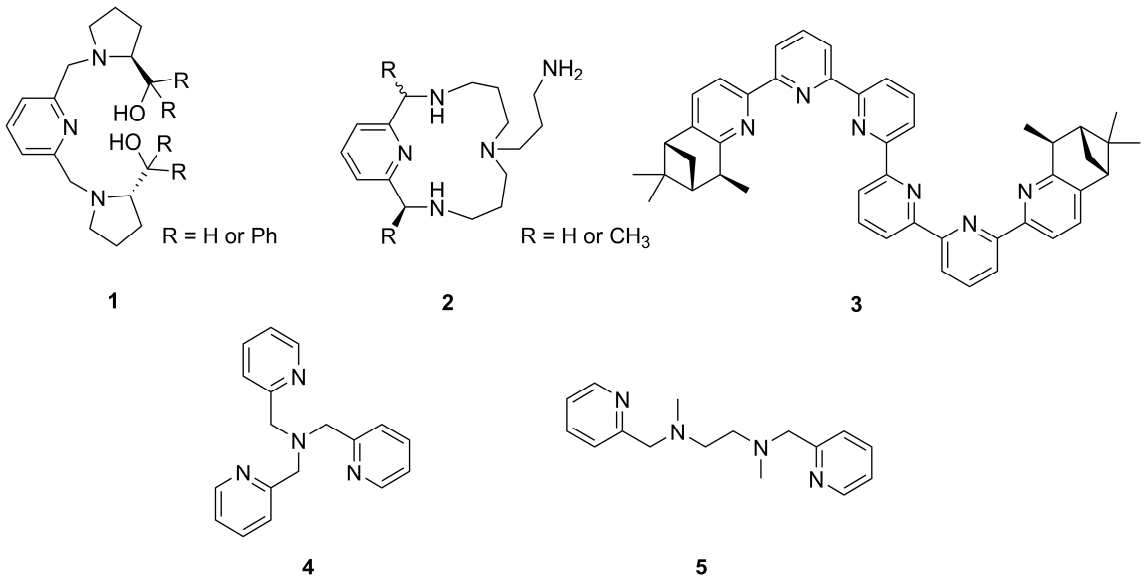

Scheme 1.7 Ligands used in iron catalyzed olefin epoxidation by hydrogen peroxide.

Other groups have also made great progress in the iron catalyzed olefin epoxidation by hydrogen peroxide, but premade iron complexes were used instead of in situ formed iron complexes. Ligands used in their studies are summarized in Scheme 1.7.

Gebbink and his coworkers synthesized iron complexes of ligand **1** and characterized their structures thoroughly by X-ray crystallography and solution spectroscopy.[61] When used as catalysts for olefin oxidation, these iron complexes showed low yield even under conditions that substrate was in large excess. In addition, even though there are two chiral centers in the ligand, no *ee* value was reported. However, this ligand presents an interesting synthetic route to introduce two chiral centers in a simple way, because it uses readily available proline or its derivatives as precursor. So it is worth further investigation.

Rybak-Akimova and her coworkers have used a pyridine-containing macrocyclic

ligand **2** with an aminopropyl pendant arm to mimic iron bleomycin, an antibiotic and anticancer drug.[62] With 5 mol% loading of iron complexes and 25 mol% non-coordinating acid HOTf, it can achieve 89% yield for cyclooctene oxidation. Mechanistic studies suggest that protonation and dissociation of the pendant amino arm facilitates olefin epoxidation. The diiron complex of polypyridine ligand **3** is developed by Kwong and his coworkers.[63] With the assistance of acetic acid, the catalyst can achieve very high yield of epoxidation and up to 43% *ee* value.

The best characterized reaction mechanism came from our lab.[64] Iron complexes of **4** and **5** can catalyze the epoxidation at 0°C in 1:2 CH_3CN / CH_3COOH in nearly quantitative yield with very low catalyst loading 0.5 mol%. These premade iron complexes enabled us to carry out a thorough study of the reaction mechanism (Scheme 1.8). Solution spectroscopic and labeling studies suggest that carboxylic acid assists the O-O bond heterolytic cleavage to form Fe^{V}=O(OOCR) species that acts as the active oxidant (Scheme 1.8, species A and B in brackets).

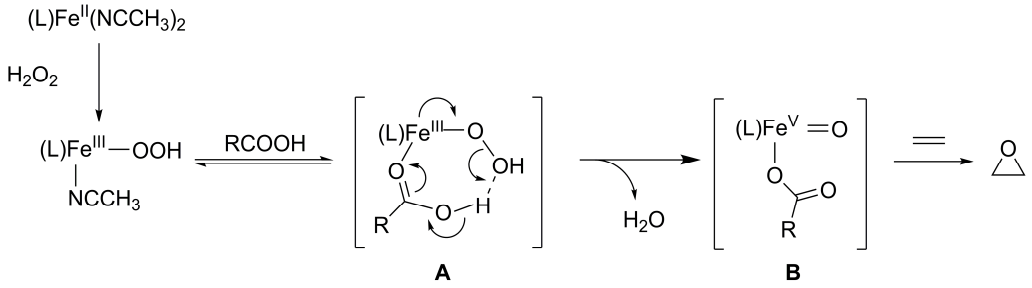

Scheme 1.8 Proposed mechanism for iron complexes with ligands **4** and **5** for olefin epoxidation.

1.3.2 Olefin *cis*-dihydroxylation

Olefin *cis*-dihydroxylation is an important chemical transformation for the synthesis of both natural products and pharmaceuticals that typically involves the use of osmium reagents.[6] Although this is a well-developed methodology, osmium has some unavoidable drawbacks due to its high toxicity and low earth abundance. People have been trying to design iron catalysts to replace osmium reagents based on the active sites of Rieske dioxygenases that degrade polyaromatic molecules by catalyzing *cis*-dihydroxylation of an aromatic double bond.[25] One example of the active site of the best studied member of Rieske dioxygenases, naphthalene 1,2-dioxygenase, is shown in Figure 1.2. The active site consists of one mononuclear iron center coordinated by two histidines and one aspartate in a facial array.[34] This common coordination motif among Rieske dioxygenases is named the 2-His-1-carboxylate facial triad. Considerable advancements have been made in the field of bio-inspired nonheme iron catalysis since our recent review.[65]

Previously ligand structures were mainly tetradentate N4 ligands: TPA and its derivatives and BPMEN and its derivatives. So far more new ligands have been developed based on bio-inspired approaches, as shown in Scheme 1.9. Cyclooctene is a common substrate for this iron-catalyzed oxidation and used as an example to compare all available iron catalysts. Selected catalytic results are summarized and compared in Table 1.3.

The best studied iron catalyst for olefin *cis*-dihydroxylation is FeTPA complex. Observation of the diol product with each oxygen atom from hydrogen peroxide and

water molecules pointed to a water assisted mechanism with Fe^{V}=O(OH) as the active oxidant (Scheme 1.10).[66] Costas and his coworkers have designed another family of tetradentate N4 ligands (Scheme 1.9, **1**).[67,68] The iron complex shows similar behavior as FeTPA complex (Table 1.3, entry 1) and similar oxygen labeling pattern is also observed. So Fe^{V}=O(OH) is proposed for this system analogous to the previous one.

In an effort to mimic the enzymatic 2-His-1-carboxylate facial triad, our group has made the Ph-DPAH *N, N, O*-facial ligand (Scheme 1.9, **2**).

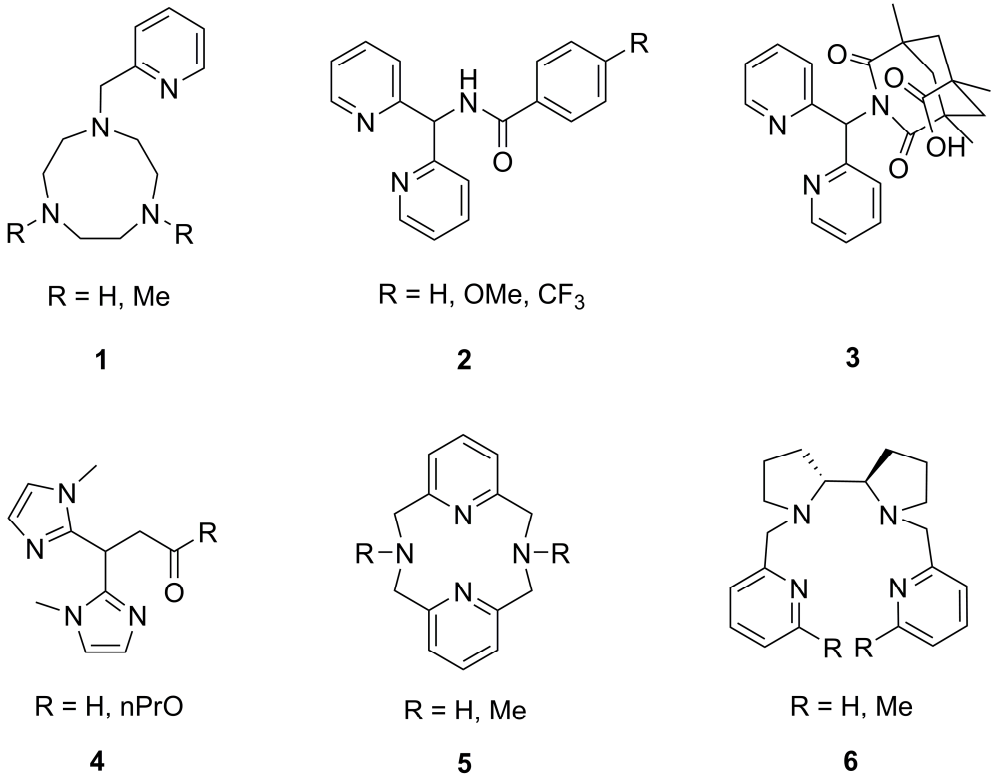

Scheme 1.9 Ligands used in iron catalysis for olefin *cis*-dihydroxylation.

Table 1.3 Cyclooctene oxidation with iron catalysts

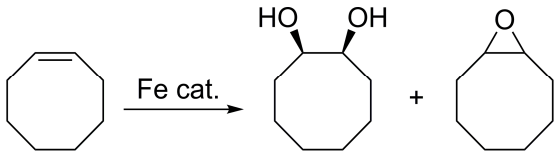

Entry	Ligand	Oxidant	Cat : Ox : S[a]	Diol[b]	Epoxide[b]
1	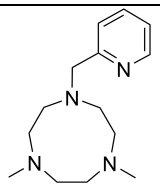	H_2O_2	1 : 10 : 1000	47%	31%
2	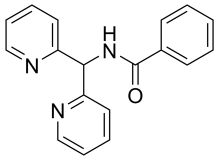	H_2O_2	1 : 10 : 1000	70%	5%
3[c]	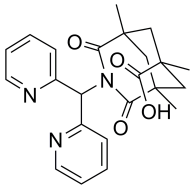	H_2O_2	1 : 10 : 1000	7%	1%
4	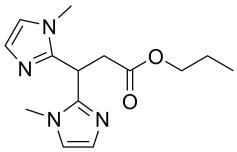	H_2O_2	1 : 10 : 1000	11%	28%
5	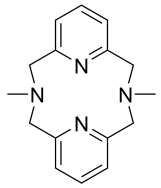	oxone	7 : 100 : 200	60%	5%

[a]Catalyst : Oxidant : Substrate. [b]Yield is based on limiting reagent. [c]1-octene is used instead of cyclooctene.

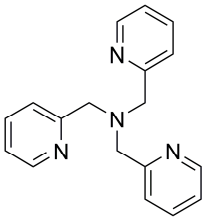

TPA

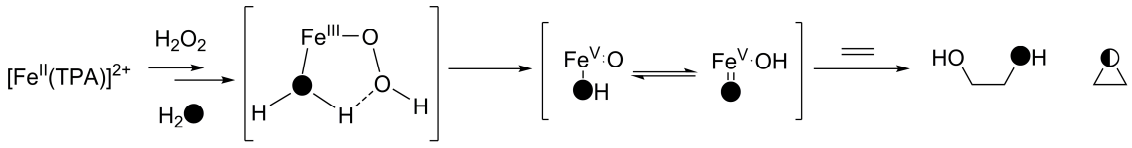

Scheme 1.10 Proposed mechanism for FeTPA-catalyzed in olefin oxidation.

Two more examples of imitating the enzymatic active sites come from our group and Gebbink's group (Scheme 1.9, **3** and **4**).[69,70] Ligand **3** contains a carboxylate group mimicking the aspartic acid in the enzyme, but the catalytic reactivity of its iron complex is very low (Table 1.3, entry 3). Mass spectrometric analysis after the reaction shows that the ligand falls off easily from the iron center. Gebbink's ligand **4** contains two imidazole rings mimicking the two histidines in the enzyme. Its iron complex shows higher reactivity, but it slightly favors epoxide over diol product (Table 1.3, entry 4). They are good structural models but not good functional models of the enzymatic systems. So far perhaps due to the lack of the secondary structure in the enzymes, biomimic iron catalysts do not have good reactivity or selectivity. In addition, mechanistic studies for both iron catalysts are lacking.

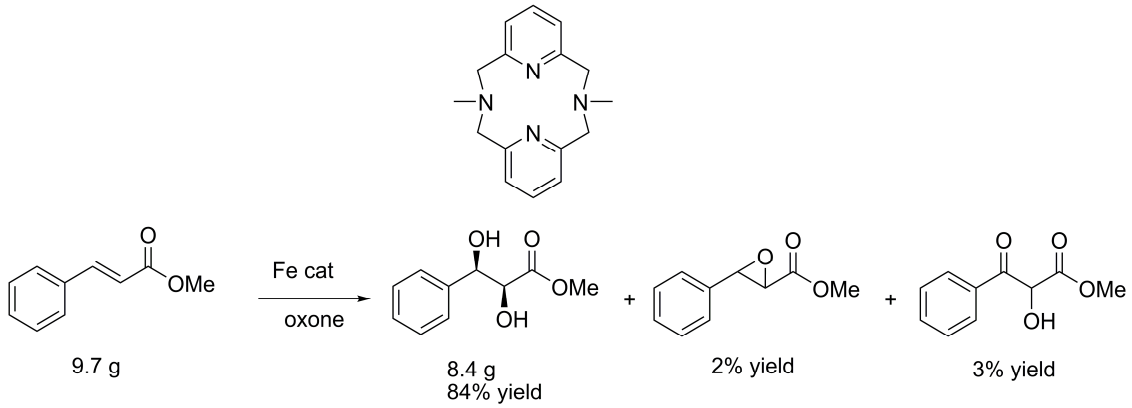

Scheme 1.11 Methyl cinnamate oxidation with Che's iron complex.

Exciting results come from Che group, with the use of a macrocyclic ligand (Scheme 1.9, **5**) containing two pyridines and two amines in the iron catalysis.[71] The iron complex has two *cis*-labile sites that are *trans* to the two pyridines. Hydrogen peroxide did not give any conversion into diol for cyclooctene oxidation, so oxone was used instead as oxidant to obtain very good results. Unlike previous studies that substrates have to be in large excess to avoid overoxidation, this system can work under substrate limiting conditions, which points to a promising direction (Table 1.3, entry 5). In addition, it is also a surprisingly robust catalyst. With very low catalyst loading, 0.7 mol%, it can achieve a 10-g-scale reaction with 84% yield of the diol (Scheme 1.11) and the iron catalyst can be reused. Preliminary mechanistic studies suggest *cis*-O=Fe^{V}=O for the active oxidant, but based only on mass spectrometric data and computational calculations.

Not much improvement has been made in the iron-catalyzed asymmetric olefin *cis*-dihydroxylation. The only example is from our lab. The iron complex of ligand **6** with

methyl groups on the C6 positions of pyridine rings can catalyze the oxidation of *trans*-2-heptene with the diol product in 52% yield and 97% *ee*.[72]

1.4 Other metals in olefin *cis*-dihydroxylation

1.4.1 Osmium catalysts

The best known and well-established catalysts for enantioselective *cis*-dihydroxylation of olefins typically involve osmium tetraoxide. [6,73-75] Major contribution to this field comes from Sharpless and his coworkers.[6] With catalytic amount of osmium compound and chiral cinchona alkaloid derived ligands shown in Figure 1.5, *cis*-dihydroxylation can be applied to nearly all alkenes with different substituents (primary, 1,1'-disubstituted, *cis*-1,2-disubstituted, *trans*-1,2-disubstituted, tri- and tetra-substituted). Both yield and enantiomer excess are very high.[6]

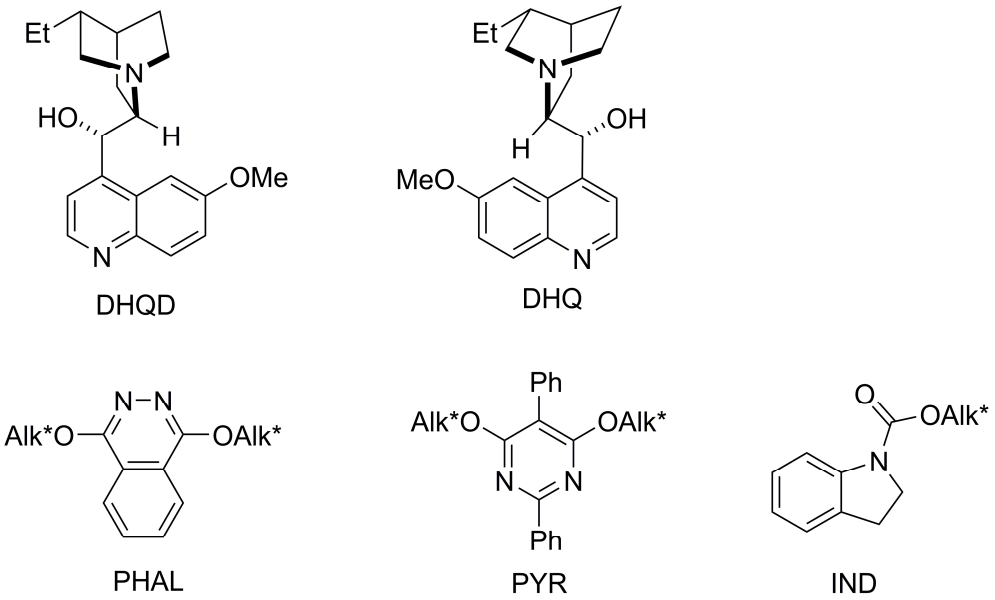

Figure 1.5 Cinchona alkaloid derived ligands used in Sharpless asymmetric dihydroxylation (AD). Alk* = DHQD or DHQ.

This is a remarkably effective catalytic system, and the 'AD-mix', containing the catalyst precursor potassium osmate dehydrate, the co-oxidant potassium ferricyanide, the base potassium carbonate, and the chiral ligand, is commercially available and the dihydroxylation transformation is easy to carry out. However, the applied co-oxidant for Os^{VI} leads to the production of overstoichiometric amount of waste. Many efforts have been made to develop more environmentally benign terminal oxidants.

Bleach is a simple and cheap oxidant and can be used in industry without problems. Beller and his coworkers has developed a catalytic system involving sodium hypochlorite as the co-oxidant.[76] Good yield and *ee* are obtained from this protocol.

H_2O_2 is especially favored as the terminal oxidant because of its low cost, low E factor, ease of handling, and the fact that its by-products are environmentally benign.[77]

When H_2O_2 is used in osmium-catalyzed olefin dihydroxylation, unproductive peroxide decomposition is the major process. Bäckvall and his coworkers discovered that with the help of electron mediators, H_2O_2 can be utilized as a terminal oxidant (Scheme 1.12).[78,79]

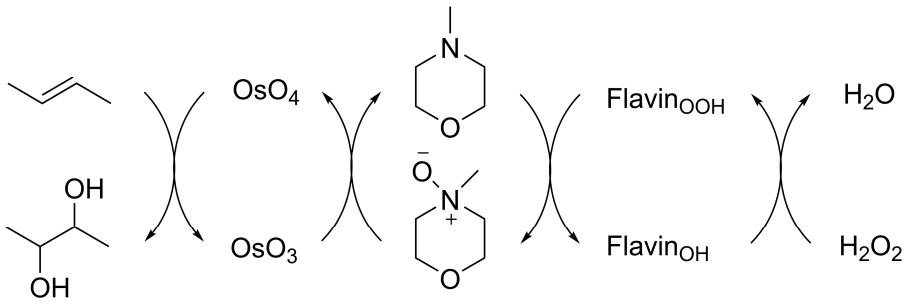

Scheme 1.12 Electron flow of osmium catalyzed dihydroxylation using H_2O_2 as the terminal oxidant.

Dioxygen is the most environmentally friendly oxidant. Beller and his coworkers developed a system that used dioxygen as the oxidant in osmium-catalyzed dihydroxylation.[80] Although this system is slow, it can achieve comparable yield and only slightly lower *ee*. Later, his group also developed a protocol that used air as the terminal oxidant.[81,82] While the total yield and selectivity of the reaction are excellent, the total turnover frequency is comparatively low.

1.4.2 Ruthenium catalysts

Ruthenium tetraoxide has been used mainly as a strong oxidizing agent in a variety of organic transformations.[83] Although it is isoelectronic to osmium tetraoxide, it was considered for a long time that it resulted in the fission of olefin to form the corresponding carbonyl compounds when alkenes are present as substrates until 1990s.

Sica and his coworkers found that ruthenium tetraoxide can dihydroxylate steroidal alkenes. This is the first time that RuO_4 transfers oxygen atoms to C=C double bond without the fragmentation of C-C bond, although a stoichiometric amount of RuO_4 is needed in the reaction.[84]

Soon after the first discovery of this application of ruthenium tetraoxide, Shing and his coworkers developed a system that uses a catalytic amount of RuO_4.[85-87] With 7 mol% $RuCl_3(H_2O)_3$ as catalyst and $NaIO_4$ as oxidant, this system can apply into a certain range of substrates. Due to the very short reaction time, it has a name, 'flash dihydroxylation', but this short reaction time also means less control over the reaction, because longer reaction time will result in the unwanted fission products.

The above problem was solved by Plietker and his coworkers by adding a catalytic amount of sulfuric acid, which accelerates the hydrolysis of products.[88-90] With this improvement, undesired fission products were suppressed and thus higher yields can be achieved by increasing the reaction time. In addition, the catalyst loading was lowered to only 0.5 mol%. Later, they replaced sulfuric acid with the Lewis acid, $CeCl_3$, to use for acid-sensitive substrates.[91]

A recent breakthrough came from Che's group.[92,93] They achieved Ru-catalyzed olefin *cis*-dihydroxylation with H_2O_2 as terminal oxidant that is desired from environmental concerns. Unlike previous systems, this ruthenium catalyst utilizes tmtacn as ligand (Figure 1.6). With [Ru(tmtacn)Cl_3] as catalyst and Al_2O_3 and NaCl as additives, it can accomplish the dihydroxylation in a 1-mol scale (Figure 1.6). So it is expected that this system could find use in the commercial world.

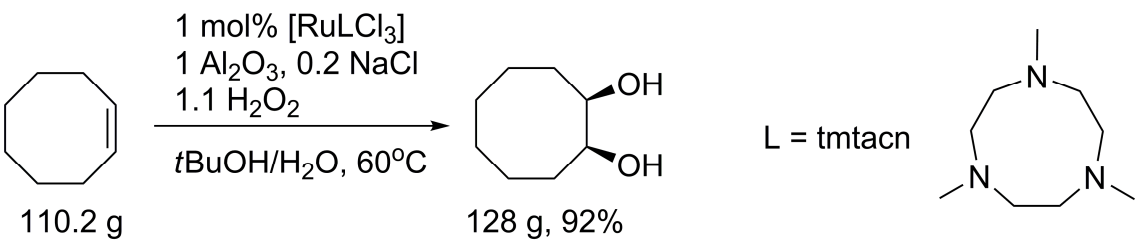

Figure 1.6 Cyclooctene dihydroxylation with [Ru(tmtacn)Cl_3] by H_2O_2 on a large scale.

1.4.3 Manganese catalysts

In the last decade, manganese complexes have been found to catalyze olefin *cis*-dihydroxylation by Feringa and his coworkers.[94-98] The first generation of manganese catalysts utilizes cyclic ligand, tmtacn (Figure 1.7). The manganese catalyst starts from dinuclear Mn^{IV} complex, $[Mn^{IV}_2O_3(tmtacn)_2]^{2+}$, and the active form is generated by 2-electron reduction and coordination of two carboxylic acid, $[Mn^{III}_2O(RCOO)_2(tmtacn)_2]^{2+}$. Studies show that the bound carboxylic acids can tune the selectivity of *cis*-dihydroxylation or epoxidation.[95] For example, with 2,6-dichlorobenzoic acid, the *cis*-diol product of *cis*-cyclooctene oxidation is 7 times of epoxide, while with salicyclic acid, epoxide product is favored 11 times over *cis*-diol. In addition, if the substrate, *cis*-cyclooctene, is maintained at pseudo-steady-state level, up to 2000 turnover numbers can be achieved for this system.

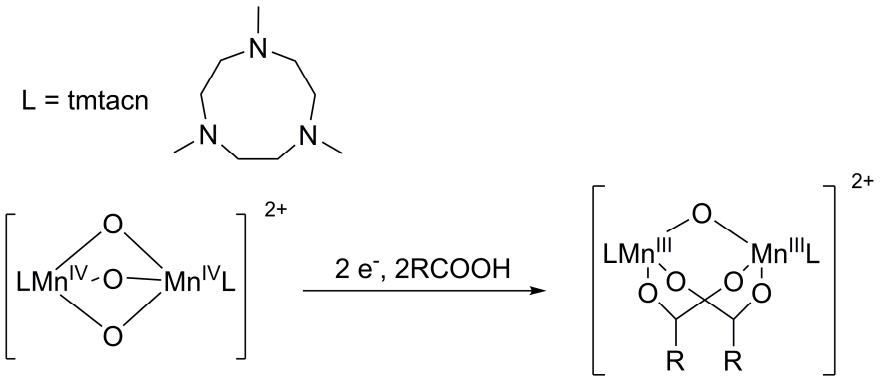

Figure 1.7 The first generation of manganese catalysts in olefin *cis*-dihydroxylation.

Since carboxylic acid can tune the chemo-selectivity, chiral carboxylic acids have been to examine the stereo-selectivity.[97] This methodology has potential application in synthetic chemistry, because protected carboxylic acids with chiral centers are much more abundantly available with lower cost than chiral ligands used in Osmium AD.[6] The independently prepared $[Mn^{III}_2O(Ac\text{-}D\text{-}Phg\text{-}OH)_2\ (tmtacn)_2]^{2+}$ with the additive of Ac-D-Phg, can catalyze the asymmetric *cis*-dihydroxylation of chromene with H_2O_2 with 54% ee. Even though the enantiometric excess is modest, this contribution is the only example of manganese-catalyzed asymmetric *cis*-dihydroxylation (AD). As the proposed mechanism implies (vide infra), the chiral centers on the carboxylic acids are far from the newly formed C-O bonds, and thus they might exert little steric effect on the product. However, this investigation provides an important direction that simple carboxylic acids can be used to introduce chiral centers into more complex products.

The proposed mechanism is shown in Scheme 1.13.[96] Water binds to one of the manganese to open the Mn-O-Mn bond, after which hydrogen peroxide replaces one binding hydroxo. This $[Mn^{III}(OOH)(RCOO)_2Mn^{III}(OH)]^{2+}$ species is responsible for the

attack of the olefin. This mechanism explains the reason that an oxygen atom from water can be incorporated into the epoxide products and the two oxygen atoms of the *cis*-diol products are from water and hydrogen peroxide each.

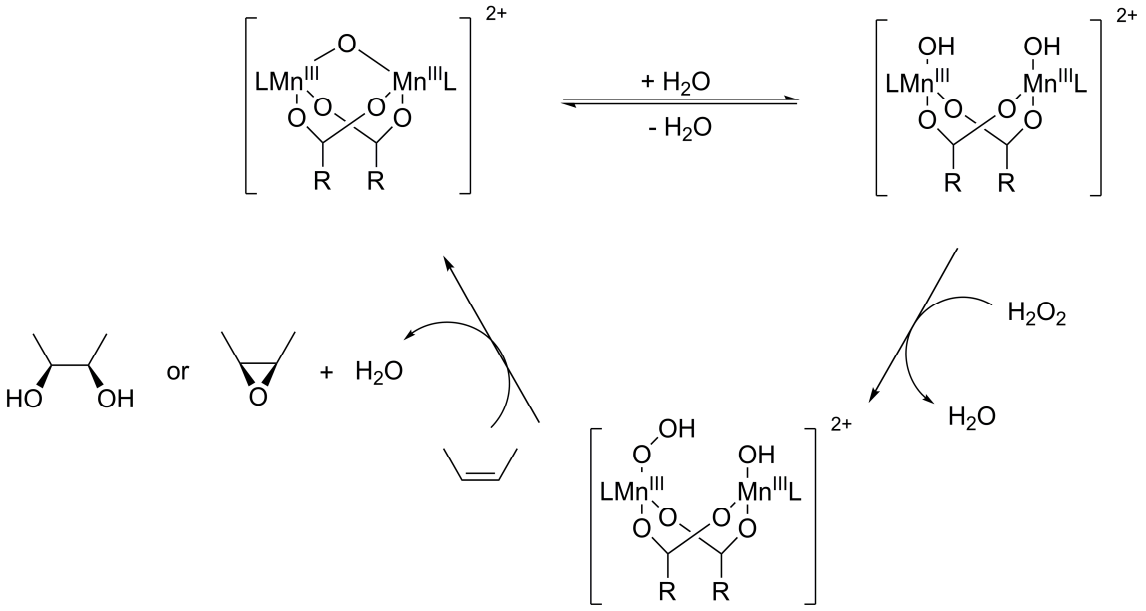

Scheme 1.13 Proposed mechanism for manganese catalysts in olefin oxidation with H_2O_2.

Although this system is efficient in converting oxidant into product, it works well only with electron-rich olefins. The second generation catalysts employ manganese salt, pyridine-2-carboxylic acid, a ketone and a base.[98] With this method, electron-deficient alkenes can be converted quantitatively to the corresponding *cis*-diol products, and it can achieve reactions on a multi-gram scale. This *in situ* preparation of the catalyst from readily available reagents makes it complimentary to the first generation,

$[Mn^{IV}_2O_3(tmtacn)_2]^{2+}$.

1.5 Problems and goals of the thesis

Understanding and extending the lifetime of N, N, O-ligand. One successful example with an *N, N, O*-ligand was reported from our group in 2005,[99] However, crystallographic studies show this iron complex employs two ligands per iron in the solid state leaving no labile sites for external oxidant to bind, while highly effective and selective *cis*-dihydroxylation is obtained from this complex in the solution of acetonitrile. So the solution structure must be different from the crystal structure. In addition, this iron catalyst undergoes deactivation along the oxidation process. Chapter 2 will give detailed studies of the solution structure and deactivation mechanism of this iron complex. Based on the mechanism, ligand modifications are made and used in iron-catalyzed reactions.

Variation of different N, N, O donors. So far, the design of *N, N, O*-ligands is still in the trial-and-error phase. Available examples are quite different from each other that no general rules can be deduced from them. Chapter 3 will show a series of structurally related ligands that give a quite remarkable pattern of reactivity and selectivity. In addition, these new catalysts also exhibit an unusual ^{18}O isotopic labeling pattern.

Inspect the effect of two cis-labile sites and iron complexes with N2Py2 ligands. Cis-labile sites have been proposed to play an important role in iron-catalyzed oxidation.[66] However, there is no direct evidence for this assumption. Chapter 4 will give an insight into this important feature with the comparison of two iron complexes that differ only in

the orientation of the two labile sites. In addition, linear N2Py2 ligands can adopt different topologies when they coordinate to the iron. Chapter 5 will try to understand the relationship between ligand topology and catalyst reactivity.

Apply cis-hydroxylation to the more difficult aromatic double bond. *Cis*-dihydroxylation of aromatic double bonds has not been accomplished by a synthetic catalyst. In Chapter 6, naphthalene, the authentic substrate of naphthalene 1,2-dioxygenase, is utilized as the substrate for iron-catalyzed oxidation reactions.

CHAPTER 2

Detailed structural and decomposition studies of R-DPAH iron complexes and improving Fe(R-DPAH) catalyst performance by ligand re-design

2.1 Introduction

Iron containing Rieske dioxygenases are involved in the biodegradation of polyaromatic molecules by catalyzing the chemo-, region- and stereo-selective *cis*-dihydroxylation of stable aromatic double bond.[4,100] The iron center in their active sites has been shown to be facially coordinated by two histidines and one aspartate residue,[34] a binding motif that is common to many oxygen-activating nonheme iron enzymes and named 2-His-1-carboxylate facial triad,[9] leaving two or three *cis* oriented labile sites around the iron center available for the binding of oxidant and substrate. Since such enzymatic systems cater to a relatively narrow range of substrates and sometimes sacrificial reductants are needed, they are now not practical oxidation catalysts. However, synthetic catalysts for olefin oxidation often involve osmium,[6,74,75] and unfortunately, osmium has some unavoidable drawbacks due to its high toxicity and low earth abundance. Therefore, inspired by the biological systems, efforts have been devoted to the exploration of bio-mimetic nonheme iron catalysts, which, coupled with H_2O_2 as oxidant, would potentially offer an attractive alternative to the more toxic and expensive osmium-based *cis*-dihydroxylation catalysts.

So far the first and most extensive studied nonheme iron catalysts for olefin *cis*-dihydroxylation contain ligands that have four nitrogen donors.[66,101,102] They lack the oxygen donor that is present in enzymatic active centers. Recently, more work with a new ligand framework having a *N, N, O* facial array about the iron center has appeared in literature.[69,70,99] Due to the close similarity to the coordination environment of enzymatic active sites, these facial *N, N, O* ligands are of great interest. The R-DPAH

ligand family stands out among these ligands because of the superior reactivity and selectivity towards *cis*-dihydroxylation of their iron complexes.[99]

This chapter describes a detailed study of the structures of R-DPAH iron complexes in solution, and an examination of deactivation pathways for these iron catalysts. These results are then used to carry out R-DPAH ligand re-design to improve catalyst performance.

2.2 Experimental section

Materials. All reagents were purchased from Sigma-Aldrich and used as received unless otherwise noted. All olefin substrates were passed over basic alumina immediately prior to use. CH_3CN was purified by Solvent Purifier from Vacuum Atmospheres Company. Synthesis of $[Fe^{II}(OTf)_2 \bullet 2NCCH_3]$ has been reported previously.[103]

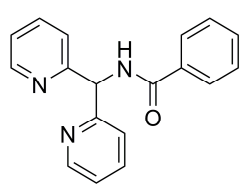

Ph-DPAH
1: $[Fe^{II}(Ph\text{-}DPAH)_2]^{2+}$

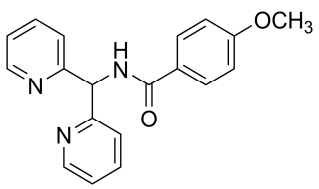

p-MeO-C_6H_4-DPAH
2: $[Fe^{II}(p\text{-}MeO\text{-}C_6H_4\text{-}DPAH)_2]^{2+}$

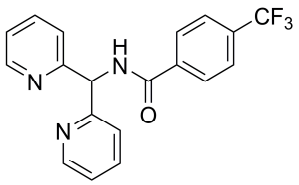

p-CF_3-C_6H_4-DPAH
3: $[Fe^{II}(p\text{-}CF_3\text{-}C_6H_4\text{-}DPAH)_2]^{2+}$

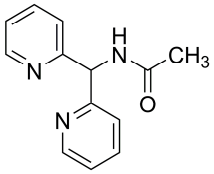

CH_3-DPAH
4: $[Fe^{II}(CH_3\text{-}DPAH)_2]^{2+}$

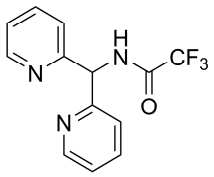

CF_3-DPAH
5: $[Fe^{II}(CF_3\text{-}DPAH)_2]^{2+}$

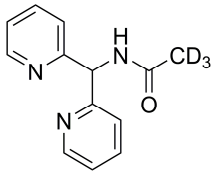

CD_3-DPAH
6: $[Fe^{II}(CD_3\text{-}DPAH)_2]^{2+}$

Scheme 2.1 R-DPAH ligand structures.

Synthesis of R-DPAH ligands. R-DPAH ligands are shown in Scheme 2.1. The synthesis of the first five ligands has been reported in the literature.[104] A new ligand with the deuterated methyl group in CH_3-DPAH is introduced. The synthesis of the CD_3-DPAH ligand is based on a similar procedure. Di-(2-pyridyl)methylamine (0.2 g, 1.1 mmol), which was synthesized according to the published literature,[105] was dissolved in deuterated acetic anhydride-d_6 $\{(CD_3CO)_2O\}$ (1 mL) and stirred for 1 hour. 10 mL water was added to quench the reaction. Dichloromethane was used to extract the product. The organic phase was collected and combined. After being dried with magnesium sulfate, the solvent was evaporated to give a white powder. The purified product was obtained from a silica gel column eluted with a gradient of hexane / ethyl acetate in 95% yield. ^{1}H-NMR ($CDCl_3$, δ ppm from TMS): 8.54(d, 2H), 7.92(d, 1H), 7.64(td, 2H), 7.42(d, 2H), 7.19(dd, 2H), 6.22(d, 1H).

Synthesis of modified R-DPAH ligands. Modified R-DPAH ligands are shown in Schemes 2.5 and 2.6. Position a of Ph-DPAH ligand can be deuterated according to a deuteration methodology developed from the Que lab.[106] 0.2 g (0.7 mmol) Ph-DPAH was combined with 0.34 g (14 mmol) NaH in CD_3CN and stirred under inert atmosphere overnight, turning the reaction solution into dark pink. Large amount of D_2O was added to quench the reaction and the organic solvent was then removed. Dichloromethane was used to extract the product from the aqueous phase and the product was purified by column chromatography. The Ph-D-DPAH ligand was obtained in 95% yield. ^{1}H-NMR ($CDCl_3$, δ ppm from TMS): 8.76(d, 1H), 8.56(dm, 2H), 7.98(dm, 2H), 7.61(dt, 2H), 7.49(m, 5H), 7.11(ddd, 2H), 6.35(d, 0.2H). ^{1}H-NMR indicated that position a of Ph-D-DPAH was 80% deuterated.

The methylation of position a of R-DPAH ligands was achieved through a two-step synthesis. The first step was to methylate the di-(2-pyridyl)methylamine to form 1,1-di(pyridin-2-yl)ethanamine based on a published procedure.[107] To a solution of 0.2 g (1.1 mmol) di-(2-pyridyl)methylamine in 5 mL dry THF was added 0.44 mL 2.5 M *n*-butyl lithium (1.1 mmol) dropwise at -78°C under Ar. Then the mixture was allowed to warm up slowly to room temperature and stirred for another 2 hours. The reaction solution turned dark. 0.07 mL (1.1 mmol) CH_3I in dry THF was then added dropwise, and the reaction was stirred for overnight. The reaction solution turned orange. 5 mL water was added slowly to quench the reaction and the solution was extracted by dichloromethane. After removal of the organic solvent, 1,1-di(pyridin-2-yl)ethanamine was obtained in 90% yield as a light yellow oil. It is pure enough that no column chromatography was

used before the next step. ^{1}H-NMR ($CDCl_3$, δ ppm from TMS): 8.55 (d, 2H), 7.65 (dd, 2H), 7.42 (d, 2H), 7.12 (dd, 2H), 2.58(broad, 2H), 1.96 (s, 3H).

Synthesis of Ph-Me-DPAH and Me-Me-DPAH was the same as Ph-DPAH and Me-DPAH. For Ph-Me-DPAH, to a solution containing 0.06 mL (0.5 mmol) benzoyl chloride and 0.09 mL (0.63 mmol) triethylamine in 2 mL THF, was slowly added 0.1 g (0.5 mmol) 1,1-di(pyridin-2-yl)ethanamine at 0°C. This solution was warmed up to 60°C and refluxed for 20 min, after which the solution was cooled down to room temperature and filtered to remove ammonium chloride. THF was removed to afford a white solid, which was redissolved in CH_2Cl_2 and 1 M NaOH solution. The aqueous phase was extracted by CH_2Cl_2. The organic phase was then collected and the solvent was removed *in vacuo*. Purified product was obtained as a white solid after recrystallizing from hot methanol. ^{1}H-NMR ($CDCl_3$, δ ppm from TMS): 9.87 (s, 1H), 8.60 (d, 2H), 7.99 (d, 2H), 7.62 (t, 2H), 7.49 (m, 3H), 7.38 (d, 2H), 7.17 (t, 2H), 2.33(s, 3H).

For Me-Me-DPAH, 0.2 g (1 mmol) 1,1-di(pyridin-2-yl)ethanamine was dissolved in 1 mL acetic anhydride and stirred for 30 min, after which ice was added to hydrolyze excess acetic anhydride. Dichloromethane was used to extract the product from the aqueous phase and removed under vacuum. Pure product was obtained after silica column chromatography (hexanes : ethyl acetate = 1 : 1). ^{1}H-NMR ($CDCl_3$, δ ppm from TMS): 8.54 (d, 2H), 7.96 (s, 1H), 7.64 (dd, 2H), 7.43 (d, 2H), 7.08 (dd, 2H), 2.43(s, 3H), 2.14(s, 3H).

The methylation of position b of R-DPAH ligands was accomplished according to the procedure in the literature for methylating amino acid NH.[108] 1 mmol Ph-DPAH, *p*-

MeO-C_6H_4-DPAH, or Me-DPAH was mixed with 1.1 mmol (0.12 g) *t*-BuOK and stirred in dry THF at room temperature under inert atmosphere overnight. The reaction solution turned orange. A large excess (10 mmol) of CH_3I was then added and the solution was stirred overnight. Water was added to quench the reaction and the organic product was extracted by dichloromethane, which was removed under vacuum. Pure product was obtained after running through a silica gel column eluted with a gradient of hexanes / ethyl acetate. Ph-NMe-DPAH (80% yield): ^{1}H-NMR ($CDCl_3$, δ ppm from TMS): 8.64 (s, 2H), 7.74(td, 2H), 7.52 (m, 2H), 7.33(m, 5H), 7.14(d, 2H), 6.35(s, 1H), 3.01(s, 3H). *p*-MeO-C_6H_4-NMe-DPAH (90% yield): ^{1}H-NMR ($CDCl_3$, δ ppm from TMS): 8.58 (d, 2H), 7.93(d, 2H), 7.65(td, 2H), 7.50(d, 2H), 7.18(dd, 2H), 6.96(d, 2H), 6.41(s, 1H), 3.86(s, 3H), 3.01(s, 3H). Me-NMe-DPAH (75% yield): ^{1}H-NMR ($CDCl_3$, δ ppm from TMS): 8.54(d, 2H), 7.64(t, 2H), 7.42(d, 2H), 7.18(dd, 2H), 6.22(s, 1H), 3.02(s, 3H), 2.14(s, 3H).

*Synthesis of complexes **1** - **6**.* Complexes **1** - **6** are synthesized by the same procedure. In an N_2-containing glovebox, a mixture of two equivalents of ligand and one equivalent of $Fe^{II}(OTf)_2$•$2NCCH_3$ was stirred overnight in 1 mL CH_3CN. Ether was added into the solution to precipitate out a green solid and this solid was redissolved in CH_3CN. Vapor diffusion of THF into this solution resulted in the formation of purified **1** - **6**.

Synthesis of complex 7. **7** was synthesized using the same procedure of **1** - **6**. 2 equiv of Ph-D-DPAH and 1 equiv $Fe(OTf)_2$ were mixed in the glovebox in MeCN and stirred overnight. Complex **7** was obtained as crystals by diffusing Et_2O into MeCN solution of **7**. Characterization of **7**: ESI/MS: *m*/*z* 785 ($\{[Fe(Ph\text{-}D\text{-}DPAH)_2](OTf)\}^+$), 495 ([Fe(Ph-

D-DPAH)(OTf)]$^{+}$), 318 ([Fe(Ph-D-DPAH)$_2$]$^{2+}$).

*Synthesis of complexes **8** and **9**.* The procedure for the synthesis of **8** and **9** was the same as for **1** - **6**. In an N_2-containing glovebox, a mixture of 2 equiv Ph-Me-DPAH or Me-Me-DPAH, and 1 equiv Fe^{II}(OTf)·2MeCN was stirred for overnight in MeCN. Vapor diffusion of Et_2O into this solution resulted in the formation of **8** or **9**. Characterization of **8**: ESI-MS: m/z 811 ({[Fe(Ph-Me-DPAH)$_2$](OTf)}$^{+}$), 629 ([(Ph-Me-DPAH)$_2$+Na]$^{+}$), 508 ([Fe(Ph-Me-DPAH)(OTf)]$^{+}$), 326, ([(Ph-Me-DPAH) +Na]$^{+}$), 304 ([(Ph-Me-DPAH)+H]$^{+}$). Characterization of **9**: ESI-MS: 687 ({[Fe(Me-Me-DPAH)$_2$](OTf)}$^{+}$), 446 ([Fe(Me-Me-DPAH)(OTf)]$^{+}$), 242 ([(Me-Me-DPAH)+H]$^{+}$). Anal. Calcd. (found) for $C_{30}H_{30}F_6FeN_6O_8S_2$: C, 43.07 (43.22); H, 3.61 (3.65); N, 10.05 (10.82).

*Synthesis of complexes **10** - **12**.* The procedure for the synthesis of **10** - **12** was the same as for **1** - **6**. In an N_2-containing glovebox, a mixture of 2 equiv Ph-NMe-DPAH or *p*-MeO-C_6H_4-NMe-DPAH or Me-NMe-DPAH, and 1 equiv Fe^{II}(OTf)·2MeCN was stirred for overnight in MeCN. Vapor diffusion of Et_2O into this solution resulted in the formation of **10** - **12**. **10** was obtained as single crystals suitable for X-ray crystallographic analysis. See Tables 2.1 for crystal data and structure refinement for **10**. Characterization of **10**: ESI/MS: *m*/*z* 811 ({[Fe(Ph-NMe-DPAH)$_2$](OTf)}$^{+}$), 508 ([Fe(Ph-NMe-DPAH)(OTf)]$^{+}$), 331 ([Fe(Ph-NMe-DPAH)$_2$]$^{2+}$), 326 ([(Ph-NMe-DPAH)+Na]$^{+}$). Anal. Calcd. (found) for $C_{40}H_{34}F_6FeN_6O_8S_2$: C, 50.01 (50.11); H, 3.57 (3.45); N, 8.75 (8.77). Characterization of **11**: ESI/MS: *m*/*z* 871 ({[Fe(*p*-MeO-C_6H_4-NMe-DPAH)$_2$](OTf)}$^{+}$), 538 ([Fe(*p*-MeO-C_6H_4-NMe-DPAH)(OTf)]$^{+}$), 361 ([Fe(*p*-MeO-C_6H_4-NMe-DPAH)$_2$]$^{2+}$), 334 ([(*p*-MeO-C_6H_4-NMe-DPAH)+H]$^{+}$). Anal. Calcd. (found) for

$C_{42}H_{38}F_6FeN_6O_{10}S_2$: C, 49.42 (49.38); H, 3.75 (3.77); N, 8.23 (8.26). Characterization of **12**: ESI/MS: *m*/*z* 687 ({[Fe(Me-NMe-DPAH)$_2$](OTf)}$^+$), 446 ([Fe(Me-NMe-DPAH)(OTf)]$^+$), 269 ([Fe(Me-NMe-DPAH)$_2$]$^{2+}$), 264 ([(Me-NMe-DPAH)+Na]$^+$). Anal. Calcd. (found) for $C_{30}H_{30}F_6FeN_6O_8S_2$: C, 43.07 (42.93); H, 3.61 (3.60); N, 10.05 (9.90).

Data collection: a crystal (approximate dimensions 0.45 x 0.35 x 0.30 mm^3) was placed onto the tip of a 0.1 mm diameter glass capillary and mounted on a CCD area detector diffractometer for a data collection at 173(2) K.[109] A preliminary set of cell constants was calculated from reflections harvested from three sets of 20 frames. These initial sets of frames were oriented such that orthogonal wedges of reciprocal space were surveyed. This produced initial orientation matrices determined from 87 reflections. The data collection was carried out using MoKα radiation (graphite monochromator) with a frame time of 25 seconds and a detector distance of 4.818 cm. A randomly oriented region of reciprocal space was surveyed to the extent of one sphere and to a resolution of 0.77 Å. Four major sections of frames were collected with 0.30º steps in ω at four different ϕ settings and a detector position of -28º in 2θ. The intensity data were corrected for absorption and decay (SADABS).[110] Final cell constants were calculated from the xyz centroids of 7601 strong reflections from the actual data collection after integration (SAINT).[111] Please refer to Table 2.11 for additional crystal and refinement information.

Structure solution and refinement: the structure was solved using Sir2004[112] and refined using SHELXL-97.[113] The space group P-1 was determined based on systematic absences and intensity statistics. A direct-methods solution was calculated which

provided most non-hydrogen atoms from the E-map. Full-matrix least squares / difference Fourier cycles were performed which located the remaining non-hydrogen atoms. All non-hydrogen atoms were refined with anisotropic displacement parameters. All hydrogen atoms were placed in ideal positions and refined as riding atoms with relative isotropic displacement parameters. The final full matrix least squares refinement converged to $R1 = 0.0312$ and $wR2 = 0.0854$ (F^2, all data).

Table 2.1 Crystal data and structure refinement for **10**

Identification code	10195	
Empirical formula	$C_{40}H_{34}F_6FeN_6O_8S_2$	
Formula weight	960.70	
Temperature	173(2) K	
Wavelength	0.71073 Å	
Crystal system	Triclinic	
Space group	P-1	
Unit cell dimensions	a = 8.311(1) Å	α = 76.910(1)°
	b = 10.168(1) Å	β = 87.001(1)°
	c = 12.875(1) Å	γ = 71.984(1)°
Volume	1007.60(18) $Å^3$	
Z	1	
Density (calculated)	1.583 Mg/m^3	
Absorption coefficient	0.568 mm^{-1}	
F(000)	492	
Crystal color, morphology	green, block	
Crystal size	0.45 x 0.18 x 0.15 mm^3	
Theta range for data collection	1.62 to 27.50°	
Index ranges	$-10 \le h \le 10$, $-13 \le k \le 13$, $-16 \le l \le 16$	
Reflections collected	12090	
Independent reflections	4560 [R(int) = 0.0213]	
Observed reflections	4116	
Completeness to theta = 27.50°	98.4%	
Absorption correction	Multi-scan	
Refinement method	Full-matrix least-squares on F^2	
Data / restraints / parameters	4560 / 0 / 287	
Goodness-of-fit on F^2	1.050	
Final R indices [I>2sigma(I)]	$R1$ = 0.0312, $wR2$ = 0.0818	
R indices (all data)	$R1$ = 0.0359, $wR2$ = 0.0854	
Largest diff. peak and hole	0.422 and -0.358 e.$Å^{-3}$	

Instrumentation. ^{1}H spectra were recorded on a Varian Unity 300 or 500 MHz spectrometer at ambient temperature. Chemical shifts (ppm) were referenced to the residual protic solvent peaks. FTIR spectra were obtained with a Thermo Nicolet Avatar 370 FT-IR instrument. X-ray crystallographic analyses were completed by mounting the crystal on a Bruker-AXS platform diffractometer with CCD area detector and sealed-tube 3-KW X-ray generators. High-resolution electrospray mass spectral (ESI-MS) experiments were performed on a Bruker (Billerica, MA) BioTOF II time-of-flight spectrometer. Product analyses from catalysis experiments were performed on a Perkin Elmer AutoSystem gas chromatograph (AT-1701 column, 30 m) with a flame ionization detector. Gas chromatography/mass spectral analyses were performed on an HP 6890 GC (HP-5 MS column, 30 m) with an Agilent 5973 mass analyzer. A 4% NH_3/CH_4 mix was used as the ionization gas for chemical ionization analyses.

Reaction conditions for catalytic oxidations. In a typical reaction, 10 equivalents of H_2O_2 (diluted from 35% H_2O_2 solution with CH_3CN resulting in a 70 mM solution) were delivered by syringe pump over a period of 5 min at room temperature (20°C) in air to a vigorously stirred CH_3CN solution containing iron catalyst and 1000 equivalents of olefin substrate. The final concentrations were 0.35 mM iron catalyst, 3.5 mM H_2O_2, and 0.35 M olefin. The solution was stirred for an additional 60 min after syringe pump addition, after which organic products were esterified by 1 mL acetic anhydride together with 0.1 mL 1-methylimidazole and extracted with $CHCl_3$. An internal standard (naphthalene) was added and the solution was washed with 1 M H_2SO_4, sat. $NaHCO_3$, and H_2O. The organic layer was dried with $MgSO_4$ and subjected to GC analysis. The

products were identified by comparison of their GC retention times and GC/MS with those of authentic compounds.

Reaction conditions for kinetics. Similar conditions as described above were used for kinetic studies except for the following details. Reactions were carried out in a mixture of 95% acetonitrile and 5% 2, 2-dimethoxylpropane. A 0.5 mL aliquot of the solution was taken out at each time spot and run through a micro silica column. The silica column was then washed by 3:1 hexanes and ethyl acetate mixture. The resulting product was the acetonide derivative of the *cis*-diol, which was analyzed by GC.

2.3 Structural studies of R-DPAH iron complexes

Structural analysis in solid state. Crystal structures of **1** - **3** have shown that two ligands bind to the iron center in a centrosymmetric fashion.[99,104] The two carbonyl groups in two ligands are *trans* to each other. Elemental analysis confirms a 1 : 2 iron-to-ligand ratio for **1** - **5**.

FT/IR analysis was carried out for **1** - **6** in the solid state. Since the distinct C=O vibration is easy to follow and the binding of the carbonyl oxygen to the iron can weaken the C=O vibration, the carbonyl stretch is a useful indicator of the coordination of the oxygen atom to the iron center. From Table 2.2, all C=O vibration show a 21 – 50 cm^{-1} downshift, which confirms the binding of the carbonyl oxygen as shown in the crystal structures of **1** - **3**.

Table 2.2 FT/IR frequencies of the carbonyl groups in solid FT/IR for **1-6**

	Ligand / cm^{-1}	Complex / cm^{-1}	$\Delta\upsilon$ / cm^{-1}
Ph-DPAH	1655	1622	33
p-MeO-C_6H_4-DPAH	1649	1616	33
p-CF_3-C_6H_4-DPAH	1668	1618	50
CH_3-DPAH	1643	1622	21
CF_3-DPAH	1707	1682	25
CD_3-DPAH	1637	1616	21

Structural analysis in solution. Since homogeneous catalysis is carried out in solution, it is very important to characterize the structures of iron complexes in solution. To determine the solution structures, ESI-MS, solution FT/IR, and NMR spectra were recorded. ESI-MS measurements of **1** - **5** were reported.[104] Figure 2.1 shows the ESI-MS spectrum of complex **6**. The following ions were observed: $\{[FeL_2](OTf)\}^+$(m/z = 665), $[FeL(OTf)]^+$(m/z = 435), $[FeL_2]^{2+}$(m/z = 258), and $L + H^+$(m/z = 231). Thus there is a ligand dissociation equilibrium as shown in Equation 2.1. In support of this equilibrium, an equimolar mixture of **1** and **2** in CH_3CN affords an ESI-MS spectrum that shows a statistical mixture of $[FeL_2]^{2+}$ ions with the mixed ligand complex $[FeLL']^{2+}$ being the most abundant species in the mixture (Figure 2.2 bottom). This spectrum is observed immediately upon mixing **1** and **2** in CH_3CN and injecting the solution into the mass spectrometer, showing that ligand scrambling occurs essentially upon dissolution.

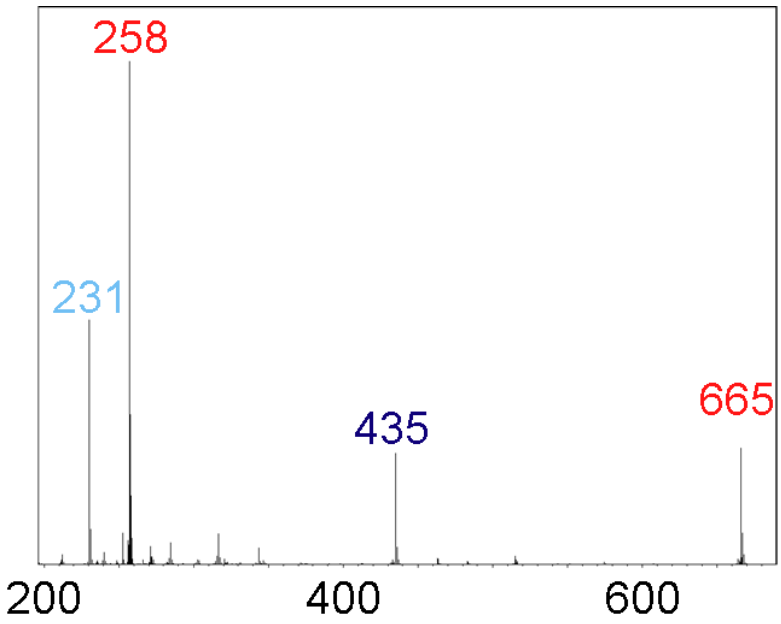

Figure 2.1 ESI-MS analysis of complex **6**. 231 = LH^+; 258 and 665 = $[Fe(L)_2]^{2+}$ and $[Fe(L)_2(OTf)]^+$; 435 = $[Fe(L)(OTf)]^+$ (L = CD_3-DPAH).

$$[FeL_2]^{2+} \rightleftharpoons [FeL]^{2+} + L$$

Equation 2.1 The ligand dissociation-association equilibrium proposed for **1-6**.

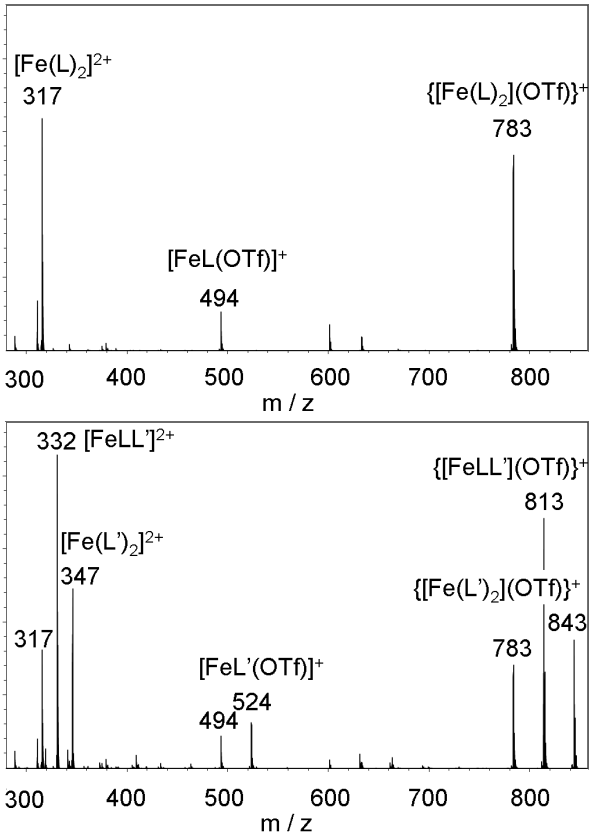

Figure 2.2 ESI-MS analysis of **1** (top) and a mixture of **1** and **2** (bottom) in CH_3CN (L = Ph-DPAH and L' = *p*-MeO-C_6H_4-DPAH).

Since the concentration of the solutions used for ESI-MS analysis (~μM) is far more dilute than that required for the catalytic reactions (0.35 mM, see section 2.2), ligand dissociation may be favored in dilute solutions. Instead of ESI-MS, FT-IR was used for solution characterization at high concentrations to simulate catalytic reaction conditions (Table 2.3). The Ph-DPAH ligand exhibits an amide $\nu_{C=O}$ at 1662 cm^{-1}. This feature downshifts by 37 cm^{-1} in the solution of the corresponding iron complex **1**, and there is no evidence for the $\nu_{C=O}$ of the free ligand in this solution. Similar results are obtained for **2** - **6**, with respective downshifts of 39, 36, 47, 95, and 40 cm^{-1} observed for these

complexes in solution. These downshifts indicate a strong interaction between the ligand amide carbonyl oxygen atoms and the metal center. Only in the case of **5** can some uncoordinated amide be discerned. Taken together, these observations indicate that complexes **1** - **6** in solution retain in large part the 1:2 metal-to-ligand composition found in the crystal structures of **1** - **3**. Furthermore, the ligand dissociation equilibrium postulated above on the basis of the ESI-MS data must lie predominantly to the left in favor of the $[FeL_2]^{2+}$complex.

Table 2.3 Solution FT/IR frequencies of the carbonyl groups in solution FT/IR for **1** - **6**[a]

	Ligand / cm^{-1}	Complex / cm^{-1}	$\Delta\upsilon$ / cm^{-1}
Ph-DPAH	1662	1625	37
p-MeO-C_6H_4-DPAH	1657	1618	39
p-CF_3-C_6H_4-DPAH	1668	1632	36
CH_3-DPAH	1677	1630	47
CF_3-DPAH	1728	1633	95
CD_3-DPAH	1669	1629	40

[a]FT/IR spectra were taken in CD_3CN.

^{1}H-NMR spectra of **1** - **6** show resonances with a large spread of chemical shifts (Figure 2.3), which is in agreement with the presence of a paramagnetic Fe(II) center that is indicated by the more than 2 Å bond lengths between the metal center and coordinating atoms in the crystal structures of **1** - **3**.[99,104] However, these spectra exhibit

many more peaks than expected if the solution structures maintain the center of symmetry found in the crystal structures. Clearly, the centrosymmetric structure alone is too simple to explain the solution behavior. However, the NMR spectrum of **5** is different from the others. Large peaks corresponding to free ligand are observed, which is in good agreement with its solution FT/IR spectrum where uncoordinated amide is discerned. Based on the equilibrium shown in equation 2.1, these complicated spectra were initially thought to be from two species: $[FeL_2]^{2+}$ and $[FeL]^{+}$, but this idea is in contradiction with the solution FT/IR spectra that do not show the C=O vibration of the free ligand. Furthermore, when ^{19}F-NMR is carried out for **3** at various concentrations (Figure 2.4), the ^{19}F-NMR spectrum of 0.35 mM **3** shows four peaks: peak d corresponding to the counter anion triflate, small peak c assigned to free ligand, and peaks a and b belonging to a species in solution that contains iron. When the concentration is doubled to 0.7 mM, the integration ratio between peaks a and b should be perturbed if they were $[FeL_2]^{2+}$ and $[FeL]^{+}$ according to equation 2.1, but the relative ratio among the peaks stayed constant and only the peak area of free ligand decreased because at higher concentration the ligand has less tendency to dissociate from the complex. The ^{19}F-NMR spectrum of a sample at even higher concentration (1.4 mM) affords the same pattern. Interestingly, the integration ratio between peaks a and b remains the same and the area of peak c becomes smaller. So the assumption that $[FeL_2]^{2+}$ and $[FeL]^{+}$ are species in solution is not appropriate. This conclusion is further evidenced by taking ^{1}H-NMR spectra of mixtures of $Fe(OTf)_2 \cdot 4MeCN$ with different ratios of CD_3-DPAH ligand (Figure 2.5). The relative size of peaks in the

paramagnetically shifted region remains unchanged. Therefore, the possibility that in solution the iron center is coordinated by different numbers of ligand is ruled out.

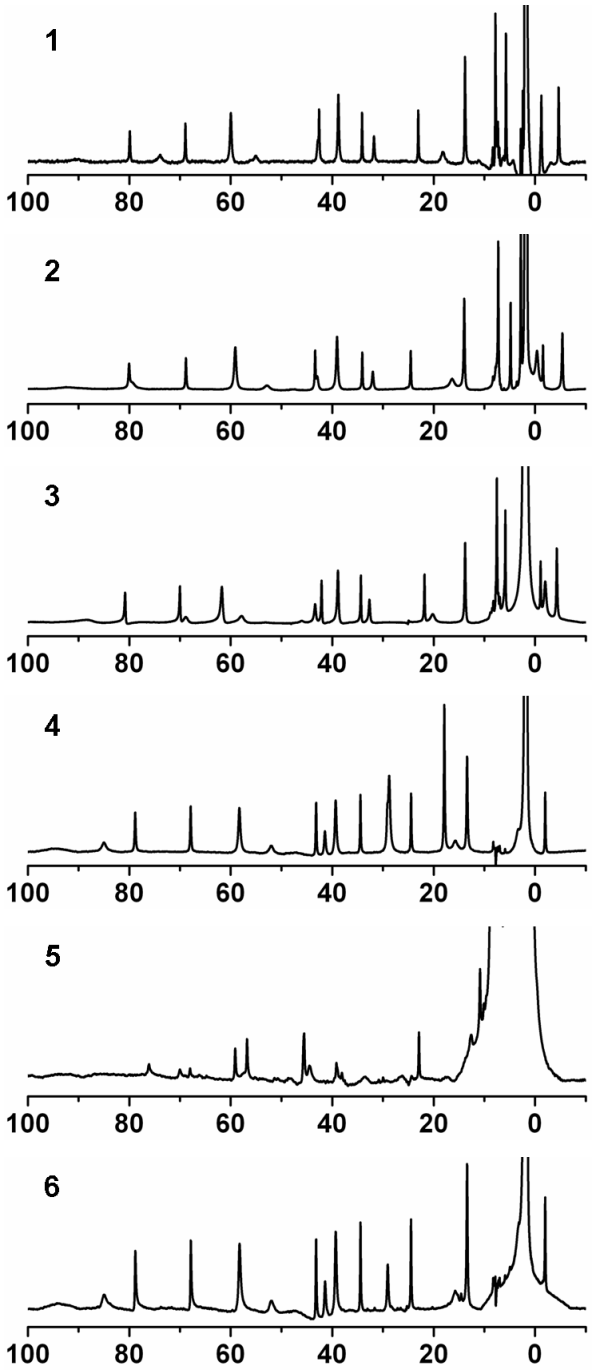

Figure 2.3 ^{1}H-NMR spectra of **1-6**.

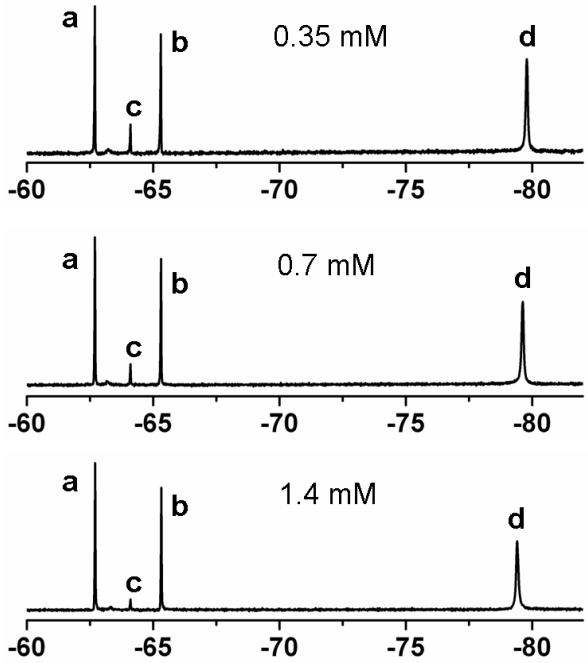

Figure 2.4 ^{19}F-NMR spectra of **3** at various concentrations.

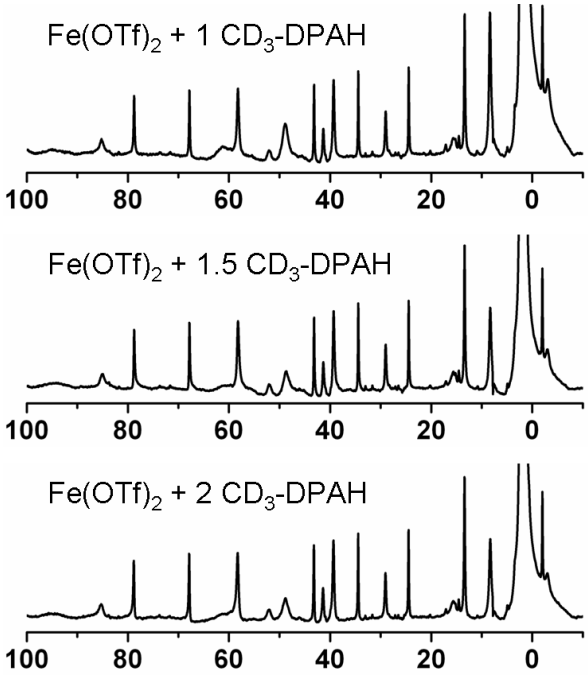

Figure 2.5 ^{1}H-NMR spectra of $Fe(OTf)_2$ with different ratios of CD_3-DPAH.

To understand the relationship between the ^{1}H-NMR spectra and the solution structures, **4** and **6** are compared, because they differ only in the methyl group next to the carbonyl group. **6** is the deuterated version of **4**, so comparison between them can give information about this methyl group. Since the methyl group is adjacent to the metal binding carbonyl functional group, the shift of the methyl group is indicative of oxygen atom binding. Figure 2.6 shows NMR spectra of **4** and **6**, and **6** shows an almost identical spectrum as **4** except that two peaks are missing, the peaks at 18 ppm and 29 ppm illustrated by the arrows in the top spectrum of Figure 2.6. The 29-ppm peak in **4** has a shoulder and its area decreases in **6**, clearly indicating that another peak is hidden in the peak and can not be resolved from it. The area ratio between these two peaks at 29 ppm and 18 ppm is approximately 1 to 1. The assignment of the methyl group is further confirmed by the ^{2}H-NMR spectrum of **6** (Figure 2.6, bottom). Two large peaks assigned to the methyl group show up at the same chemical shifts as in the ^{1}H-NMR of spectrum of **4**. A small peak is also observed and assigned to the methyl group of the free ligand. So there are two types of methyl groups and thus two types of carbonyl oxygen binding environments in solution for complexes **4** and **6**. This conclusion thus far is also in agreement with the ^{19}F-NMR spectrum of **3** (Figure 2.4). There are two peaks corresponding to the CF_3 group in the complex. Since the CF_3 group is on the phenyl ring that is connected to the binding carbonyl group, the CF_3 shift can also shed light on the binding mode of the carbonyl group. The centrosymmetric structure as shown from crystal structures is expected to contain only one type of binding oxygen atom. Clearly, another structure other than the centrosymmetric one exists in solution.

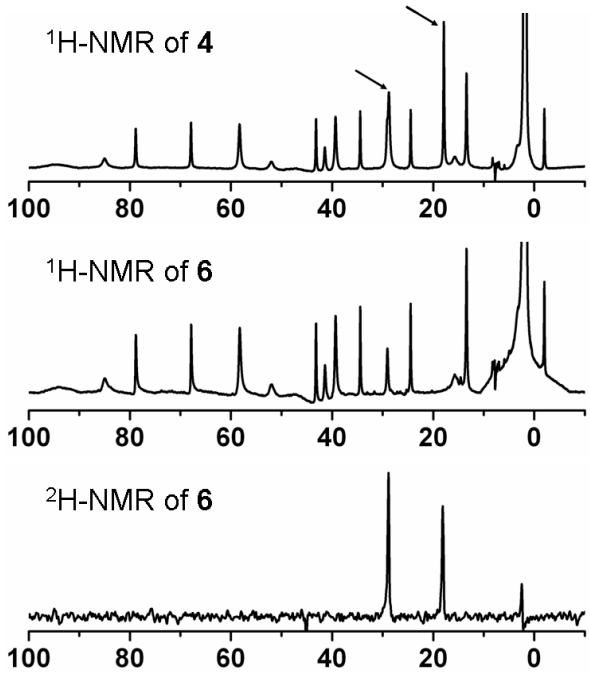

Figure 2.6 NMR spectra of **4** and **6**.

The 2D-^{1}H-NMR spectrum of **6** was investigated (Figure 2.7 top) to gain insight into the pyridine ligands. The coupling interactions among pyridine protons are illustrated in the 1D-^{1}H-NMR spectrum of **6** (Figure 2.7 bottom). Because the α proton on the pyridine ring is too close to the nitrogen atom that coordinates the paramagnetic iron center, it does not show up as a sharp peak and coupling to the adjacent β peak can not be detected. So this makes the γ peak the only one that can couple to two other peaks. Based on this knowledge, the β and γ peaks can all be assigned (Figure 2.7, labels above the peaks). As shown in Figure 2.7, there are three types of pyridines. The area ratios among these three types are roughly 2 : 1 : 1. Considering that the two types of methyl groups have approximately the same area, presumably the first type of pyridine belongs to one structure and the second and the third belong to another one.

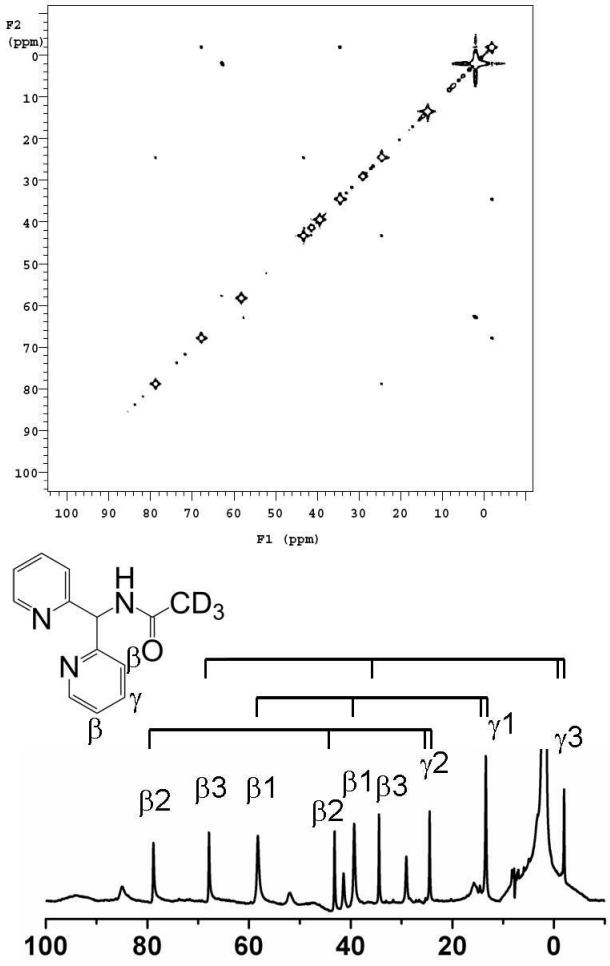

Figure 2.7 2D-^{1}H-NMR of **6** and assignment of pyridine protons.

Taken together, in solution there are two structures: one with one kind of oxygen donor and nitrogen donor and the other with one kind of oxygen donor and two kinds of nitrogen donors. Thus I propose an equilibrium between two structures in solution (Scheme 2.2). The first structure is in agreement with the one observed in the crystal. The two oxygen atoms are *trans* to each other (Scheme 2.2, trans), so only one type of oxygen and nitrogen ligand is observed. In the other structure, the two oxygen atoms are *cis* to each other (Scheme 2.2, cis). Two nitrogen atoms are *trans* to each other and the

other nitrogens are *trans* to oxygens, so there are two types of nitrogen donors and one type of oxygen donor. Since the free ligand can also be detected in the NMR spectra, the ligand can dissociate from the iron center to some degree. Therefore, this is the first time that solution characterization of iron complexes with the *N,N,O*-facial ligand can be fully accomplished.

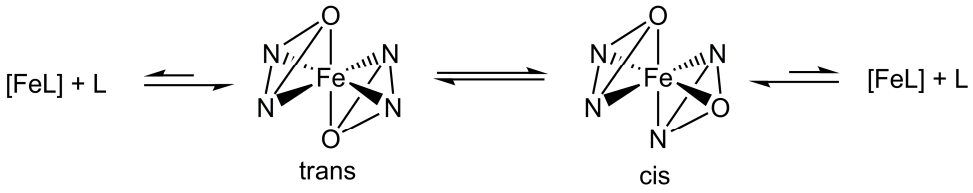

Scheme 2.2 Proposed structures for **1-6** in acetonitrile.

2.4 Reactivity of R-DPAH iron complexes

Reactions catalyzed by the combination of $Fe(OTf)_2$ and ligand. Catalytic studies have shown that R-DPAH iron complexes are good catalysts for converting olefin into *cis*-diol in very high yield with H_2O_2 as oxidant.[104] Control experiments without iron complexes give no turnovers for olefin oxidation, suggesting that H_2O_2 binds to the iron center to form a $Fe(H_2O_2)$ adduct that effects the oxidation of olefin. Formation of such an adduct has been considered and found to be energetically reasonable in computational studies of Fenton chemistry[114,115] and of an iron complex of a tetradentate bispidine ligand that is capable of olefin oxidation catalysis.[116] For the R-DPAH family of catalysts, such an $Fe(O_2H_2)$ adduct may be formed either by a) dissociation of the two carbonyl ligands upon addition of H_2O_2 or b) loss of one of the R-DPAH ligands.

To assess the viability of option a, a 1:2 ratio of $Fe(OTf)_2$ and dipyridin-2-ylmethanone (DPK) in CH_3CN was tested for whether it could catalyze the *cis*-dihydroxylation of 1-octene. However, with 1 and 4 equivalents of H_2O_2, no product can be detected from the reaction, and less than 0.1 equiv diol is obtained upon addition of 10 equiv H_2O_2, suggesting that the four-pyridine ligand combination postulated for option a is not able to catalyze olefin *cis*-dihydroxylation under the conditions that R-DPAH iron complexes can (Table 2.4). In addition, there must be an additional metal coordination site to bind water to account for the observed label scrambling.[104] For option a, this would require formation of a 7-coordinate $Fe(N2)_2(O_2H_2)(H_2O)$ intermediate, which may be too sterically crowded.

To assess the viability of option b, a 1:1 ratio of $Fe(OTf)_2$ and Ph-DPAH was tested and found to be active in catalyzing 1-octene *cis*-dihydroxylation. Addition of 1 equiv H_2O_2 afforded 0.7(1) TON of the *cis*-diol, while addition of 4 equiv H_2O_2 resulted in 2.9(2) TON, for about a 73% efficiency in the conversion of H_2O_2 into *cis*-diol, just slightly below that observed for **1**.[99] However, addition of 10 equiv H_2O_2 afforded only 4.1(2) TON of the *cis*-diol, suggesting significant catalyst deterioration after 3 turnovers (Table 2.4). Delaying this outcome may be the role played by the additional Ph-DPAH ligand in **1**. This option, on the other hand, is particularly attractive as it can provide three coordination sites on one face of the six-coordinate iron center to allow binding of both a side-on bound H_2O_2 and a water molecule. Evidence that the proposed ligand dissociation equilibrium is established rapidly has been presented in Figure 2.2. Upon addition, H_2O_2 would then most likely interact with the 1:1 $[Fe(L)]^{2+}$ species and shift

the dissociation equilibrium to the right to form the 6-coordinate Fe $(L)(O_2H_2)(H_2O)$ intermediate.

Table 2.4 Reactivity of 1-octene oxidation with $Fe(OTf)_2$ and various ligands as catalyst[a]

Ligand	Fe : L	H_2O_2	epoxide	*cis*-diol
DPK[b]	1 : 2	1	-	-
DPK[b]	1 : 2	4	-	-
DPK[b]	1 : 2	10	-	0.1
Ph-DPAH	1 : 1	1	-	0.7(1)
Ph-DPAH	1 : 1	4	-	2.9(2)
Ph-DPAH	1 : 1	10	0.1(1)	4.1(2)

[a]Reaction conditions: H_2O_2 was added by syringe pump at a rate of 0.5 min per equivalent of H_2O_2 (to minimize H_2O_2 disproportionation) to a solution of catalyst (0.35 mM) and 1-octene (0.35 M) in CH_3CN. This solution was stirred for an additional 60 min prior to workup. See section 2.2 for further details. Yields expressed as turnover numbers, TON, (μmol product/μmol catalyst). [b]DPK stands for dipyridin-2-ylmethanone.

Oxidation of naphthalene. Naphthalene can be oxidized by H_2O_2 into *cis*-1,2-dihydronaphthalene-1,2-diol catalyzed by $[Fe(TPA)(MeCN)_2](OTf)_2$,[117] and a Fe^{V}=O(OH) species is proposed to be the active oxidant. To understand the nature of the active oxidant for R-DPAH iron complexes in olefin catalysis, it is interesting to study

whether naphthalene oxidation can be catalyzed by R-DPAH iron complexes. Different from what was reported for $[Fe(TPA)(MeCN)_2](OTf)_2$,[117] no *cis*-dihydroxylation of naphthalene was observed. This observation leads to the assumption that R-DPAH iron complexes form an oxidant that is less powerful than Fe^{V}=O(OH). This oxidant is presumably in the Fe^{IV} oxidation state.

Oxidation of cyclohexene. Cyclohexene has a weak allylic C-H bond that is susceptible to oxidation, and the facile formation of allylic oxidation products has been observed for some nonheme iron complexes.[61,118-121] On the other hand, the C=C bond can also be readily oxidized. Therefore, cyclohexene functions as a good mechanistic probe, as it can undergo different oxidation pathways. With cyclohexene as substrate, 10 equiv H_2O_2 afforded 5.7 equiv *cis*-cyclohexane-1,2-diol, 0.5 equiv cyclohexenol, 0.4 equiv cyclohexenone, and no cyclohexene oxide for **1** and **4**. The high conversion to the *cis*-diol product is quite remarkable. The products observed in the reaction of cyclohexene with **1** or **4** / H_2O_2 are quite indicative of the active oxidant formed in the catalytic cycle, where the dominant product is the *cis*-diol, representing 90% of the products formed. Cyclohexenol and cyclohexenone make up the remaining 10%, and no epoxide was observed. This outcome is distinctly different from oxidations catalyzed by other nonheme iron complexes. For example, in the case of Fe^{II}(cyclam)/H_2O_2, only cyclohexene oxide was observed.[122] On the other hand, allylic oxidation products were the dominant. The very low extent of allylic oxidation in the case of the R-DPAH complexes suggests the involvement of an oxidant with a much lower hydrogen-atom abstraction capability than is associated with nonheme oxoiron(IV) complexes, which

have been shown to be quite facile at carrying out hydrogen-atom abstractions, particularly of allylic C-H bonds.[120,123-125] A recent comparison of oxoiron(IV) and hydroxoiron(IV) species supported by the same tetradentate ligand showed the former to have a 100-fold higher H-atom abstracting ability than the latter.[126] A similar comparison of Mn(IV) complexes also revealed the same trend.[127-129] With a lower hydrogen-atom affinity than its oxoiron(IV) counterpart, the dihydroxoiron(IV) oxidant is proposed and consequently well suited to carry out the highly selective *cis*-dihydroxylation of the cyclohexene double bond.

Taken together, a mechanism for olefin oxidation catalyzed by R-DPAH iron complexes can be formulated (Scheme 2.3). R-DPAH iron complexes in acetonitrile solution lose one ligand initially to open three *cis* sites that can accommodate the binding of H_2O_2 and H_2O. The thus formed $Fe^{II}(\eta^2\text{-}H_2O_2)$ adduct undergoes O-O homolytic cleavage to generate the active oxidant $Fe^{IV}(OH)_2$, responsible for oxidizing olefin to form the *cis*-diol product.

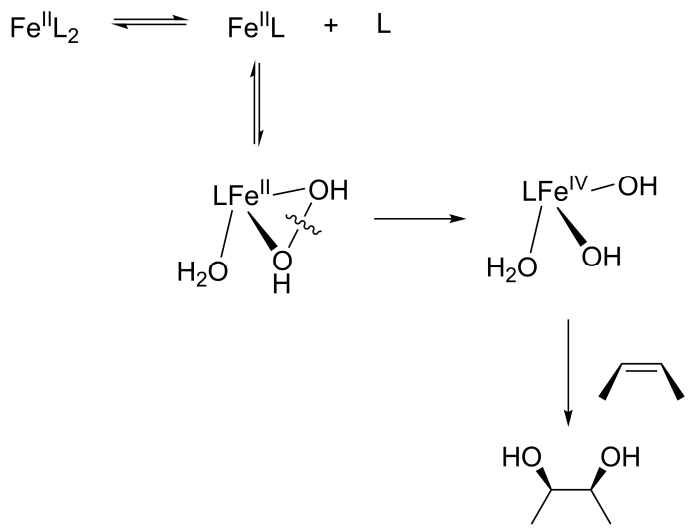

Scheme 2.3 Mechanism of olefin oxidation catalyzed by R-DPAH iron complexes.

2.5 Kinetic studies of R-DPAH iron complexes

*Kinetics of 1-octene oxidation catalyzed by **1***. Monitoring kinetics of oxidation reaction is an important way to study the reaction mechanism. However, in the case of iron-catalyzed olefin oxidation by H_2O_2, the H_2O_2 solution has to be injected via a syringe pump over a period of time to minimize of the disproportionation of H_2O_2, thus hampering kinetic studies. In addition, the two-step workup procedure (see section 2.2) could introduce new error into kinetic studies.

The optimized reaction conditions for olefin oxidation catalyzed by R-DPAH iron complexes required 5 minutes for the addition of H_2O_2 solution and another 60 minutes for stirring. This time requirement is quite puzzling, as the long stirring time suggests that H_2O_2 can stay in the reaction solution intact for later use, which is contradictory to the requirement of slow injection.

To solve this puzzle and study the kinetics, alternative reaction conditions were

employed. 5% 2, 2-dimethoxylpropane was used as a co-solvent of pure acetonitrile as solvent, so the resulting *cis*-diol product is converted into its acetonide derivative. The two-step workup procedure is thus eliminated, and the product can be analyzed by GC just after running the reaction solution through silica gel to remove the iron complex. In this way, kinetics can be carried out more conveniently and with fewer errors.

Preliminary kinetic results with 1-octene as a model substrate are illustrated in Figure 2.8. Each point in the graph was repeated three times. From the graph, the number of turnovers after 60 minutes is lower than under standard conditions where H_2O_2 was injected in 5 min, indicating that the slow injection still helps prevent from disproportionation. In addition, product formation exhibits two phases. In the first five minutes, the product formation is very slow, but starting from the fifth minute, the rate of product formation increases significantly and shows a first order behavior. The second phase from 5 min to 60 min can be fit to a first order kinetics model and the observed rate constant, k_{obs}, was 0.11 per min. This behavior indicates that the R-DPAH iron complexes are pre-catalysts and they need to form the active catalysts in the solution in the first five minutes, which is consistent with the proposal that one ligand falls off the iron center to open three *cis* sites for oxidant to bind before olefin oxidation occurs. In addition, the initial delay time can also explain the requirement of the five minutes injection time.

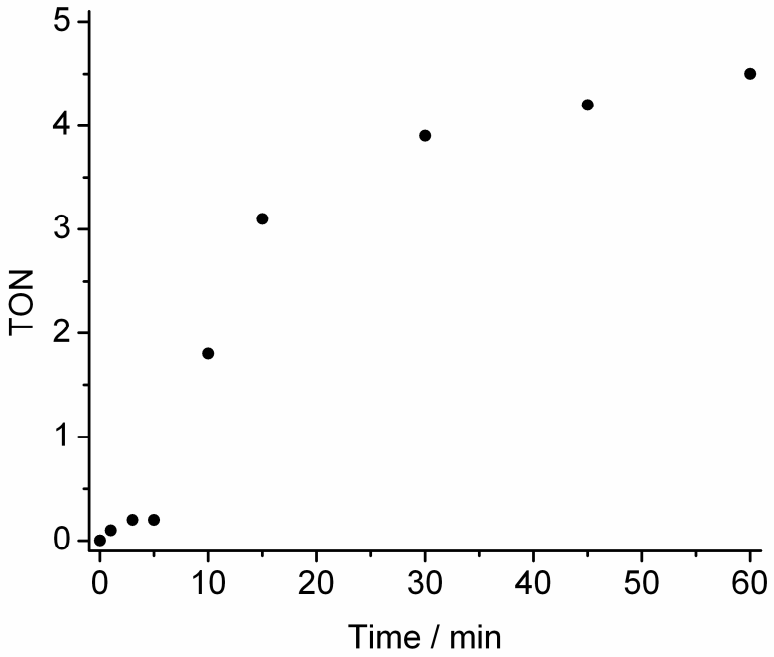

Figure 2.8 Kinetics of 1-octene oxidation catalyzed by **1**. Details of reaction conditions are in section 2.2.

2.6 Catalyst deactivation studies of R-DPAH iron complexes

*^{19}F-NMR studies of **3***. It has been discovered that R-DPAH iron complexes lose their catalytic reactivity after about 10 turnovers, so it is important to study the deactivation mechanism in order to lengthen the catalysts lifetime. The trifluoromethyl group on the *p*-CF_3-C_6H_4-DPAH ligand of **3** provides a convenient method to monitor the reaction by ^{19}F-NMR. 1-octene oxidation catalyzed by **3** was explored by this method with parabromofluorobenzene used as chemical shift internal reference. H_2O_2 was added all at once and ^{19}F-NMR spectra were collected immediately. 128 scans were collected for every spectrum, spanning about 7 minutes (Figure 2.9). From the top spectrum of Figure 2.9, the free ligand peak can be observed immediately, suggesting that ligand

dissociation occurs immediately upon adding H_2O_2. As the oxidation reaction progressed, the peaks corresponding to the iron complex became smaller and smaller. At the end of the reaction, only the ligand peak was clearly seen in the last collected spectrum (Figure 2.9, bottom after 50 min). In all these spectra, the ligand peak is always bigger than the peaks from the iron complex. These spectra are quite different from the ^{19}F-NMR spectrum of **3** in acetonitrile without any substrate and oxidant, in which the free ligand peak is very small compared to iron complex peaks (Figure 2.4). It can be concluded that ligand dissociation is one reason that R-DPAH iron complexes deactivate. The easy dechelation of the R-DPAH ligands could be due to the fact that the tridentate ligand has a smaller binding affinity for the iron than the tetradentate ligand.

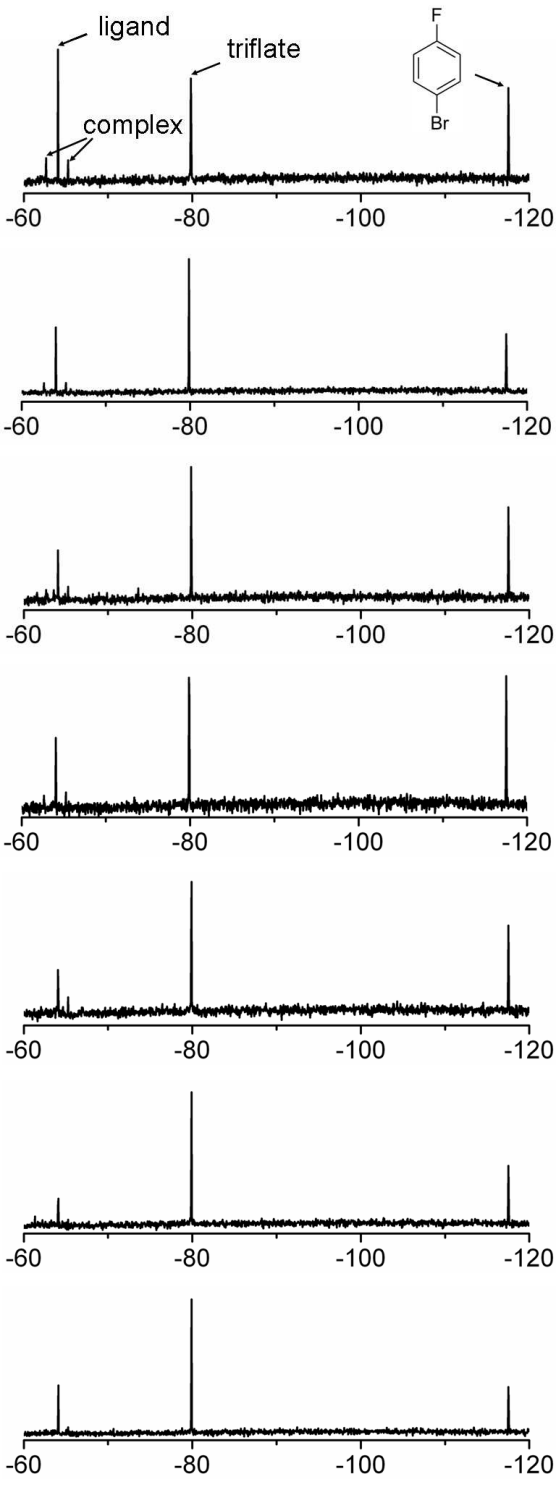

Figure 2.9 ^{19}F-NMR of **3** in the 1-octene oxidation.

*Ligand decomposition studies of **1***. As previous studies demonstrate, the ligand easily dissociates from the iron center, so free ligand in the solution could act as substrate. Considering that the tertiary CH of Ph-DPAH is adjacent to two pyridine rings and one amide group, it should be quite readily oxidized. So the solution of **1** after reaction was examined by ESI-MS, but the spectrum was so complicated that hardly anything can be deduced. To simplify this problem, Na_2EDTA solution was added into the solution after a typical catalytic reaction of 1-octene oxidation to remove iron from the solution, and then the resulting solution without iron was analyzed by ESI-MS. The ESI-MS spectrum showed the presence of peaks arising from species other than the free ligand peaks, indicating ligand oxidation (Figure 2.10). These peaks correspond to N-(dipyridin-2-ylmethylene)benzamide, benzamide and dipyridin-2-ylmethanone. These products indicate that the Ph-DPAH ligand is oxidized into its imine derivative, which then hydrolyzed into the observed ketone and amide (Scheme 2.4). A similar oxidation of the related N-(bis(2-pyridyl)methyl) pyridine-2-carboxamide ligand has been reported.[130]

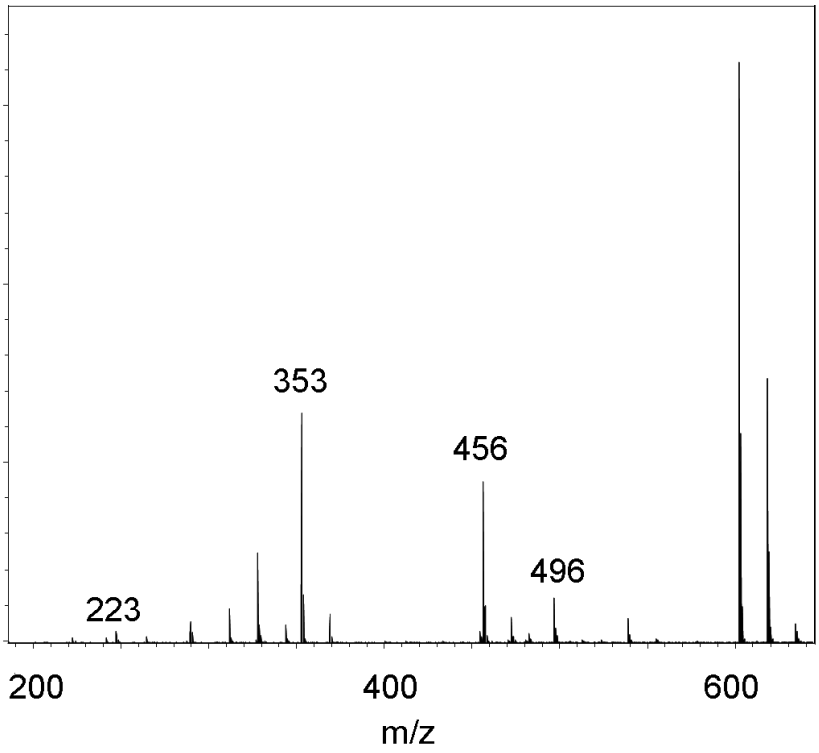

Figure 2.10 ESI-MS analysis of reaction solution of **1** at the end of a typical reaction after removing iron by Na_2EDTA. Selected peaks: 223 (dipyridin-2-ylmethanone + K^+), 353 (dipyridin-2-ylmethanone + *cis*-diol + Na^+), 456 (N-(dipyridin-2-ylmethylene) benzamide + *cis*-diol + Na^+), 496 (ligand + dipyridin-2-ylmethanone + Na^+)

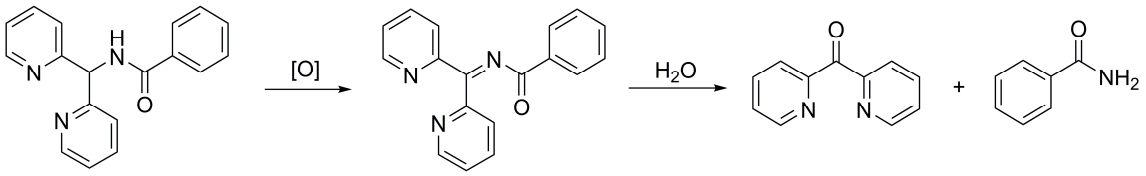

Scheme 2.4 Ligand decomposition pathway.

The products from ligand decomposition were further investigated in olefin oxidation to reveal their effects on the catalysis. Catalytic results are summarized in

Table 2.5. Combination of $Fe(OTf)_2$ with either dipyridin-2-ylmethanone or benzamide or both can not catalyze 1-octene oxidation, indicating that the Ph-DPAH ligand is actually the effective ligand instead of any derivatives. When benzamide was added in a typical catalytic reaction, the *cis*-diol yield was only slightly lowered compared with standard **1**-catalyzed 1-octene oxidation. However, when dipyridin-2-ylmethanone was used in the reaction, the *cis*-diol was formed merely in trace amounts. When both dipyridin-2-ylmethanone and benzamide were added, still only trace amounts of the *cis*-diol product can be observed. In sum, as long as dipyridin-2-ylmethanone was present in the solution, the catalyst deteriorates significantly. Therefore, these results show that the decayed product dipyridin-2-ylmethanone is detrimental to the catalyst.

So far, the catalyst deactivation studies suggest that deactivation goes through two steps. The first step is the dissociation of the ligand from the iron center due to the lower binding constant for the tridentate ligand; next the free ligand in solution acts as a readily oxidized substrate and decomposes into dipyridin-2-ylmethanone, which deactivates the catalyst.

Table 2.5 Catalytic results with ligand decomposed products[a]

Iron source	Additive 1	Additive 2	*cis*-diol
1	N/A	N/A	7.6
$Fe(OTf)_2$	dipyridin-2-ylmethanone	N/A	0
$Fe(OTf)_2$	benzamide	N/A	0
$Fe(OTf)_2$	dipyridin-2-ylmethanone	benzamide	0
1	dipyridin-2-ylmethanone	N/A	<0.1
1	benzamide	N/A	6.6
1	dipyridin-2-ylmethanone	benzamide	<0.1

[a]Reaction conditions: 10 equivalents of H_2O_2 was added by syringe pump over a period of 5 min(to minimize H_2O_2 disproportionation) to a solution of iron (0.35 mM), 1 equivalent of additive 1, 1 equivalent of additive 2, and 1000 equivalents of 1-octene (0.35 M) in CH_3CN. This solution was stirred for an additional 60 min prior to workup. See section 2.2 for further details. Yields expressed as turnover numbers, TON, (μmol product/μmol catalyst).

2.7 Increasing catalyst longevity by R-DPAH ligand re-design

Logic of ligand modification. The R-DPAH iron complexes deactivate after about 10 turnovers due to the oxidation of R-DPAH ligands to their imine derivatives (Scheme 2.5, top). If this unwanted oxidation is prevented, the resulting harmful dipyridin-2-ylmethanone can not be formed. So the iron catalysts may be expected to live longer and their catalytic reactivity will be improved.

As mentioned in previous sections, the tertiary C-H bond of the R-DPAH ligands is very weak (position a in Scheme 2.5) because it is adjacent to two pyridine rings and an amide group. This position a can be strengthened by two ways by making the C-H bond into a C-D bond or by substituting the hydrogen atom with a methyl group.

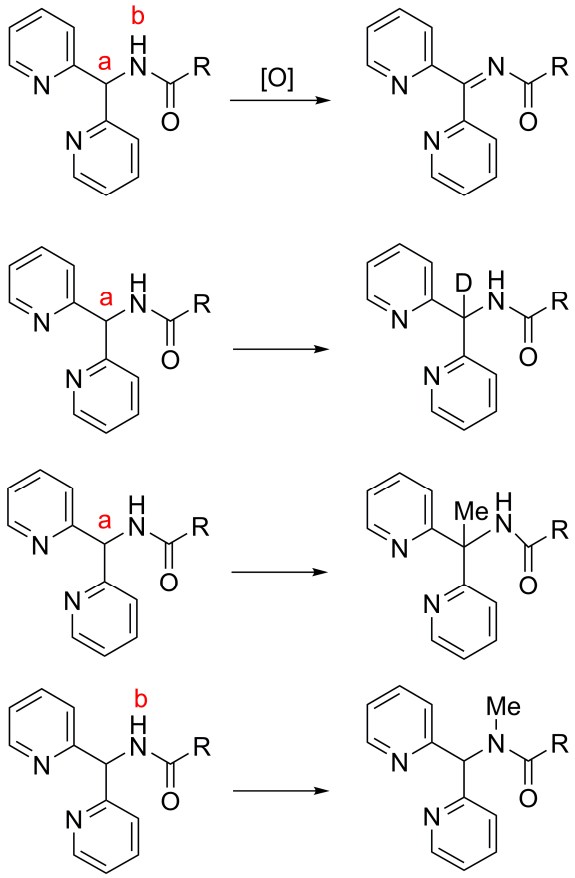

Scheme 2.5 Modification of R-DPAH ligands.

An alternative approach to block the pathway to form the C=N imine double bond is to put a methyl group on position b (Scheme 2.5). Although the weak tertiary C-H bond is still in the ligand structure, the resulting adjacent N-C bond is not easy to break and

and formation of the corresponding imine would be prevented and thus the harmful dipyridin-2-ylmethanone can not be generated. All modified ligands and their iron complexes are summarized in Scheme 2.6.

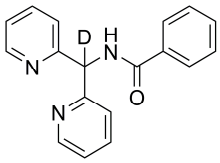

Ph-D-DPAH
7: $[Fe^{II}(Ph\text{-}D\text{-}DPAH)_2]^{2+}$

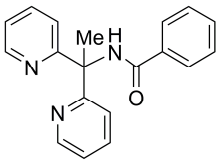

Ph-Me-DPAH
8: $[Fe^{II}(Ph\text{-}Me\text{-}DPAH)_2]^{2+}$

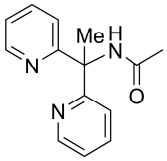

Me-Me-DPAH
9: $[Fe^{II}(Me\text{-}Me\text{-}DPAH)_2]^{2+}$

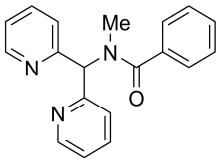

Ph-NMe-DPAH
10: $[Fe^{II}(Ph\text{-}NMe\text{-}DPAH)_2]^{2+}$

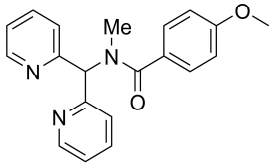

p-MeO-C_6H_4-NMe-DPAH
11: $[Fe^{II}(p\text{-}MeO\text{-}C_6H_4\text{-}NMe\text{-}DPAH)_2]^{2+}$

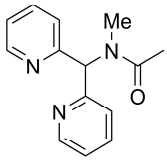

Me-NMe-DPAH
12: $[Fe^{II}(Me\text{-}NMe\text{-}DPAH)_2]^{2+}$

Scheme 2.6 Modified ligands structures.

2.7.1 Deuteration of position a

Characterization of complex 7. ESI-MS analysis shows that Ph-D-DPAH ligand maintains 80% deuteration in the complex (Figure 2.11). Both solid and solution FT/IR show a downshift of 39 and 38 cm^{-1} for the carbonyl group of **7** compared with Ph-D-DPAH ligand (Table 2.6), indicating that the carbonyl oxygen atom binds to the iron center in both solid and solution state. The ^{1}H-NMR spectrum shows the same pattern as **1**, so the deuteration of position a in the Ph-DPAH ligand does not change the structure of its iron complex. Therefore, it is believed that **7** maintains the same structure in

MeCN solution illustrated in Scheme 2.2.

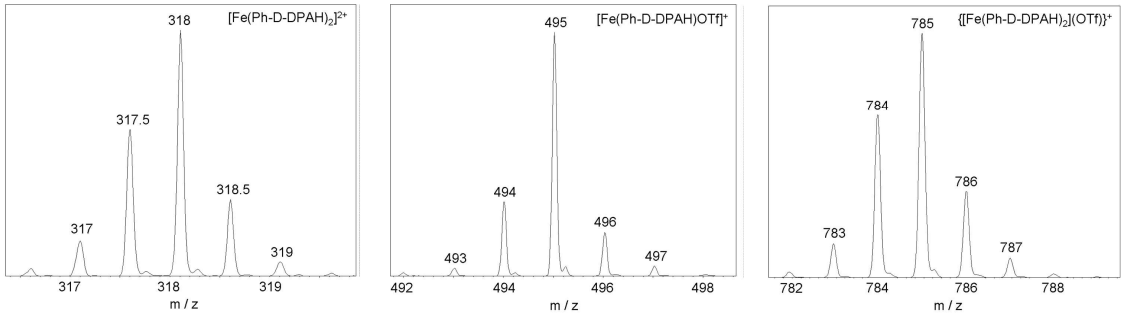

Figure 2.11 ESI-MS of **7** in MeCN.

Table 2.6 Vibration frequencies of the carbonyl group of **7** and the Ph-D-DPAH ligand by FT/IR

	ligand / cm^{-1}	complex / cm^{-1}	$\Delta\upsilon$ / cm^{-1}
Solid	1655	1616	39
Solution (CD_3CN)	1662	1624	38

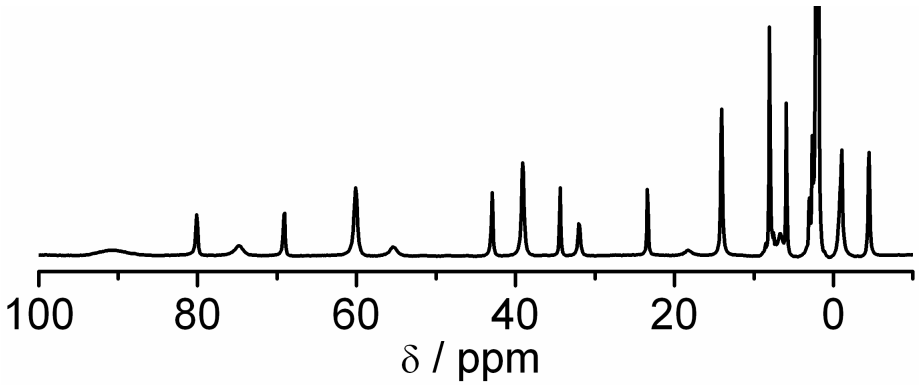

Figure 2.12 ^{1}H-NMR of **7**.

Catalytic reactivity. Table 2.7 compares the catalytic activities of **7** and its parent complex **1** in the oxidation of 1-octene using H_2O_2 as oxidant. With 10 equiv of H_2O_2, **7** converted 81% of H_2O_2 into the *cis*-diol product (Table 2.7, entry 1), which is slightly higher than the 76% conversion of catalyst **1** (Table 2.7, entry 4). When 20 equiv H_2O_2 were used, **1** can only catalyze 10.1 turnovers (Table 2.7, entry 5), while the deuterated **7** has a catalytic activity of 13.1 turnovers (Table 2.7, entry 2). After 20 equiv H_2O_2, **1** lost its reactivity completely, while **7** can still catalyze another 2 turnovers when another 10 equiv H_2O_2 was added (Table 2.7, entry 3). The 80% deuterated iron catalyst **7** is better behaved than its parent complex **1**, although the percentage conversion still decreases as more H_2O_2 is used. Therefore, deuteration enhances the stability of iron catalysts, but the ligand is still susceptible to oxidation.

Table 2.7 Oxidation of 1-octene catalyzed by **1** and **7** with H_2O_2 as oxidant[a]

Entry	complex	H_2O_2	epoxide	*cis*-diol
1	**7**	10	0.1(1)	8.1(0.3)
2	**7**	20	0.1(1)	13.1(0.3)
3	**7**	30	0.2(1)	15.4(1.2)
4	**1**	10	0.1(1)	7.6(0.3)
5	**1**	20	0.1(1)	10.1(0.1)

[a]Reaction conditions: H_2O_2 was added by syringe pump at a rate of 2 equiv per minute (to minimize H_2O_2 disproportionation) to a solution of iron (0.35 mM) and 1000 equiv of 1-octene (0.35 M) in CH_3CN. This solution was stirred for an additional 60 min prior to workup. See section 2.2 for further details. Yields expressed as turnover numbers, TON, (μmol product/μmol catalyst).

2.7.2 Methylation of position a

Deuteration of position a gave positive results, but it was not sufficient to extend catalyst lifetime significantly. So the picolyl position was further protected by installing a methyl group (Scheme 2.5), in which the ligand decay pathway can be fully blocked. The new C-C bond is even harder to break than C-D bond, so further improved catalytic results would be expected for this methodology.

*Characterization of complexes **8** and **9**.* The carbonyl vibrations of **8** and **9** were examined by FT/IR (Table 2.8). For **8**, the downshift of the $\upsilon_{C=O}$ from that in the ligand was only 22 cm^{-1} in the solid state, while in solution this downshift was even smaller (17

cm^{-1}). This indicates that the carbonyl oxygen atom binds the iron center loosely. Similarly, the $\upsilon_{C=O}$ for **9** downshifted only 10 cm^{-1} in the solid state, while there was no shift at all in solution. So the carbonyl group of Me-Me-DPAH does not even bind to the iron in acetonitrile. This phenomenon is quite surprising considering the similarity between R-DPAH ligands and the position a methylated derivatives. This methyl group must introduce extra unexpected strain that makes R-Me-DPAH poor ligands to the iron.

Table 2.8 Vibration frequencies of carbonyl group **8** and **9** by FT/IR

		ligand / cm^{-1}	complex / cm^{-1}	$\Delta\upsilon$ / cm^{-1}
8	Solid	1720	1698	22
	Solution (CD_3CN)	1720	1703	17
9	Solid	1645	1635	10
	Solution (CD_3CN)	1676	1676	0

In addition, the ^{1}H-NMR spectra were examined for **8** and **9** in CD_3CN (Figure 2.13). In both spectra, large peaks corresponding to free ligands were observed, indicating that the ligands can not coordinate to the metal center properly in solution. This phenomenon is in good agreement with the FT/IR studies.

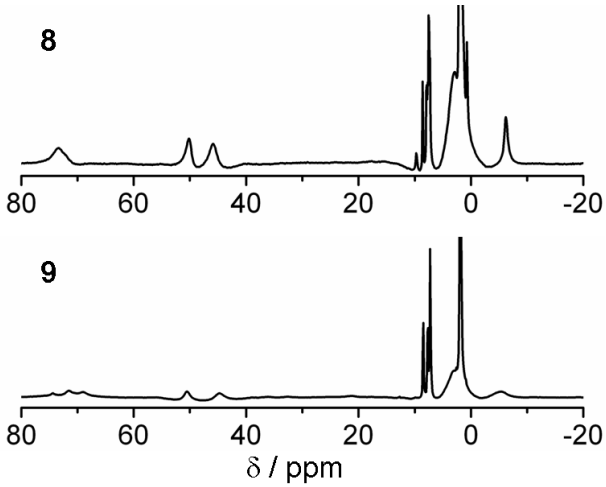

Figure 2.13 ^{1}H-NMR of **8** and **9** in CD_3CN.

Catalytic activities. Table 2.9 compares the catalytic reactivities of **8** and **9** with their parent complexes **1** and **4** in the oxidation of 1-octene and styrene. **8** showed very limited conversion of 1-octene into 1,2-octane-diol compared with **1**-catalyzed 1-octene oxidation (Table 2.9, entries 1 and 4). With styrene as substrate, **1** catalyzes 8 turnovers in the formation of the *cis*-diol product, while the position a methylated derivative **8** can not even affect a single turnover (Table 2.9, entries 2 and 5). Comparison between **9** and **4** also demonstrates the same effect of methylation of position a, which is that the methylation hampers the catalytic activity of R-DPAH ligands in the iron-catalyzed olefin oxidation.

Table 2.9 Catalytic results catalyzed by **8** and **9** wit H_2O_2 as oxidant[a]

Entry	complex	olefin	epoxide	*cis*-diol
1	**8**	1-octene	0.1(1)	0.7(2)
2[b]	**8**	styrene	0.3(1)	0.7(3)
3	**9**	1-octene	0.1(1)	0.7(2)
4	**1**	1-octene	0.1(1)	7.6(3)
5[b]	**1**	styrene	0.1(1)	8.0(5)
6	**4**	1-octene	<0.1	7.7(2)

[a]Reaction conditions: 10 equiv H_2O_2 was added by syringe pump at a rate over a period of 5 min (to minimize H_2O_2 disproportionation) to a solution of iron (0.35 mM) and 1000 equiv substrate (0.35 M) in CH_3CN. This solution was stirred for an additional 60 min prior to workup. See section 2.2 for further details. Yields expressed as turnover numbers, TON, (μmol product/μmol catalyst). [b]Reactions were carried out under Ar. 1.3(1) TON of benzaldehyde is observed for **8**. 0.4(1) TON of benzaldehyde is observed for **1**.

Since the crystal structure could not be obtained for **8**, the structure of its parent complex **1** was used for the analysis (Figure 2.14). The picolyl position C1 is connected with three substituents. The three angles of N1-C1-C7, N1-C1-C2, C2-C1-C7 are 113.6°, 114.9°, and 112.4° respectively, which are larger than those in an perfect tetrahedron structure. This indicates that the tripod constructed by N1, C2, C7, and center atom C1 is more open. Methylation at position a will make N1, C2, and C7 move closer to each

other and thus introduce extra strain in the ligand, which makes the coordination to the iron not feasible. Based on this structural analysis, the limited oxidation reactivity of **8** and **9** is not surprising.

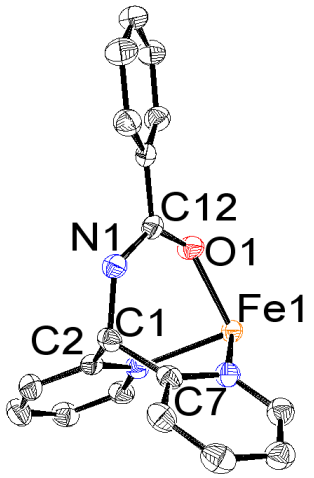

Figure 2.14 ORTEP plot of the crystal structure of **1**. Asymmetric unit is shown. Hydrogen atoms, counter-ions and non-coordinating solvent molecules have been omitted for clarity.

Table 2.10 Selected angles observed in **1**

N1-C1-C7 / °	N1-C1-C2 / °	C2-C1-C7 / °
113.6	114.9	112.4

2.7.3 Methylation of position b

To prevent the oxidative decay of R-DPAH ligands and formation of their imine derivatives, an alternative way is to methylate position b (Scheme 2.5). In position a, the

carbon is already connected to three large substituents before any modification. Methylation would introduce a fourth substituent that could make the environment of the carbon too bulky and thus give the three coordination arms less freedom to find the proper angle to bind the iron center. In contrast, methylation of position b should not have the same problem. Firstly, this position is one more atom farther from the two pyridine rings, and thus the influence on them, if any, would be very little. Secondly, methylating position b makes the central nitrogen atom only tri-substituted, so the oxygen binding arm should have enough freedom to find a suitable angle to bind to the iron. Therefore, improved results were expected for this modification.

*Characterization of complexes **10** - **12***. The crystal structure of **10** is shown Figure 2.15, and it resembles that of **1**,[99] with a center of inversion present at each iron center. Upon iron coordination, the Ph-NMe-DPAH ligand provides a facial array of two pyridines and a carbonyl oxygen in a good approximation of the facial 2-His-1-carboxylate ligand environment found in a number of oxygen activating mononuclear nonheme iron enzymes.[9,12] Table 2.11 compares bond lengths around the iron center and selected angles of **10** and its parent complex **1**. The Fe-N bonds in **10** are 2.126 and 2.116 Å, respectively, and interestingly these numbers are shorter than those in **1**. The Fe-O bond distance in **10** is 2.036 Å, which is also shorter that in **1**. The shorter distances between the iron center and the coordinating atoms indicate that, instead of introducing extra strain in the ligand as in **8**, methylation of position b makes the derivative ligand bind to the iron center even more strongly. Corresponding angles are also compared in Table 2.11. The three angles around the picolyl carbon are similar for

both **10** and **1**, which means that methylation of position b does not affect position a at all. The angle of position b (123.2 °) is smaller than without introducing a methyl group here, as in structure **1** (128.6 °). As the nitrogen is linked with only three substituents in **10**, the change in the bond angle does not cause an unfavorable steric effect.

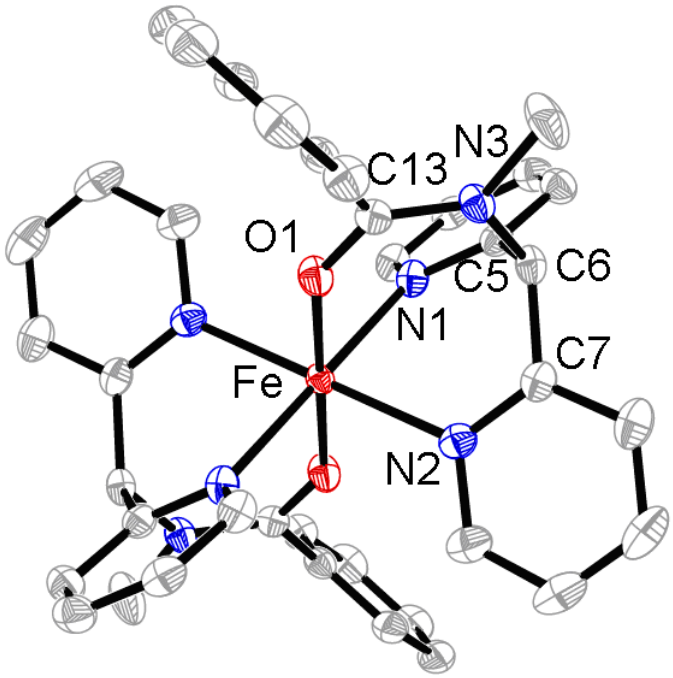

Figure 2.15 ORTEP plot of complex **10**. Hydrogen atoms, counter-ions and non-coordinating solvent molecules have been omitted for clarity.

Table 2.11 Comparison of bond lengths and angles observed in **10** and **1**[a]

	10	**1**
Bond length / Å	2.126 (Fe-N1)	2.171 (Fe-N2)
	2.116 (Fe-N2)	2.181 (Fe-N3)
	2.036 (Fe-O1)	2.043 (Fe-O1)
Angle / °	113.5 (C5-C6-C7)	112.4 (C2-C1-C7)
	114.2 (N3-C6-C5)	113.6 (N1-C1-C7)
	114.0 (N3-C6-C7)	114.9 (N1-C1-C2)
	123.2 (C6-N3-N13)	128.6 (C1-N1-C12)

[a]Please check Figures 2.14 and 2.15 for the labels in parenthesis.

Solution FT/IR was used to assess the coordination of the carbonyl group in **10** - **12** (Table 2.12). Downshifts of the $\upsilon_{C=O}$ by 33, 55, and 41 cm^{-1} were observed for **10** - **12** in acetonitrile solution, respectively, which is in agreement with the crystal structure of **10**. The ^{1}H-NMR spectra of these complexes in acetonitrile show similar patterns as **1** (Figure 2.16). The methylation of position b did not change the structures of their iron complexes in solution. Therefore, it is believed that **10** - **12** maintain the same structure in MeCN solution illustrated in Scheme 2.2.

Table 2.12 Vibration frequencies of the carbonyl groups of **10** - **12** by solution FT/IR for in CD_3CN

	ligand / cm^{-1}	complex / cm^{-1}	$\Delta\upsilon$ / cm^{-1}
10	1635	1602	33
11	1658	1603	55
12	1648	1607	41

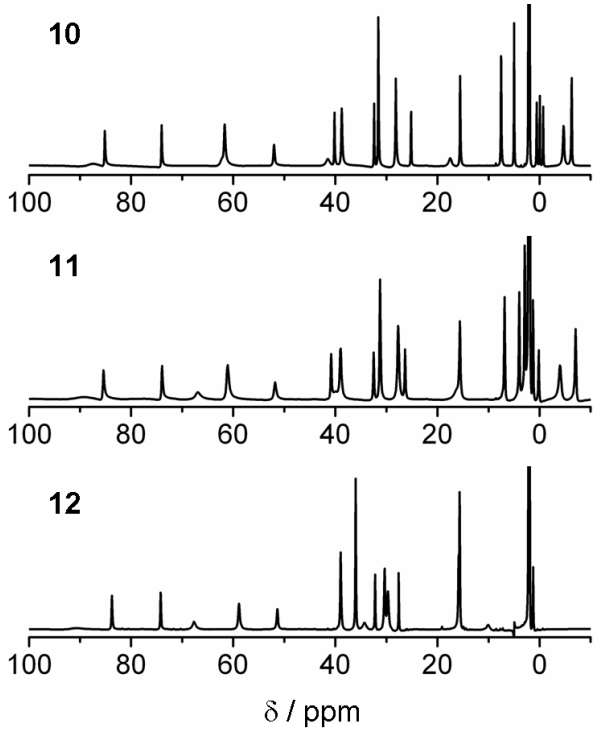

Figure 2.16 ^{1}H-NMR of **10-12** in CD_3CN.

Catalytic reactivity. Table 2.13 compares the catalytic activities of **10** and its parent complex **1** in the oxidation of 1-octene using H_2O_2 as oxidant. With 10 equiv of H_2O_2, **10** converted 78% of H_2O_2 into the *cis*-diol product (Table 2.13, entry 1), which is only

slightly higher the 76% conversion of catalyst **1** (Table 2.13, entry 4). When 20 equiv H_2O_2 are used, **1** can only catalyze 10.1 turnovers (Table 2.13, entry 5), while the new complex **10** gave 14.7 turnovers (Table 2.13, entry 2). The conversion of **10** at 20 equiv H_2O_2 is 74%, which is only slightly lower the conversion of 78% for 10 equiv H_2O_2. After 20 equiv H_2O_2, **1** lost its reactivity completely, while **10** could still catalyze another 2 turnovers when another 10 equiv H_2O_2 was added (Table 2.13, entry 3). The methylation of position b indeed had a protective effect on the ligand, although the percentage conversion still decreased as more H_2O_2 was used. The decay mechanism for this new complex will be further explored. The results of **10** were also compared with those of **7**. Both complexes showed improved catalytic results for 10 equiv H_2O_2, while **10** exhibited better results than **7** when 20 equiv H_2O_2 was used. This discrepancy in reactivity demonstrates the stronger protective effect on the ligand for methylation than deuteration. Unfortunately, both **7** and **10** showed decreased conversion of oxidant when 30 equiv H_2O_2 was added, suggesting that more protection for the ligand is needed for this system.

Table 2.13 Catalytic oxidation of 1-octene with H_2O_2 as oxidant[a]

Entry	complex	H_2O_2	epoxide	*cis*-diol
1	**10**	10	<0.1	7.8(0.1)
2	**10**	20	0.1	14.7(0.5)
3	**10**	30	0.2	16.3(1.1)
4	**1**	10	0.1(1)	7.6(0.3)
5	**1**	20	0.1(1)	10.1(0.1)
6	**7**	10	0.1(1)	8.1(0.3)
7	**7**	20	0.1(1)	13.1(0.3)
8	**7**	30	0.2(1)	15.4(1.2)

[a]Reaction conditions: H_2O_2 was added by syringe pump at a rate of 2 equiv per minute (to minimize H_2O_2 disproportionation) to a solution of iron (0.35 mM) and 1000 equiv of 1-octene (0.35 M) in CH_3CN. This solution was stirred for an additional 60 min prior to workup. See section 2.2 for further details. Yields expressed as turnover numbers, TON, (μmol product/μmol catalyst).

2.8 Catalytic reactivity at various temperatures

So far, most iron-catalyzed olefin oxidation reactions by H_2O_2 have been carried out at room temperature. Considering that catalyst deactivation is also an oxidative reaction, varying the temperatures may differentiate the reaction rates between the olefin oxidation and ligand oxidation pathway. Based on this idea, increased temperatures were explored for **1**-catalyzed 1-octene oxidation.

Table 2.14 summarizes catalytic results of 1-octene oxidation by **1** at different temperatures. The overall results are also illustrated in Figure 2.17. When temperature was raised to 40°C, 10 equiv H_2O_2 gives 8.9 turnovers of 1,2-octane diol (Table 2.14, entry 1), which is higher than at room temperature (Table 2.14, entry 10). This observation suggests that the rate of 1-octene oxidation must increase more than that of ligand decay. This initial promising result prompted experiments with more oxidant. Indeed, with 20 equiv H_2O_2, the turnovers nearly doubled to 17.4 (Table 2.14, entry 2), while the turnover number increased further with another 10 equiv H_2O_2 (Table 2.14, entry 3). Two other higher temperatures, 60°C and 75°C, were attempted. Figure 2.17 clearly shows the trend: at temperatures higher from 40°C, the reactivity became inferior. For example, with the same amount of H_2O_2 added, 40°C always give the highest turnovers.

This preliminary set of experiments with various temperatures indicates that room temperature may not be necessarily the best condition. In the future, temperature should be considered as a variable in optimizing the reaction conditions.

Table 2.14 Oxidation of 1-octene catalyzed by **1** at various temperatures[a]

Entry	Temperature / °C	H_2O_2	epoxide	*cis*-diol
1	40	10	0.1(1)	8.9 (0.5)
2	40	20	0.2(1)	17.4 (0.4)
3	40	30	0.3(2)	20.6 (1.8)
4	60	10	0.2(1)	6.6 (0.2)
5	60	20	0.2(2)	14.5 (0.5)
6	60	30	0.3(2)	19.6 (1.2)
7	75	10	0.2(1)	5.6 (0.9)
8	75	20	0.3(2)	10.5 (0.3)
9	75	30	0.5(2)	14.5 (0.1)
10	20	10	0.1(1)	7.6(0.3)
11	20	20	0.1(1)	10.1(0.1)

[a]Reaction conditions: H_2O_2 was added by syringe pump at a rate of 2 equiv per minute (to minimize H_2O_2 disproportionation) to a solution of iron (0.35 mM) and 1000 equiv of 1-octene (0.35 M) in CH_3CN. This solution was stirred for an additional 60 min prior to workup. See section 2.2 for further details. Yields expressed as turnover numbers, TON, (μmol product/μmol catalyst).

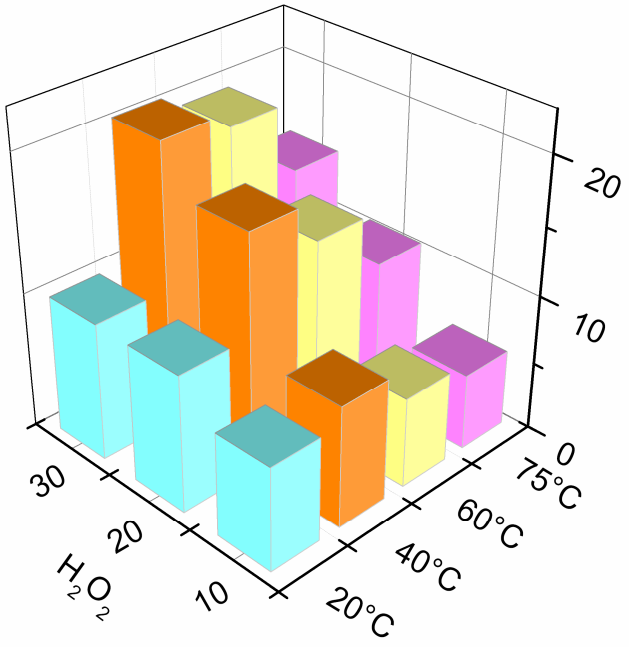

Figure 2.17 Oxidation of 1-octene catalyzed by **1** with H_2O_2 as oxidant.

2.9 Conclusions

In this work, R-DPAH iron complexes are for the first time fully characterized in solution. There exists an equilibrium between two coordination isomers in acetonitrile. More mechanistic studies have been attempted, and $Fe^{IV}(OH)_2$ is proposed for the active oxidant. Catalyst deactivation for R-DPAH iron complexes has been thoroughly studied, and various protection pathways involving modification of the R-DPAH ligands have been tried. Lastly, catalytic reactions at various temperatures have been explored, suggesting that room temperature might not be the optimized reaction temperature for catalysis.

2.10 Acknowledgements

I would like to thank Mr. Gregory Rohde and Dr. Victor Young, Jr. for solving the structure for **10** at the X-Ray Crystallographic Laboratory in the Chemistry Department at the University of Minnesota. Also deserving acknowledgements are Dr. Lei Yang and Prof. Williams Tolman for helping me use FT/IR in their laboratory.

CHAPTER 3

Olefin *cis*-dihydroxylation catalyzed by a series of iron complexes containing facial *N, N, O*-ligands: an unusual pattern of oxygen-atom incorporation into products

3.1 Introduction

Enzymes can catalyze the stereospecific oxidation of C=C bonds under environmentally friendly conditions.[1,4] Among these enzymes there are two families: heme and nonheme enzymes. The most extensively studied is a heme enzyme, cytochromes P450, consisting of a heme that is attached to the protein backbone via an iron-coordinating cysteinate residue.[131,132] More recently, nonheme iron enzymes have become better characterized and understood and have been shown to promote novel oxidative chemistry.[4,133] Of particular interest is a nonheme enzyme family called Rieske dioxygenases, which catalyze the *cis*-dihydroxylation of C=C bonds in the process of biodegradation of arenes in the environment.[26,29] A common motif among mononuclear nonheme iron enzymes exists in the active site of these enzymes, consisting of an iron center coordinated by two histidine residues and one carboxylate.[34,134] This recurring motif, named the 2-His-1-carboxylate facial triad,[9,12] is illustrated by the active site of the best studied of these enzymes, naphthalene 1,2-dioxygenase (NDO) (Figure 3.1).[34,38] As demonstrated from X-ray crystallographic data,[38] there are two potential *cis*-coordination sites around the iron center and these sites are used for the side-on binding of O_2. According to biochemical studies, this O_2 adduct either is the active oxidant to attack the C=C bond or must undergo O-O bond cleavage to form the high-valent iron species that oxidizes the C=C bond.[41,44]

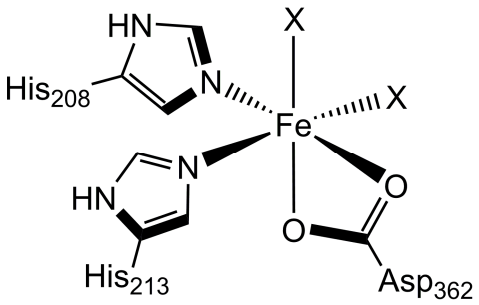

Figure 3.1 Naphthalene 1,2-dioxygenase (NDO) active site.

In the synthetic world, olefin *cis*-dihydroxylation is an important chemical transformation in both natural product and drug syntheses and traditionally involves heavy metal osmium compounds.[6,73-75] However, more benign catalysts are needed to replace osmium compounds to meet the ever increasingly stringent environmental regulation and green chemistry concerns.[135,136] The established key role of the mononuclear iron center in the Rieske dioxygenases has thus inspired efforts to design nonheme iron catalysts that mimic the action of these enzymes and develop a more environmentally friendly alternative to the osmium based *cis*-dihydroxylation. In the last decade, our group and others have developed many examples of first-row transition metal catalysts for olefin *cis*-dihydroxylation.[70,71,97,98,101,104] H_2O_2 is preferred in our work, because it is environmentally benign, of low cost and easily handled.[77] In addition, the demonstration of iron-catalyzed *cis*-dihydroxylation using H_2O_2 as oxidant is a particularly significant development, as iron centers typically react with H_2O_2 to generate hydroxyl radicals that give rise to nonspecific oxidation products. Thus far, all active iron catalysts are supported by tetradentate ligands with four nitrogen donors.[66,102] or facial tridentate *N, N, O* ligands[69,70,99,137,138] They are structurally very different from

each other and thus difficult to compare and to gain any insight into the relationship between ligand structures and catalytic reactivity.

In this chapter, I have designed and synthesized a series of structurally similar *N, N, O*-ligands that all contain two pyridyl nitrogen donors and various oxygen donors. This similarity provides the basis for a direct comparison among their iron(II) complexes. Different degrees of catalytic capacity can help us understand how different ligand structures affect reactivity. Therefore, these systems for the first time provide a basis for the subsequent development of catalysts suitable for applications in synthetic world. In addition, these systems show an unusual oxygen incorporation pattern that is not seen before. Based on this observation, the proposed active oxidant results from O-O bond cleavage and can live long enough to exchange with labeled water to a very large degree.

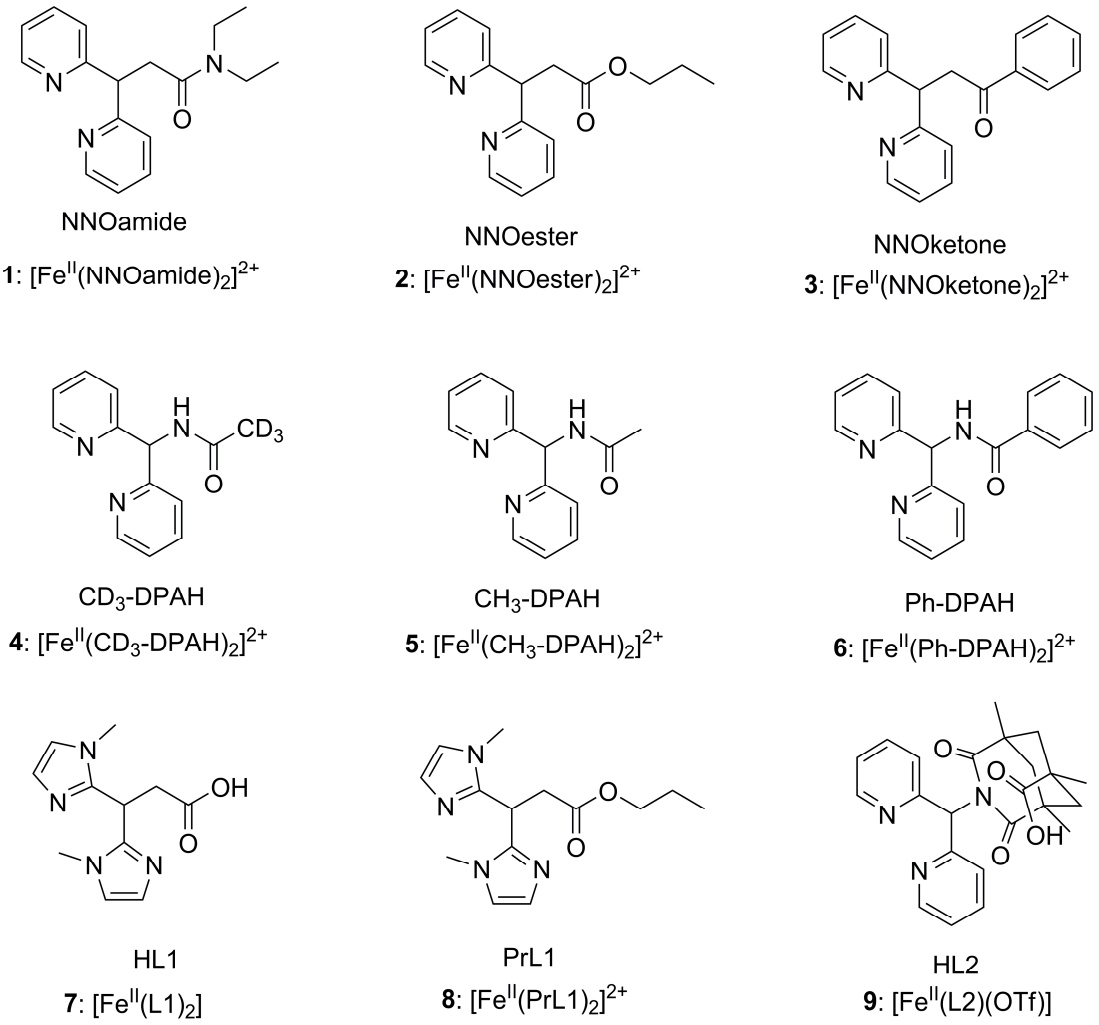

Scheme 3.1 Typical *N, N, O*-facial ligands in iron based olefin oxidation catalysis.

3.2 Experimental Section

Materials and Synthesis. All reagents were purchased from Sigma-Aldrich and used as received unless otherwise noted. All olefin substrates were passed over basic alumina immediately prior to use. CH_3CN was purified by Solvent Purifier from Vacuum Atmospheres Company. $H_2{}^{18}O_2$ (90% ^{18}O-enriched, 2 wt% solution in $H_2{}^{16}O$) was obtained from Sigma-Aldrich. $H_2{}^{18}O$ (97% ^{18}O enriched) was obtained from Shanghai Engineering Research Center of Stable Isotope. Synthesis of $[Fe^{II}(OTf)_2{\bullet}2NCCH_3]$ has

been reported previously.[103]

Synthesis of dipyridin-2-ylmethane. Dipyridin-2-ylmethane is prepared in over 90% yield by Wolf-Kishner-Huang reduction with some modifications of literature procedure.[139] Mixture of di(2-pyridyl)ketone (2 g, 0.011 mol), potassium hydroxide (2.4 g, 0.037 mol), and hydrazine hydrate (18 mL, 0.37 mol) was heated to 110 °C. The reaction was kept at this temperature and stirred for 3 h with the mouth opened to evaporate the resulting water. Upon cooling, 50 ml water was added, and the solution was extracted by dichloromethane. The organic phase was collected and washed by brine solution. After it was dried by magnesium sulfate, solvent was removed in vacuo resulting in pale yellow oil with 94% yield. ^{1}H-NMR ($CDCl_3$, δ ppm from TMS): 8.55(d, 2H), 7.60(td, 2H), 7.26(d, 2H), 7.11(dd, 2H), 4.33(s, 2H).

Synthesis of N,N-diethyl-3,3-di(pyridin-2-yl)propanamide (**NNOamide**). A solution of *n*-butyllithium in hexanes (0.42 mL, 1.0 mmol, 2.5 M in hexane) was added dropwise to a stirred solution of dipyridin-2-ylmethane (0.16 g, 0,94 mmol) in dry THF (10 mL) at -78 °C under Ar. The solution was stirred at -78 °C for 1 hour and allowed to warm up to room temperature slowly. *N, N*-diethylchloroacetamide (0.15 mL, 1.1 mmol) was added dropwise and stirred overnight. The reaction mixture was quenched with water (20 mL) and THF was removed by rotavap. The aqueous phase was extracted with dichloromethane and the combined organic phase was dried with magnesium sulfate and filtered. The solvent was evaporated to dryness. The purified product was obtained from a silica gel column eluted with a hexane / ethyl acetate gradient in 80% yield as colorless oil. ^{1}H-NMR ($CDCl_3$, δ ppm from TMS): 8.55(d, 2H), 7.58(m, 2H), 7.27(d, 2H), 7.09(dd,

2H), 4.97(t, 1H), 3.40(d, 2H), 3.37(q, 2H), 3.26(q, 2H), 1.18(t, 3H), 0.98(t, 3H). IR (in CD_3CN sol'n): ν(C=O) 1637 cm^{-1}.

Synthesis of propyl 3,3-di(pyridin-2-yl)propanoate (**NNOester**). The ligand NNOester was synthesized using the same procedure described above for NNOamide except that *n*-propyl bromoacetate was used. The purified product was obtained from a silica gel column eluted with a hexane / ethyl acetate gradient in 84% yield as yellow oil. ^{1}H-NMR ($CDCl_3$, δ ppm from TMS): 8.48(d, 2H), 7.58(td, 2H), 7.27(d, 2H), 7.12(dd, 2H), 4.81(t, 1H), 3.95(t, 2H), 3.33(d, 2H), 1.51(m, 2H), 0.83(t, 3H). IR (in CD_3CN sol'n): ν(C=O) 1731 cm^{-1}.

Synthesis of 1-phenyl-3,3-di(pyridin-2-yl)propan-1-one (**NNOketone**). The ligand NNOketone was synthesized using the same procedure described above for NNOamide except that phenacyl chloride was used. The purified product was obtained from a silica gel column eluted with a hexane / ethyl acetate gradient in 84% yield as white solid. ^{1}H-NMR ($CDCl_3$, δ ppm from TMS): 8.67(dm, 1H), 8.52(dm, 1H), 7.65(td, 2H), 7.38(td, 2H), 7.26(m, 2H), 7.15(m, 2H), 7.09(d, 1H), 7.03(dd, 1H), 6.91(d, 1H), 5.22(t, 1H), 4.41(d, 2H). IR (in CD_3CN sol'n): ν(C=O) 1713 cm^{-1}.

Synthesis of **CD_3-DPAH**. The di-(2-pyridyl)methylamine (0.2 g, 1.1 mmol), which was synthesized according the published literature,[105] was dissolved in deuterated acetic anhydride-d_6 {$(CD_3CO)_2O$} (1 mL) and stirred for 1 hour. 10 ml water was added to quench the reaction. Dichloromethane was used to extract the product. The organic phase was collected and combined. After being dried by magnesium sulfate, the solvent was evaporated to give white powder. The purified product was obtained from a silica

gel column eluted with a hexane / ethyl acetate gradient in 95% yield. ^{1}H-NMR ($CDCl_3$, δ ppm from TMS): 8.54(d, 2H), 7.92(d, 1H), 7.64(td, 2H), 7.42(d, 2H), 7.19(dd, 2H), 6.22(d, 1H). IR (in CD_3CN sol'n): ν(C=O) 1669 cm^{-1}.

Synthesis of $[Fe^{II}(NNOamide)_2](OTf)_2$ (**1**). In an N_2-containing glovebox, a mixture of the NNOamide ligand (79 mg, 0.28 mmol) and $Fe^{II}(OTf)_2$•$2NCCH_3$ (61 mg, 0.14 mmol) was stirred overnight in 1 mL CH_3CN. Ether was added into the solution to precipitate out green solid and this solid was redissolved in CH_3CN. Vapor diffusion of THF into this solution resulted in the formation of purified **1** after 5 days as green crystal in 70% yield, which is suitable for X-ray crystallographic analysis. See *vide infra* for details regarding X-ray crystallographic analysis and Table 3.1 for crystal data and structure refinement for **1**. Characterization of **1**: Elemental analysis: $C_{36}H_{42}F_6FeN_6O_8S_2$ (920.72) calcd. C 46.96, H 4.60, N 9.13; found C 46.89, H 4.55, N 9.27. IR (in CD_3CN sol'n): ν(C=O) 1600 cm^{-1}. ESI-MS: *m/z* = 771 ($[Fe(NNOamide)_2(OTf)]^+$), 488 ($[Fe(NNOamide)(OTf)]^+$), 311 ($[Fe(NNOamide)_2]^{2+}$), 306 ($[NNOamide + Na]^+$).

Synthesis of $[Fe^{II}(NNOester)_2](OTf)_2$ (**2**). **2** was synthesized using the same procedure described above for **1**. Purified **2** can be obtained by vapor diffusion of THF into CH_3CN solution of **2** in 5 days as light green crystal in 80% yield, which is suitable for X-ray crystallographic analysis. See *vide infra* for details regarding X-ray crystallographic analysis and Table 3.2 for crystal data and structure refinement for **2**. Characterization of **2**: Elemental analysis: $C_{34}H_{36}F_6FeN_4O_{10}S_2$ (894.64) calcd. C 45.65, H 4.06, N 6.26; found C 45.65, H 3.98, N 6.36. IR (in CD_3CN sol'n): ν(C=O) 1681 cm^{-1}. ESI-MS: *m/z* = 745 ($[Fe(NNOester)_2(OTf)]^+$), 475 ($[Fe(NNOester)(OTf)]^+$), 306

([NNOester + Na]$^+$).

Synthesis of [Fe^{II}(NNOketone)$_2$](OTf)$_2$ (**3**). **3** was synthesized using the same procedure described above for **1**. Purified **3** can be obtained by vapor diffusion of THF into CH_3CN solution of **3** in 5 days as brown powder in 60% yield. Characterization of **3**: Elemental analysis: $C_{40}H_{32}F_6FeN_4O_8S_2 + H_2O + CH_3CN$ (989.74) calcd. C 50.97, H 3.77, N 7.08; found C 51.28, H 3.79, N 7.55. IR (in CD_3CN sol'n): ν(C=O) 1627 cm^{-1}. ESI-MS: *m/z* = 781 ([Fe(NNOketone)$_2$(OTf)]$^+$), 493 ([Fe(NNOketone)(OTf)]$^+$), 316 ([Fe(NNOketone)$_2$]$^{2+}$), 306 ([NNOester + H]$^+$).

Synthesis of [Fe^{II}(CD_3-DPAH)$_2$](OTf)$_2$ (**4**). **4** was synthesized using the same procedure described above for **1**. Purified **4** can be obtained by vapor diffusion of THF into CH_3CN solution of **4** in 5 days as green powder in 73% yield. Characterization of **4**: IR (in CD_3CN sol'n): ν(C=O) 1669 cm^{-1}. ESI-MS: *m/z* = 665 ([Fe(CD_3-DPAH)$_2$(OTf)]$^+$), 435 ([Fe(CD_3-DPAH)(OTf)]$^+$), 258 ([Fe(CD_3-DPAH)$_2$]$^{2+}$), 231 ([CD_3-DPAH + H]$^+$).

X-ray crystallography

[Fe(NNOamide)$_2$](OTf)$_2$

Data collection. A crystal (approximate dimensions 0.45 x 0.35 x 0.13 mm^3) was placed onto the tip of a 0.1 mm diameter glass capillary and mounted on a CCD area detector diffractometer for a data collection at 173(2) K.[109] A preliminary set of cell constants was calculated from reflections harvested from three sets of 20 frames. These initial sets of frames were oriented such that orthogonal wedges of reciprocal space were surveyed. This produced initial orientation matrices determined from 35 reflections. The data collection was carried out using MoKα radiation (graphite monochromator) with a

frame time of 60 seconds and a detector distance of 4.928 cm. A randomly oriented region of reciprocal space was surveyed to the extent of one sphere and to a resolution of 0.77 Å. Four major sections of frames were collected with 0.30º steps in ω at four different ϕ settings and a detector position of -28º in 2θ. The intensity data were corrected for absorption and decay.[110] Final cell constants were calculated from the xyz centroids of 2820 strong reflections from the actual data collection after integration.[111] Please refer to Table 3.1 for additional crystal and refinement information.

Structure solution and refinement. The structure was solved using SHELXS-97 (Sheldrick, 1990)[112] and refined using SHELXL-97 (Sheldrick, 1997).[113] The space group P-1 was determined based on systematic absences and intensity statistics. A direct-methods solution was calculated which provided most non-hydrogen atoms from the E-map. Full-matrix least squares / difference Fourier cycles were performed which located the remaining non-hydrogen atoms. All non-hydrogen atoms were refined with anisotropic displacement parameters. All hydrogen atoms were placed in ideal positions and refined as riding atoms with relative isotropic displacement parameters. The final full matrix least squares refinement converged to $R1 = 0.0412$ and $wR2 = 0.0860$ (F^2, all data).

Table 3.1 Crystal data and structure refinement for **1**

Identification code	10175	
Empirical formula	C_{36} H_{42} F_6 Fe N_6 O_8 S_2	
Formula weight	920.73	
Temperature	173(2) K	
Wavelength	0.71073 Å	
Crystal system	Triclinic	
Space group	P-1	
Unit cell dimensions	a = 9.3804(10) Å	α= 09.946(2)°
	b = 10.4290(11) Å	β = 98.046(2)°
	c = 11.5094(12) Å	γ = 97.591(2)°
Volume	1028.23(19) $Å^3$	
Z	1	
Density (calculated)	1.487 Mg/m^3	
Absorption coefficient	0.552 mm^{-1}	
F(000)	476	
Crystal color, morphology	green, plate	
Crystal size	0.45 x 0.35 x 0.13 mm^3	
Theta range for data collection	1.92 to 27.55°	
Index ranges	$-12 \le h \le 12$, $-13 \le k \le 13$, $-14 \le l \le 14$	
Reflections collected	12111	
Independent reflections	4658 [R(int) = 0.0339]	
Observed reflections	3401	
Completeness to theta = 27.55°	98.1%	
Absorption correction	Multi-scan	
Max. and min. transmission	0.931 and 0.793	
Refinement method	Full-matrix least-squares on F^2	
Data / restraints / parameters	4658 / 0 / 270	
Goodness-of-fit on F^2	1.033	
Final R indices [I>2sigma(I)]	R1 = 0.0412, wR2 = 0.0785	
R indices (all data)	R1 = 0.0685, wR2 = 0.0860	
Largest diff. peak and hole	0.359 and -0.330 e.$Å^{-3}$	

$[Fe(NNOester)_2](OTf)_2$

Data collection. A crystal (approximate dimensions 0.30 x 0.13 x 0.10 mm^3) was placed onto the tip of a 0.1 mm diameter glass capillary and mounted on a CCD area detector diffractometer for a data collection at 173(2) K.[109] A preliminary set of cell constants was calculated from reflections harvested from three sets of 20 frames. These initial sets of frames were oriented such that orthogonal wedges of reciprocal space were surveyed. This produced initial orientation matrices determined from 51 reflections. The data collection was carried out using MoKα radiation (graphite monochromator) with a frame time of 30 seconds and a detector distance of 4.818 cm. A randomly oriented region of reciprocal space was surveyed to the extent of one sphere and to a resolution of 0.77 Å. Four major sections of frames were collected with 0.30º steps in ω at four different ϕ settings and a detector position of -28º in 2θ. The intensity data were corrected for absorption and decay.[110] Final cell constants were calculated from the xyz centroids of 4094 strong reflections from the actual data collection after integration.[111] Please refer to Table 3.2 for additional crystal and refinement information.

Structure solution and refinement. The structure was solved using SHELXS-97[112] and refined using SHELXL-97.[113] The space group $P2_1/n$ was determined based on systematic absences and intensity statistics. A direct-methods solution was calculated which provided most non-hydrogen atoms from the E-map. Full-matrix least squares / difference Fourier cycles were performed which located the remaining non-hydrogen atoms. All non-hydrogen atoms were refined with anisotropic displacement parameters. The ester (atoms O2 C14 C15 C16) was modeled as a 55% / 45% disorder over two

positions. The bond lengths of identical atom pairs of the disordered ester were restrained to be equal. The triflate ion was modeled over two positions (84%/16%) and the bond lengths of the identical atom pairs were restrained to be equal. All hydrogen atoms were placed in ideal positions and refined as riding atoms with relative isotropic displacement parameters. The final full matrix least squares refinement converged to $R1 = 0.0496$ and $wR2 = 0.1480$ (F^2, all data).

Table 3.2 Crystal data and structure refinement for **2**

Identification code	10160	
Empirical formula	C_{34} H_{36} F_6 Fe N_4 O_{10} S_2	
Formula weight	894.64	
Temperature	173(2) K	
Wavelength	0.71073 Å	
Crystal system	Monoclinic	
Space group	$P2_1/n$	
Unit cell dimensions	a = 9.0497(16) Å	α = 90°
	b = 16.409(3) Å	β = 98.449(2)°
	c = 13.173(2) Å	γ = 90°
Volume	1935.0(6) $Å^3$	
Z	2	
Density (calculated)	1.536 Mg/m^3	
Absorption coefficient	0.587 mm^{-1}	
F(000)	920	
Crystal color, morphology	green, plate	
Crystal size	0.30 x 0.13 x 0.10 mm^3	
Theta range for data collection	2.00 to 27.52°	
Index ranges	$-11 \le h \le 11$, $-20 \le k \le 21$, $-17 \le l \le 16$	
Reflections collected	22347	
Independent reflections	4420 [R(int) = 0.0349]	
Observed reflections	3265	
Completeness to theta = 27.52°	99.1%	
Absorption correction	Multi-scan	
Max. and min. transmission	0.9436 and 0.8436	
Refinement method	Full-matrix least-squares on F^2	
Data / restraints / parameters	4420 / 63 / 299	
Goodness-of-fit on F^2	1.052	
Final R indices [I>2sigma(I)]	$R1$ = 0.0496, $wR2$ = 0.1302	
R indices (all data)	$R1$ = 0.0726, $wR2$ = 0.1480	
Largest diff. peak and hole	0.475 and -0.390 e.$Å^3$	

Instrumentation. ^{1}H spectra were recorded on a Varian Unity 300 or 500 MHz spectrometer at ambient temperature. Chemical shifts (ppm) were referenced to the residual protic solvent peaks. FTIR spectra were obtained with a Thermo Nicolet Avatar 370 FT-IR instrument. X-ray crystallographic analyses were completed by mounting the crystal on a Bruker-AXS platform diffractometer with CCD area detector and sealed-tube 3-KW X-ray generators. High-resolution electrospray mass spectral (ESI-MS) experiments were performed on a Bruker (Billerica, MA) BioTOF II time-of-flight spectrometer. Product analyses from catalysis experiments were performed on a Perkin Elmer AutoSystem gas chromatograph (AT-1701 column, 30 m) with a flame ionization detector. Gas chromatography/mass spectral analyses were performed on an HP 6890 GC (HP-5 MS column, 30 m) with an Agilent 5973 mass analyzer. A 4% NH_3/CH_4 mix was used as the ionization gas for chemical ionization analyses.

Reaction conditions for catalytic oxidations. In a typical reaction, 10 equivalents of H_2O_2 (diluted from 35% H_2O_2 solution with CH_3CN resulting in a 70 mM solution) were delivered by syringe pump over a period of 5 min at room temperature (20 ^oC) in air to a vigorously stirred CH_3CN solution containing iron catalyst and 1000 equivalents of olefin substrate. The final concentrations were 0.35 mM iron catalyst, 3.5 mM H_2O_2, and 0.35 M olefin. The solution was stirred for an additional 60 min after syringe pump addition, after which organic products were esterified by 1 mL acetic anhydride together with 0.1 mL 1-methylimidazole and extracted with $CHCl_3$. An internal standard (naphthalene) was added and the solution was washed with 1 M H_2SO_4, sat. $NaHCO_3$, and H_2O. The organic layer was dried with $MgSO_4$ and subjected to GC analysis. The

products were identified by comparison of their GC retention times and GC/MS with those of authentic compounds.

Isotope labeling studies. Similar conditions as described above were used for isotope labeling studies except for the following details. In experiments involving $H_2{}^{18}O$, 1000 equivalents of $H_2{}^{18}O$ were added to reaction solution prior to the injection of $H_2{}^{16}O_2$. In experiments involving $H_2{}^{18}O_2$, 10 equivalents of $H_2{}^{18}O_2$ (diluted by CH_3CN from the commercially available 2% $H_2{}^{18}O_2/H_2O$ solution, which contains 1:100 molar ratio of $H_2{}^{18}O$ to $H_2{}^{16}O$) was used instead of H_2O_2. The diol esterification procedure was the same as that diagrammed above. The data reported either summarize a single reaction or are the average of 2 reactions and the % ^{18}O values reported were calculated based on the ^{18}O-enrichment of the reagents containing the isotope.

3.3 Catalyst preparation and characterization

Ligand design and synthesis. In an effort to pursue iron substitution to replace toxic and expensive osmium reagents, our group and others have been developing many ligands used in iron catalysis based on the imitation or inspiration of the biological systems.[67,140] These successful examples mainly use tetradentate N4 ligands. Recently, emphasis switched to the design of facial N, N, O ligands, because this new family of ligands is more similar to the enzymatic 2-His-1-carboxylate facial triad coordination environment. Gebbink's group synthesized a biomimetic ligand HL1 that contains two imidazole rings and one carboxylate.[70] This ligand is a good structural model of the 2-His-1-carboxylate facial triad, but its iron complex **7** is not a active catalyst for olefin

oxidation. So far the reactive iron catalysts are only complexes **6**, **8** and **9**.[69,70,104] Because the ligand structures are very different from each other, it is difficult to formulate ligand design rules from the reactivity comparison. In addition, they all have some serious problems. The amide CH-NH group of the Ph-DPAH ligand is susceptible to oxidation and ligand decomposition leads to the catalyst deactivation.[104] Complex **8** is an active catalyst, but the selectivity towards olefin *cis*-dihydroxylation is low.[70] The ligand HL2 in complex **9** falls off the iron center so easily that the catalyst barely achieves any turnovers.[69]

To avoid these problems, a series of structurally related new ligands has been designed in this study (Scheme 3.2). To circumvent the susceptibility of amide CH-NH bond in Ph-DPAH to oxidation, two changes were made to the Ph-DPAH structure. The first way is to move the amide N to the other side of the amide C=O function group and protect it by two ethyl groups. In this way, the new ligand is named NNOamide. The other way is to replace the NH group by CH_2, making the amide functionality into a ketone and the new ligand is named NNOketone. The PrL1 ligand is also modified to have two pyridine rings instead of two imidazole rings and the new ligand is NNOester. These three newly designed ligands all contain the same nitrogen donors, two pyridine rings, but different oxygen donors. The comparison of the catalytic reactivity of their iron complexes is more meaningful and can give us the insight of effect of different oxygen donor. Similarly, PrL1 and NNOester have the same oxygen donor, ester oxygen, but different nitrogen donors. Comparison between them will indicate the effect of nitrogen donors.

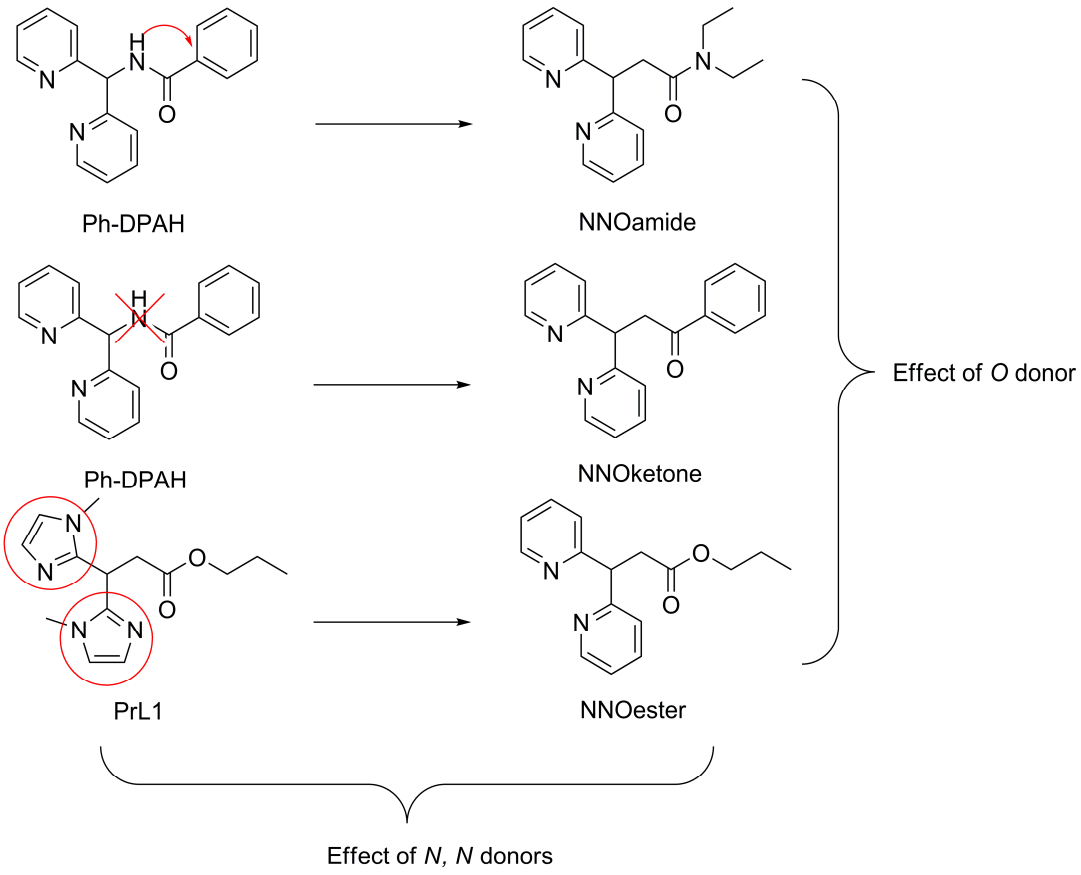

Scheme 3.2 Logic of new ligands design.

Synthesis of the three new ligands starts from the same chemical, di(2-pyridyl) ketone. It is reduced to di(2-pyridyl) methane by the Wolf-Kishner-Huang method.[139] Lithiation of the resulting di(2-pyridyl) methane at the bridging methylene group with *n*-butyllithium at -78°C in dry THF and subsequent dropwise addition of *N, N*-diethylchloroacetamide, *n*-propyl bromoacetate and phenacyl chloride result in the clean formation of NNOamide, NNOester and NNOketone. The overall synthetic routes are shown in Scheme 3.3.

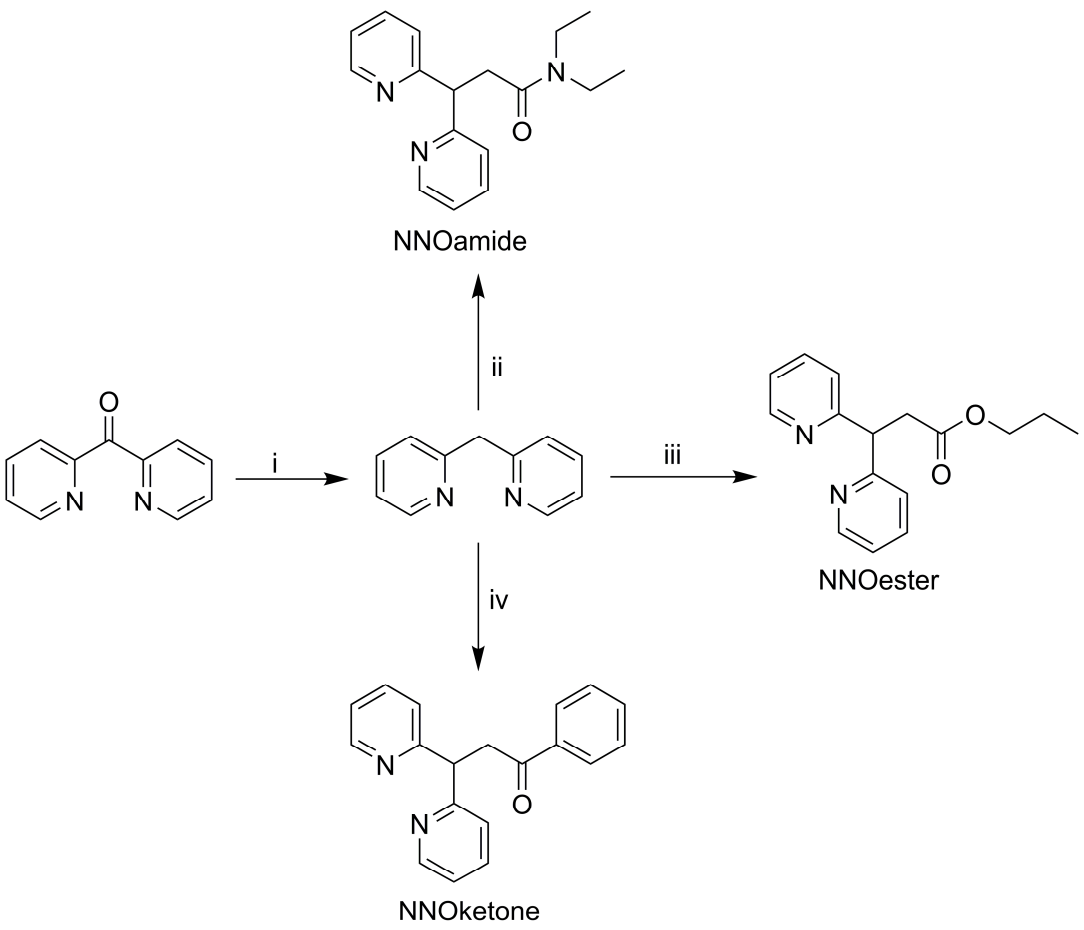

Scheme 3.3 Synthesis of new ligands in this chapter. i) H_2NNH_2, KOH, 100°C, 3h; ii) a. *n*-butyllithium, -78°C, b. *N, N*-diethylchloroacetamide, overnight; iii) a. *n*-butyllithium, -78°C, b. *n*-propyl bromoacetate, overnight; iv) a. *n*-butyllithium, -78°C, b. phenacyl chloride, overnight.

Synthesis and solid characterization of Fe^{II} complexes. Complexes **1** – **3** are synthesized via combination of $[Fe^{II}(OTf)_2(CH_3CN)_2]$ and two equivalents of ligand. Single crystals suitable for X-ray analysis were obtained for **1** and **2**, and their structures are shown in Figure 3.2. Upon iron coordination, the NNOamide and NNOester ligands

provide a facial array of two pyridines and a carbonyl oxygen. The structures of **1** and **2** closely resemble that of **6** with a center of symmetry at each iron center.[104] Table 3.3 summarizes bond distances between the iron center and coordinating atoms in **1**, **2**, **6**,[99] **8**,[70] **9**[69] and two forms of naphthalene 1,2-dioxygenase (NDO).[34,38] **6** and **8** are iron(II) complexes with facial *N, N, O* ligand sets developed respectively by our lab[99] and Klein Gebbink.[70] Complex **9** is different from others in having a tetradentate *N, N, O, O* ligand set derived from two pyridines and a bidentate carboxylate.[69] Fe-N distances all fall between 2.1 and 2.2 Å, typical of high spin iron(II) complexes, and are generally longer than those found for the enzymatic active center. Shorter Fe-O distances are observed for the Fe amide O in **1** and **6** than those of the Fe ester O in **2** and **8**. This difference clearly reflects the fact that the more electron rich amide O binds the iron center more strongly than the ester O. Solid FT/IR studies showed downshifts of 38 and 57 cm^{-1} for the carbonyl groups of complexes **1** and **2** compared with their ligands in solid state (Table 3.4). These vibrations at distinct wavenumbers corroborate the structural information provided by the crystal structures that carbonyl oxygen atoms bind to the iron center.

Diffraction quality crystals can not be obtained for **3**, but elemental analysis shows a 1:2 metal-ligand stoichiometry as found for **1** and **2**. In addition, solid FT/IR also shows a downshift of 85 cm^{-1} for the carbonyl group confirming the binding of carbonyl oxygen to the iron center (Table 3.4). Therefore, a centrosymmetric structure is also proposed for complex **3** in solid state.

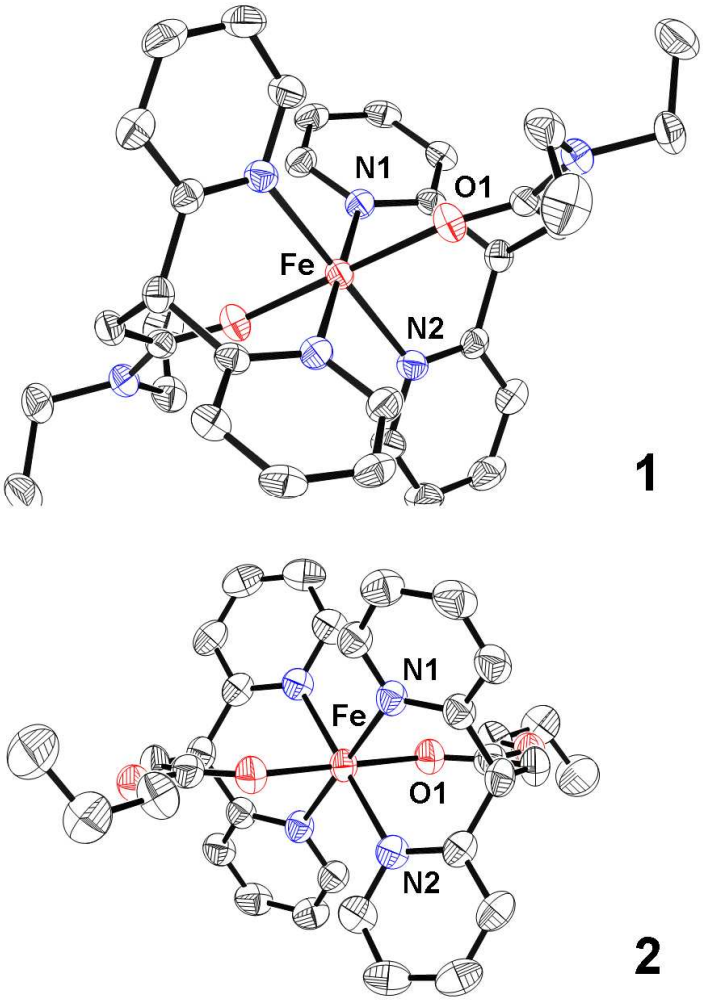

Figure 3.2 ORTEP plots of complexes **1** and **2**. Hydrogen atoms, counter-ions and non - coordinating solvent molecules have been omitted for clarity.

Table 3.3 Comparison of iron-ligand bond distances

	Fe-N1 / Å	Fe-N2 / Å	Fe-O1 / Å	Fe-O2 / Å	ref
1	2.162(1)	2.172(2)	2.043(1)		This work
2	2.151(2)	2.167(2)	2.102(2)		This work
6	2.171	2.181	2.043		99
8	2.122(2)	2.120(2)	2.228(2)		70
9[a]	2.124	2.137	2.145	2.150	69
NDO[b]	2.0	2.1	2.2	2.6	34
NDO[c]	2.1	2.0	2.3	2.4	38

[a]Structure was obtained for related $[Fe^{II}(L2)(Cl)]$ complex. [b]1NDO.pdb. [c]1O7G.pdb

Table 3.4 FT/IR frequencies for the carbonyl groups in **1 - 3**

	Ligand / cm^{-1}	Complex / cm^{-1}	$\Delta\upsilon$ / cm^{-1}
oil or solid			
NNOamide	1636	1598	38
NNOester	1731	1674	57
NNOketone	1715	1630	85
in CD_3CN			
NNOamide	1637	1600	37
NNOester	1731	1681	50
NNOketone	1713	1627	86

Solution characterization of Fe^{II} complexes. Since homogeneous catalysis is carried out in solution, it is very important to clarify the solution structures of **1** - **3**. To determine the structures of the complexes in solution, ESI-MS, solution FT/IR, and NMR spectra were recorded. ESI-MS measurements of CH_3CN solutions of the

complexes indicate the presence of the mononuclear iron species with two coordinated ligands. Interestingly, the 1:1 iron / ligand species and free ligand are also observed in the ESI-MS spectra (Figure 3.3). For example for **1**, $\{[FeL_2](OTf)\}^+$(m/z = 771), $[FeL(OTf)]^+$(m/z = 488), $[FeL_2]^{2+}$(m/z = 311), and L + Na^+(m/z = 306) are observed. This spectral pattern is also observed for our previously reported complex **6**. It is reasonable that complexes **1 - 3** and **6** share similar structures in solution (Equation 3.1). However, since the concentration of the solution used for ESI-MS analysis (~μM) is far more dilute than that for catalytic reactions (0.35 mM, see experimental section), a ligand dissociation-association equilibrium may be present under such dilute conditions but not necessarily under reaction conditions. Therefore, solution characterization at similar concentration to the catalytic reaction is also carried out.

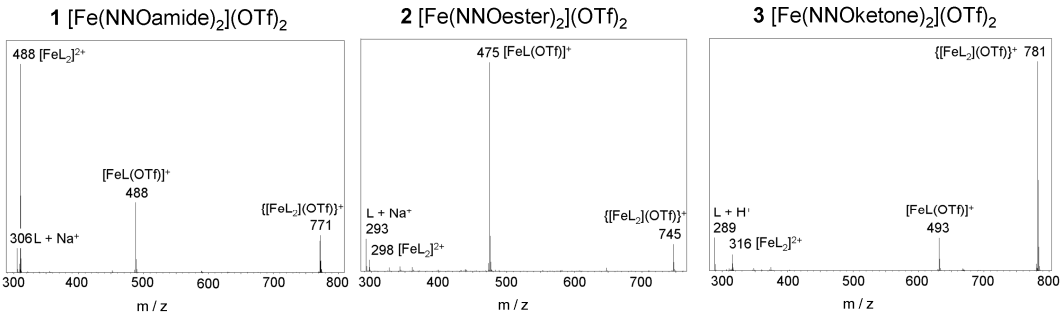

Figure 3.3 ESI-MS spectra of complexes **1 - 3** in CH_3CN.

$$[FeL_2]^{2+} \rightleftharpoons [FeL]^{2+} + L$$

Equation 3.1 A ligand dissociation-association equilibrium proposed for **1 - 3**.

The position of the carbonyl stretch vibration was found to be indicative of the coordination mode of the ligand in the solid state (Table 3.4). The solution FT/IR spectra were also collected and used to inspect the solution structure. The NNOamide ligand exhibits a carbonyl vibration at 1637 cm^{-1}. The absorption downshifts by 37 cm^{-1} in the CH_3CN solution of the corresponding iron complex **1**. Similar results are obtained for **2** and **3**, with respective downshifts of 50 and 86 cm^{-1} observed for these complexes in solution (Experimental section), but the $\upsilon_{C=O}$ of the free ligand can also be discerned for **2** and **3**. These downshifts indicate the interaction between the ligand carbonyl oxygen atoms and the metal center. So far FT/IR and ESI-MS studies in solution indicate that complexes **1** - **3** retain in large part the 1:2 metal-to-ligand composition as found in the crystal structures of **1** and **2**, but there still exists a ligand dissociation association equilibrium (equation 3.1).

The ^{1}H-MR spectrum of **1** shows a large spread of chemical shift (Figure 3.4), which is in agreement with the paramagnetic Fe(II) center indicated by the more than 2 Å bond lengths between the metal center and coordinating atoms in the crystal structure. However, this spectrum exhibits many more peaks than expected if the solution structure maintains the inversion center shown by the crystal structure. Clearly, the centro-symmetric structure is too simple to explain the solution structure. At first, based on the equilibrium shown in equation 3.1, this complicated spectrum was thought to be from two species: $[FeL_2]^{2+}$ and $[FeL]^+$, but this is in contradiction with that solution FT/IR does not show C=O vibration of free ligand for **1**. Furthermore, addition of free ligand into the solution should push the equilibrium to the left and the spectrum should be

simplified as the $[FeL_2]^{2+}$ would be the predominant species in solution. However, adding ligand does not perturb the ratio among these peaks and the spectrum remains the same except that free ligand peaks show up. The possibility that in solution the iron center is thus coordinated by different numbers of ligand is ruled out.

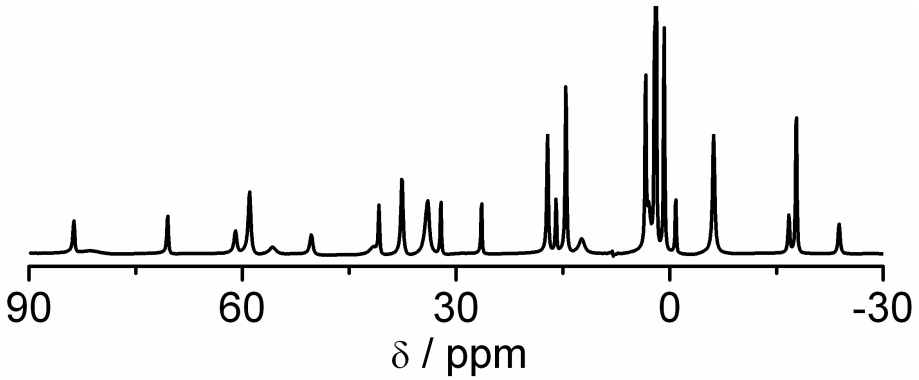

Figure 3.4 ^{1}H-NMR spectrum of **1**.

To understand the ^{1}H-NMR spectra and solution structures of this family of complexes, two other ligands are synthesized: CH_3-DPAH and its deuterated derivative CD_3-DPAH. Their corresponding complexes are **4** and **5** (Scheme 3.1). Since both ligands contain two pyridine nitrogen donors and one amide oxygen donor as NNOamide, their structures in solution should be similar to each other. In addition, the previously characterized complex **4**[104] and new complex **5** both show the same ESI-MS pattern and downshifts of the carbonyl frequency as **1**, which validates the methodology of the usage of the simplified ligands. Both CH_3-DPAH and CD_3-DPAH have a methyl group that is close to the binding carbonyl oxygen atom, so the shift of the methyl group

is indicative of oxygen atom binding to the metal. Similarly the pyridine proton shifts reflect coordination of nitrogen atoms to the metal center.

^{1}H-NMR spectra of **4** and **5** were collected and compared (Figure 3.5, top and middle). **5** shows an almost identical spectrum as **4** except that two peaks are missing, the peaks at 18 ppm and 29 ppm illustrated by the arrows in the top spectrum of Figure 3.5. The 29 ppm peak in **4** has a shoulder and its area decreases in **5**, clearly indicating that another peak is hidden in the peak and can not be resolved from it. The area ratio between these two peaks at 29 ppm and 18 ppm is approximately 1 to 1. The assignment of the methyl group is further confirmed by the ^{2}H-NMR spectrum of **5** (Figure 3.5, bottom). Two large peaks assigned to methyl group show up at the same chemical shifts as the ^{1}H-NMR of **4**. A small peak is also observed and assigned to the methyl group of free ligand. So there are two types of methyl group, reflecting two types of amide carbonyls in the solution of complexes **4** and **5**. The centrosymmetric structure shown from the crystal structure is expected to contain only one type of amide C=O; clearly, another structure other than the centrosymmetric one exists in the solution.

Since the coupling interactions among pyridine protons contain information of coordinating nitrogen atoms, 2D-^{1}H-NMR of **5** was investigated (Figure 3.6). The coupling pattern among pyridine protons is shown on the 1D-^{1}H-NMR spectrum of **5** (Figure 3.7). Because the α proton on the pyridine ring is too close to the binding nitrogen atom that coordinates the paramagnetic iron center, it does not show up as a sharp peak and coupling to the adjacent β peak can not be detected. So this makes the γ peak the only one that can couple to two other peaks. Based on this knowledge, the β

and γ peaks are all assigned (Figure 3.7, labels above the peaks). As shown in Figure 3.7, there are three types of pyridines. The area ratio among these three types are roughly 2 : 1 : 1. Considering the two types of methyl groups that have approximately the same area, presumably the first type of pyridine belongs to one structure and the second and the third belong to another one.

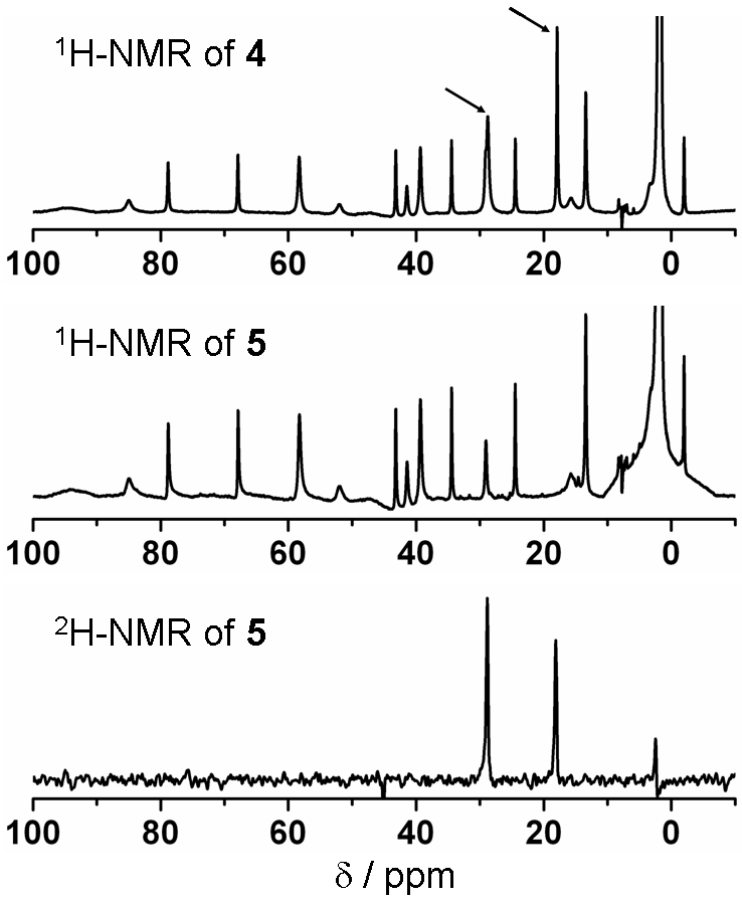

Figure 3.5 NMR spectra of **4** and **5**.

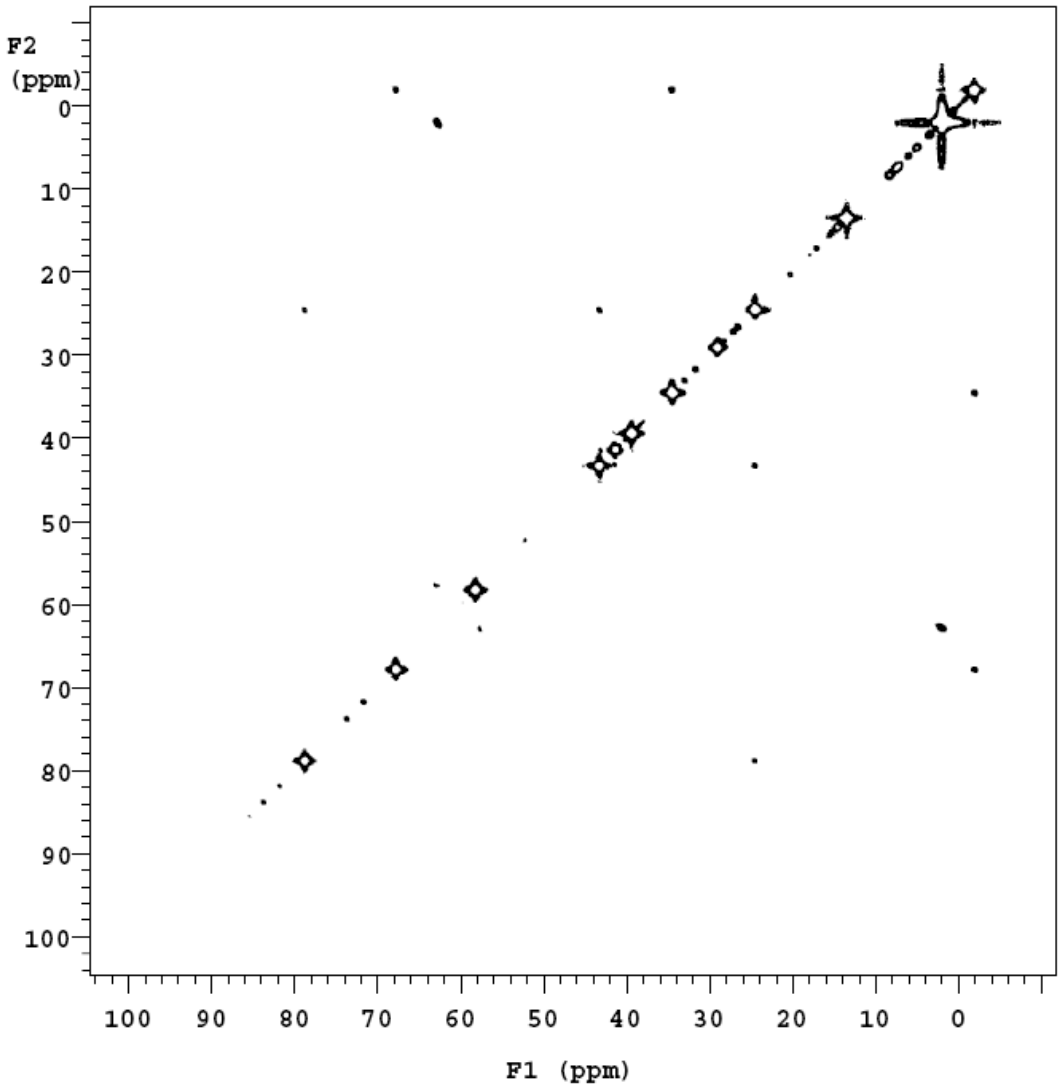

Figure 3.6 2D-^{1}H-NMR spectrum of **5**.

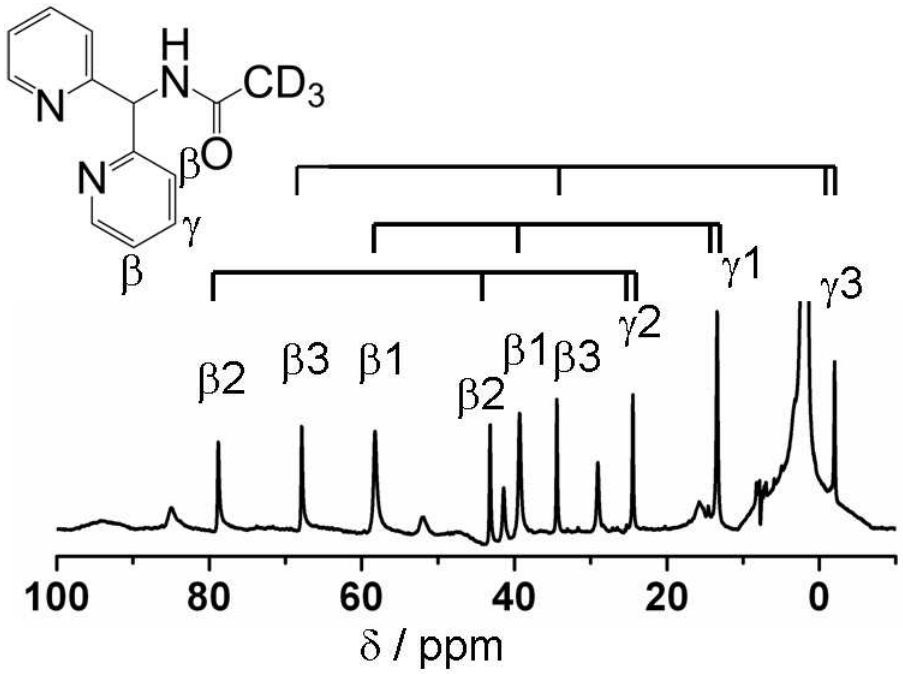

Figure 3.7 Coupling among pyridine protons shown on the 1D-^{1}H-NMR spectrum of **5**.

Taken together, in solution there are two structures: one with one kind of oxygen donor and nitrogen donor and the other with one kind of oxygen donor and two kinds of nitrogen donors. Thus we propose an equilibrium between two structures in solution (Scheme 3.4). The first structure is in agreement with the centrosymmetric one observed in the crystal. The two C=O groups are *trans* to each other (Scheme 3.4, trans). Due to the inversion center, only one methyl resonance and one set of pyridine protons are observed. In the other structure, the two C=O groups are *cis* to each other (Scheme 3.4, cis). Two nitrogen atoms are *trans* to each other and the other nitrogens are *trans* to oxygens, so there are two types of nitrogen donors and one type of oxygen donor. Since the free ligand can also be detected in the NMR spectra, the ligand can dissociate from

the iron center to some degree. Therefore, this is the first time that solution characterization of iron complexes with *N,N,O*-facial ligand can be fully accomplished.

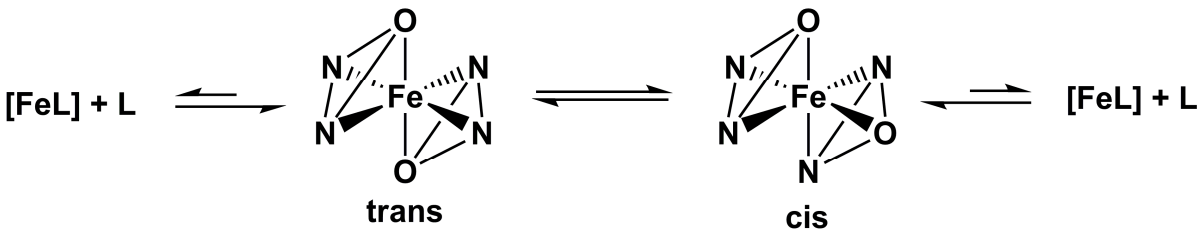

Scheme 3.4 Proposed structures for **1-3** in solution of CH_3CN.

The solution characterization strategy for **1** is based on the solution characterization of **4** and **5**. The assignment of pyridine protons of **1** is shown in Figure 3.8 and can be confirmed by 2D-^{1}H-NMR of **1** (Figure 3.9). Similarly three types of pyridine are observed and the ratio among them is about 2.5 : 1 : 1. The trans structure is slightly more favored than the cis structure (Scheme 3.4) and presumably is the more stable form in solution. Lowering the temperature should shift the equilibrium to the left trans structure. This hypothesis is proved by the low temperature ^{1}H-NMR of **1** (Figure 10). The area ratio of β1 : β2 : β3 shifts from 2.5 : 1 : 1 at room temperature to 5 : 1 :1 at -35°C, confirming the existence of the equilibrium in solution.

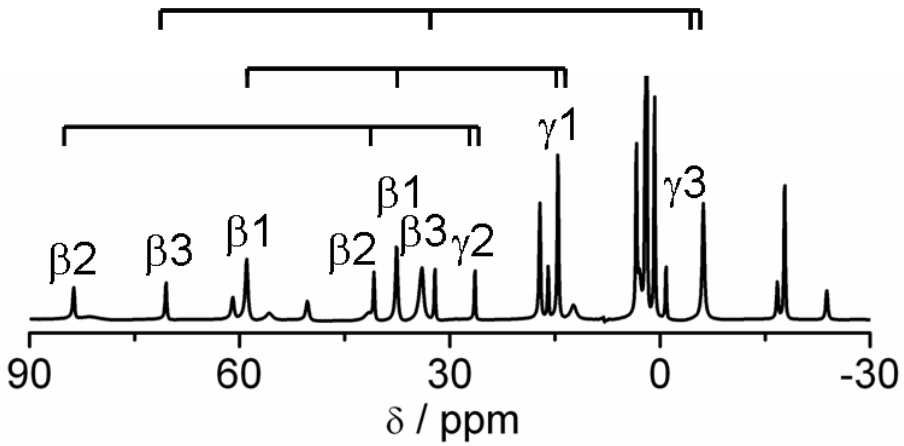

Figure 3.8 Assignment of pyridine protons for **1**.

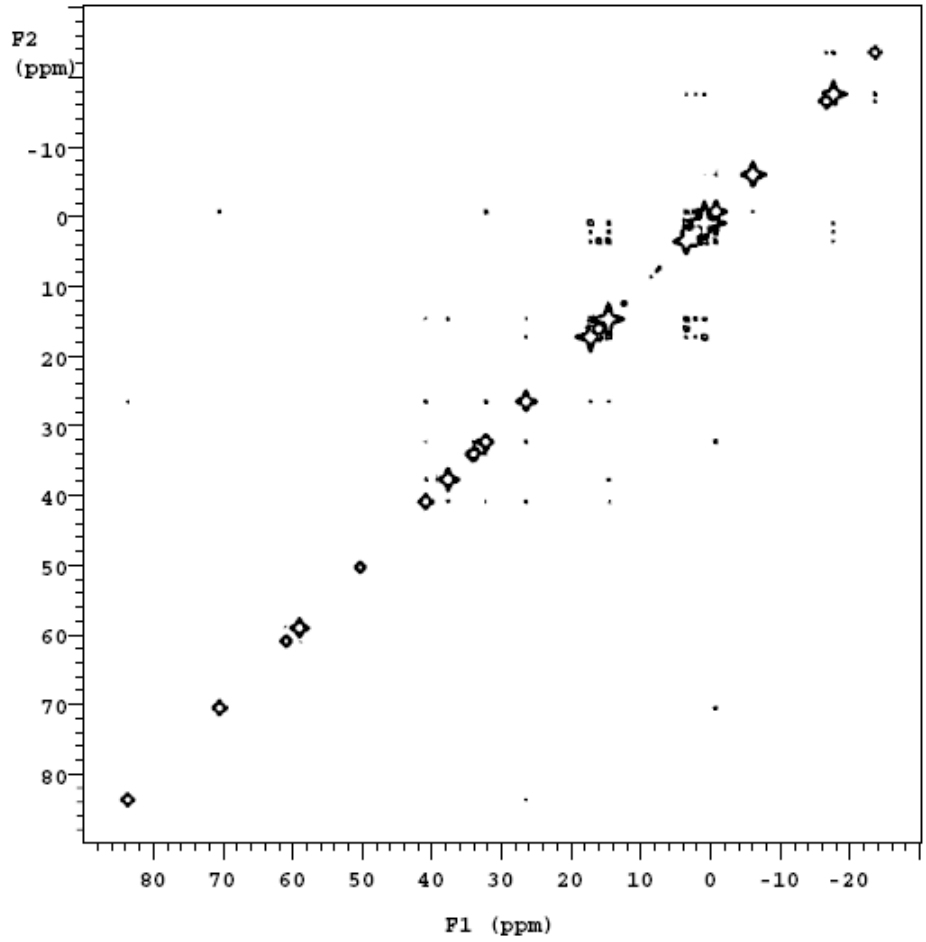

Figure 3.9 2D-^{1}H-NMR spectrum of **1**.

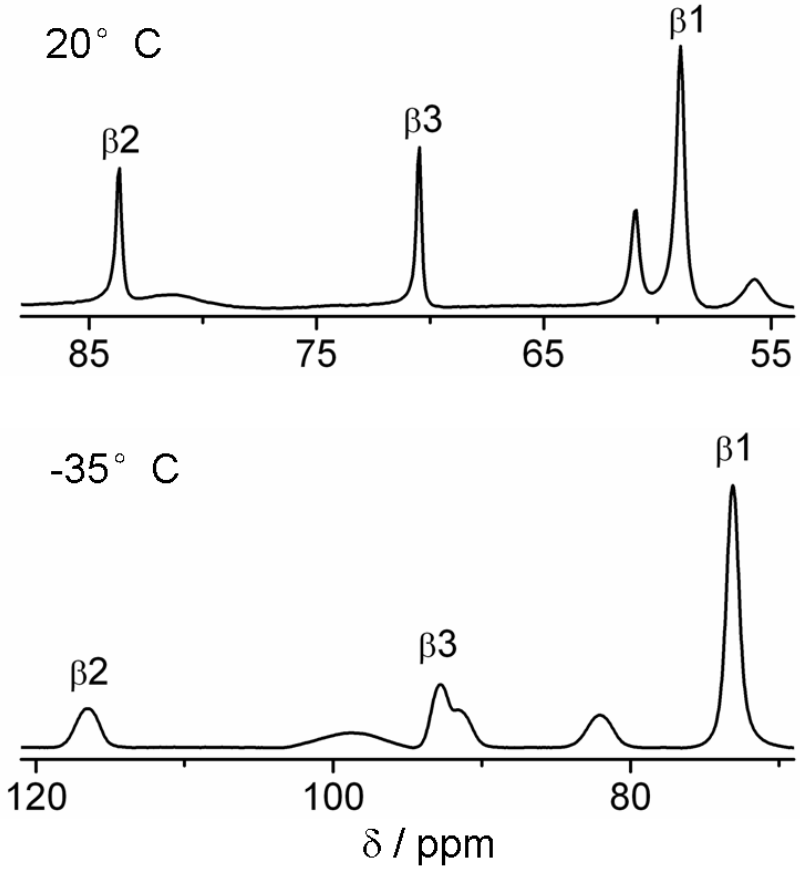

Figure 3.10 ^{1}H-NMR of **1** at different temperatures.

The ^{1}H-NMR spectra of **2** and **3** were also examined (Figure 3.11). They both show more peaks than expected from a centrosymmetric structure and free ligand peaks are observed. Considering the solution ESI-MS and FT/IR studies and by analogy to **1**, the same equilibrium was also proposed for **2** and **3** (Scheme 3.4).

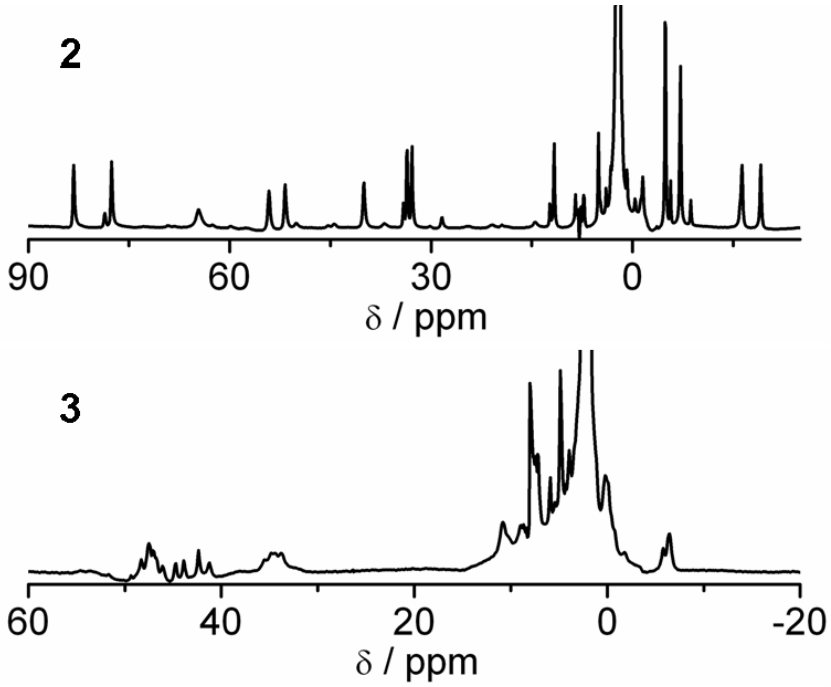

Figure 3.11 ^{1}H-NMR spectra of **2** (top) and **3** (bottom).

3.4 Catalytic activity

Table 3.5 summarizes the catalytic activities of active iron complexes with facial *N, N, O* ligands in the oxidation of a variety of olefins using H_2O_2 as oxidant. Our lab has previously developed a series of facial *N, N, O* ligands based on the structure of Ph-DPAH and they all show very similar catalytic behavior, so Table 3.5 uses only **6** with the parent Ph-DPAH ligand to represent the whole family. As mentioned in a previous paragraph, complex **7** with HL1 is the good structural model of Rieske dioxygenases, but it is not active in the olefin oxidation catalysis.[70] Its ester derivative **8** with PrL1, on the other hand, is catalytically active and used for comparison in Table 3.5.[70] Complex **9** is another iron catalyst with the facial *N, N, O* ligand, but its reactivity is so low that it can not achieve any turnovers due to the easy falloff of the ligand,[69] so HL2 is not

included in the Table 3.5. The purpose of catalytic studies of iron catalysts with newly designed *N, N, O*-facial ligands is to derive the relationship between the ligand structure and the catalytic reactivity. To make the comparison valid, reaction conditions for **1 - 3** are kept the same as previously reported active iron catalysts. Thus for these experiments to achieve the desired catalytic outcomes, the substrate olefins must be present in large excess to trap the iron oxidant as soon as it is formed, and the H_2O_2 must be introduced by syringe pump to keep the H_2O_2 concentration low and avoid H_2O_2 disproportionation and generation of hydroxyl radicals. As such, these reaction conditions are not very practical for synthetic chemists. However, these are the only iron catalysts thus far for the conversion of olefins into *cis*-diol products that use H_2O_2 as the oxidant. Thus, the insights from ligand variations obtained from this study will be useful for the later ligand design in the bio-inspired iron catalysts.

Table 3.5 Oxidation of olefins catalyzed by iron complexes with facial *N, N, O* ligands[a]

	1	**2**	**3**	**6**[b]	**8**[c]
1-octene					
diol	8.2(3)	2.1(1)	1.2(1)	7.6(3)	2.7
epoxide	0.1(1)	0.1(1)	n. d.[f]	0.1(1)	1.6
***cis*-cyclooctene**					
diol	5.4(1)	1.1(1)	1.3(1)	7.0(6)	1.1
epoxide	0.3(1)	0.6(1)	0.6(1)	0.5(1)	2.8
styrene[d]					
diol	8.2(3)	2.0(4)	1.8(2)	8.0(5)	1.7
epoxide	0.2(1)	0.3(1)	<0.1	0.1(1)	2.3
***cis*-2-heptene**					
diol	4.2(1)	1.6(1)	2.2(1)	4.9(4)	6.3[g]
[RC%][e]	[100]	[100]	[100]	[99]	[92]
epoxide	0.6(1)	0.8(1)	0.4(1)	0.7(1)	6.2[g]
[RC%][e]	[38]	[50]	[10]	[57]	[84]
t-butyl acrylate					
diol	7.5(2)	1.4(1)	1.6(1)	5.5(2)	
epoxide	n. d.[f]	n. d.[f]	0.1(1)	--	
dimethyl fumarate					
diol	6.5(2)	0.9(1)	2.2(2)	5.3(4)	
epoxide	n. d.[f]	n. d.[f]	n. d.[f]	--	

[a]Reaction conditions: H_2O_2 was added by syringe pump over a 5-min period to a solution of catalyst (0.35 mM) and substrate (0.35 M) in CH_3CN. This solution was stirred for an additional 60 min prior to workup. See section 3.2 for further details. Yields expressed as turnover numbers, TON, (μmol product/μmol catalyst). [b]Results from ref 99. [c]Results from ref 70. Reaction conditions are slightly different with 20-min

H_2O_2 addition followed by 40 min additional stirring. See original paper for further details. [d]Results were obtained under inert atmosphere by degassing solutions prior to oxidant introduction so that only a minor amount of the benzaldehyde autoxidation product was observed. See Table 3.6 for the quantification of this product. [e]RC%: retention of configuration. RC = 100 × (A – B)/(A + B), where A = yield of *cis*-configuration product with retention and B = yield of epimer. [f]n. d. : not detected. [g]20 equiv H_2O_2 were used.

Complexes **1** - **3** are all active iron catalysts in olefin *cis*-dihydroxylation with H_2O_2 as oxidant. For all olefins used in this study, **1** is a better catalyst in efficiency than **2** and **3**, and **2** and **3** are comparable to each other in oxidation reactivity. *Cis*-diol is the major product for all reactions, while epoxide is obtained in small amounts for olefins with electron donating substituents or not detected for olefins with electron withdrawing substituents. Complexes **1** and **6** are structurally related and **1** shows slightly more efficient catalytic capability than **6** except *cis*-cyclooctene and *cis*-2-heptene with two alkyl substituents. The longevity of **1** was examined by injecting 20 equiv H_2O_2, and 14.1 turnovers were obtained. The conversion is not as good as 10 equiv H_2O_2, but **1** is fairly robust. New complexes **1-3** are also examined with *cis*-2-heptene as substrate, all the diol products are observed with retention of configuration while loss of retention is detected for the epoxide products, suggesting that the dihydroxylation is indeed *cis*-only but the epoxidation might use a different pathway.

More insightful results come from the comparison among these complexes. As

mentioned in the ligand design section, NNOester and PrL1 have the same oxygen donor, ester oxygen but different nitrogen donors. NNOester has two pyridine rings while PrL1 contains two imidazole rings. Reactivity comparison between their corresponding iron complexes, **2** and **8**, can shed light on the effect of nitrogen donors on the reactivity. There are only three substrates that are common for both catalysts. From Figure 3.12, complex **8** shows a better overall reactivity including both *cis*-diol and epoxide products, and for *cis*-cyclooctene and styrene, epoxide is the favored product over *cis*-diol. On the other hand, **2** gives lower conversion of H_2O_2, but the *cis*-diol yield is almost the same as that from **8**. So the lower amount of epoxide from **2** is the cause for the overall lower reactivity. In other words, complex **2** greatly suppresses the formation of epoxide, and thus the selectivity is greatly enhanced. Therefore, the two pyridines in the NNOamide ligand increase the selectivity for *cis*-diol compared with the two imidazoles in the PrL1 ligand.

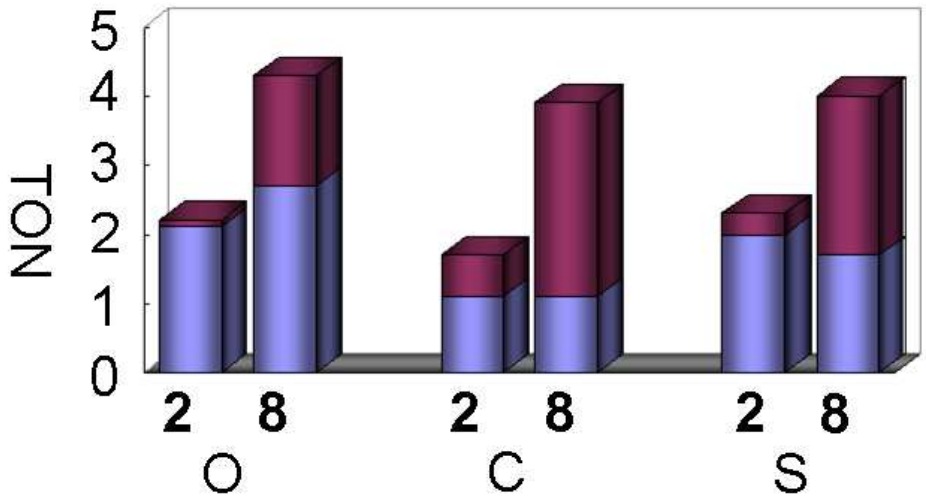

Figure 3.12 Reactivity comparison between **2** and **8** for oxidation of 1-octene (O), *cis*-cyclooctene (C) and styrene (S). Blue bar: *cis*-diol product; purple bar: epoxide product.

The three new ligands, NNOamide, NNOester, and NNOketone, all share the two pyridines but have various oxygen donors (Scheme 3.1). Comparison of catalytic reactivity will show the effect of different oxygen donors. As illustrated in Figure 3.13, for all cases, the selectivity towards *cis*-dihydroxylation is excellent. This is in good agreement with the results from the last paragraph that the two pyridines help increase the selectivity of *cis*-diol product. In addition, **1** is a much better catalyst than either **2** or **3**, while **2** and **3** are comparable to each other. For example, 82% of H_2O_2 is converted into *cis*-diol product for the oxidation of 1-octene by **1**, while only 21% and 12% of H_2O_2 are converted by **2** and **3**, respectively. To examine the effect of the ligand, the amide oxygen in NNOamide has higher electron density than ester oxygen and ketone oxygen in NNOester and NNOketone. So the observation that **1** is the best catalyst among **1** - **3** clearly connects the electron density on the binding oxygen with the

catalytic reactivity.

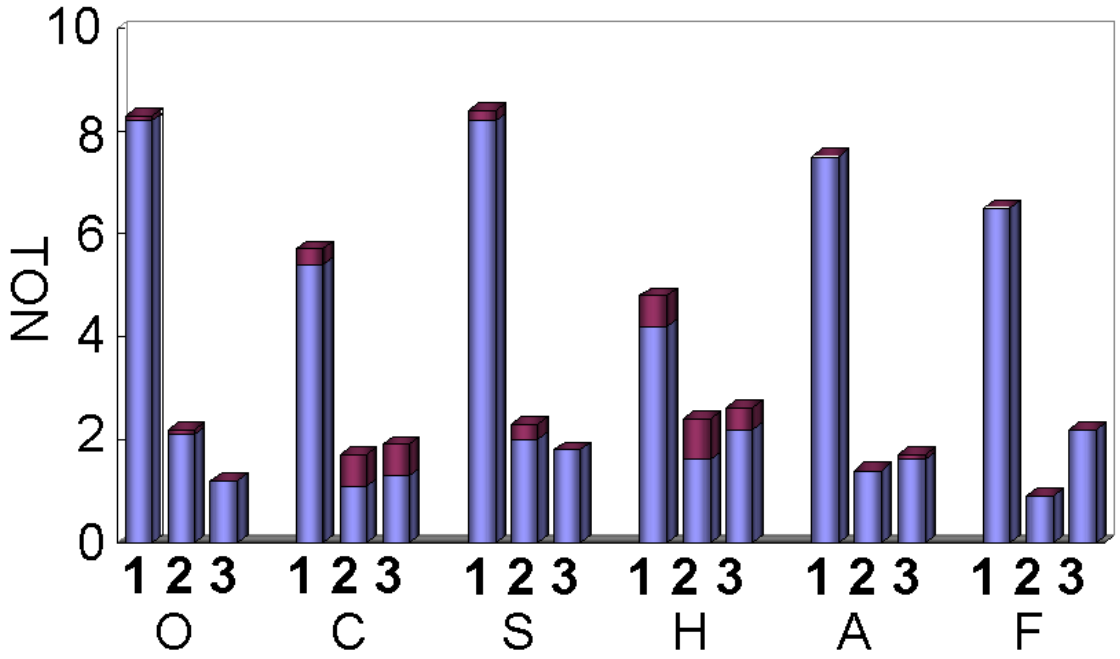

Figure 3.13 Reactivity comparison of **1-3** for oxidation of 1-octene (O), *cis*-cyclooctene (C), styrene (S), *cis*-2-heptene (H), *t*-butyl acrylate (A) and dimethyl fumarate (F). Blue bar: *cis*-diol product; purple bar: epoxide product.

3.5 Competition reactions

1 represents the most reactive and selective iron catalyst thus far, so the active oxidant formed from **1** in the course of catalysis is of great interest to us. To gather information regarding the nature of this active oxidant, its interaction with substrates is examined by substrate competition studies. Reactions are carried out with pairs of olefin substrates substituted by groups with different electron donating / withdrawing abilities, and based on the preference of substrates the property of the active oxidant can be

concluded. Equimolar amounts of two substrates are used in the reaction under normal catalytic and work-up conditions, and the results are represented by the percentage of each *cis*-diol product as illustrated in Figure 3.14. When dimethyl fumarate with two electron withdrawing groups is presented in the reaction, it is always the greatly preferred substrate no matter what the other substrate is. When *t*-butyl acrylate with only one electron withdrawing substituent is mixed with either 1-octene or *cis*-cyclooctene, it is largely favored. Finally, when 1-octene and *cis*-cyclooctene compete for the oxidation, *cis*-cyclooctene is slightly favored. So an interesting trend is observed: dimethyl fumarate > *t*-butyl acrylate > *cis*-cyclooctene ≈ 1-octene. Notably, when the most favorable substrate, dimethyl fumarate, is mixed with the least favorable substrate, 1-octene in equal amounts, no product is observed for 1-octene. So a 1 : 9 ratio of dimethyl fumarate and 1-octene is used in the competition reactions. Still the *cis*-diol product from dimethyl fumarate is 10 times (TON = 6.0) more than that from 1-octene (TON = 0.7). Clearly the more electron-deficient olefin is favored in these oxidations. This trend has been previously reported for **6**.[104] Considering the similarity between **1** and **6**, it is not surprising that the active oxidants formed from **1** and **6** are both nucleophilic.

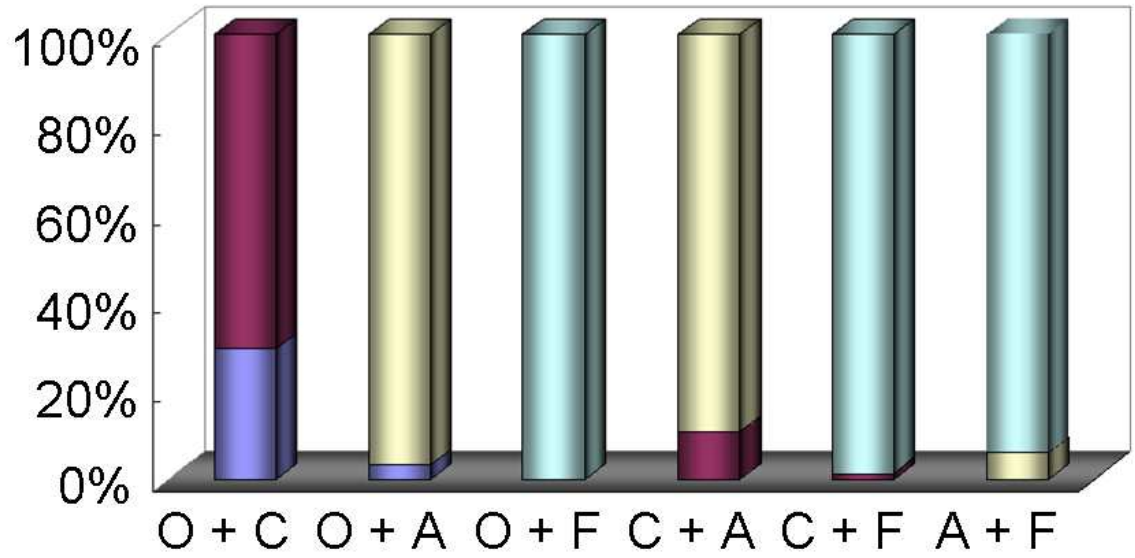

Figure 3.14 Percentage of different *cis*-diol products resulting from the oxidations of equimolar mixtures of substrates. C: *cis*-cyclooctene (purple); O: 1-octene (blue); A: *t*-butyl acrylate (yellow); F: dimethyl fumarate (green).

3.6 Isotopic labeling studies

Isotopic labeling studies. For the olefin *cis*-dihydroxylation reactions, two oxygen atoms are incorporated into the *cis*-diol products. Tracing the source of oxygen atoms is a useful mechanistic tool, especially in the case of H_2O_2 as oxidant, to understand when O-O bond cleaves in the course of reaction. As indicated by the *cis*-dihydroxylation of *cis*-2-heptene, reactions undergo *cis*-only metal based fashion instead of autoxidation by dioxygen from the air, which makes the hydrogen peroxide and water only sources for incorporated oxygen atoms. ^{18}O-labeled hydrogen peroxide, $H_2{}^{18}O_2$, is used in the reaction, but as commercially available $H_2{}^{18}O_2$ comes as a 2 wt% solution in $H_2{}^{16}O$, every equivalent of $H_2{}^{18}O_2$ added in the labeling studies is accompanied by 100 equiv

$H_2{}^{16}O$. To corroborate these results, complementary labeling experiments with 10 equiv $H_2{}^{16}O_2$ / 1000 $H_2{}^{18}O$ are also carried out. Previous experiments have shown two patterns of labeling results. One is that the two oxygen atoms in the products are each from H_2O_2 and H_2O, and this pattern is represented by $[Fe^{II}(TPA)]^{2+}$.[66] The other is that part or all portion of products are derived from both oxygen atoms from H_2O_2, as represented by **6**.[104]

1 - **3** are tested in the labeling experiments described above. Complete results are summarized in Table 3.6 and Figure 3.15 graphically illustrates the percentage of different isotopomers of the *cis*-diol products obtained from $H_2{}^{18}O_2$ / $H_2{}^{16}O$ experiments. Data from Table 3.6 demonstrate agreement between the complementary $H_2{}^{18}O_2$ and $H_2{}^{18}O$ studies. Most importantly, some portion of the *cis*-diol products have both oxygen atoms derived from water for all complexes **1** - **3** and all substrates used in these studies. In contrast, for complex **6**, no *cis*-diol product derives both oxygen atoms from water (Table 3.6). This unprecedented observation will be discussed in the later section. When 1-octene, *cis*-cyclooctene, *t*-butyl acrylate, and dimethyl fumarate are used in an order of increasing preference as demonstrated in the previous section, water incorporation into the *cis*-diol products with one or two oxygen atoms from water decreases in proportion for each catalyst as presented in Figure 3.15. These results suggest that olefin oxidation by the iron-derived oxidant competes with the label scrambling between H_2O_2 and H_2O at the iron center.

Table 3.6 Percentage of isotopomers found in the *cis*-diol products with $H_2{}^{18}O_2$ or $H_2{}^{18}O$ used as sources of ^{18}O atoms in olefin oxidations catalyzed by **1** - **3** and **6**[a]

cata lyst	substrate	10 $H_2{}^{16}O_2$ / 1000 $H_2{}^{18}O$			10 $H_2{}^{18}O_2$ / 1000 $H_2{}^{16}O$		
		$O^{16}O^{16}$	$O^{16}O^{18}$	$O^{18}O^{18}$	$O^{16}O^{16}$	$O^{16}O^{18}$	$O^{18}O^{18}$
1	1-octene	46	36	17	20	37	43
	cis-cyclooctene	62	31	6	11	31	56
	t-butyl acrylate	90	10	0	4	14	82
	dimethyl fumarte	98	2	0	3	6	90
2	1-octene	49	19	28	23	28	45
	cis-cyclooctene	59	24	15	9	19	71
	t-butyl acrylate	79	14	7	8	17	75
	dimethyl fumarte	95	5	0	3	11	86
3	1-octene	57	27	16	19	25	56
	cis-cyclooctene	67	16	16	12	20	67
	t-butyl acrylate	80	12	5	7	17	75
	dimethyl fumarte	96	4	0	4	9	86
6[b]	1-octene	67	29		4	32	64
	t-butyl acrylate	92	8		0	13	87
	dimethyl fumarte	98	2		1	4	95

[a]Please check section 3.2 for more details of reaction conditions. [b]Results from 104.

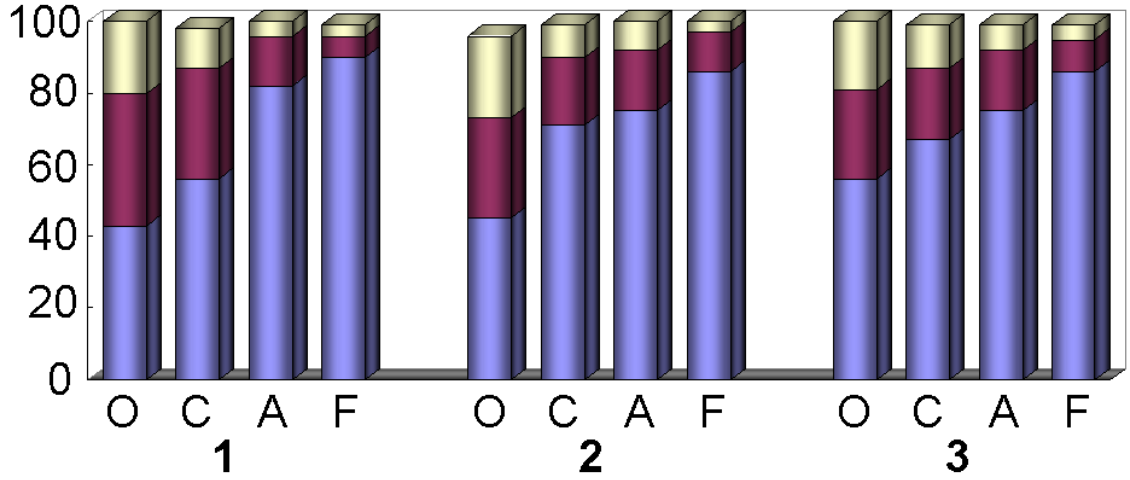

Figure 3.15 Percentage of *cis*-diol products with 2 ^{18}O atoms (blue), with 1 ^{18}O atom and 1 ^{16}O atom (purple) and with 2 ^{16}O atoms (yellow) in olefin *cis*-dihydroxylation reactions catalyzed by **1** - **3** (0.35 mM) with 10 equiv $H_2{}^{18}O_2$ and 1000 equiv $H_2{}^{16}O$ in CH_3CN at room temperature in the presence of 1000 equiv olefin. O, C, A, and F stand for 1-octene, *cis*-cylcooctene, *t*-butyl acrylate, and dimethyl fumarate, respectively.

Temperature dependent isotopic labeling studies. The competition between olefin oxidation and label scrambling can be tested if the rates for both are perturbed. Experiments with labeled water at different temperatures for 1-octene oxidation catalyzed by **1** are examined (Figure 3.16). When the temperature is increased from room temperature (20°C) to 40°C, it is interesting to find that the percentage for each product keeps the same, indicating that both rates increase proportionally. However, when the temperature is further increased to 60°C, the portion of the *cis*-diol products with one or two oxygen atoms from water is decreased, suggesting that at high temperature, the rate for olefin oxidation is enhanced more than that of label scrambling.

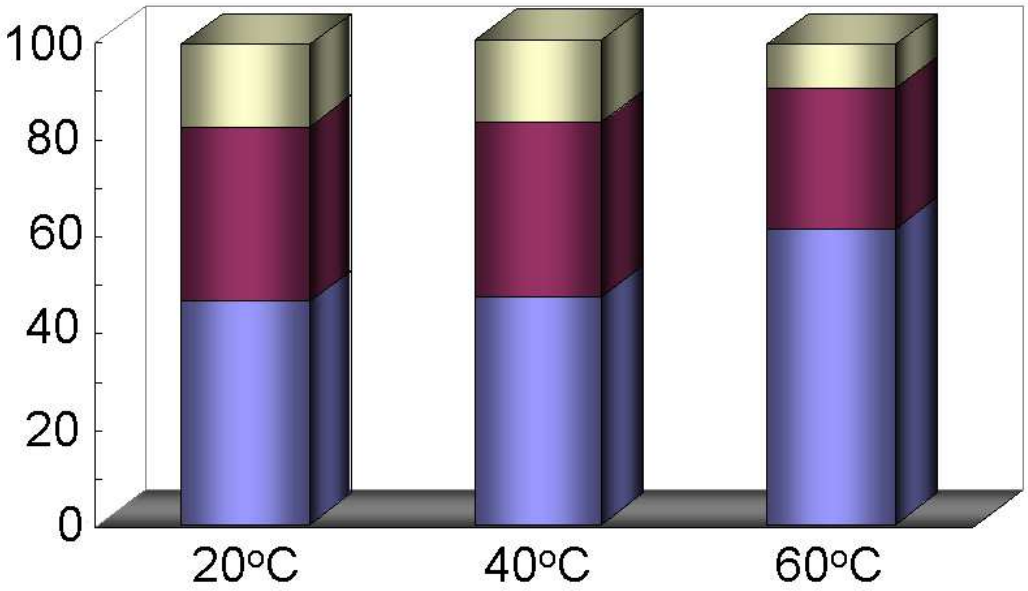

Figure 3.16 Percentage of *cis*-diol products with 2 ^{16}O atoms (blue), with 1 ^{18}O atom and 1 ^{16}O atom (purple) and with 2 ^{18}O atoms (yellow) in olefin *cis*-dihydroxylation reactions catalyzed by **1** (0.35 mM) with 10 equiv $H_2{}^{16}O_2$ and 1000 equiv $H_2{}^{18}O$ in CH_3CN at different temperatures in the presence of 1000 equiv 1-octene.

Water labeling effect. Since water plays an important role in the mechanism, more labeling experiments with labeled water are carried out catalyzed by **1**. The *cis*-diol products with one or two oxygen atoms from water are checked by increasing the amount of labeled water present in the reaction system. In the case of the *cis*-diol product with one oxygen atom from water and the other from hydrogen peroxide, the label incorporation from water exhibits a saturation behavior with increasing water concentration, suggesting an equilibrium binding of one water molecule to the iron center during the catalytic cycle. This is also supported by the linearity of the double

reciprocal plot of this data (Figure 3.17, up, inset). This phenomenon is not surprising, as it was previously observed for **6**.[104] Intriguing results come from the *cis*-diol products with both oxygen atoms from water. The label incorporation percentage also shows a saturation behavior, but this saturation curve is obtained against the square of water concentration instead of water concentration. The double reciprocal plot of label incorporation and the square of water concentration is linear (Figure 3.17, down). This unusual labeling pattern implies that another equilibrium also exists with two water molecules bind to the iron center.

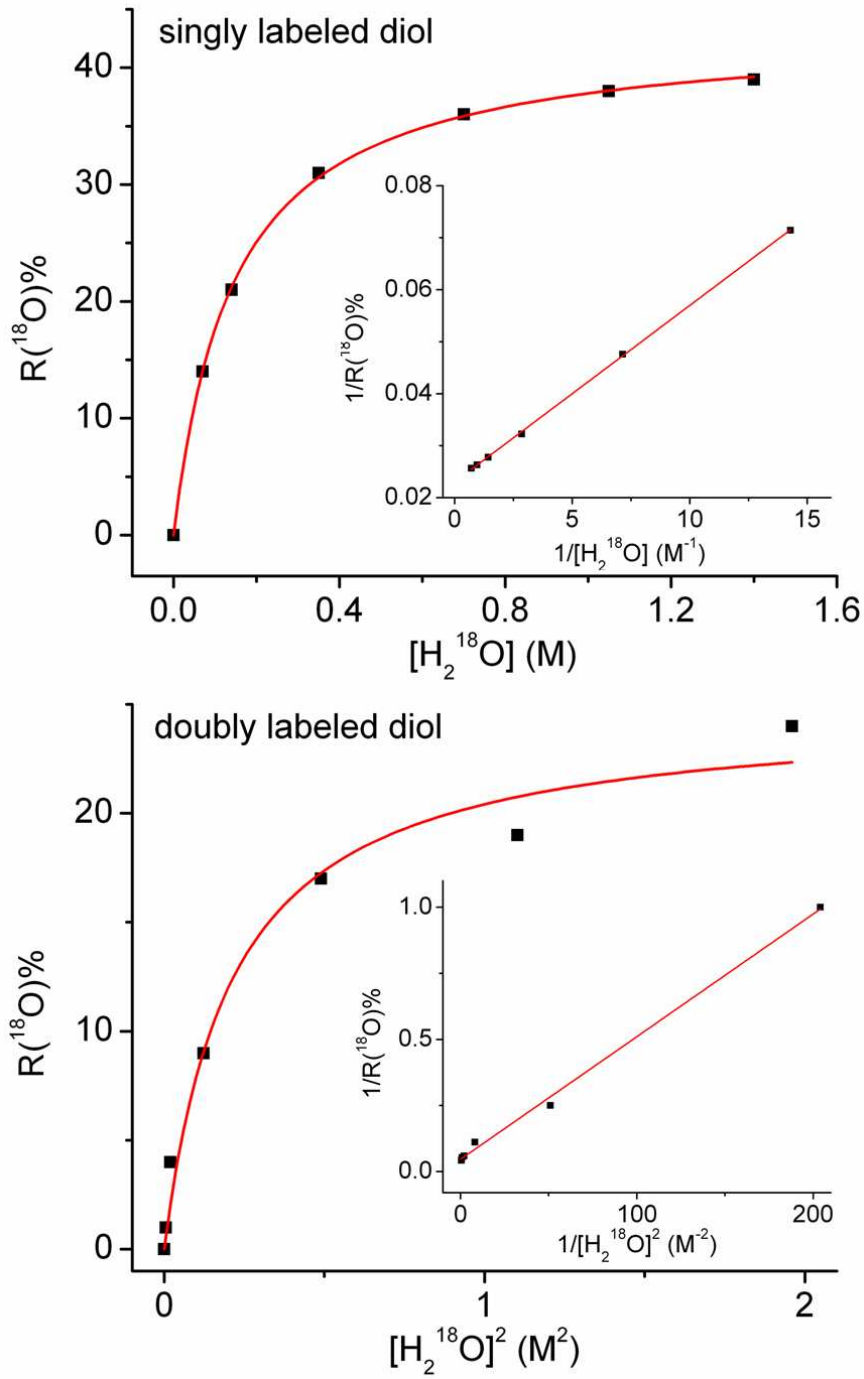

Figure 3.17 Percentage of ^{18}O-labeled diol obtained in the oxidation of 1-octene catalyzed by **1** with H_2O_2 as a function of the concentration of $H_2{}^{18}O$. Top: singly labeled product; bottom: doubly labeled product. Inset: double reciprocal plot.

3.7 Discussions

Structural considerations of catalysts. Previous structural studies on iron complexes with facial *N, N, O* ligands represented by **6** and **8** are limited.[70,104] Solid state structural information is from X-ray crystallography, showing a centrosymmetric structure, while structural information in solution is obtained through ESI-MS and solution FT/IR. ESI-MS indicates a ligand dissociation-association equilibrium, but since the concentration for doing ESI-MS analysis is very low, further evidence for the equilibrium under reaction conditions would be useful. Solution FT/IR only confirms that the carbonyl oxygen atoms bind the iron center as shown in the crystal structures. So this work demonstrates the actual structures in the solution of CH_3CN for iron complexes with facial *N, N, O* ligands by analyzing NMR spectra of **4** and its deuterated derivative **5**. The concentration for NMR is about the same magnitude as reaction conditions, which makes the NMR analysis the most valid method. The better resolution of NMR can also tell the difference between structures in solution. After analysis, the presence of two different oxygen donors and three different nitrogen donors leads us to propose the equilibrium between *cis* and *trans*-structures in solution shown in Scheme 3.4 for **4** and **5**. Analogous spectra are obtained for **1** and the same equilibrium is proposed. This equilibrium is evidenced by low temperature NMR showing that the peak area ratio between two structures changes and the centrosymmetric isomer as shown in crystal structure becomes more predominant at -35°C. Significant amounts of free ligand are observed for **2** and **3**. Due to the similarity to **1**, the same equilibrium is proposed for them too, but some free ligand presumably dissociates from the metal center. Therefore,

overall equilibrium is summarized in Scheme 3.4, but for different complexes, this equilibrium can shift in different directions.

Ligand Effect. The logic behind the design of the new structurally related ligands is clearly shown in Scheme 3.2. From reactivity comparisons of their iron complexes, insight into the ligand effect is expected to be obtained. Indeed, catalytic results turn out to be very interesting and insightful. NNOester and PrL1 both have the same ester oxygen donor to the iron center, but they have different nitrogen donors. NNOester has two pyridines and PrL1 has two imidazoles. From Figure 3.11, **8** with PrL1 as ligand is a more reactive catalyst than **2** with NNOester as ligand, but the selectivity toward *cis*-dihydroxylation of **2** is worse than **1**. The two pyridine nitrogen donors help with enhancing the selectivity. To explain this discrepancy, the pKa values of both nitrogen donors are checked and shown in Equation 3.2. The pKa for pyridine is 5.2, while the pKa for 1-methyl imidazole is 7.4. These values were determined in aqueous solution, but they clearly show that pyridine is less basic than 1-methyl imidazole. The Fe-N bond distances in the crystal structures demonstrate this subtle difference. Fe-N distances in **8** are shorter than those in **2** (Table 3.3). The more basic imidazoles in PrL1 make the iron center so reactive that it can not differentiate the *cis*-dihydroxylation and epoxidation pathways, while the basicity of pyridines is appropriate for only the *cis*-dihydroxylation pathway. This conclusion is also evidenced by catalytic results of **1** - **3**. Their ligands all contain two pyridines and the *cis*-diol products are all selectively formed.

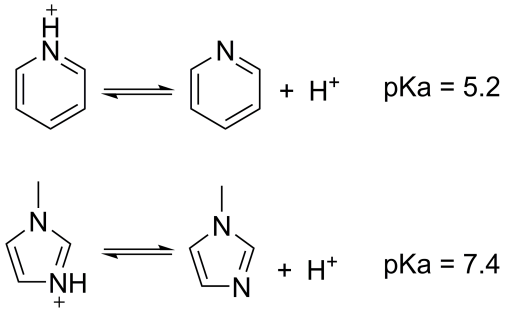

Equation 3.2 pKa values for pyridine and 1-methyl imidazole.

Results for **1** - **3** are compared in Figure 3.12. **1** with an amide oxygen donor is much more reactive than the other two catalysts. This clearly indicates that the electron density on the oxygen atom affects the reactivity. Amide oxygen atom is the most electron rich among these three, and thus it donates more electron density to the iron center. On the other hand, electron densities for ester and ketone are similar but lower than the amide oxygen, so catalytic reactivities of **2** and **3** are comparable but lower than **1**. Therefore, from the studies so far, the facial *N, N, O* ligands need two pyridines to have good selectivity and one amide to obtain high reactivity. This makes the NNOamide and similar Ph-DPAH family ligands the best facial *N, N, O* ligands thus far.

Mechanistic considerations. Isotopic labeling studies provide us information about the source of the incorporated oxygen atoms. Since dioxygen in the air is not involved in the reaction, only hydrogen peroxide and water are possible oxygen sources. The *cis*-diol products with at least one oxygen atom from hydrogen peroxide are commonly observed for all non-heme iron catalysts so far.[66,99,102] However, in this work, **1** - **3** exhibit an unprecedented labeling pattern with both oxygen atoms in the *cis*-diol products from

water, in addition to the common patterns observed before. This unusual labeling pattern is very insightful into the mechanism as discussed below. Further labeling experiments are carried out for **1** by adding increasing amount of $H_2{}^{18}O$. The saturation curve is observed for the percentage of the *cis*-diol product with one oxygen from hydrogen peroxide and the other from water against water concentration, which has been seen for the non-heme iron catalysts that give *cis*-diol products with one oxygen atom from water. More interestingly, another saturation behavior is illustrated by plotting the percentage of the *cis*-diol product with both oxygen atoms from water versus the square of water concentration.

Both of the above results indicate that one or two water molecules bind to the iron center. Since the hydrogen peroxide is the terminal oxidant and it can not accomplish the *cis*-dihydroxylation alone, it has to bind to the metal iron and be activated. So in the case of two water molecules binding, there are a total of three extra ligands that need to bind to the iron center, two water molecules and one hydrogen peroxide, and at least three sites are needed for their coordination. The most reasonable hypothesis is that one tridentate ligand dissociates from the metal center and hydrogen peroxide binds in an end-on η^1 fashion, $Fe(\eta^1\text{-}O_2H_2)(OH_2)_2$ (Figure 3.18 left). On the other hand, With one water molecule binding, an $Fe(\eta^2\text{-}O_2H_2)$ adduct is proposed (Figure 3.18 right). The same adduct was proposed for the structurally similar complex **6**, and is also found to be energetically reasonable in computational studies of Fenton chemistry[114,115] and of an iron complex of a tetradentate bispidine ligand that is capable of olefin oxidation catalysis.[116]

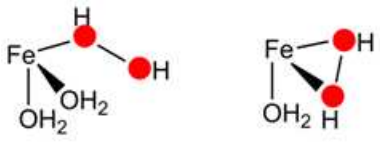

Figure 3.18 Proposed iron hydrogen peroxide aqua adducts.

Another implication of the unusual labeling pattern is that the $Fe(\eta^1\text{-}O_2H_2)(OH_2)_2$ adduct has to undergo O-O bond cleavage to have the *cis*-diol product with both oxygen atoms from water. If the $Fe(\eta^1\text{-}O_2H_2)(OH_2)_2$ attacked the substrate directly, it would be expected that at least one oxygen atom in the product was from hydrogen peroxide and it would be impossible to have *cis*-diol with both oxygen atoms from water. The *cis*-dihydroxylation of *cis*-2-heptene shows nearly complete retention of configuration and no radical is involved in the mechanism. Therefore, the O-O bond cleavage for this adduct is heterlytic to avoid the formation of hydroxyl radical (Scheme 3.5 up). After losing one water molecule, it forms an iron dihydroxo aqua species. The proton on the aqua ligand can shift to any other oxygen atom, thus making all the three oxygen atoms possible to be incorporated into the *cis*-diol products. So the *cis*-diol products with both oxygen atoms from water can be explained. The other $Fe(\eta^2\text{-}O_2H_2)(OH_2)$ adduct is the same as that proposed for **6**. Because of the similarity between **6** and **1**, a homolytic O-O bond cleavage is also proposed here (Scheme 3.5 down). Two bonded oxygen atoms are from hydrogen peroxide, which can explain the *cis*-diol products with both oxygen atoms from hydrogen peroxide.

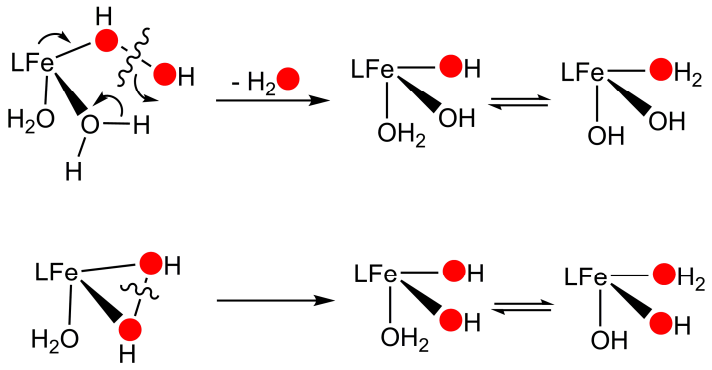

Scheme 3.5 O-O bond cleavage for iron hydrogen peroxide aqua adducts. Oxygen atoms in hydrogen peroxide are illustrated in red.

After the O-O bond cleavage, the valence state of the iron center will go up two units. So the active oxidant is either Fe^{V} from Fe^{III} or Fe^{IV} from Fe^{II}. The best studied non-heme iron catalyst is $[Fe^{II}(TPA)]^{2+}$ with a tetradentate ligand TPA. Its extensive work pointed to a proposed active oxidant of high valent HO-Fe^{V}=O species.[66] This high valent Fe^{V} species was also proposed to be the active oxidant for naphthalene *cis*-dihydroxylation catalyzed by $[Fe^{II}(TPA)]^{2+}$.[117] Our previous work of **6** did not show any reactivity using naphthalene as product and prompted us to propose the Fe^{II} / Fe^{IV} cycle, instead of the well established Fe^{III} / Fe^{V} cycle. When **1** is used as a catalyst in naphthalene oxidation, naphthalene stays intact, which is not surprising considering the structural similarity between **1** and **6**. Therefore, we propose Fe^{IV} is the oxidation state in the active oxidant. This hypothesis is consistent with the substrate competition reactions that electron deficient olefins are more favored in the reaction. Thus the active oxidant of **1** must have the nucleophilic property, while substrates competition reactions demonstrated that $[Fe^{II}(TPA)]^{2+}$ prefers electron rich olfins showing its electrophilic

property. So these are in agreement with their respective assignment of valence state for the active oxidants.

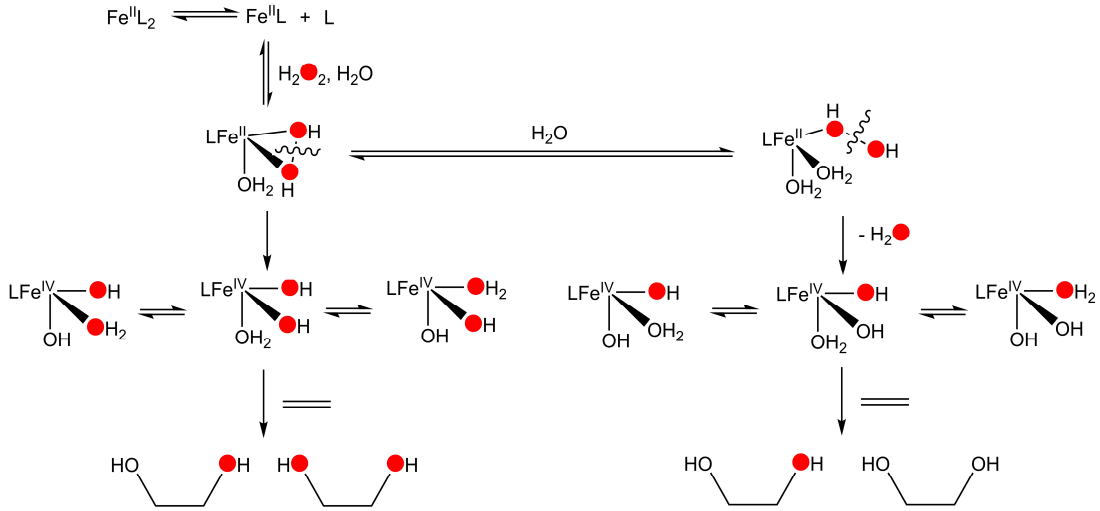

Scheme 3.6 Mechanistic overview. Oxygen atoms in hydrogen peroxide are illustrated in red.

Taken together, the overall mechanism is shown in Scheme 3.6. Iron complexes at first lose one ligand from the metal center to provide three sites for the binding of oxidant and water molecules. As the pre-equilibrium saturation curves of water coordination show, water binds to the iron center afterwards before the rate determining O-O bond cleavage. When one hydrogen peroxide and one water are involved, side-on binding adduct $Fe^{II}(\eta^2\text{-}O_2H_2)(OH_2)$ occurs. On the other hand, based on the new labeling observation, another water can also bind and an end-on adduct $Fe^{II}(\eta^1\text{-}O_2H_2)(OH_2)_2$ is formed. From here, these two adducts undergo different ways of O-O bond cleavage to generate a similar active oxidant $Fe^{IV}(OH)_2(OH_2)$. The O-O bond in side-on adduct takes

the homolytic cleavage pathway, while O-O bond in end-on adduct is heterolytically cleaved. The resulting intermediates contain different numbers of oxygen atoms from water and hydrogen peroxide. This high valent species Fe^{IV} dihydroxo is proposed to be responsible for attacking olefins to make the final *cis*-diol products, but the proton on the aqua can scramble among the three oxygen atoms, which competes with the olefin attack. So depending on the relative rates of proton scrambling and substrate attack, different degrees of water oxygen incorporation into products will be detected. *cis*-Diol products from the side-on adduct contain one or two oxygen atoms from hydrogen peroxide, while at least one oxygen atom in the *cis*-diol products from the end-on adduct will be from water.

This proposed mechanism is consistent with all the experimental data thus far, and the competition between proton exchange and substrate attack determines the amount of water oxygen incorporation into products. Therefore, if their relative rates can be perturbed, different levels of water oxygen incorporation should be detected. In this way, the competition and thus the mechanism can be tested. The most straightforward idea is that reaction rates change by varying the temperature. So the reaction with 1-octene as substrate is carried out at 40°C instead of the 20°C normal reaction temperature. Unexpectedly, percentages of products with different oxygen sources remain almost identical to the lower temperature conditions. Even higher temperature, 60°C, is utilized, and at this temperature, the ratio of different isotopomers changes, with isotopomers with one or two oxygen atoms from water generated in lower amounts (Figure 3.16). So obviously, from 20°C to 40°C, both proton scrambling and substrate attack increase their

rates to the same degree that relative ratio of isotopomers does not change. However, by raising the temperature to 60°C, the rate of substrate attack increases more dramatically than that of proton scrambling, and thus the *cis*-diol product with both oxygens from hydrogen peroxide become more predominant.

Another method is used to test the hypothesis. According to the results of substrates competition reactions, the order of preference is dimethyl fumarate, *t*-butyl acrylate, *cis*-cyclooctene and 1-octene. The rate of substrate attack can be tuned by using different substrates, while the same reaction temperature keeps the proton scrambling rate constant. Results are graphically illustrated in Figure 3.15. The predicted trend is indeed evidenced for complexes **1** - **3** (Figure 3.15). For example, with the most favorite substrate, dimethyl fumarate, the rate of substrate attack is the fastest, and thus the time left for proton scrambling is the least among the four used substrates. Significant less amount of product with one oxygen from water is observed, and only trace amount of product with both oxygens from water is detected.

3.8 Conclusions

In sum, I have designed and synthesized a series of novel structurally related facial *N, N, O* ligands based on the inspiration of biological systems. The structures of their respective iron complexes with two ligands are studied thoroughly for the first time in both solid state and in solution. The comparison of their reactive activity demonstrates various ligand effects. So far, two pyridines and one amide are the best combination for facial *N, N, O* ligands. Mechanistic examination with labeling studies reveals an

unprecedented pattern that two oxygen atoms in the *cis*-diol products are from water molecules. This observation is the most convincing evidence for ligand dissociation and O-O bond cleavage. Since one ligand is actually not functioning, future efforts will be directed toward designing ligands employing the rules concluded from this work that coordinate to the iron center in a 1 : 1 ratio.

3.9 Appendix

Table 3.7 Oxidation of styrene catalyzed by iron complexes with *N, N, O*-facial ligands with H_2O_2 as oxidant[a, b]

	1	**2**	**3**	**6**[c]	**8**[d]
diol	8.2(3)	2.0(4)	1.8(2)	8.0(5)	1.7
epoxide	0.2(1)	0.3(1)	<0.1	0.1(1)	2.3
benzaldehyde	0.6(1)	0.8(1)	0.7(1)	0.4(1)	0.6

[a]Reaction conditions: H_2O_2 was added by syringe pump over a 5 min period to a solution of catalyst (0.35 mM) and substrate (0.35 M) in CH_3CN. This solution was stirred for an additional 60 min prior to workup. See Experimental section for further details. Yields expressed as turnover numbers, TON, (μmol product/μmol catalyst). [b]Results were obtained under inert atmosphere by degassing solutions prior to oxidant introduction. [c]Results from ref [99]. [d]Results from ref [70]. Reaction conditions are slightly different in 20 min H_2O_2 addition followed by 40 min additional stirring. See original paper for further details.

Table 3.8 Product analysis from the competition reactions[a]

	epoxide	diol
cis-cyclooctene / 1-octene	0.1(1) / 0	2.4(2) / 1.0(1)
cis-cyclooctene / *t*-butyl acrylate	0.2(1) / 0	0.7(1) / 5.8(2)
cis-cyclooctene / dimethyl fumarate	0.2(1) / 0	0.1(1) / 6.5(1)
1-octene / *t*-butyl acrylate	0 / 0	0.2(1) / 6.2(1)
1-octene / dimethyl fumarate	0 / 0	0 / 6.0(3)
t-butyl acrylate / dimethyl fumarate	0 / 0	0.4(1) / 6.3(2)

[a]Reaction conditions: 10 equiv H_2O_2 was added by syringe pump over a 5-min period (to minimize H_2O_2 disproportionation) at room temperature in air to a solution of catalyst (0.35 mM), 500 equiv substrate 1 and 500 equiv substrate 2 in CH_3CN. This solution was stirred for an additional 60 min before workup. See section 3.2 for further details. Yields expressed as turnover numbers, TON, (μmol product/μmol catalyst).

3.10 Acknowledgements

I would like to thank Mr. Gregory Rohde and Dr. Victor Young, Jr. for solving the structures for **1** and **2** at the X-Ray Crystallographic Laboratory in the Chemistry Department at the University of Minnesota. Also deserving acknowledgements are Dr. Lei Yang and Prof. William Tolman for helping me use FT/IR in their laboratory.

CHAPTER 4

Iron catalyzed olefin epoxidation and *cis*-dihydroxylation by tetraalkylcyclam complexes: the importance of *cis*-labile sites

4.1 Introduction

The mononuclear nonheme oxygenase superfamily of enzymes has been found to be capable of catalyzing a startling array of chemical transformations, including epoxidation and *cis*-dihydroxylation of C=C bonds.[4,133] Of our particular interest in this regard are the Rieske dioxygenases, a class of enzymes that catalyze the *cis*-dihydroxylation of aromatic C=C bonds in the biodegradation of arenes.[26,29] The iron containing active sites of these Rieske dioxygenases[134] are supported by the '2-His-1-carboxylate facial triad' structural motif that characterizes the superfamily to which they belong, leaving up to three *cis*-labile sites for oxygen and/or substrate binding (Figure 4.1).[9,12] Reaction with dioxygen occurs upon $1e^-$ reduction of the ferric resting state of the enzyme and reduction on the Rieske center, which is itself initiated by substrate binding within the active site domain. Injection of a second electron yields a $Fe^{III}(\eta^2\text{-}O_2)$ intermediate that in the case of naphthalene 1,2-dioxygenase (NDO) has been crystallographically characterized.[38] Protonation activates the peroxo for reaction with the substrate, but it is a matter of some debate whether the putative $Fe^{III}(\eta^2\text{-}OOH)$ intermediate *cis*-dihydroxylates the substrate directly, or first undergoes O-O bond heterolysis to form a $HO\text{-}Fe^{V}=O$ active oxidant.[39-44]

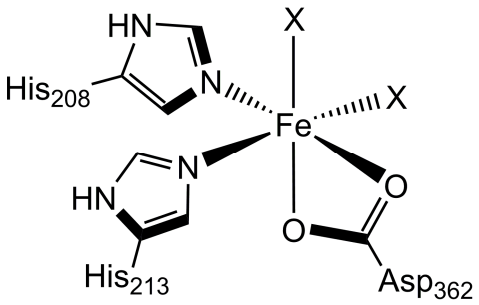

Figure 4.1 Naphthalene 1,2-dioxygenase (NDO) active site.

Catalytic olefin *cis*-dihydroxylation is also an important chemical transformation in synthetic chemistry, where it is usually performed using the OsO_4-based 'Sharpless Asymmetric Dihydroxylation'.[6,73-75] This is a remarkably effective catalytic system, but concerns regarding the high toxicity and cost of osmium and the oxidants used has led to a search for alternatives.[135,136] In the last decade, our group and others have developed examples of first row transition metal catalysts for olefin *cis*-dihydroxylation.[66,67,70,71,95-98,101,104] Of particular note in this regard was a report by Che and co-workers detailing the use of an iron complex of a tetradentate macrocyclic ligand with pyridine and tertiary amine donors to achieve high turnovers on a large reaction scale with oxone as the oxidant,[71] though the E factor (kg waste per kg product) is quite high.[135] Inspired by the Rieske dioxygenases, our own efforts have also focused upon the use of nonheme monoiron catalysts, but we prefer to use H_2O_2 as the terminal oxidant because of its low cost, low E factor, ease of handling, and the fact that its by-products are environmentally benign.[77] Thus far, all effective iron catalysts contain either tetradentate or tridentate ligands, with at least two *cis*-oriented labile coordination sites. On this basis, *cis*-labile sites were proposed to be a key requirement for successful catalytic olefin

dihydroxylation. However, major differences in the donor properties of the ligands used in these studies raises questions regarding the validity of this conclusion. In an effort to clarify this matter, we sought to compare the catalytic properties of the $Fe^{II}(OTf)_2$ complexes of Me_2EBC and TMC (Scheme 4.1), two tetradentate ligands with near identical donor atoms that enforce different coordination geometries. TMC prefers to coordinate in an equatorial fashion and Me_2EBC coordinates facially, which results in a pair of *trans*-labile sites in the former case and *cis*-labile sites in the latter. The resulting systematic study of $[Fe^{II}(TMC)(OTf)](OTf)$ and $[Fe^{II}(Me_2EBC)(OTf)_2]$, and comparison with existing iron(II) catalysts, is rationalized on a mechanistic basis herein and provides unambiguous conclusions regarding the impact of labile site orientation upon the catalytic oxidation of olefins using hydrogen peroxide as the terminal oxidant.

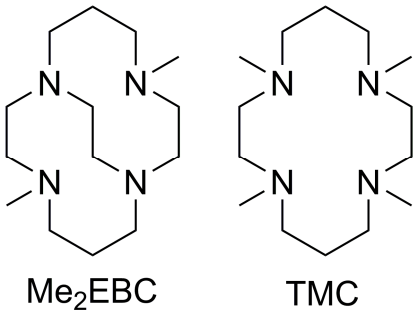

Scheme 4.1 Ligand structures.

4.2 Experimental section

Materials and Synthesis. All reagents and anhydrous diethyl ether (Et_2O) were obtained from Sigma-Aldrich and used as received, unless otherwise noted. All olefin

substrates were passed over basic alumina immediately prior to use. The solvents tetrahydrofuran (THF), dichloromethane (DCM), and acetonitrile (CH_3CN) were purified using a Vacuum Atmospheres Solvent Purifier and degassed prior to use. $H_2{}^{18}O_2$ (90% ^{18}O-enriched, 2 wt% solution in $H_2{}^{16}O$) and $H_2{}^{18}O$ (97% ^{18}O enriched) were purchased from Sigma-Aldrich and Shanghai Engineering Research Center of Stable Isotopes, respectively. $Fe(OTf)_2(CH_3CN)_2$,[103] $Fe(TMC)(OTf)_2$,[141] and $Fe(Me_2EBC)Cl_2$[142,143] were prepared according to literature procedures.

Synthesis of [Fe(Me$_2$EBC)(OTf)$_2$]. A mixture of [$Fe(Me_2EBC)Cl_2$] (265 mg, 0.7 mmol) and AgOTf (358 mg, 1.4 mmol) was stirred overnight in 5 mL CH_2Cl_2. The AgCl precipitate formed during this time was removed by filtration, and the filtrate was reduced in volume and layered with Et_2O. The colorless crystals thereby obtained were isolated by filtration, washed with Et_2O and dried under vacuum to give the product as a white solid (381 mg, 90%). Crystals of [$Fe(Me_2EBC)(OTf)_2$] suitable for X-ray analysis were obtained by vapor diffusion of Et_2O into a concentrated CH_2Cl_2 solution of the complex. See *vide infra* for details regarding X-ray crystallographic analysis and Table 4.1 for crystal data and structure refinement. Characterization of [$Fe(Me_2EBC)(OTf)_2$]: ESI/MS: *m/z* 459 ($[Fe^{II}(Me_2EBC)(OTf)]^+$), 155 ($[Fe^{II}(Me_2EBC)]^{2+}$), both with the expected isotope distribution patterns (Figure 4.5). Anal. Calcd. (found) for $C_{16}H_{30}F_6FeN_4O_6S_2$: C, 31.59 (31.56); H, 4.97 (5.14); N, 9.21 (9.16).

X-ray crystallography analysis of [$Fe(Me_2EBC)(OTf)_2$].

Data collection. A crystal (approximate dimensions 0.36 x 0.16 x 0.10 mm^3) was placed onto the tip of a 0.1 mm diameter glass capillary and mounted on a CCD area

detector diffractometer for a data collection at 123(2) K.[109] A preliminary set of cell constants was calculated from reflections harvested from three sets of 20 frames. These initial sets of frames were oriented such that orthogonal wedges of reciprocal space were surveyed. This produced initial orientation matrices determined from 38 reflections. The data collection was carried out using MoK_α radiation (graphite monochromator) with a frame time of 20 seconds and a detector distance of 4.9 cm. A randomly oriented region of reciprocal space was surveyed to the extent of one sphere and to a resolution of 0.78 Å. Four major sections of frames were collected with 0.30º steps in ω at four different ϕ settings and a detector position of -28º in 2θ. The intensity data were corrected for absorption and decay (SADABS).[110] Final cell constants were calculated from 2493 strong reflections from the actual data collection after integration (SAINT).[111] Please refer to Table 4.1 for additional crystal and refinement information.

Structure solution and refinement. The structure was solved using Bruker SHELXTL[112] and refined using Bruker SHELXTL.[113] The space group Fdd2 was determined based on systematic absences and intensity statistics. A direct-methods solution was calculated which provided most non-hydrogen atoms from the E-map. Full-matrix least squares / difference Fourier cycles were performed which located the remaining non-hydrogen atoms. All non-hydrogen atoms were refined with anisotropic displacement parameters. All hydrogen atoms were placed in ideal positions and refined as riding atoms with relative isotropic displacement parameters. The final full matrix least squares refinement converged to $R1 = 0.0213$ and $wR2 = 0.0551$ (F^2, all data).

Table 4.1 Crystal data and structure refinement for $[Fe(Me_2EBC)(OTf)_2]$

Identification code	07218b	
Empirical formula	$C_{16}\ H_{30}\ F_6\ Fe\ N_4\ O_6\ S_2$	
Formula weight	608.41	
Temperature	123(2) K	
Wavelength	0.71073 Å	
Crystal system	orthorhombic	
Space group	Fdd2	
Unit cell dimensions	a = 8.8289(8) Å	α = 90.00°
	b = 32.69(3) Å	β = 90.00°
	c = 16.3726(15) Å	γ = 90.00°
Volume	4723.8(7) $Å^3$	
Z	8	
Density (calculated)	1.711 Mg/m^3	
Absorption coefficient	0.904 mm^{-1}	
F(000)	2512	
Crystal color, morphology	Colorless, Plate	
Crystal size	0.35 x 0.16 x 0.10 mm^3	
Theta range for data collection	2.49 to 27.49°	
Index ranges	$0 \le h \le 11$, $0 \le k \le 42$, $-20 \le l \le 21$	
Reflections collected	13810	
Independent reflections	2681 [R(int) = 0.0256]	
Observed reflections	2593	
Completeness to theta = 27.49°	99.9%	
Absorption correction	Multi-scan	
Max. and min. transmission	0.9150 and 0.7426	
Refinement method	Full-matrix least-squares on F^2	
Data / restraints / parameters	2681 / 1 / 160	
Goodness-of-fit on F^2	1.097	
Final R indices [I>2sigma(I)]	$R1$ = 0.0213, $wR2$ = 0.0544	
R indices (all data)	$R1$ = 0.0224, $wR2$ = 0.0551	
Largest diff. peak and hole	0.561 and -0.213 $e.Å^{-3}$	

Instrumentation. ^{1}H NMR spectra were recorded on either a Varian Unity 300 or 500 MHz spectrometer at ambient temperature. Chemical shifts (ppm) were referenced to residual protic solvent peaks. High-resolution electrospray mass spectral (ESI-MS) experiments were performed on a Bruker (Billerica, MA) BioTOF II time-of-flight spectrometer, using a spray chamber voltage of 4000 V and a gas carrier temperature of 70°C. Analysis of products from catalytic experiments were performed using a Perkin Elmer AutoSystem gas chromatograph (AT-1701 column, 30 m) with a flame ionization detector. Gas chromatography/mass spectral analyses were performed on an HP 6890 GC (HP-5 MS column, 30 m) with an Agilent 5973 mass analyzer. A 4% NH_3/CH_4 mix was used as the ionization gas for chemical ionization analyses.

Reaction conditions for catalytic oxidations. In a typical reaction, 10 equivalents of H_2O_2 (diluted from 35% H_2O_2 solution with CH_3CN resulting in a 70 mM solution) were delivered by syringe pump under air over a period of 30 min at room temperature (20 ^{o}C) to a vigorously stirred CH_3CN solution containing iron complex and 1000 equivalents of olefin substrate. The final concentrations were 0.7 mM iron complex, 7 mM H_2O_2, and 0.7 M olefin. The solution was stirred for an additional 5 min upon completion of H_2O_2 addition, after which organic products were esterified using 1 mL acetic anhydride together with 0.1 mL 1-methylimidazole. Subsequent to extraction using $CHCl_3$, an internal standard (naphthalene) was added and the solution washed with 1 M H_2SO_4, sat. $NaHCO_3$, and H_2O. The organic layer was dried with $MgSO_4$ and subjected to GC analysis. The products were identified by comparison of their GC retention times with those of authentic compounds.

Substrate limiting reaction conditions. In a typical reaction, H_2O_2 (diluted from 35% H_2O_2 solution with CH_3CN resulting in a 1 M solution) was delivered by syringe pump at a rate of 5 equiv (relative to iron) per minute at room temperature (20 ^oC) in air to a vigorously stirred CH_3CN solution containing iron complex, olefin substrate and additive. The final concentration of iron complex was 0.7 mM. The solution was stirred for an additional 30 min after syringe pump addition, after which organic products were esterified using 1 mL acetic anhydride together with 0.1 mL 1-methylimidazole. Subsequent to extraction using $CHCl_3$, an internal standard (naphthalene) was added and the solution was washed with 1 M H_2SO_4, sat. $NaHCO_3$, and H_2O. The organic layer was dried with $MgSO_4$ and subjected to GC analysis. The products were identified by comparison of their GC retention times with those of authentic compounds.

Isotope labeling studies. Conditions similar to those described above were used for isotope labeling studies, with the following exceptions. In experiments involving $H_2{}^{18}O$, 1000 equivalents of $H_2{}^{18}O$ were added to reaction solution prior to the injection of $H_2{}^{16}O_2$. In experiments involving $H_2{}^{18}O_2$, 10 equivalents of $H_2{}^{18}O_2$ (diluted by CH_3CN from the commercially available 2% $H_2{}^{18}O_2/H_2O$ solution, which contains 1:100 molar ratio of $H_2{}^{18}O$ to $H_2{}^{16}O$) was used instead of H_2O_2. The diol esterification procedure used was the same as that detailed above. The data reported either represent a single reaction, or are the average of 2 reactions. The % ^{18}O values reported were calculated based on the ^{18}O-enrichment of the reagents containing the isotope.

4.3 Structural analysis

The crystal structure of [Fe(Me_2EBC)($OTf)_2$] is shown in Figure 4.2. It shows a C_2-symmetric six-coordinate iron center with the two triflate ligands occupying sites *cis* to each other. The Me_2EBC ligand adopts a *cis*-V stereochemistry associated with tetraalkylcyclam macrocycles due to the constraints imposed by the ethylene bridge that connects N1 and N1',[144] much like the structures of the [Fe(Me_2EBC)Cl_2] and [Mn(Me_2EBC)$(OH)_2]^{2+}$ complexes reported by Busch and co-workers.[143,145] In contrast, the structure of [Fe(Me_2EBC)($OTf)_2$] is clearly distinct from that of the related TMC complex [Fe(TMC)(O_2SPh)](O_2SPh),[146] with the most obvious difference being the binding mode of the macrocyclic ligand to the metal center. Whereas the two remaining coordinating sites on [Fe(Me_2EBC)($OTf)_2$] are oriented *cis* relative to each other and occupied by the triflate anions, the two sites on [Fe(TMC)(O_2SPh)](O_2SPh) are oriented *trans* to one another. However the latter complex is 5-coordinate, with only the site *syn* to the methyl groups being occupied by a ligand. Table 4.2 compares the bond lengths of [Fe(Me_2EBC)($OTf)_2$] with related complexes. [Fe(Me_2EBC)($OTf)_2$] exhibits nearly identical Fe-N bond lengths averaging 2.198 Å, while [Fe(TMC)(O_2SPh)](O_2SPh) has Fe-N bond lengths ranging from 2.176(2) to 2.258(3) Å and averaging 2.215 Å.[146] These distances are typical of high spin iron(II) complexes such as [Fe(Me_2EBC)$(Cl)_2$] (ave. Fe-N = 2.27 Å) and $[Fe(6\text{-}Me_3\text{-}TPA)(CH_3CN)]^{2+}$ (ave. Fe-N = 2.21 Å; 6-Me_3-TPA = tris((6-methylpyridin-2-yl) methyl)amine) but much longer than those of low-spin $[Fe(TPA)(CH_3CN)_2]^{2+}$ (ave. Fe-N = 1.96 Å).[147]

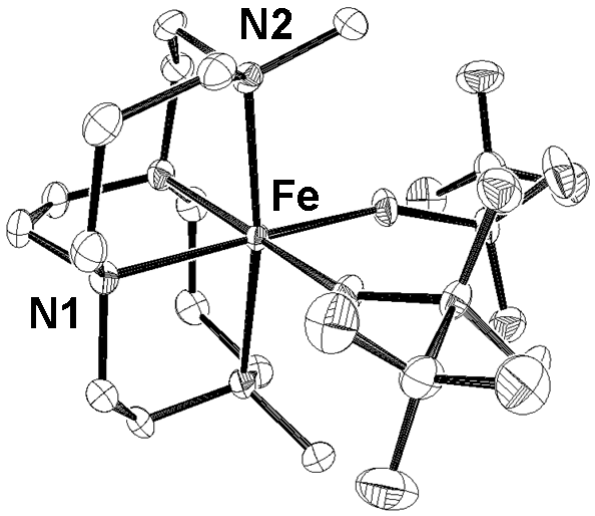

Figure 4.2 ORTEP plot of [Fe(Me_2EBC)($OTf)_2$] showing 50% probability thermal ellipsoids. Hydrogen atoms have been omitted for clarity.

Table 4.2 Bond lengths (Å) observed in complexes mentioned in this work

	Fe-N1	Fe-N2	Fe-N3	Fe-N4	ref
[Fe(Me_2EBC)($OTf)_2$]	2.197(1)	2.199(1)			This work
[Fe(Me_2EBC)Cl_2]	2.2574(13)	2.2634(13)	2.2866(14)	2.2748(13)	143
[Fe(TMC)(O_2SPh)]$^+$	2.231(3)	2.176(2)	2.258(3)	2.196(2)	146
[Fe(TPA)($CH_3CN)_2$]$^{2+}$	1.99(1)	1.97(1)	1.92(1)	1.95(1)	147
[Fe(6-Me_3-TPA)($CH_3CN)_2$]$^{2+}$	2.15(1)	2.25(1)	2.18(1)	2.24(1)	147

NMR spectroscopy is a useful tool for assessing solution structure. Consistent with having an S = 2 spin-state, [Fe^{II}(Me_2EBC)($OTf)_2$] exhibits a ^{1}H NMR spectrum in CD_3CN solution with a series of well-defined paramagnetically shifted and broadened resonances (Figure 4.3A). The number of peaks observed indicates that the C_2-

symmetric solid-state structure of the complex is retained in solution. In contrast, the ^{1}H-NMR spectrum of [Fe^{II}(TMC)(OTf)](OTf) has a smaller number of resonances (Figure 4.3B) due to its C_{2V} symmetry. Notably, the CD_3CN solution ^{19}F NMR spectra of both complexes exhibit a single peak at -79.6 ppm (Figure 4.3C and D), which is associated with free triflate. In contrast, the ^{19}F-NMR spectrum of [Fe^{II}(Me_2EBC)$(OTf)_2$] in CD_2Cl_2 shows only one peak but with a chemical shift associated with bound triflate (Figure 4.3E), while the ^{19}F-NMR spectrum of [Fe^{II}(TMC)(OTf)](OTf) shows two peaks associated with one free triflate and one bound triflate (Figure 4.3F). The ^{19}F-NMR data in acetonitrile solution thus indicate that the triflate ligands are displaced by solvent molecules and that the catalyst precursors are in fact the dicationic complexes $[Fe^{II}(Me_2EBC)(MeCN)_2]^{2+}$ and $[Fe^{II}(TMC)(MeCN)_2]^{2+}$.

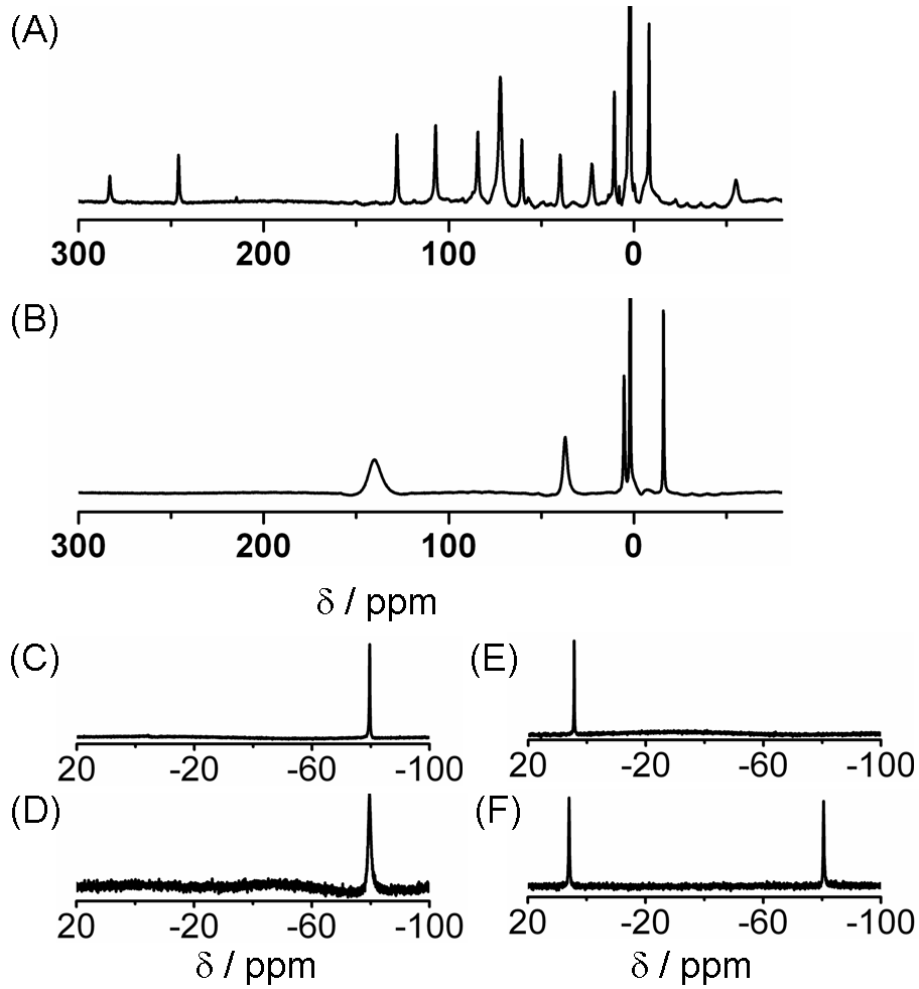

Figure 4.3 NMR spectra of [Fe(Me_2EBC)($OTf)_2$] and [Fe(TMC)(OTf)](OTf). (A) ^{1}H NMR of [Fe(Me_2EBC)($OTf)_2$] in CD_3CN; (B) ^{1}H NMR of [Fe(TMC)($OTf)_2$] in CD_3CN; (C) ^{19}F-NMR of [Fe(Me_2EBC)($OTf)_2$] in CD_3CN; (D) ^{19}F-NMR of [Fe(TMC)(OTf)](OTf) in CD_3CN; (E) ^{19}F-NMR of [Fe(Me_2EBC)($OTf)_2$] in CD_2Cl_2; (F) ^{19}F-NMR of [Fe(TMC)(OTf)](OTf) in CD_2Cl_2.

ESI-MS shows that [Fe(Me_2EBC)($OTf)_2$] maintains the same structure as shown in the crystal and it exhibits the same pattern as predicted from the molecule (Figure 4.4).

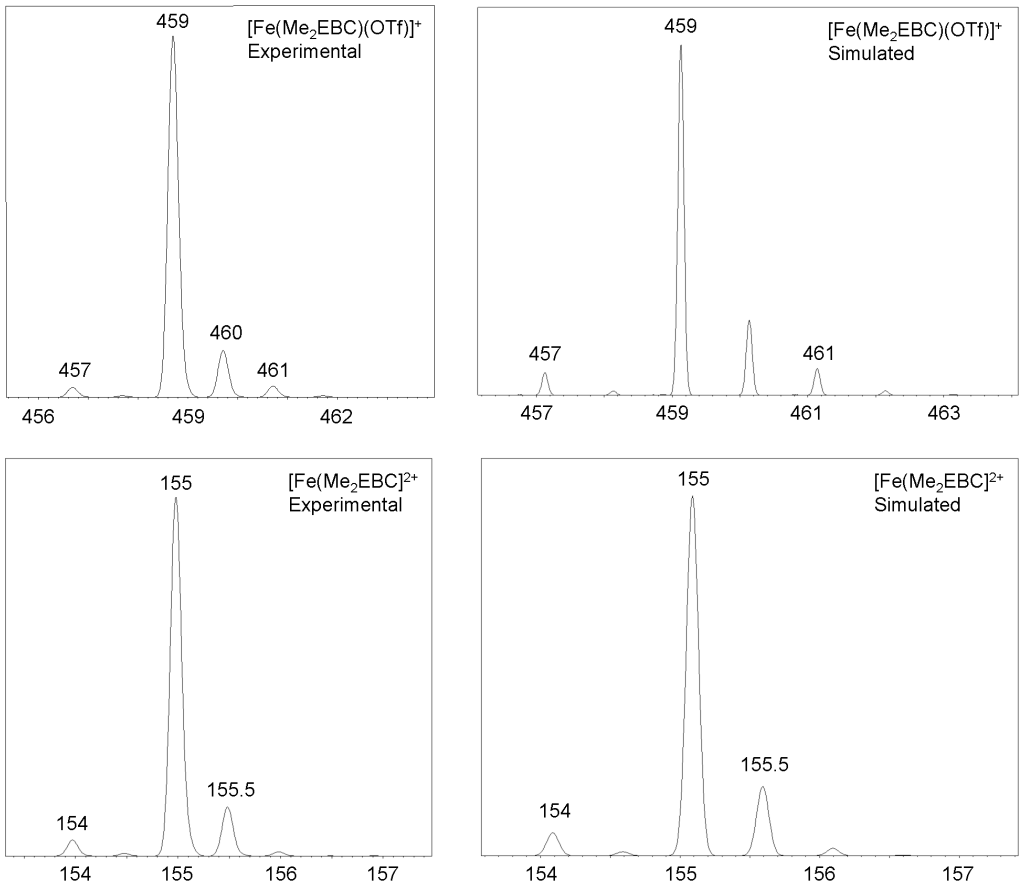

Figure 4.4 Isotope distribution patterns for the major peaks in the ESI-MS spectrum of [Fe(Me$_2$EBC)(OTf)$_2$].

4.4 Catalytic activities

Olefin oxidation. Table 4.3 lists the catalytic activities of [Fe(Me$_2$EBC)(OTf)$_2$] in the oxidation of various olefins with H_2O_2 as the oxidant. To allow direct comparison with published data, reactions were conducted using the conditions previously detailed for studies with [Fe(TPA)(OTf)$_2$].[66] To simplify mechanistic studies and achieve high conversion of H_2O_2 into olefin oxidation product, a large excess of substrate was used and the H_2O_2 solution was introduced to the reaction system by a syringe pump over a

period of 30 min to avoid its disproportionation.

Table 4.3 shows that [Fe(Me_2EBC)($OTf)_2$] is a more effective catalyst for the oxidation of electron-rich olefins than for electron-poor ones (Table 4.3, entries 1 – 5). With cyclooctene as substrate, a 62% conversion of H_2O_2 into products was observed, with a diol-to-epoxide ratio of 2.4. With *cis*-2-heptene as substrate, a 52% conversion of H_2O_2 into products was achieved, with a diol-to-epoxide ratio of 3.7. In the case of 1-octene as substrate, the percentage conversion of H_2O_2 into products decreased to 24%, but the diol-to-epoxide ratio increased to 7. For the oxidation of electron-poor olefins like *t*-butyl acrylate and dimethyl fumarate, *cis*-dihydroxylation was strongly favored, but the yields of diol were low. Oxidation of *cis*-2-heptene as a probe substrate yielded the major *cis*-diol product with >99% retention of configuration, while the minor epoxide product showed a 60% retention of configuration. Retention of configuration at these levels precludes *cis*-diol formation via epoxide ring opening and provides strong evidence for the involvement of a metal-based oxidant because values of this magnitude cannot be obtained with a free radical oxidant like HO•.

Interestingly, the closely related [Fe(TMC)(OTf)](OTf) complex is inactive as a catalyst for olefin oxidation. No *cis*-dihydroxylation of *cis*-cyclooctene was observed, and at best one turnover of the epoxide product was obtained (Table 4.3, entry 6). As [Fe(Me_2EBC)($OTf)_2$] and [Fe(TMC)(OTf)](OTf) differ primarily in the orientation of the two potential labile sites at the iron center, the difference in their catalytic behavior supports the notion that two *cis*-labile sites are needed to promote this type of catalytic reactivity.

Table 4.3 Olefin oxidation catalyzed by [$Fe^{II}(Me_2EBC)(OTf)_2$] and related complexes[a]

entry	ligand	olefin	epoxide [%RC][b]	*cis*-diol [%RC][b]	ref
1	Me_2EBC	*cis*-cyclooctene	1.8(1)	4.4(1)	This work
2	Me_2EBC	1-octene	0.3(1)	2.1(4)	This work
3	Me_2EBC	*cis*-2-heptene	1.1(1) [60]	4.1(1) [100]	This work
4	Me_2EBC	*t*-butyl acrylate	0.1(1)	0.9(3)	This work
5	Me_2EBC	dimethyl fumarate	0	0.4(1)	This work
6	TMC	*cis*-cyclooctene	1.0(1)	0	This work
7	TPA	*cis*-cyclooctene	3.4(1)	4.0(2)	66
8	6-Me_3-TPA	*cis*-cyclooctene	0.7(2)	4.9(6)	66
9	No complex	*cis*-cyclooctene	0	0	This work

[a]Reaction conditions: 10 equiv H_2O_2 was added by syringe pump over a 30-min period (to minimize H_2O_2 disproportionation) at room temperature under air to a solution of 0.7 mM catalyst and 1000 equiv substrate in CH_3CN. This solution was stirred for an additional 5 min before workup. See Experimental section for further details. Yields expressed as turnover numbers, TON, (μmol product/μmol catalyst). [b]%RC, the percentage of retention of configuration of stereochemistry in the products of *cis*-2-heptene oxidation, expressed as $100 \times (A - B)/(A + B)$, where A = yield of *cis*-diol or *cis*-epoxide with retention of configuration and B = yield of epimer.

Catalytic oxidation with additives. In previous work, the catalytic behavior of [Fe(TPA)$(OTf)_2$] and [Fe(BPMEN)$(OTf)_2$] was found to be influenced by the presence of additives, with the addition of acetic acid resulting in increased turnover numbers and near exclusive formation of epoxide.[64,148,149] Similarly, the addition of 10 equiv AcOH to

[$Fe(Me_2EBC)(OTf)_2$]-catalyzed *cis*-cyclooctene oxidation reactions led to increased yields of products, with the overall conversion of H_2O_2 to product rising from 62% to 75%, and the product distribution shifted to favor almost exclusive formation of epoxide (Table 4.4, entry 4). On the other hand, the addition of 10 equiv of $HClO_4$ essentially killed the reaction, and even 1 equiv $HClO_4$ was sufficient to inhibit catalysis significantly (Table 4.4, entry 12 and 13). These observations show that the role of acetic acid is not just to serve as a proton source. Catalytic activity was also almost completely lost with the addition of 10 equiv NaOAc or 2,6-lutidine (Table 4.4, entries 14 and 15, respectively), which suggests that bases, whether coordinating or non-coordinating, are inimical to catalysis. The addition of 1000 equiv HOAc to the [Fe(TMC)(OTf)](OTf)-catalyzed *cis*-cyclooctene oxidation reaction only served to decrease the yield of epoxide from 1 turnover to 0.3 (Table 4.4, entry 16).

In a more systematic study of the effect of acetic acid (Figure 4.5 and Table 4.4, entries 2 – 7), we found that even as little as 0.5 equiv HOAc was sufficient to perturb the epoxide-to-diol ratio, and the maximum effect was attained with as little as 10 equiv. Carboxylic acids with lower pKa (i.e. chloroacetic acid (pK_a = 2.9) and dichloroacetic acid (pK_a = 1.3)) were also effective at suppressing diol formation and shifting the product mixture only to epoxide, but the percentage conversion of H_2O_2 to product was lower than that for acetic acid (Table 4.4, entries 8 and 10). Adding more equivalents of chloroacetic acid and dichloroacetic acid increased conversion of H_2O_2 to epoxide (Table 4.4, entries 9 and 11). The overall effect of acetic acid and its derivatives is illustrated in Figure 4.6. Taken together, these results can be rationalized by the

existence of a binding equilibrium resulting from coordination the added acid to the iron center, as postulated previously for [Fe(TPA)$(OTf)_2$], with the acid having the largest pK_a being a better ligand. The coordination of the carboxylic acid to the iron center promotes the epoxidation of *cis*-cyclooctene. The effect of acetic acid is also examined for other substrates (Figure 4.7). The similar pattern was also observed for 1-octene and *cis*-2-heptene. With 1000 equiv AcOH, both reactions are shifted towards epoxidation.

Table 4.4 Olefin oxidation catalyzed by [Fe(Me_2EBC)($OTf)_2$] with different additives[a]

Entry	additive	epoxide	*cis*-diol
1	—	1.8(1)	4.4(1)
2	0.5 AcOH	2.2	2.1
3	1 AcOH	3.8	1.7
4	10 AcOH	7.5	0.2
5	100 AcOH	7.6	0.1
6	1000 AcOH	7.3(1)	0
7	3000 AcOH	7.6	0
8	10 $ClCH_2COOH$	4.5	0.3
9	100 $ClCH_2COOH$	5.6	0
10	10 $Cl_2CHCOOH$	1.4	0.1
11	100 $Cl_2CHCOOH$	3.1	0
12	1 $HClO_4$	0.2	0.9
13	10 $HClO_4$	0.2(1)	0.3(1)
14	10 NaOAc	0.5(1)	0
15	10 2,6-lutidine	0.1	0.5
16[b]	1000 AcOH	0.3	0

[a]Reaction conditions: 10 equiv H_2O_2 was added by syringe pump over a 30 min period (to minimize H_2O_2 disproportionation) at room temperature in air to a solution of catalyst (0.7 mM), 1000 equiv *cis*-cyclooctene and additive in CH_3CN. This solution was stirred for an additional 5 min before workup. See section 4.2 for further details.

Yields expressed as turnover numbers, TON, (μmol product/μmol catalyst). [b]Olefin oxidation carried out by [Fe(TMC)(OTf)](OTf).

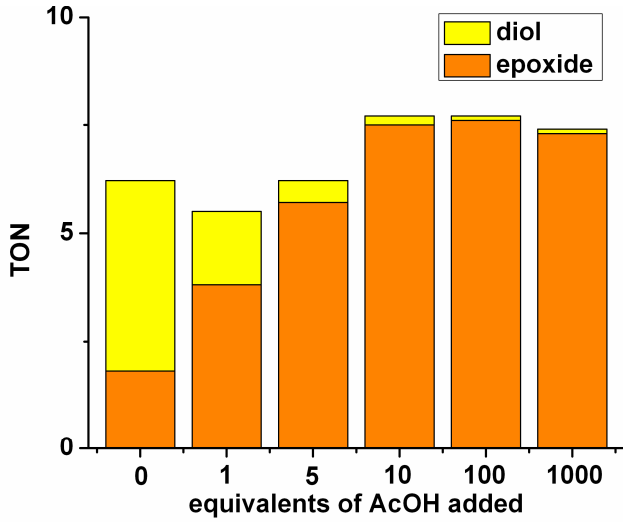

Figure 4.5 *cis*-Cyclooctene oxidation catalyzed by [Fe(Me_2EBC)($OTf)_2$] with various equivalents of AcOH as additives.

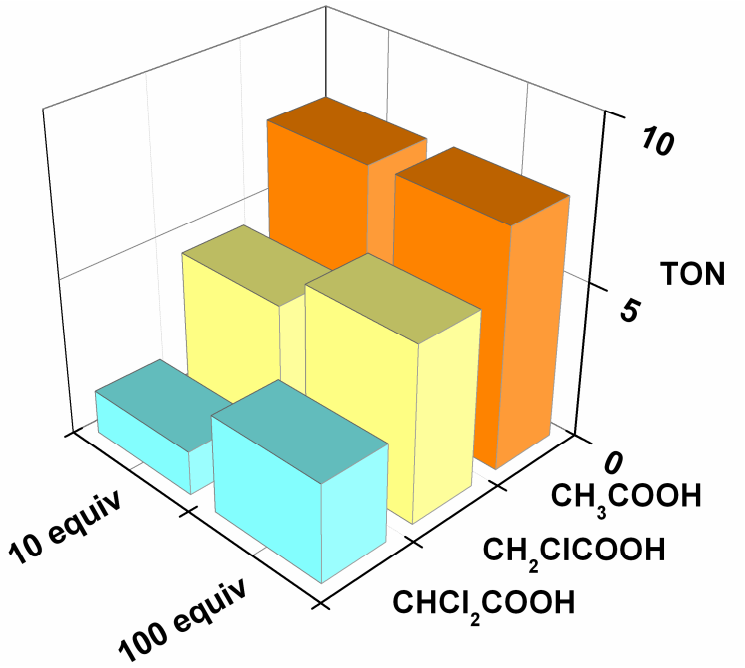

Figure 4.6 Effect of acids with various pKa values.

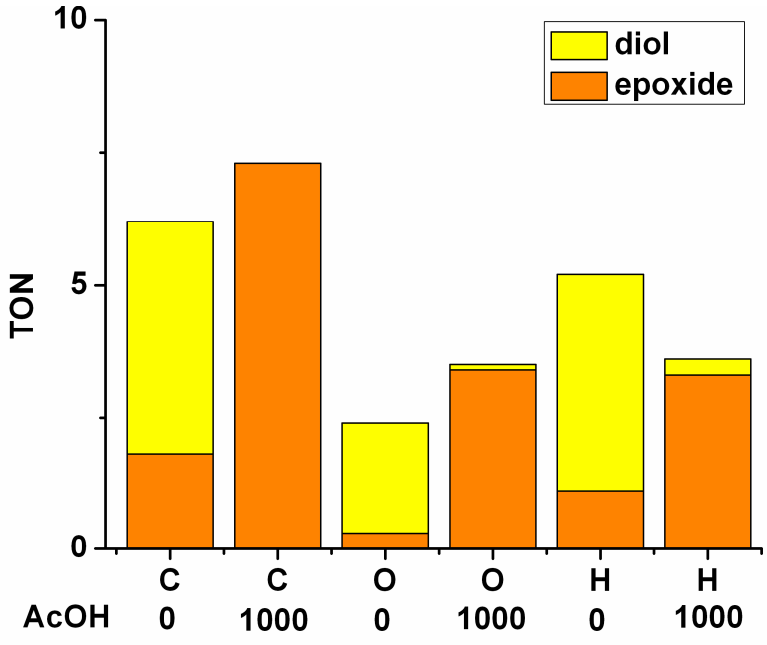

Figure 4.7 AcOH effect in the [Fe(Me_2EBC)($OTf)_2$] catalyzed olefin oxidation. C: *cis*-cyclooctene; O: 1-octene; H: *cis*-2-heptene.

Substrate limiting conditions. Given the positive effects of adding HOAc to the yield of epoxide, we explored more synthetically practical reaction conditions using 0.14 M *cis*-cyclooctene and 0.21 M H_2O_2, where substrate was the limiting reagent (Table 4.5). With 0.5 mol% [Fe(Me_2EBC)($OTf)_2$] catalyst, 13% of substrate was converted into *cis*-diol (TON = 26) and 10% for epoxide (TON = 20). Upon addition of 0.7 M HOAc to the reaction mixture, the epoxide yield increased fivefold to 62% (TON = 124) and the diol yield was suppressed to only 1%. While the overall yield of products in the absence of HOAc was lower for [Fe(Me_2EBC)($OTf)_2$] than for [Fe(TPA)($OTf)_2$] (69%), the overall yield improved significantly in the presence of 0.7 M HOAc for [Fe(Me_2EBC)($OTf)_2$], while it dropped to 42% for [Fe(TPA)($OTf)_2$].[64] On the other hand, comparisons with the epoxide-selective complex [Fe(BPMEN)($OTf)_2$][64] showed that [Fe(Me_2EBC)($OTf)_2$] was less effective as a catalyst, with or without adding AcOH. These results raise the possibility of developing practical applications of these complexes in synthetic chemistry.

Table 4.5 *cis*-Cyclooctene oxidation catalyzed by iron complexes at 0.5 mol% catalyst loading[a]

entry	Complex	Temp (°C)	additive	Conv-ersion	Yield epoxide[c]	*cis*-diol[c]
1	$[Fe(Me_2EBC)(OTf)_2]$	20	—	44%	10%	13%
2	$[Fe(Me_2EBC)(OTf)_2]$	20	0.07 M HOAc	64%	55%	2%
3	$[Fe(Me_2EBC)(OTf)_2]$	20	0.7 M HOAc	77%	62%	1%
4[b]	$[Fe(Me_2EBC)(OTf)_2]$	20	0.7 M HOAc	52%	35%	1%
5	$[Fe(Me_2EBC)(OTf)_2]$	0	—	25%	5%	10%
6	$[Fe(Me_2EBC)(OTf)_2]$	0	0.7 M HOAc	77%	67%	1%
7[c]	$[Fe(TPA)(OTf)_2]$	0	—	n.r.	32%	37%
8[c]	$[Fe(TPA)(OTf)_2]$	0	0.7 M HOAc	n.r.	40%	2%
9[c]	$[Fe(BPMEN)(OTf)_2]$	0	—	n.r.	72%	3%
10[c]	$[Fe(BPMEN)(OTf)_2]$	0	0.7 M HOAc	n.r.	93%	1%

[a]Reaction conditions: H_2O_2 was added by syringe pump at a rate of 5 equiv/min (relative to catalyst, to minimize H_2O_2 disproportionation) in air to a CH_3CN solution of 0.7 mM catalyst, 0.14 M *cis*-cyclooctene. After syringe pump addition was completed, the reaction was stirred for another 30 min. [b]Oxidant is injected all at once. [c]Results from 64. Experiments were done at a catalyst concentration of 1 mM. [c]Yield is based on the substrate.

4.5 Competition reactions

Substrate competition studies provided further insight into the nature of the iron-based oxidant. Four substrates were selected for pairwise competition experiments, where equimolar amounts of two different substrates were oxidized under normal catalytic and work-up conditions. As shown in Figure 4.8 and Table 4.6, the [Fe(Me_2EBC)($OTf)_2$] catalyst favored the oxidation of the more electron-rich olefin, with the order of oxidation preference found to be *cis*-cyclooctene > 1-octene > *t*-butyl acrylate > dimethyl fumarate. This order implicates the formation of an electrophilic oxidant, which indicates that [Fe(Me_2EBC)($OTf)_2$] is a Class A catalyst. Class A catalysts, such as [Fe(TPA)($OTf)_2$], preferentially oxidize electron-rich olefins and carry out both epoxidation and *cis*-dihydroxylation of olefins (Table 4.3, entry 7). On the other hand, Class B catalysts, exemplified by [Fe(6-Me_3-TPA)($OTf)_2$] (Table 4.3, entry 8), selectively perform olefin *cis*-dihydroxylation and oxidize electron-poor olefins like acrylate and fumarate more rapidly than electron-rich olefins.[150]

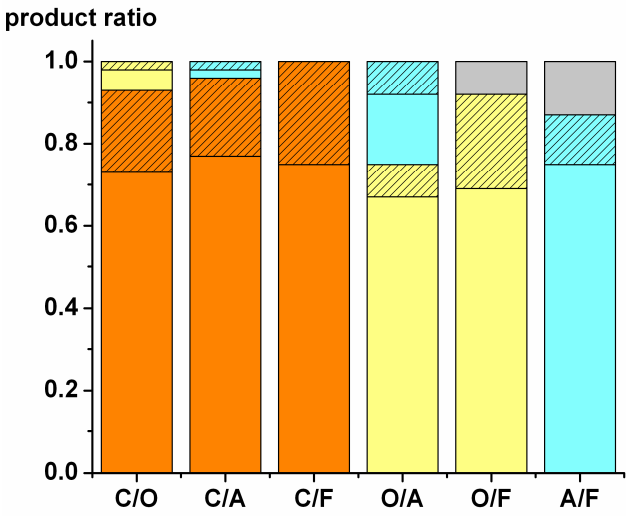

Figure 4.8 Competition oxidation results with equal amounts of two substrates catalyzed by [Fe(Me_2EBC)($OTf)_2$]. C: *cis*-cyclooctene oxidation products in orange; O: 1-octene oxidation products in yellow; A: *t*-butyl acrylate oxidation products in cyan; F: dimethyl fumarate oxidation product in grey. Solid bars correspond to amount of *cis*-diol formed, while shaded bars correspond to amount of epoxide formed.

Table 4.6 Product analysis from the competition reactions[a]

	epoxide	diol
cis-cyclooctene / 1-octene	1.0(1) / <0.1	3.6(2) / 0.2(1)
cis-cyclooctene / *t*-butyl acrylate	0.9(2) / 0.1(1)	3.7(2) / 0.1(1)
cis-cyclooctene / dimethyl fumarate	1.4(1) / 0	4.1(2) / 0
1-octene / *t*-butyl acrylate	0.1(1) / 0.1(1)	0.8(1) / 0.2(1)
1-octene / dimethyl fumarate	0.3(1) / 0	0.9(2) / <0.1
t-butyl acrylate / dimethyl fumarate	0.1(1) / 0	0.6(1) / 0.1(1)

[a]Reaction conditions: 10 equiv H_2O_2 was added by syringe pump over a 30 min period (to minimize H_2O_2 disproportionation) at room temperature in air to a solution of catalyst (0.7 mM), 500 equiv substrate 1 and 500 equiv substrate 2 in CH_3CN. This solution was stirred for an additional 5 min before workup. See Experimental section for further details. Yields expressed as turnover numbers, TON, (μmol product/μmol catalyst).

4.6 Isotopic labeling studies

^{18}O labeling experiments have proven useful in previous studies for deducing whether peroxide O-O bond cleavage occurs prior to the attack of substrate by establishing the source of the oxygen atoms incorporated into product.[66,104] As commercially available $H_2{}^{18}O_2$ usually comes as a 2 wt% solution in $H_2{}^{16}O$, the 10 equivalents of $H_2{}^{18}O_2$ typically added in our labeling experiments was accompanied by 1000 equiv $H_2{}^{16}O$. To corroborate these results, complementary labeling experiments

with 10 equiv $H_2{}^{16}O_2$ and 1000 equiv $H_2{}^{18}O$ were also carried out. Previous experiments carried out for [Fe(TPA)$(OTf)_2$] and [Fe(6-Me_3-TPA)$(OTf)_2$] with *cis*-cyclooctene as substrate revealed two distinct labeling patterns.[66] For Class A catalyst [Fe(TPA)$(OTf)_2$], the *cis*-diol product incorporated one oxygen atom from H_2O_2 and the other from H_2O, results that led us to postulate a water-assisted mechanism for activating the peroxo O-O bond for cleavage. In contrast, for Class B catalyst [Fe(6-Me_3-TPA)$(OTf)_2$], both diol oxygens derived exclusively from H_2O_2, thereby requiring a non-water-assisted pathway for H_2O_2 activation.

Analogous ^{18}O labeling experiments were carried out with [Fe(Me_2EBC)$(OTf)_2$]. Table 4.7 shows the percentage of ^{18}O incorporation into the epoxide and *cis*-diol products obtained from both $H_2{}^{18}O_2/H_2{}^{16}O$ and $H_2{}^{16}O_2/H_2{}^{18}O$ experiments. The [Fe(Me_2EBC)$(OTf)_2$]-catalyzed oxidation of *cis*-cyclooctene with $H_2{}^{18}O_2$ in the presence of 1000 equiv of $H_2{}^{16}O$ afforded epoxide with 82% incorporation of the ^{18}O label. When $H_2{}^{16}O_2$ was used in the presence of 1000 equiv of $H_2{}^{18}O$, 16% of the epoxide was ^{18}O-labeled, a result complementary to the $H_2{}^{18}O_2$ experiment. Distinct from the epoxide labeling pattern, the *cis*-diol product showed dominant incorporation of one oxygen atom each from H_2O_2 and H_2O. Thus, all the oxygen present in both epoxide and diol products derived either from H_2O_2 or H_2O for epoxide and diol, with essentially no involvement of O_2 from air due to autoxidation. Additional labeling experiments were carried out as a function of $H_2{}^{18}O$ concentration. As shown in Figure 4.9 and previously demonstrated for [Fe(TPA)$(OTf)_2$],[66] the incorporation of ^{18}O from $H_2{}^{18}O$ into the epoxide and *cis*-diol products exhibits saturation behavior. This saturation behavior

suggests a pre-equilibrium binding of H_2O to the iron center during the catalytic cycle, which is also illustrated by the linearity of the double reciprocal plot of the data (Figure 4.9, insets).

Table 4.7 Labeling results of *cis*-cyclooctene oxidation catalyzed by $[Fe(L)(OTf)_2]$[a]

		epoxide		*cis*-diol		
		unlabeled	labeled	unlabeled	singly labeled	doubly labeled
Me_2EBC	$H_2{}^{18}O_2$ (2%)[a]	18%	82%	5%	88%	7%
Me_2EBC	1000 $H_2{}^{18}O$[b]	84%	16%	13%	86%	1%
TPA[c]	1000 $H_2{}^{18}O$[b]	90%	9%	14%	86%	—
BPMEN[d]	1000 $H_2{}^{18}O$[b]	70%	30%	40%	60%	—
^{Me2}PyTACN[e]	1000 $H_2{}^{18}O$[b]	35%	65%	12%	88%	—

[a]Reaction conditions: 10 equiv $H_2{}^{18}O_2$ was added by syringe pump over a 30 min period at room temperature in air to a solution of catalyst (0.7 mM) and 1000 equiv *cis*-cyclooctene in CH_3CN. [b]Reaction conditions: 10 equiv H_2O_2 was added by syringe pump over a 30 min period at room temperature in air to a solution of catalyst (0.7 mM), 1000 equiv *cis*-cyclooctene and 1000 equiv $H_2{}^{18}O$ in CH_3CN. [c]Results from ref. 66. [d]Results from ref 151. [e]Results from ref 67.

The incorporation of label from water into the oxidation products requires the participation of an oxidant that is able to undergo exchange with water in the course of

the catalytic cycle. These labeling results are similar to those observed for *cis*-cyclooctene oxidation catalyzed by other [Fe(L)(OTf)$_2$] complexes (L = TPA, BPMEN, and ^{Me2}PyTACN) (Table 4.7), but the extent of label incorporation from water into the epoxide product depends on the nature of tetradentate ligand. These variations are likely controlled by several factors including: a) the affinity of the iron center for the water ligand, b) the rate of label exchange with the oxidant, and c) the rate of reaction between the oxidant and the olefin. The labeling results for [Fe(Me$_2$EBC)(OTf)$_2$] most closely resemble those of [Fe(TPA)(OTf)$_2$].

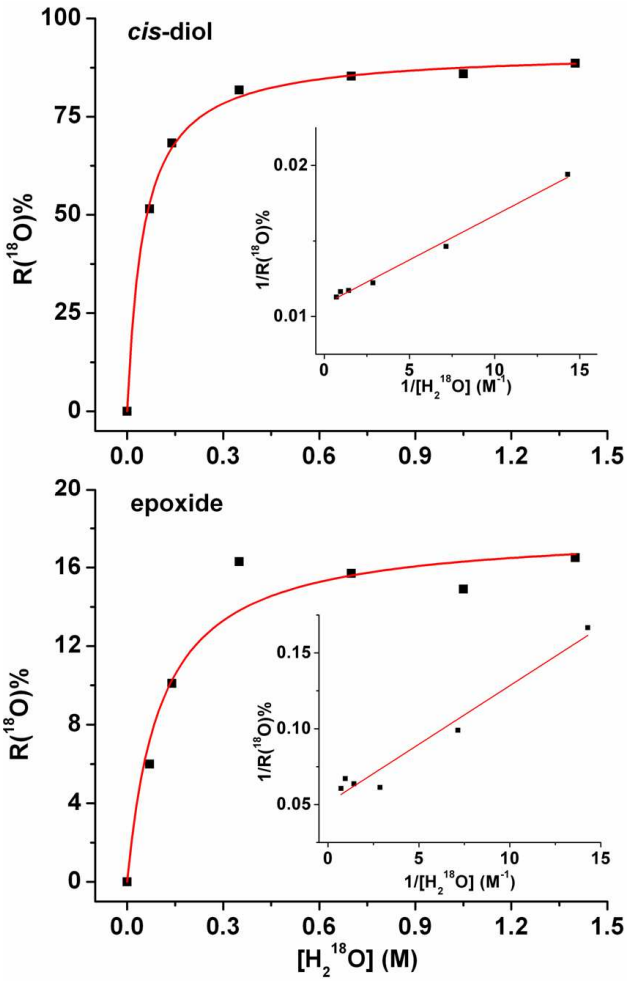

Figure 4.9 Percentage of ^{18}O-labeled epoxide and *cis*-diol product in the oxidation of *cis*-cyclooctene catalyzed by [Fe(Me$_2$EBC)(OTf)$_2$] with H_2O_2 as a function of the concentration of $H_2{}^{18}O$. Inset: double-reciprocal plot.

4.7 Mechanistic considerations

For [Fe(TPA)(OTf)$_2$], the prototypical Class A catalyst, it is generally accepted that an Fe^{III}/Fe^{V} pair is involved in the catalytic cycle with an HO-Fe^{V}=O species as the active oxidant,[66] a notion supported by DFT calculations.[152,153] This proposed mechanism is outlined in Scheme 1 and is based on the following observations: (1) the

characterization of a low spin Fe^{III}-OOH complex in CH_3CN at -40 °C; (2) ^{18}O labeling experiments showing that one atom of the *cis*-diol product derives from water; and (3) the more rapid oxidation of more electron-rich olefins over electron-poor ones, implicating an electrophilic oxidant. This mechanism is distinct from that developing for Class B catalysts, which is proposed to involve an Fe^{II}/Fe^{IV} cycle with $Fe^{IV}(OH)_2$ as the active oxidant.[104]

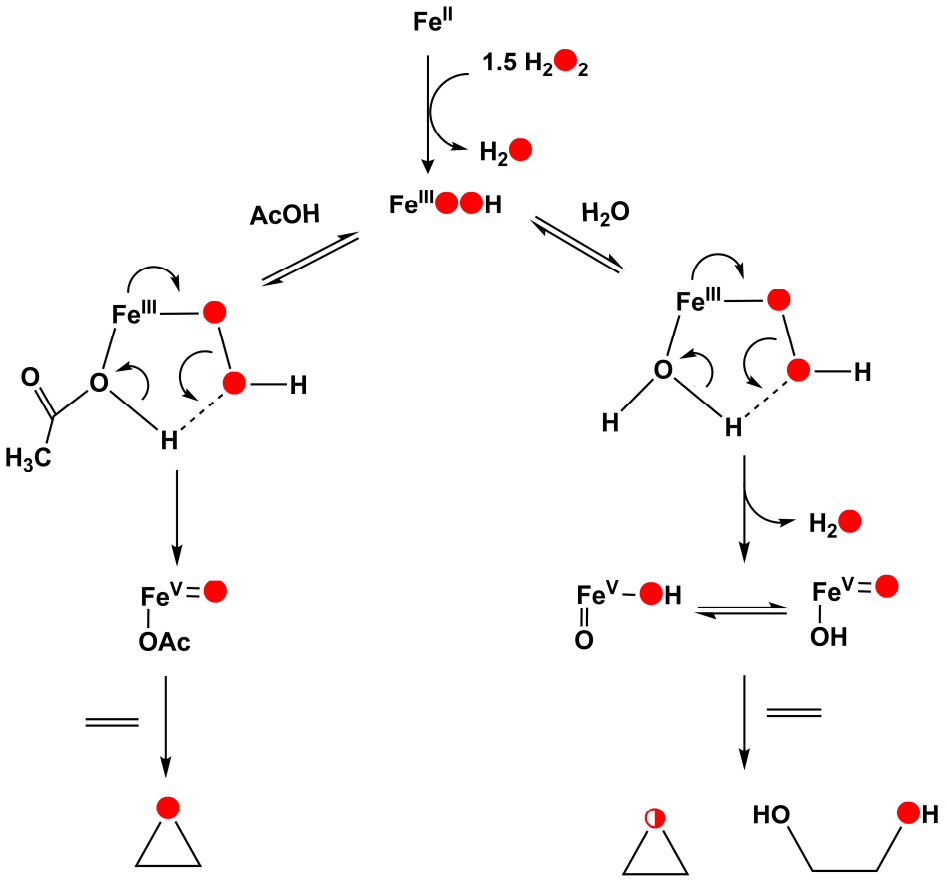

Scheme 4.2 Proposed mechanism.

The catalytic results with $[Fe(Me_2EBC)(OTf)_2]$ show a reactivity pattern very

similar to that for [Fe(TPA)(OTf)$_2$][66] and therefore classify [Fe(Me$_2$EBC)(OTf)$_2$] as a Class A catalyst. As implied in Scheme 4.2, the iron(II) catalyst must first be oxidized to iron(III) before the Fe^{III}–OOH intermediate can be formed and catalysis initiated. Such a lag phase was indeed observed for [Fe^{II}(TPA)(OTf)$_2$], with the first 0.5 equiv H_2O_2 added not producing any product.[66] Similarly, the addition of 0.5 equiv H_2O_2 to [Fe^{II}(Me$_2$EBC)(OTf)$_2$] afforded negligible quantities of product in both the absence and presence of added HOAc (Table 4.8, Appendix).

Labeling studies show that water is involved in the mechanism and the observed saturation behavior in the extent of label incorporation from water suggests pre-equilibrium water binding to the metal center prior to O–O bond cleavage. Water is postulated to bind to a Fe^{III}–OOH center, which has yet to be observed for [Fe^{II}(Me$_2$EBC)(OTf)$_2$], to form a five-membered ring by hydrogen bonding to the terminal oxygen atom of the hydroperoxide. This interaction is thought to promote heterolytic cleavage of the O–O bond to form an HO–Fe^{V}=O oxidant that is responsible for olefin epoxidation and *cis*-dihydroxylation, thereby rationalizing the ^{18}O labeling results that show water incorporation into both epoxide and *cis*-diol products. HOAc added in the reaction replaces the water ligand and serves as the proton donor that promotes O–O bond heterolysis. The resultant AcO–Fe^{V}=O oxidant is only capable of oxo transfer to the olefin substrate leading to exclusive epoxide formation.

4.8 Conclusions

Considering the structural similarity of the macrocyclic ligands in

[Fe(TMC)(OTf)](OTf) and [Fe(Me_2EBC)($OTf)_2$], it is remarkable that the latter is so much more reactive than the former in catalyzing olefin oxidation. The positive effect of HOAc addition on product yield and epoxide selectivity for [Fe(Me_2EBC)($OTf)_2$] catalysis is attributed to acetic acid binding to the iron center and its facilitation of O–O bond cleavage due to its proximity to the Fe^{III}–OOH unit, as previously proposed for [Fe(TPA)($OTf)_2$].[64] This is not possible for [Fe(TMC)(OTf)](OTf). Not only does HOAc addition not exert an enhancing effect, it is in fact inimical to the reactivity of the complex, The difference in catalytic activity between [Fe(TMC)(OTf)](OTf) and [Fe(Me_2EBC)($OTf)_2$] emphasizes the importance of the *cis* orientation of the two labile sites in [Fe(Me_2EBC)($OTf)_2$] and supports the proposed mechanism.

4.9 Appendix

Table 4.8 Olefin oxidation by [Fe(Me_2EBC)($OTf)_2$] with 0.5 equiv H_2O_2[a]

Additive	epoxide	*cis*-diol
N/A	<0.1	0
1000 AcOH	0.1(1)	0

[a]Reaction conditions: 0.5 equiv H_2O_2 was added by syringe pump over a 1.5 min period at room temperature in air to a solution of catalyst (0.7 mM) and 1000 equiv *cis*-cyclooctene in CH_3CN. This solution was stirred for an additional 5 min before workup. See Experimental section for further details. Yields expressed as turnover numbers, TON, (μmol product/μmol catalyst).

4.10 Acknowledgements

I would like to thank Dr. Jason England for introducing the complex $[Fe(Me_2EBC)(OTf)_2]$ into our laboratory and providing valuable suggestions. I also would like to thank Mr. Gregory Rohde and Dr. Victor Young, Jr. for solving the structure for $[Fe(Me_2EBC)(OTf)_2]$ at the X-Ray Crystallographic Laboratory in the Chemistry Department at the University of Minnesota.

CHAPTER 5

Reactivity studies of iron complexes with tetradentate N2Py2 ligands

5.1 Introduction

Nature has evolved a number of nonheme iron oxygenases capable of the stereoselective oxidation of C=C bonds.[4,20] Among these enzymes, Rieske dioxygenases are of particular interest to us, because they are bacterial enzymes that can catalyze the O_2-dependent enantioselective *cis*-dihydroxylation of arene and olefin double bonds.[29,32,33,40,41,154,155] These enzymes utilize a mononuclear nonheme iron center coordinated to a 2-histidine-1-carboxylate facial triad motif that leaves at least two labile sites available for catalysis.[9,12] The best studied member in Rieske dioxygenases is naphthalene 1,2-dioxygenase (NDO), which has been crystallographically characterized (Figure 5.1).[34,38] Naphthalene oxidation with dioxygen occurs upon $1e^-$ reduction of the ferrous resting state of the enzyme, which is itself initiated by substrate binding within the active site domain. Injection of a second electron yields a $Fe^{III}(\eta^2\text{-}O_2)$ intermediate.[38] Protonation activates the peroxo for reaction with the substrate, and from here it is under debate whether the putative $Fe^{III}(\eta^2\text{-}OOH)$ intermediate *cis*-dihydroxylates the substrate directly, or first undergoes O-O bond heterolysis to form a HO-Fe^{V}=O active oxidant.[39-44]

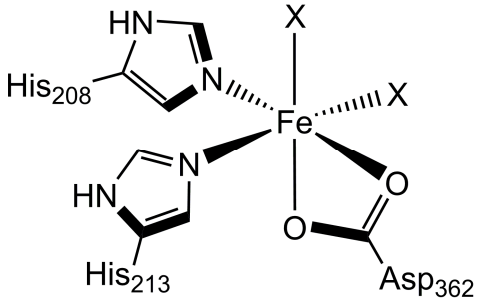

Figure 5.1 Naphthalene 1,2-dioxygenase (NDO) active site.

Catalytic olefin *cis*-dihydroxylation is an important chemical transformation in pharmaceuticals and natural product synthesis, and it usually involves osmium compounds.[6,73-75] Although this methodology, 'Sharpless Asymmetric Dihydroxylation', is a remarkably effective catalytic system, concerns regarding the high toxicity and cost of osmium and the oxidants used has led to a search for alternatives.[135,136] In the last decade, our group and others have developed examples of iron catalysts for olefin *cis*-dihydroxylation.[66,67,70,71,101,104] Inspired by the Rieske dioxygenases, my own efforts have also focused upon the use of nonheme monoiron catalysts, but I prefer to use H_2O_2 as the terminal oxidant because of its low cost, low E factor, ease of handling, and the fact that its by-products are environmentally benign.[77]

Tetradentate ligands consist of a big family of iron catalysts capable of olefin *cis*-dihydroxylation, and they usually contain amine and pyridine donors. Table 5.1 summarizes the catalytic results of typical tetradentate ligands with various numbers of amines and pyridines. From the table, the four ligands picked contain different numbers of amines and pyridines. Me_2EBC has four amine donors, ^{Me2}PyTACN has three amines and one pyridine, BPMEN has two amines and two pyridines, and TPA has one amine and three pyridines. *Cis*-cyclooctene, 1-octene, and *cis*-2-heptene are three common substrates catalyzed by the four iron complexes with these ligands. For Me_2EBC, ^{Me2}PyTACN and TPA, the catalytic results all show the slight preference of diol product, while BPMEN as N2Py2 ligand is distinct from others in favoring epoxidation over *cis*-dihydroxylation. So catalytic reactivities with N2Py2 ligands deserve further studies.

Table 5.1 Comparison of olefin oxidation catalyzed by iron complexes with different tetradentate ligands[a]

Ligand	Coord.	*cis*-cyclooctene		1-octene		*cis*-2-heptene [RC][b]	
	Atoms	epox	diol	epox	diol	epox	diol
Me_2EBC	N4	1.8(1)	4.4(1)	0.3(1)	2.1(4)	1.1(1) [60]	4.1(1) [100]
^{Me2}PyTACN	N3Py	4.0[c]	4.1[c]	1.1[d]	6.3[d]	1.2[d]	3.0[d]
BPMEN[e]	N2Py2	7.5(6)	0.9(2)	4.1(1)	1.3(1)	5.5(3)[92]	0.9(1)[79]
TPA[e]	NPy3	3.4(1)	4.0(2)	2.2(1)	5.3(3)	1.9(1)[80]	3.0(3)[96]

[a]Reaction conditions: 10 equiv H_2O_2 was added by syringe pump over a 30 min period (to minimize H_2O_2 disproportionation) at room temperature in air to a solution of catalyst (0.7 mM), 1000 equiv substrate in CH_3CN. This solution was stirred for an additional 5 min before workup. See section 5.2 for further details. Yields expressed as turnover numbers, TON, (μmol product/μmol catalyst). [b]RC, the percentage of retention of configuration in the *cis*-dihydroxylation and in the epoxidation of *cis*-2-heptene, expressed as $100 \times (A - B)/(A + B)$, where A = yield of *cis*-diol or *cis*-epoxide with retention of configuration and B = yield of epimer. [c]Results from ref 68. [d]Results from ref 67. 1000 $H_2{}^{18}O$ was added in the reaction. [e]Results from ref 66

Unlike other ligands in Table 5.1, N2Py2 ligands are linear structures. When they coordinate to the ferrous center in an octahedral geometry, they in principle can adopt three topologies: *trans*, *cis*-α, and *cis*-β (Scheme 5.1). This chapter will discuss catalytic reactivities tuned by ligand topologies and comparison of reactivities of available N2Py2

ligands (Scheme 5.2).

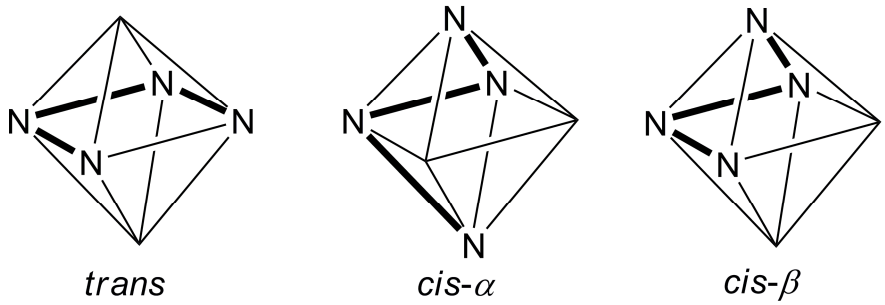

Scheme 5.1 Three different topologies that can be adopted by N2Py2 tetradentate ligands.

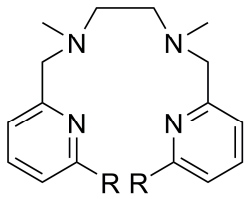

R = H, BPMEN
R = Me, 6-Me$_2$-BPMEEN

1: [Fe^{II}(BPMEN)]$^{2+}$
2: [Fe^{II}(6-Me$_2$-BPMEN)]$^{2+}$

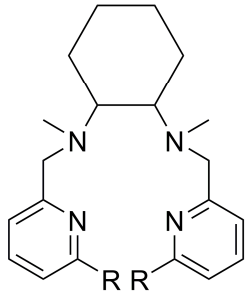

R = H, BPMCN
R = Me, 6-Me$_2$-BPMCN

3: α-[Fe^{II}(BPMCN)]$^{2+}$
4: β-[Fe^{II}(BPMCN)]$^{2+}$
5: β-[Fe^{II}(6-Me$_2$-BPMCN)]$^{2+}$

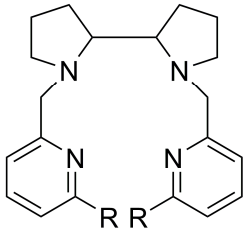

R = H, BPBP
R = Me, 6-Me$_2$-BPBP

6: [Fe^{II}(BPBP)]$^{2+}$
7: [Fe^{II}(6-Me$_2$-BPBP)]$^{2+}$

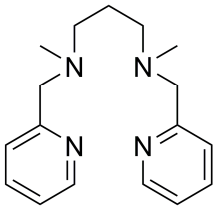

BPMPN

8: [Fe^{II}(BPMPN)]$^{2+}$

Scheme 5.2 N2Py2 ligand structures.

5.2 Experimental section

Materials and Synthesis. All reagents and anhydrous diethyl ether (Et_2O) were obtained from Sigma-Aldrich and used as received, unless otherwise noted. All olefin substrates were passed over basic alumina immediately prior to use. The solvents tetrahydrofuran (THF), dichloromethane (DCM), and acetonitrile (CH_3CN) were purified using a Vacuum Atmospheres Solvent Purifier and degassed prior to use. $H_2{}^{18}O_2$

(90% ^{18}O-enriched, 2 wt% solution in $H_2{}^{16}O$) and $H_2{}^{18}O$ (97% ^{18}O enriched) were purchased from Sigma-Aldrich and Shanghai Engineering Research Center of Stable Isotopes, respectively. $Fe(OTf)_2(CH_3CN)_2$ was prepared according to literature procedures.[103]

Instrumentation. ^{1}H NMR spectra were recorded on either a Varian Unity 300 or 500 MHz spectrometer at ambient temperature. Chemical shifts (ppm) were referenced to residual protic solvent peaks. High-resolution electrospray mass spectral (ESI-MS) experiments were performed on a Bruker (Billerica, MA) BioTOF II time-of-flight spectrometer, using a spray chamber voltage of 4000 V and a gas carrier temperature of 70°C. Analysis of products from catalytic experiments were performed using a Perkin Elmer AutoSystem gas chromatograph (AT-1701 column, 30 m) with a flame ionization detector. Gas chromatography/mass spectral analyses were performed on an HP 6890 GC (HP-5 MS column, 30 m) with an Agilent 5973 mass analyzer. A 4% NH_3/CH_4 mix was used as the ionization gas for chemical ionization analyses.

Reaction conditions for catalytic oxidations. In a typical reaction, 10 equivalents of H_2O_2 (diluted from 35% H_2O_2 solution with CH_3CN resulting in a 70 mM solution) were delivered by syringe pump under air over a period of 30 min at room temperature (20 ^{o}C) to a vigorously stirred CH_3CN solution containing iron complex and 1000 equivalents of olefin substrate. The final concentrations were 0.7 mM iron complex, 7 mM H_2O_2, and 0.7 M olefin. The solution was stirred for an additional 5 min upon completion of H_2O_2 addition, after which organic products were esterified using 1 mL acetic anhydride together with 0.1 mL 1-methylimidazole. Subsequent to extraction using $CHCl_3$, an

internal standard (naphthalene) was added and the solution washed with 1 M H_2SO_4, sat. $NaHCO_3$, and H_2O. The organic layer was dried with $MgSO_4$ and subjected to GC analysis. The products were identified by comparison of their GC retention times with those of authentic compounds.

Isotope labeling studies. Conditions similar to those described above were used for isotope labeling studies, with the following exceptions. In experiments involving $H_2{}^{18}O$, 1000 equivalents of $H_2{}^{18}O$ were added to reaction solution prior to the injection of $H_2{}^{16}O_2$. In experiments involving $H_2{}^{18}O_2$, 10 equivalents of $H_2{}^{18}O_2$ (diluted by CH_3CN from the commercially available 2% $H_2{}^{18}O_2/H_2O$ solution, which contains 1:100 molar ratio of $H_2{}^{18}O$ to $H_2{}^{16}O$) was used instead of H_2O_2. The diol esterification procedure used was the same as that detailed above. The data reported either represent a single reaction, or are the average of 2 reactions. The % ^{18}O values reported were calculated based on the ^{18}O-enrichment of the reagents containing the isotope.

Synthesis of BPMCN. The ligand BPMCN is synthesized in a three-step procedure. To a vigorously stirring aqueous solution of NaOH at 0°C, was added 5.3 mL (0.044 mol) 1,2-cyclohexanediamine. A solution of ethyl chloroformate (9.1 mL, 0.095 mol) in 40 mL benzene was then added dropwise over a period of 30 min. The reaction mixture was stirred for 3 hours. The precipitate was filtered, washed by cold water, and dried under vacuum. Pure product, diethyl cyclohexane-1,2-diyldicarbamate, was obtained by recrystallization from hot ethanol.

4.5 g diethyl cyclohexane-1,2-diyldicarbamate was added in small portions into a three neck round bottom flask containing 5 g $LiAlH_4$ and 150 mL dry diethyl ether under

nitrogen. The mixture was stirred at room temperature for about 30 min and then refluxed overnight. Water was used to quench the reaction at 0°C. The precipitate was removed by filtering. Solvent was evaporated under vacuum to give an oil, which was the product, N1,N2-dimethylcyclohexane-1,2-diamine.

Without further purification, 2.8 g (0.02 mol) N1,N2-dimethylcyclohexane -1,2-diamine, 7.2 g (0.04 mol) picolyl chloride, and 10 g (0.09 mol) Na_2CO_3 were mixed in acetonitrile and stirred for three days. After removing the solid, an oil was obtained by evaporating the solvent. The crude product was purified by running through a silica gel column eluted with a hexanes / ethyl acetate gradient. The overall yield was 48%. ^{1}H-NMR ($CDCl_3$, δ ppm from TMS): 8.24 (d, 2H), 7.61 (dd, 2H), 7.12 (m, 4H), 3.85 (dd, 4H), 2.65 (t, 2H), 2.29 (s, 6H), 1.99 (m, 2H), 1.75 (m, 2H), 1.22 (dm, 4H).

*Synthesis of **3***. 0.162 g (0.5 mmol) BPMCN and 0.063 g $FeCl_2$ are mixed in 1 mL acetonitrile in glovebox and stirred overnight. It afforded a yellow precipitate, which was filtered, washed by CH_3CN and then dried under vacuum. This yellow solid was presumably α-[Fe(BPMCN)Cl_2]. 0.196 g (0.4 mmol) α-[Fe(BPMCN)Cl_2] was suspended in 2 mL CH_3CN. 0.237 g AgOTf was added to this solution. After stirring overnight, AgCl was removed by filtering. Solvent was evaporated under vacuum to yield a green powder. Pure **3** was obtained after recrystallization by layering diethyl ether on a CH_2Cl_2 solution. Overall yield is 80%. ESI-MS: *m/z* 190 ($[Fe^{II}(BPMCN)]^{2+}$), 529 ($[Fe^{II}(BPMCN)(OTf)]^{+}$), 1208 ($[Fe_2(BPMCN)_2(OTf)_3]^{+}$), all with the expected isotope distribution patterns.

*Synthesis of **4***. 0.162 g (0.5 mmol) BPMCN and 0.218 g (0.5 mmol)

$Fe(OTf)_2(CH_3CN)_2$ were mixed in 1 mL CH_2Cl_2 in glovebox and stirred for overnight. Removal of solvent under vacuum afforded a white solid. Pure **4** was obtained from recrystallization by layering hexane on a CH_2Cl_2 solution.

5.3 Olefin oxidation tuned by different topologies

*^{1}H-NMR of **3** and **4** in solution.* The BPMCN can coordinate to the iron center in different topologies with different synthetic procdures.[102,156] Figure 5.2 shows the ^{1}H-NMR spectra of **3** and **4**. **3** adopts *cis-*α topology, so the overall structure is C_2 symmetric and it displays fewer peaks than **4**. **4** has *cis-*β topology and is less symmetric than **3**, so it shows more peaks and covers a larger range of chemical shifts. This structural study indicates that **3** and **4** maintain their structures in acetonitrile solution at room temperature.

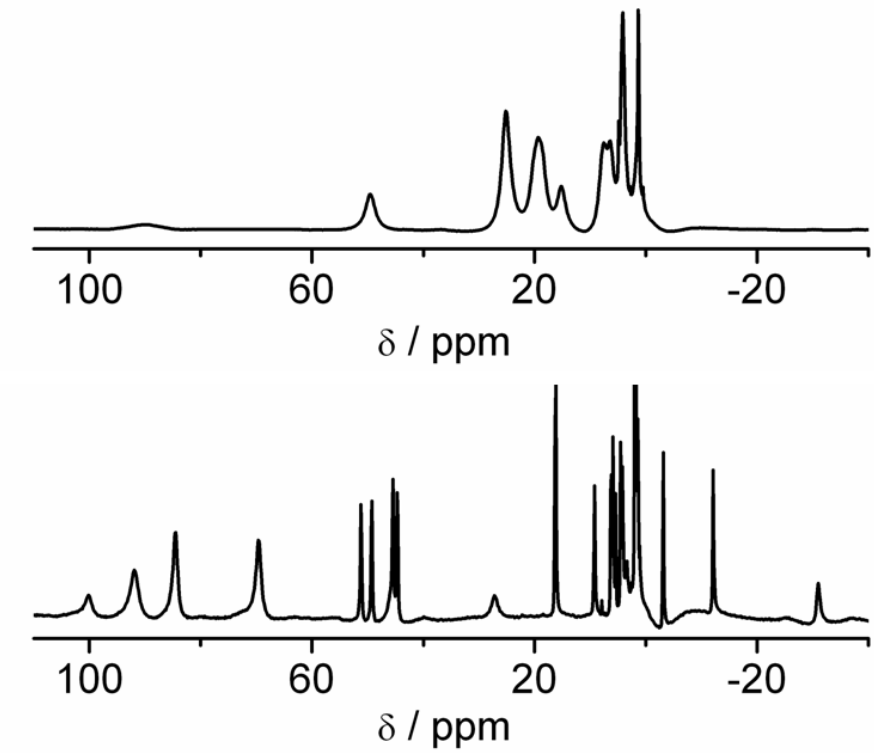

Figure 5.2 ^{1}H-NMR spectra of **3** (up) and **4** (down) in CD_3CN at 20°C.

Olefin oxidation. Table 5.2 summarizes the catalytic olefin oxidation results catalyzed by **3** and **4**, which shows very different reactivities. With *cis*-cyclooctene as substrate, they both show very high conversion of the oxidant and prefer epoxidation over *cis*-dihydroxylation. **3** makes more epoxide than **4**, but **4** generates more diol product. With 1-octene as substrate, **3** still favors epoxidation, while **4** shifts its preference to *cis*-dihydroxylation. When *cis*- or *trans*-2-heptene is used, **3** shows larger favor over epoxidation, while **4** gives relatively equal amounts of epoxide and diol products. This pattern is inversed when electron withdrawing olefins are used. With ethyl crotonate and *t*-butyl acrylate, **3** gives comparable amounts of epoxide and diol,

while **4** demonstrates its preference of diol products. Epoxidation of dimethyl fumarate is very difficult, so both complexes give similar turnovers of diol products. This reactivity study clearly demonstrates that although **3** and **4** contain exactly the same ligand, they have very different reactivities when ligand coordinates to the iron center in different topologies.

Table 5.2 Olefin oxidation catalyzed by **3** and **4**[a]

	3		**4**	
	epoxide	diol	epoxide	diol
cis-cyclooctene	8.2(1)	0.3(1)	6.2(2)	2.9(2)
1-octene	3.1(1)	0.9(2)	0.7(0)	3.7(1)
cis-2-heptene	6.3(1)	0.4(1)	3.2(1)	2.7(0)
[RC][b]	[94%]	[68%]	[81%]	[69%]
trans-2-heptene	5.8(1)	0.4(1)	1.9(2)	2.1(1)
[RC][b]	[98%]	[73%]	[84%]	[73%]
ethyl-crotonate	2.6(2)	2.3(1)	0.2(0)	3.6(3)
t-butyl acrylate	2.1(3)	1.3(1)	0.2(0)	3.5(1)
dimethyl fumarate	0	1.0(1)	0	4.8(1)

[a]Reaction conditions: 10 equiv H_2O_2 was added by syringe pump over a 30 min period (to minimize H_2O_2 disproportionation) at room temperature in air to a solution of catalyst (0.7 mM), 1000 equiv substrate in CH_3CN. This solution was stirred for an additional 5 min before workup. See section 5.2 for further details. Yields expressed as turnover numbers, TON, (μmol product/μmol catalyst). [b]RC, the percentage of retention of configuration in the *cis*-dihydroxylation and in the epoxidation of *cis*-2-heptene, expressed as $100 \times (A - B)/(A + B)$, where A = yield of *cis*-diol or *cis*-epoxide with retention of configuration and B = yield of epimer.

Competition reactions. Substrate competition studies provide further different

reactivities of iron complexes with different topologies. Four substrates were selected for pairwise competition experiments, where equimolar amounts of two different substrates are oxidized under normal catalytic and work-up conditions. As shown in Figure 5.3 and Table 5.3, when the electron-rich olefin, *cis*-cyclooctene or 1-octene, is mixed with the electron-poor olefin, *t*-butyl acrylate or dimethyl fumarate, **3** shows great preference of the olefin with electron donating substituents. Only trace amounts of products can be detected for electron-deficient olefins. On the other hand, **4** with *cis*-β topology does not exhibit such a clear preference. Products from electron-rich or electron-deficient olefins are comparable to each other when both are present in the reaction. This competition study demonstrates that the ligand topology can have an impact on the substrate preference.

Table 5.3 Product analysis from the competition reactions[a]

	3		**4**	
	epoxide	diol	epoxide	Diol
cis-cyclooctene / *t*-butyl acrylate	8.2 (4) / 0	0.4 (1) / 0.1(1)	2.8 (3) / 0	1.7 (2) / 1.2(2)
1-octene / *t*-butyl acrylate	2.3 (1) / 0	0.9 (1) / 0.2(1)	0.2 (1) / 0	1.0 (1) / 3.5 (1)
cis-cyclooctene / dimethyl fumarate	9.1(7) / 0	0.3 (1) / 0	2.7 (2) / 0	1.4 (1) / 3.4 (3)
1-octene / dimethyl fumarate	2.9(1) / 0	1.0 (1) / 0	0.4 (1) / 0	1.5 (1) / 4.2 (1)

[a]Reaction conditions: 10 equiv H_2O_2 was added by syringe pump over a 30 min period (to minimize H_2O_2 disproportionation) at room temperature in air to a solution of catalyst (0.7 mM), 500 equiv substrate 1 and 500 equiv substrate 2 in CH_3CN. This solution was stirred for an additional 5 min before workup. See section 5.2 for further details. Yields expressed as turnover numbers, TON, (μmol product/μmol catalyst).

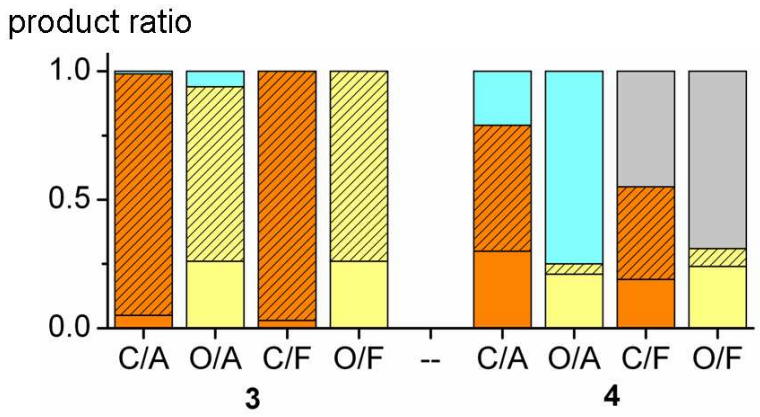

Figure 5.3 Competition oxidation results with equal amounts of two substrates catalyzed by **3** and **4**. C: *cis*-cyclooctene oxidation products in orange; O: 1-octene oxidation products in yellow; A: *t*-butyl acrylate oxidation products in cyan; F: dimethyl fumarate oxidation product in grey. Solid bars correspond to amount of *cis*-diol formed, while shaded bars correspond to amount of epoxide formed.

5.4 Comparison among iron complexes with N2Py2 ligands

As mentioned in the part of introduction, the catalytic behavior of **1** is different from other iron complexes with tetradentate ligands. Since N2Py2 ligand can adopt three topologies when it binds to the metal center (Scheme 5.1), **1** could change into *trans* topology in solution, which lacks the *cis* two labile sites required for olefin *cis*-dihydroxylation (Chapter 4). This explanation can be evidenced by the related complex **8** with BPMPN as ligand. The two amines are linked by propylene in BPMPN instead of ethylene in BPMEN, which gives the iron complex more flexibility. X-ray crystallographic and NMR studies show that **8** can adopt all possible topologies in solution and each topology can convert to another.[157] However, in case of **1**, only *cis*-α

topology is observed crystallographically.[158] Solution NMR also indicates that it maintains the same structure.[159] In addition, acetic acid assisted epoxidation catalyzed by **1**[64,148,149] behaves quite similarly as $[Fe^{II}(TPA)]^{2+}$ with two *cis* labile sites.[64] Another two related ligands, BPMCN and BPBP, have the same backbone as BPMEN, but they are more rigid than BPMEN. When they form the iron complexes with *cis*-α topology, it will be very unlikely that this topology can convert to any other topologies. These two complexes, **3** and **6**, both exhibit quite similar catalytic behavior in favoring the epoxidation over *cis*-dihydroxylation (Table 5.4). Therefore, **1** is likely to keep its topology in solution and the epoxidation is likely to be determined by this *cis*-α topology.

Interestingly, when the sixth position of pyridine is substituted by a methyl group, the preference for products is completely converted to *cis*-diol (Table 5.4, **2** and **7**). This observation is detected for $[Fe^{II}(TPA)]^{2+}$ too, which was explained by the spin state of the starting Fe(II) complex. Methyl groups push the pyridine far away from the iron center, thus making iron center high spin. Depending on the spin state, low spin complexes, like $[Fe^{II}(TPA)]^{2+}$, are Class A, while high spin complexes, like $[Fe^{II}(6\text{-}Me_3\text{-}TPA)]^{2+}$, are Class B. So far more experimental results demonstrate that this classification is quite preliminary. For example, **3** starts from high spin (Figure 5.2), but it behaves like **1** that is low spin and classified as Class A. I am trying to explain in a different way. Fe^{V}=O(OH) is putative intermediate that is responsible for both epoxidation and *cis*-dihydroxylation,[66] and computational calculation shows that its formation is feasible.[151] Whether the product is epoxide or *cis*-diol depends on whether oxo or peroxo attacks the double bond. When oxo attacks, it forms epoxide, and when

peroxo attacks, it forms diol product. Supposedly, methyl groups introduce steric effect, but Fe-OH is less affected by the methyl groups on the sixth position than Fe=O, and thus this substitution can alternate the preference of product. Anyways, this is only an assumption, and it needs further investigation.

Complexes **4** and **5** adopt *cis*-β topology. **4** has the same ligand, BPMCN, as **3**, but it has quite distinct catalytic results. The epoxide is less, while increasing amount of diol is formed. This clearly indicates that different topologies can affect the final catalytic turnout. Methyl substitution on the sixth position has the same effect as above, indicating that they are all due to the same reason behind these observations. Very recently, Nam had a paper studying different reactivities of Fe(IV)-oxo with different ligand topology.[160] In this paper, they used a very similar ligand as BPMCN, which can adopt *cis*-α and *cis*-β topologies in iron complexes. The Fe^{IV}/Fe^{III} redox potential of *cis*-α isomer is 0.11 V higher than that of *cis*-β isomer, indicating that the high valent species of the *cis*-α isomer is a stronger oxidant than the *cis*-β isomer. This is in agreement with the studies that the *cis*-α isomer has a better reactivity towards oxygen atom transfer. Computational calculation explains the different by put the oxo opposite to different donors. In the *cis*-α isomer, oxo is *trans* to amine nitrogen, while the *cis*-β isomer is *trans* to quinolyl nitrogen (equivalent to pyridyl nitrogen in BPMCN). The *cis*-α isomer is 2.4 kcal mol^{-1} less stable than the *cis*-β isomer. This could potentially explains the preference of epoxidation for α-topology complexes. Since the oxo in the high valent species of β-topology complexes has lower reactivity to transfer oxygen, there is greater chance for the formation of the *cis*-diol product.

Table 5.4 Olefin oxidation catalyzed by iron complexes with N2Py2 ligands[a]

		1[b]	**2**[b]	**3**	**4**	**5**[c]	**6**[e]	**7**[e]
cis-	epox	7.5(6)	1.5(1)	8.2(1)	6.2(2)	3.5		0.7(1)
cyclooctene	diol	0.9(2)	6.4(1)	0.3(1)	2.9(2)	5.8		4.0(5)
1-octene	epox	4.1(1)	0.7(1)	3.1(1)	0.7(0)	1.3[d]	2.6(3)	0.1(1)
	diol	1.3(1)	5.3(1)	0.9(2)	3.7(1)	8.1[d]	1.7(1)	6.4(3)
cis-2	epox	5.5(3)	2.0(1)	6.3(1)	3.2(1)	4.5[d]		0.6(1)
-heptene	diol	0.9(1)	4.6(2)	0.4(1)	2.7(0)	7.8[d]		3.4(1)
trans-2	epox	5.3(1)	1.5(3)	5.8(1)	1.9(2)	2.4[d]	5.1(1)	0.2(1)
-heptene	diol	0.6(1)	2.6(2)	0.4(1)	2.1(1)	7.5[d]	1.1(4)	5.2(2)
t-butyl	epox			2.1(3)	0.2(0)	0.5[d]	3.0(1)	<0.1
acrylate	diol			1.3(1)	3.5(1)	10.1[d]	0.1(1)	5.3(5)

[a]Reaction conditions: 10 equiv H_2O_2 was added by syringe pump over a 30 min period (to minimize H_2O_2 disproportionation) at room temperature in air to a solution of catalyst (0.7 mM), 1000 equiv substrate in CH_3CN. This solution was stirred for an additional 5 min before workup. See Experimental section for further details. Yields expressed as turnover numbers, TON, (μmol product/μmol catalyst). [b]Results from [66]. [c]Results from [102]. [d]20 equiv H_2O_2 is used. [e]Results from [72].

5.5 Conclusions

N2Py2 ligands can adopt three topologies. This chapter first examines two complexes with the same ligand but different topologies and shows that topology is an

important factor in catalysis. Comparison of available iron complexes with N2Py2 ligands implies that *cis*-α topology favors epoxidation, but this can be shifted to *cis*-dihydroxylation when methyl groups are introduced at positions that can exert steric effect.

5.6 Acknowledgements

I would like to thank Dr. Paul Oldenburg for all his help when I first joined the laboratory. Without his help, I could not have started this project (my first project) so smoothly.

CHAPTER 6

Naphthalene oxidation by a variety of iron complexes with N4 ligands

6.1 Introduction

Nature has evolved a pathway to degrade arenes by soil bacteria.[4,25,26] The bio-degradation of aromatic compounds is initiated by the *cis*-dihydroxylation of an arene double bond by Rieske dioxygenases,[32,33,134,155] which belong to a family of non-heme enzymes with mononuclear iron active sites that share a common 2-His-1-carboxylate facial triad motif.[9] The best characterized of these Rieske dioxygenases is naphthalene 1,2-dioxygenase (NDO),[34,38] which catalyzes the conversion of naphthalene to *cis*-(1R,2S)-1,2-dihydro-1,2-naphthalenediol (Scheme 6.1).[161] An important goal in my biomimetic efforts has been to identify or design iron catalysts that mimic the functions of Rieske dioxygenases in order to gain better insight into the mechanisms of these unique transformations and discover new synthetic reactions that may be useful in synthetic organic and/or environmental applications.[6,162]

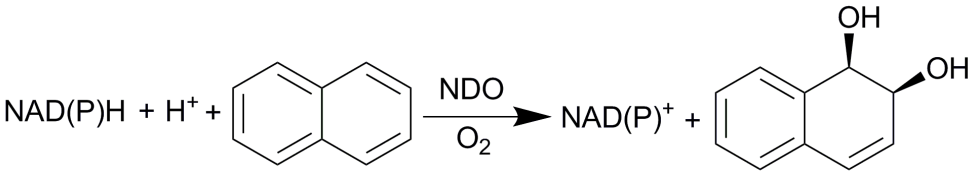

Scheme 6.1 Naphthalene oxidation by naphthalene 1,2-dioxygenase (NDO).

In the past few years, the Que laboratory and others have been successful in finding non-heme iron catalysts that catalyze the *cis*-dihydroxylation of olefins.[61,66,99,150,157,163] However, the *cis*-dihydroxylation of aromatic double bonds has thus far not been reported. This chapter describes for the first time non-heme iron complexes that

catalyzes the *cis*-dihydroxylation of naphthalene and thus serves as a functional model for naphthalene 1,2-dioxygenase.

6.2 Experimental section

Materials. All reagents were purchased from Sigma-Aldrich and used as received unless otherwise noted. All olefin substrates were passed over basic alumina immediately prior to use. CH_3CN was purified by Solvent Purifier from Vacuum Atmospheres Company. Synthesis of $[Fe^{II}(OTf)_2 \bullet 2NCCH_3]$ and **1-4** have been reported previously.[102,103,147,156,158]

Instrumentation. ^1H spectra were recorded on a Varian Unity 300 or 500 MHz spectrometer at ambient temperature. Chemical shifts (ppm) were referenced to the residual protic solvent peaks. High-resolution electrospray mass spectral (ESI-MS) experiments were performed on a Bruker (Billerica, MA) BioTOF II time-of-flight spectrometer. Product analyses from catalysis experiments were performed on a Perkin Elmer AutoSystem gas chromatograph (AT-1701 column, 30 m) with a flame ionization detector. Gas chromatography/mass spectral analyses were performed on an HP 6890 GC (HP-5 MS column, 30 m) with an Agilent 5973 mass analyzer. A 4% NH_3/CH_4 mix was used as the ionization gas for chemical ionization analyses.

Reaction conditions for catalytic oxidations. In a typical reaction, 10 equivalents of H_2O_2 (diluted from 35% H_2O_2 solution with CH_3CN resulting in a 0.5 M solution) were delivered by syringe pump over a period of 5 min at room temperature (20°C) in air to a vigorously stirred CH_3CN solution containing iron catalyst and 1000 equivalents of

olefin substrate. The final concentrations were 1 mM iron catalyst, 10 mM H_2O_2, and 0.5 M olefin. The solution was stirred for an additional 20 min after syringe pump addition, after which organic products were esterified by 1 mL acetic anhydride together with 0.1 mL 1-methylimidazole and extracted with $CHCl_3$. An internal standard (naphthalene) was added and the solution was washed with 1 M H_2SO_4, sat. $NaHCO_3$, and H_2O. The organic layer was dried with $MgSO_4$ and subjected to GC and GC/MS analysis. The products were identified by comparison of their GC retention times and GC/MS with those of authentic compounds. The reported results are the average of at least three trials.

Isotope labeling studies. Similar conditions as described above were used for isotope labeling studies except for the following details. In experiments involving $H_2{}^{18}O$, 1000 equivalents of $H_2{}^{18}O$ were added to reaction solution prior to the injection of $H_2{}^{16}O_2$. In experiments involving $H_2{}^{18}O_2$, 10 equivalents of $H_2{}^{18}O_2$ (diluted by CH_3CN from the commercially available 2% $H_2{}^{18}O_2/H_2O$ solution, which contains 1:100 molar ratio of $H_2{}^{18}O$ to $H_2{}^{16}O$) was used instead of H_2O_2. The diol esterification procedure was the same as that diagrammed above. The data reported either summarize a single reaction or are the average of 2 reactions and the % ^{18}O values reported were calculated based on the ^{18}O-enrichment of the reagents containing the isotope.

Synthesis of D_6-TPA. All ligands structures are listed in Scheme 6.2. They all can be synthesized based on known procedures, except the novel ligand, D_6-TPA. Its synthesis starts from the ligand TPA (tris(pyridin-2-ylmethyl)amine) that was synthesized according to literature procedures.[147] Deuteration of the picolyl positions of TPA ligand was achieved based on a published procedure developed from our laboratory.[106] 0.29 g

(1 mmol) of the TPA ligand and 0.48 (20 mmol) sodium hydride were suspended in 15 mL of acetonitrile-d_3, and the mixture was then stirred at 50°C under Ar for 24 h. A total of 15 mL D_2O is then introduced to quench the reaction. Upon removal of acetonitrile under vacuum, the residue was extracted with dichloromethane and the organic layer was collected and washed with 20 mL brine solution. Pure product was obtained in 85% yield after running through silica gel eluted with a gradient of hexanes / ethyl acetate. ^{1}H-NMR ($CDCl_3$, δ ppm from TMS): 8.62 (d, 3H), 7.73 (dd, 3H), 7.61 (d, 3H), 7.15 (dd, 3H). ESI-MS: *m / z* 297 ($[TPA + H]^+$), 319 ($[TPA + Na]^+$), 335 ($[TPA + K]^+$). Both ^{1}H-NMR and ESI-MS analyses showed that >99% of the protons on the picolyl methylene groups were deuterated.

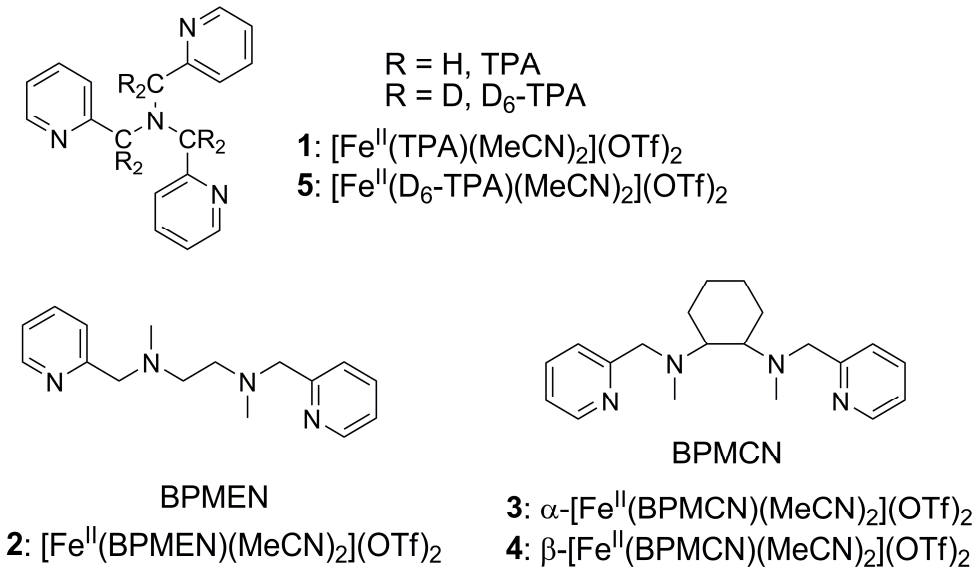

Scheme 6.2 Ligand structures in Chapter 6.

*Synthesis of [Fe(D$_6$-TPA)(MeCN)$_2$](OTf)$_2$ complex (**5**).* In an N_2-containing

glovebox, a mixture of the D_6-TPA ligand (0.5 mmol) and [$Fe^{II}(OTf)_2$•$2NCCH_3$] (0.5 mmol) is stirred overnight in 5 ml acetonitrile, after which diethyl ether is added into this solution to precipitate a red solid. After filtration, the red solid is redissolved in acetonitrile and vapor diffusion of Et_2O into this solution results in the formation of purified product in 80% yield. Characterization: ESI-MS: 501 ({[Fe(D_6-TPA)(OTf)]}$^+$). ^{1}H-NMR (CD_3CN, δ ppm from TMS): 11.26 (s, 3H), 8.58 (m, 6H), 7.37 (t, 3H).

6.3 Identification and quantification of products from naphthalene oxidation

1 is a complex that has been shown to catalyze olefin epoxidation and *cis*-dihydroxylation with H_2O_2 as oxidant.[66] When naphthalene is used instead of an olefin under nearly identical reaction conditions (1 mM catalyst and 0.5 M naphthalene in CH_3CN at 20 °C under air with 10 mM H_2O_2 syringed-pumped into the reaction mixture at a rate of 2 equivalents per minute followed by 20 min additional stirring), **1** is found to catalyze the oxidation of naphthalene. Four oxidation products from these reactions are identified, namely *cis*-1,2-dihydro-1,2-naphthalenediol, 1-naphthol, 2-naphthol, and 1,4-naphthoquinone (Scheme 6.3). The diol product represents the major product of naphthalene oxidation and is identical to that produced in the NDO-catalyzed reaction.[161] Since these three products are of great interest to us, their analysis by GC/MS, HPLC, and quantification by GC are shown in the following paragraphs.

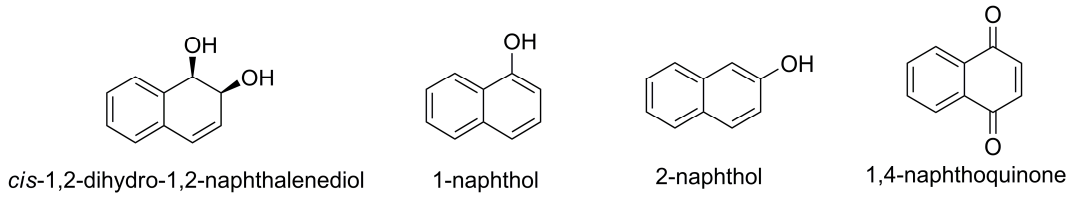

cis-1,2-dihydro-1,2-naphthalenediol 1-naphthol 2-naphthol 1,4-naphthoquinone

Scheme 6.3 Identified products from naphthalene oxidation by H_2O_2.

Identification by GC/MS. At first, only 1,4-naphthoquinone can be identified. After treatment of the reaction mixture with acetic anhydride and 1-methyl-imidazole to acetylate the alcohol functions, three other oxidation products from these reactions are identified, namely *cis*-1,2-dihydro-1,2-diacetoxynaphthalene, 1-acetonaphthalene, and 2-acetonaphthalene. The correspondence to the enzyme-produced product is demonstrated by the appearance of a peak that gave rise to ions with mass corresponding to the *cis*-diol derived products in GC/MS analysis. The three ions observed for this peak are 264, 204, and 187. Since the mass spectrometer uses chemical ionization to generate ion with NH_3 / CH_4 gas, M + 1 ($M + H^+$) or M + 18 ($M + NH_4^+$) is commonly seen. 264 is assigned to the molecular ion of the acetylated *cis*-diol product with ammonium (*cis*-1,2-dihydro- 1,2-diacetoxynaphthalene + NH_4^+). 187 is corresponding to the fragmented ion of the acetylated *cis*-diol product losing one acetate ([*cis*-1,2-dihydro- 1,2-diacetoxynaphthalene – OAc^-]$^+$), while 204 is the ion of 187 plus ammonia ([*cis*-1,2-dihydro-1,2-diacetoxynaphthalene – OAc^- + NH_3]$^+$). The peak that assigned to the acetylated *cis*-diol product is also demonstrated by the fact that it co-migrats in the GC/MS analysis with the acetylated derivative of a commercially available authentic sample, which indicates that the orientation of the two newly formed C-O bonds are *cis*

to each other, because the *trans* isomer would be expected to have a different retention time. The other two products, 1-acetonaphthalene and 2-acetonaphthalene, can not be resolved in the GC/MS column, so they display only one single peak in the GC trace. No fragmentation is observed for these two products and only molecular ions are detected, which are 187 (acetonaphthalene + H^+) and 204 (acetonaphthalene + NH_4^+). They also co-migrate with the acetylated commercially available naphthols.

Identification by HPLC. The *cis*-1,2-dihydro-1,2-naphthalenediol has to be acetylated to be analyzed by GC/MS, but HPLC provides an alternative way to detect *cis*-1,2-dihydro-1,2-naphthalenediol directly. The reaction solution is subject to HPLC analysis without workup process, which can eliminate any other factors that could complicate the system. Figure 6.1 shows two HPLC traces: the black line is from the reaction solution and the red line is from the commercially available authentic sample. The reaction solution trace exhibits a peak that has exactly the same retention (within the error) time with the authentic sample. This observation demonstrates two important conclusions: firstly, the dihydroxylated product of naphthalene is indeed formed from the oxidation reaction catalyzed by **1**; and secondly, the stereochemistry of the diol product is the same as the authentic sample, which is *cis*. Therefore, based on GC/MS and HPLC analysis, it is confident that the enzyme-produced product can be generated by a synthetic iron complex. These results represent the first example of iron-catalyzed arene *cis*-dihydroxylation, thereby mimicking NDO in its ability to use H_2O_2 as the oxidant in a peroxide shunt pathway.[40,41]

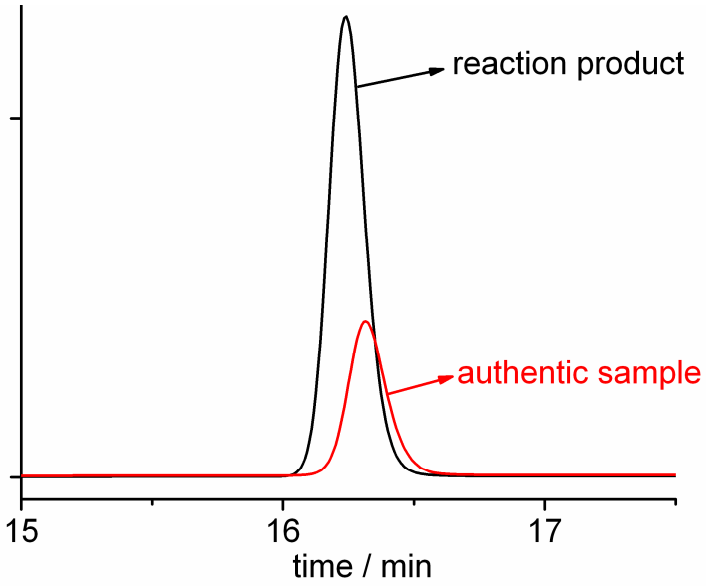

Figure 6.1 HPLC analysis of *cis*-1,2-dihydro-1,2-naphthalenediol. Black: product from reaction; red: authentic sample from commercial source.

Quantification by GC. The yield of the *cis*-diol product is determined as its di-acetylated derivative by gas chromatography (GC). When 10 equivalents of H_2O_2 are used as oxidant, approximately 30% conversion relative to the oxidant is observed, corresponding to about 3 turnovers relative to the iron. The other three products of naphthalene oxidation were obtained in much lower yields, namely 5% for 1-naphthol, 2% for 2-naphthol and 3% for 1,4-naphthoquinone (relative to H_2O_2). Since *cis*-1,2-dihydro-1,2-diacetoxynaphthalene undergoes thermal decomposition of losing one acetic acid to become 1- or 2-acetonaphthalene (GC/MS analysis demonstrates the possibility that the acetate can be eliminated easily, please check previous paragraphs), the actual yields of 1- or 2-naphthol are adjusted from the observed yields. Control experiments showed that 5% of the observed *cis*-1,2-dihydro-1,2-diacetoxynaphthalene was

converted into acetonaphthalenes. Based on the prevailing mechanistic notion that arene hydroxylation involves the initial attack of a metal-oxo species on the arene C=C double bond,[164-167] the two naphthol products may be considered as corresponding to the epoxide products obtained in the **1**-catalyzed oxidations of olefins.[66] From this perspective, the diol/naphthol ratio of 4:1 can be compared to diol/epoxide ratios of 1.2:1 for cyclooctene and 5:1 for 1-octene. Thus, naphthalene is comparable to 1-octene in having a much stronger preference to undergo *cis*-dihydroxylation than monooxygenation. However the overall percentage conversion of oxidant into naphthalene oxidation products is about a factor of 2 lower than corresponding values for olefin oxidation,[66] perhaps reflecting the greater oxidative stability of naphthalene.

6.4 Naphthalene oxidation catalyzed by various nonheme iron complexes

Other nonheme iron complexes with N4 ligands have also been explored in this novel arene *cis*-dihydroxylation. **2** with the BPMEN ligand is a good catalyst in olefin oxidation, especially epoxidation.[64] **3** and **4** contain the same ligand, BPMCN, but adopt different topologies. **3** adopts the α topology, in which the two pyridines are *trans* to each other, while **4** adopts the β topology, in which the two pyridines are *cis* to each other. No matter what topology, **3** and **4** both have the two labile sites *cis* to each other. **5** is the deuterated version of **1** with the picolyl methylene groups deuterated, since these positions are adjacent to pyridines and likely to be attacked. So deuteration is to extend the catalyst lifetime and increase the yield of the *cis*-diol.

Table 6.1 summarizes the catalytic results of naphthalene oxidation by iron

complexes. Among the first four complexes, **1** has the best catalytic ability in converting naphthalene into *cis*-1,2-dihydro-1,2-naphthalenediol with 3 turnovers (Table 6.1, entry 1). The oxidation results for **2-4** are comparable to each other, with about 1 turnover (Table 6.1, entries 2-4). The difference between **1** and **2-4** could possibly lie in the ligand structures. TPA ligand has a tripodal structure, while BPMEN is linear. BPMCN has the backbone of BPMEN (Scheme 6.2). However, how the ligand structure influences the catalytic results is not quite clear for now. Further investigation is needed.

As a control experiment, $[Fe^{II}(OTf)_2(NCMe)_2]$ is also tested as a catalyst for this reaction, but the result is negative (Table 6.1, entry 6). This observation indicates that iron alone does not have the ability to catalyze arene oxidation and ligands play an important role, which in agreement with the assumption in the last paragraph that ligand structure affects the catalytic reactivity.

Interestingly, **5** catalyzes the naphthalene oxidation only as well as **1**. Deuterated complex **5** might have been expected to produce a higher yield of diol than **1** because of retardation of ligand oxidation. However, their results are comparable to each other (Table 6.1, entries 1 and 5), showing that catalyst **1** does not deactivate via oxidation of the picolyl methylene groups. It is likely that **1** is robust enough to survive more turnovers when more oxidant is added.

Another two iron complexes have been examined in naphthalene oxidation. Even though $[Fe^{II}(Me_2EBC)(OTf)_2]$ behaves like **1** in the oxidation of aliphatic olefins (Chapter 4), it can not catalyze arene oxidation (Table 6.1, entry 7). The reason is probably attributed to the fact that the strain of the macrocyclic ligand drags the amine

donors away from the metal center and thus less electron density is donated, making the complex less powerful. $[Fe^{II}(Ph\text{-}DPAH)_2](OTf)_2$ does not catalyze this reaction either (Table 6.1, entry 8), but lower oxidation state of the active oxidant is proposed in explaining the lack of reactivity towards naphthalene oxidation (Chapter 2).

Table 6.1 Oxidation of naphthalene by nonheme iron complexes[a]

Entry	complex	diol	1-naphthol	2-naphthol	quinone
1	**1**	3.0(1)	0.5(1)	0.2(1)	0.3(1)
2	**2**	0.9(2)	0.5(1)	0.1(1)	0.4(1)
3	**3**	1.2(1)	0.3(1)	0.1(1)	0.4(1)
4	**4**	0.8(2)	0.2(1)	0.1(1)	0.2(1)
5	**5**	2.9(2)	0.5(1)	0.1(1)	0.2(1)
6	$[Fe^{II}(OTf)_2(MeCN)_2]$	0	0	0	0
7[b]	$[Fe^{II}(Me_2EBC)(OTf)_2]$	0	0	0	0
8[c]	$[Fe^{II}(Ph\text{-}DPAH)_2](OTf)_2$	0	0	0	0

[a]Reaction conditions: 10 equiv H_2O_2 (relative to complex) in CH_3CN solution is delivered by syringe pump over a period of 5 min at room temperature under air to a vigorously stirred CH_3CN solution containing 1 mM iron catalyst and 500 equiv naphthalene. The solution is stirred an additional 20 min after syringe pump addition and products are determined by GC analysis. Yields expressed as μmol product/μmol catalyst. [b]Results from Chapter 4. [c]Results from Chapter 2.

6.5 Naphthalene oxidation with various amounts of oxidant and substrate

Studies of **5** demonstrate that catalyst **1** at least does not deactivate through the oxidation of the picolyl positions. The 30% conversion of 10 equivalents of H_2O_2 is much lower than for **1**-catalyzed olefin oxidations. To investigate whether the lower oxidant conversion observed for naphthalene reflects catalyst deactivation by other pathways or just a lower efficiency in oxidizing naphthalene relative to olefins, the effect of adding more equivalents of H_2O_2 is thus examined.

The catalytic results with increasing equivalents of H_2O_2 are summarized in Table 6.2. All the reactions are carried out under the same conditions with the additional equivalents of H_2O_2 being added into the reaction system at the same constant injection rate of 2 equiv per minute. Figure 6.2 illustrates that there is a linear relationship between the amount of H_2O_2 added and the amount of diol produced and a 30% conversion of H_2O_2 to product is maintained. From this figure, it also shows that the catalyst remains comparably active even after addition of 100 equiv H_2O_2. This demonstrates that **1** is a robust catalyst for *cis*-dihydroxylation of naphthalene.

Table 6.2 Naphthalene oxidation catalyzed by **1** with varying amounts of H_2O_2 and substrate [a]

Entry	H_2O_2	Naphthalene	Diol
1	10	500	3.0(1)
2	20	500	5.6(1)
3	40	500	12.3(5)
4	60	500	18.0(9)
5	80	500	24.6(1.1)
6	100	500	28.5(4)
7	100	400	24.9(9)
8	100	300	20.8(6)
9	100	200	16.2(9)
10	100	100	12.1(8)

[a]Reaction conditions: H_2O_2 in CH_3CN solution is delivered by syringe pump at a rate of 2 equiv per minute at room temperature under air to a vigorously stirred CH_3CN solution containing 1 mM iron catalyst and naphthalene. The solution is stirred an additional 20 min after syringe pump addition and products are determined by GC analysis. Yields expressed as μmol product/μmol catalyst.

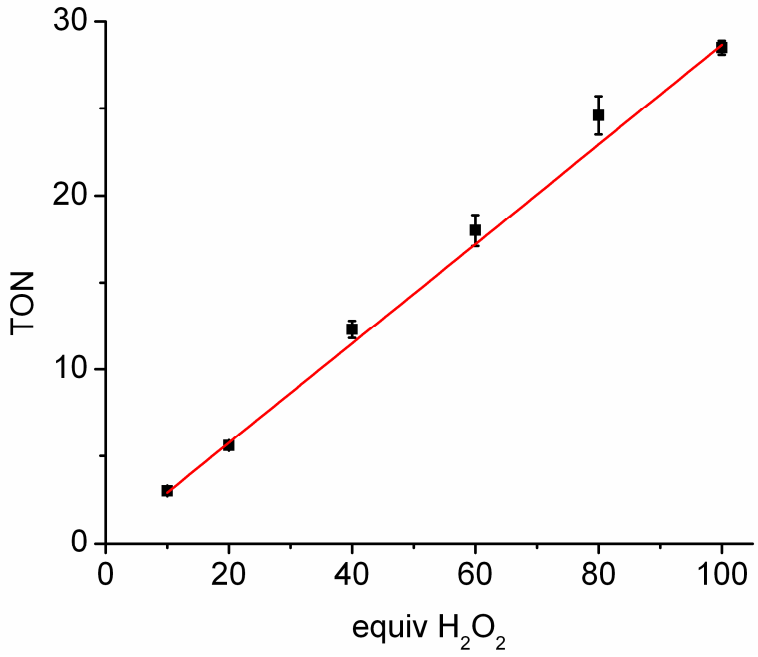

Figure 6.2 Yield of naphthalene *cis*-dihydroxylation in CH_3CN using **1** as catalyst as a function of H_2O_2 equivalents added (relative to catalyst).

With the notion that the catalyst **1** remains active even when 100 equivalents of H_2O_2 are used, lower amounts of naphthalene were used in the reaction system in order to achieve the substrate limiting condition. Unfortunately, decreasing the naphthalene amount to below 500 equivalents relative to iron results in lower yields (Table 6.2, entries 6-10, Figure 6.3), and the lower the concentration of naphthalene added, the fewer turnovers the reaction can generate. This phenomenon clearly demonstrates that a high concentration of naphthalene is necessary to intercept the oxidant efficiently, which is also true in case of olefin oxidation catalyzed by nonheme iron complexes.

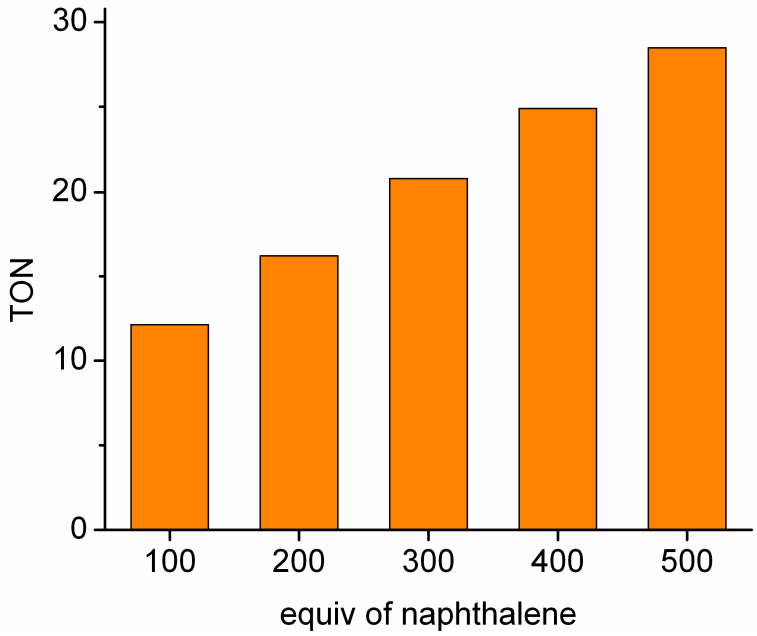

Figure 6.3 Yield of naphthalene *cis*-dihydroxylation in CH_3CN using **1** as catalyst as a function of naphthalene used (relative to catalyst).

6.6 Competition reactions

1-catalyzed olefin oxidation is well established.[66] To gain insight into the nonheme iron-catalyzed naphthalene oxidation, 1-octene was added in the reaction to examine whether the active oxidant formed in this system can also attack olefins. Table 6.3 summarizes the competition results. With 1/10 equiv of 1-octene relative to naphthalene as co-substrate, products from naphthalene oxidation slightly decrease and 1,2-octane diol is observed (Table 6.3, entry 2). The naphthalene conversion is only half effective, when 1-octene is doubled (Table 6.3, entry 3). Finally, when equal amounts of 1-octene and naphthalene are used, products from 1-octene increase and products from naphthalene decrease. So 1-octene can intercept the active oxidant in naphthalene

oxidation. These observations indicate that naphthalene oxidation is likely to share the same pathway as other **1**-catalyzed olefin oxidations.

Table 6.3 Competitive oxidation of naphthalene and 1-octene catalyzed by **1**[a]

1-octene	naphthalene	1-octene		naphthalene		
		epox	diol	diol	naphthol[b]	quinone
0	500	0	0	3.0	0.7	0.3
50	500	0	0.1	2.5	0.4	0.3
100	500	0	0.2	1.6	0.3	0.1
500	500	0.1	0.7	1.5	0.3	0.1

[a]Reaction conditions: 10 equiv H_2O_2 in CH_3CN solution was delivered by syringe pump over a period of 5 minutes at room temperature under air to a vigorously stirred CH_3CN solution containing 1 mM iron catalyst, naphthalene and 1-octene. The solution was stirred an additional 20 min after syringe pump addition and products were determined by GC analysis. Yields expressed as μmol product/μmol catalyst. [b]Includes 1-naphthol and 2-naphthol.

6.7 Isotopic labeling studies

*Isotope labeling studies of **1**.* ^{18}O labeling studies have proven very useful in our earlier studies of iron-catalyzed olefin oxidation for determining the sources of the oxygen atoms incorporated into products.[66] Thus analogous studies were carried out for naphthalene oxidation, focusing on the diol and naphthol products. When 10 equiv 2%

$H_2{}^{18}O_2$ (100 equiv H_2O per $H_2{}^{18}O_2$) is used as oxidant, more than 90% of the diol product is singly labeled (Figure 6.4, column 1 and Table 6.4, entry 1). The complementary experiment carried out with 10 equiv H_2O_2 and 1000 equiv $H_2{}^{18}O$ (relative to catalyst) also affords more than 90% of the singly labeled diol product (Figure 6.4, column 2 and Table 6.4, entry 2). These results show that the cis-diol product of naphthalene oxidation derives one O atom from H_2O_2 and the other from H_2O, following the labeling pattern found in cyclooctene *cis*-dihydroxylation by **1**, in which most diol product derives the two oxygen atoms each from hydrogen peroxide and water (Table 6.4, entries 3 and 4).

In the experiments, 1-naphthol and 2-naphthol can be resolved on the GC column used for quantification but can not be resolved on the GC-MS column used for determining the ^{18}O label incorporation. Thus the reported label incorporation for naphthols represents a composite value. ^{18}O-labeling studies of the naphthol products with 2% $H_2{}^{18}O_2$ show that 72% of the naphthols incorporated the ^{18}O label while 27% was unlabeled (Figure 6.4, column 3 and Table 6.4, entry 1). The complementary experiment with 1000 equiv added $H_2{}^{18}O$ confirmed this pattern (Figure 6.4, column 4 and Table 6.4: entry 2). (When corrected for the contribution from the thermal decomposition of the labeled diol product, the value for % incorporation from H_2O decreases to 21%.) Compared with epoxide in the oxidation of cyclooctene (Table 6.4, entries 3 and 4) where lower incorporation from water was observed, this reflects the higher difficulty of naphthalene as oxidation substrate, which gives the active oxidant HO-Fe^V=O more time to scramble.

Table 6.4 Isotope labeling results for naphthalene oxidation catalyzed by **1**[a]

Entry	*cis*-diol			naphthol	
	unlabeled	singly labeled	doubly labeled	unlabeled	labeled
naphthalene					
1: $H_2{}^{18}O_2$ / $H_2{}^{16}O$[b]	6%	93%	<1%	27%	72%
2: $H_2{}^{16}O_2$ / $H_2{}^{18}O$[c]	3%	96%	0	73%	26%
cyclooctene[d]					
3: $H_2{}^{18}O_2$ / $H_2{}^{16}O$[b]	3%	97%	0	n.r.[e]	90%
4: $H_2{}^{16}O_2$ / $H_2{}^{18}O$[c]	n.r.[e]	86%	1%	n.r.[e]	9%

[a]Please check Experimental section for details of reaction conditions. [b]10 equiv $H_2{}^{18}O_2$ (2% aqueous solution) relative to catalyst is used as oxidant. [c]10 equiv H_2O_2 (0.5 M in CH_3CN from 35% aqueous solution) diluted with 1000 equiv $H_2{}^{18}O$ is used as oxidant. [d]Results from 66 [e]n.r. stands for not reported.

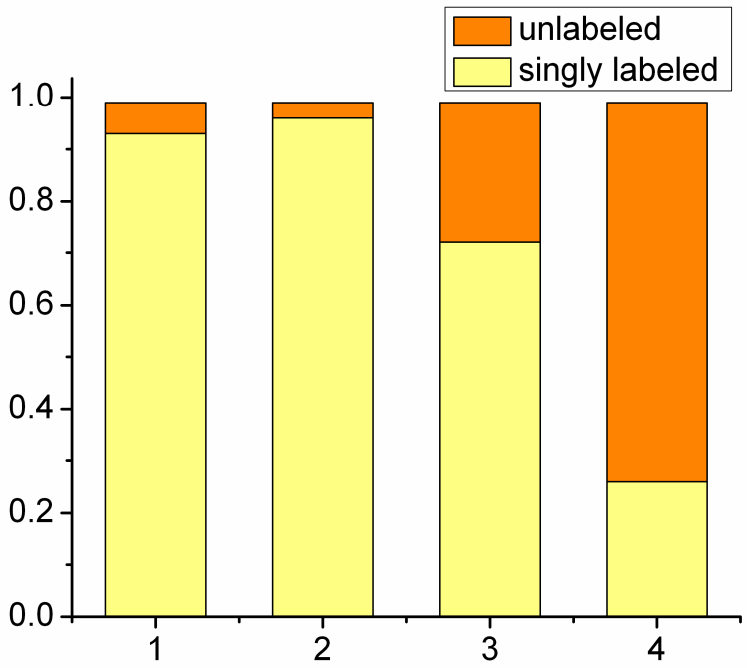

Figure 6.4 Isotope labeling results from **1**-catalyzed oxidations of naphthalene in CH_3CN. Entries 1 and 2 show the labeling patterns for the *cis*-diol product, while entries 3 and 4 show the labeling patterns for the naphthol products. For entries 1 and 3, 10 equiv $H_2{}^{18}O_2$ (2% aqueous solution) relative to catalyst is used as oxidant; for entries 2 and 4, 10 equiv H_2O_2 (0.5 M in CH_3CN from 35% aqueous solution) diluted with 1000 equiv $H_2{}^{18}O$ is used as oxidant. See Table 6.4 for numerical values.

Effect of labeled water. Experiments varying the amount of added labeled water were carried out with **1** as catalyst (Figure 6.5). ^{18}O incorporation from $H_2{}^{18}O$ into *cis*-1,2-dihydro-1,2-naphthalenediol in the **1**-catalyzed reaction displays saturation behavior. Interestingly, the $H_2{}^{18}O$ labeling results previously reported for **1**-catalyzed cyclooctene *cis*-dihydroxylation[66] also fit onto this curve (Figure 6.6). This behavior indicates the involvement of a pre-equilibrium binding of water to the metal center during turnover.

The congruence in the labeling results suggests that *cis*-dihydroxylation of naphthalene by **1** utilizes the same pathway as *cis*-dihydroxylation of olefins by **1**.[66,168]

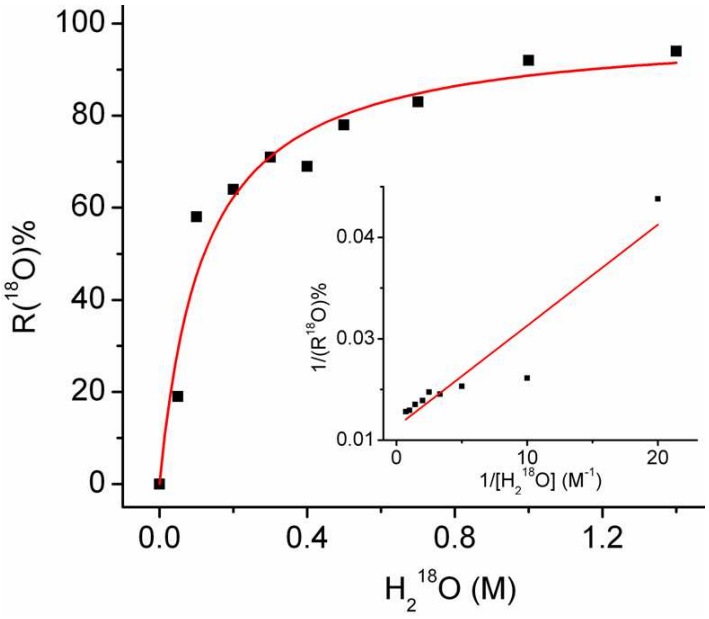

Figure 6.5 Fraction of ^{18}O-labeled *cis*-1,2-dihydro-1,2-naphthalenediol obtained in the oxidation of naphthalene catalyzed by **1**.

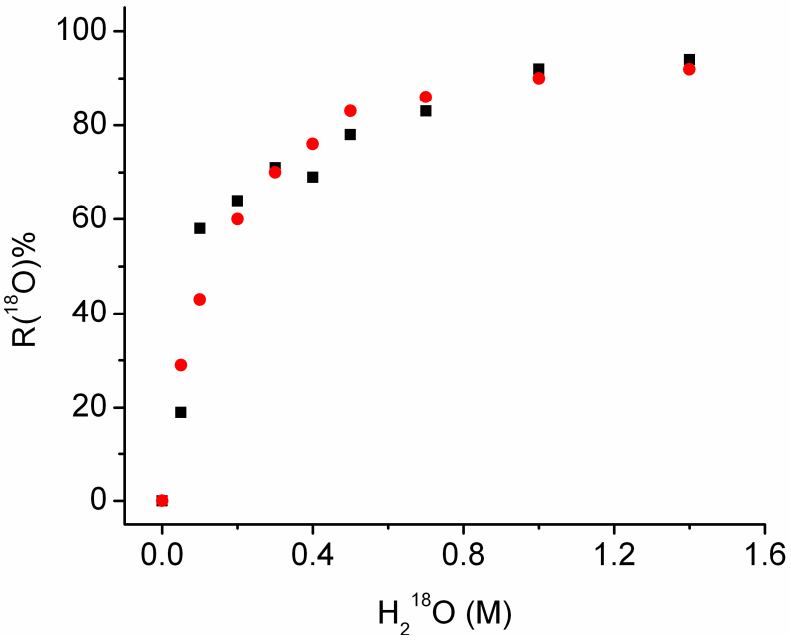

Figure 6.6 Fraction of ^{18}O-labeled *cis*-1,2-dihydro-1,2-naphthalenediol (black squares) and *cis*-1,2-cyclooctanediol (red dots) obtained in the oxidation of naphthalene and cyclooctene catalyzed by **1**.

6.8 Mechanistic considerations

The competition reactions of naphthalene and 1-octene show that 1-octene can intercept the active oxidant formed in oxidation of naphthalene. The *cis*-diol product of naphthalene oxidation derives one O atom from H_2O_2 and the other from H_2O, following the labeling pattern found in cyclooctene *cis*-dihydroxylation by **1**. All these experimental results strongly suggest that the water-assisted mechanism previously proposed for the **1**-catalyzed *cis*-dihydroxylation of olefins[66] applies to naphthalene *cis*-dihydroxylation as well (Scheme 6.4). The water-assisted mechanism involves initial formation of a low-spin Fe^{III}-OOH species to which water can bind. The coordinated

water is proposed to facilitate the heterolytic cleavage of the O-O bond to form the *cis*-HO-Fe^{V}=O oxidant that adds across the substrate double bond to form *cis*-diol and give rise to the signature labeling pattern observed.

Around 70% - 80% of naphthol oxygen derives from H_2O_2. For comparison, 90% of the epoxide oxygen derived from H_2O_2 in the **1**-catalyzed epoxidation of cyclooctene. These results support the mechanism proposed in Scheme 6.4. The observed incorporation of water into the epoxide or the naphthol products cannot be rationalized by invoking the Fe^{III}-OOH intermediate as oxidant and requires oxo-hydroxo tautomerism of the putative HO-Fe^{V}=O oxidant and transfer of the oxo atom to the substrate. So far, the naphthol products are considered as epoxide analogue in arene oxidation. Previous studies show that acetic acid can shift the product formation from diol to epoxide in **1**-catalyzed cyclooctene oxidation.[64] When acetic acid is added, 200 equiv (relative to iron) suppress the formation of the diol product, but the yield of naphthols is also significantly lowered, suggesting that the naphthols and epoxide are not formed in exactly the same way.

It is interesting to note that $H_2{}^{18}O$ incorporation into the naphthol products under the same conditions is twofold higher than for cyclooctene oxide in the epoxidation of cycloctene by **1**[66] but somewhat lower than the 27% value reported for cyclohexanol in the hydroxylation of cyclohexane by the same catalyst.[169] These results are interpreted as reflecting the different activation barriers associated with the attack of the putative HO-Fe^{V}=O oxidant on the various substrates. The more difficult the substrate is to oxidize, the greater the extent of oxo-hydroxo tautomerism before substrate attack, so more label

from water would be introduced into the oxidized product for the substrates with the higher activation barriers. Thus the observed progression for % label incorporation, cyclooctene < naphthalene < cyclohexane, is in accord with this notion.

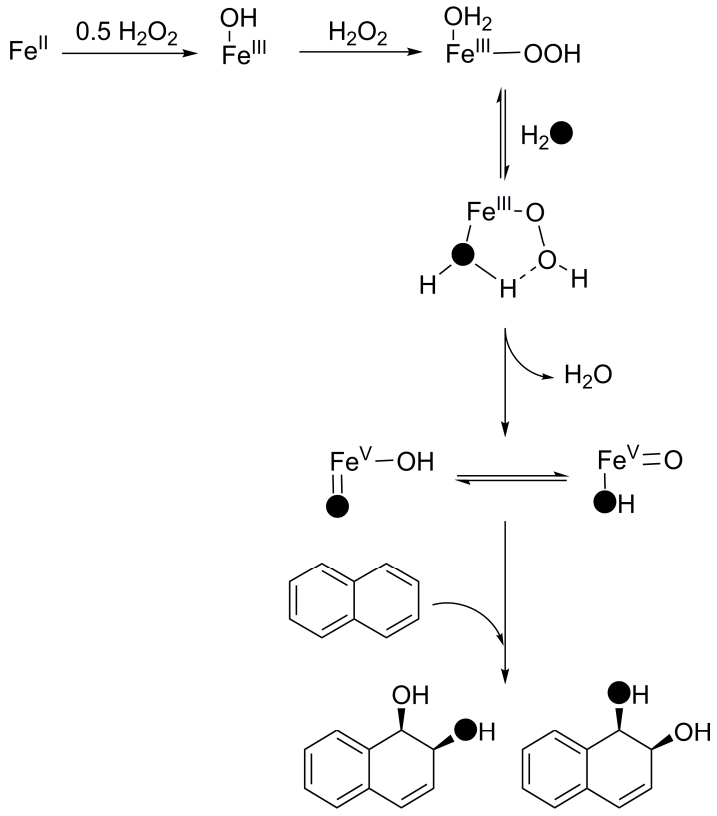

Scheme 6.4 Proposed mechanism for the *cis*-dihydroxylation of naphthalene catalyzed by **1**.

6.9 Conclusions

In summary, the first examples of synthetic non-heme iron complexes capable of catalyzing the *cis*-dihydroxylation of naphthalene are reported. This transformation can be carried out under ambient conditions with H_2O_2 as oxidant and thus models the action

of naphthalene 1,2-dioxygenase, via the peroxide shunt pathway.[40,41] ^{18}O labeling experiments strongly implicate a HO-Fe^{V}=O oxidant that is formed via a water-assisted mechanism originally proposed for the **1**-catalyzed hydroxylation of alkanes[169] and *cis*-dihydroxylation of olefins.[66] By extension, this work suggests that the crystallographically characterized side-on peroxo intermediate of NDO[34,38] could convert to a similar high-valent HO-Fe^{V}=O oxidant that is responsible for the biological *cis*-dihydroxylation of naphthalene.

6.10 Acknowledgements

I would like to thank Dr. Chunyen Ke for initiating this project and Dr. Genqiang Xue for his valuable suggestions. I am also grateful to Dr. Rubén Mas-Ballesté and Dr. Paul Oldenburg for their discussions.

CHAPTER 7

Conclusions and perspectives

7.1 Introduction

This thesis has focused on the design of bio-inspired nonheme iron catalysts in olefin oxidations, especially olefin epoxidation and *cis*-dihydroxylation. There were two strategies used to design the ligands. One was to use *N, N, O*-ligands that directly mimic the active site of nonheme monoiron oxygenases (Chapters 2 and 3), and the other was to use N4 tetradentate ligands (Chapters 4-6). Studies with these two strategies have resulted in a number of new iron catalysts, many of which exhibit better reactivity and selectivity. This chapter will first summarize these two strategies, and then provide some future directions for research in this area.

7.2 *N, N, O*-ligands vs. N4 ligands

As currently reported *N, N, O*-ligands for iron catalysts are quite different in their structures, a series of structurally related *N, N, O*-ligands have been designed and synthesized. Based on the comparison of their reactivity, ligand design rules are generated. *N, N, O*-ligands with two pyridine nitrogen donors and one amide oxygen donor have the best reactivity and selectivity towards olefin *cis*-dihydroxylation. However, iron catalysts need two *N, N, O*-ligands per iron and dissociate one ligand in the solution, which means that this way wastes one ligand. In addition, perhaps due to the fact that a tridentate ligand donates less electron density to the metal center than tetradentate ligands, iron catalysts with *N, N, O*-ligands can not accomplish the oxidation of naphthalene as those with N4 ligands. And for the same reason, tridentate ligands can not support the iron center to go to the Fe(V) state as proposed with N4 ligands.

N4 tetradentate ligands bind to the iron center more strongly than *N, N, O*-ligands, as no free ligand is observed when ESI-MS is examined for iron complexes with N4 ligands in solution. One more electron donor can lead the iron catalysts to go to Fe(V) state and catalyze the oxidation of the very stable aromatic double bond. However, without any oxygen atom donor, the selectivity towards olefin *cis*-dihydroxylation of iron catalysts with N4 ligands is not as remarkable as those with *N, N, O*-ligands.

7.3 Prospective tetradentate ligands with oxygen atom donor(s)

Ligands influence the electronic and geometric properties of the metal center and may direct the orientation of reactants attaching to and products dissociating from the catalyst, thereby controlling catalytic activity and selectivity. Accordingly, the role of ligands and their interactions with metals are a central theme in understanding the catalytic process and in designing and optimizing catalysts.[5] From previous chapters, *N, N, O*-ligands and N4 ligands both have their own advantages. Here I propose some new ligands for the future directions. They are all tetradentate ligands so that iron catalysts need only one ligand in their structure and ligands can also bind the metal center more strongly and donate more electron density to the iron center. In addition, they all incorporate one or two oxygen donors in their structures to maintain the high reactivity and selectivity. Scheme 7.1 summarizes some prospective tetradentate ligands that incorporate one or two oxygen atom donors.

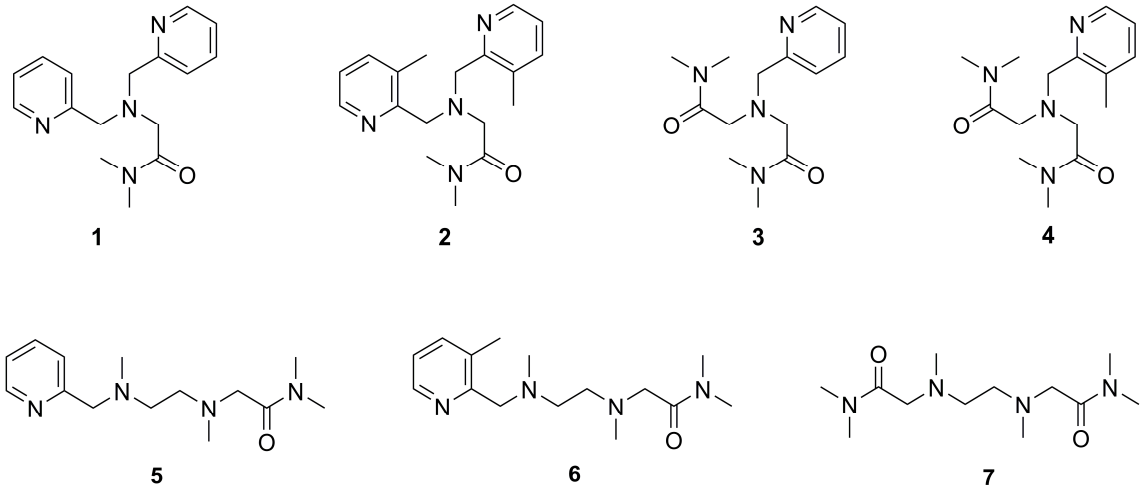

Scheme 7.1 Prospective tetradentate ligands employing one or two oxygen atom donors.

The first row of Scheme 7.1 represents variations of the TPA ligand that include one or two oxygen donors, while the second row contains similar variations of the BPMEN ligand. For ligand **1**, one arm of pyridine is replaced with one dimethyl amide oxygen donor. Ligand **2** has two methyl groups in the C6 positions of the remaining two pyridine rings. As the carboxylate bidentately binds the mononuclear center in the active site of naphthalene 1,2-dioxygenase, two oxygen atom donors are incorporated into **3** and **4**, with the difference in C6 position of the remaining pyridine ring. On the other hand, BPMEN represents a different ligand family with a linear N2Py2 structure. Based on the same strategy, one oxygen donor substitutes one pyridine ring to give **5** and **6** that differ in the C6 position of pyridine ring, and two oxygen donors replace both pyridine rings to give ligand **7**.

7.4 Concluding remarks

As Alwin Mittasch, the inventor of cheap and efficient iron-based catalysts for the synthesis of ammonia in the Haber-Bosch process, said, ‘Chemistry without catalysis would be a sword without a handle, a light without brilliance, a bell without sound.’ I feel pleasured to be in this exciting field of catalysis. As more concern about the environment leads to more stringent regulations, there will be an increasing need for alternative green catalysts to replace traditional catalysts. This thesis summarizes my efforts in the past six years to design novel bio-inspired nonheme mononuclear iron catalysts for the olefin oxygenation. I am sincerely grateful to all who have helped me and accompanied me along the way. Thanks for reading.

BIBLIOGRAPHY

(1) *Biological Inorganic Chemistry*; Bertini, I.; Gray, H. B.; Stiefel, E. I.; Valentine, J. S., Eds.; University Science Books: Sausalito, 2007.

(2) *Cytochrome P-450. Structure, Mechanism and Biochemistry*; 3rd ed.; Ortiz de Montellano, P. R., Ed.; Kluwer Academic/Plenum Publishers: New York, 2005.

(3) Lange, S. J.; Que, L., Jr. *Curr. Op. Chem. Biol.* **1998**, *2*, 159-172.

(4) Costas, M.; Mehn, M. P.; Jensen, M. P.; Que, L., Jr. *Chem. Rev.* **2004**, *104*, 939-986.

(5) *Fundamentals of industrial catalytic processes*; Farrauto, R. J.; Bartholomew, C. H., Eds.; John Wiley & Sons, Inc.: Hoboken, New Jersey, 2006.

(6) Kolb, H. C.; VanNieuwenhze, M. S.; Sharpless, K. B. *Chem. Rev.* **1994**, *94*, 2483-2547.

(7) Que, L., Jr.; Ho, R. Y. N. *Chem. Rev.* **1996**, *96*, 2607-2624.

(8) Wallar, B. J.; Lipscomb, J. D. *Chem. Rev.* **1996**, *96*, 2625-2658.

(9) Koehntop, K. D.; Emerson, J. P.; Que, L., Jr. *J. Biol. Inorg. Chem.* **2005**, *10*, 87-93.

(10) Bruijnincx, P. C. A.; van Koten, G.; Gebbink, R. J. M. K. *Chemical Society Reviews* **2008**, *37*, 2716-2744.

(11) Kloer, D. P.; Ruch, S.; Al-Babili, S.; Beyer, P.; Schulz, G. E. *Science* **2005**, *308*, 267-269.

(12) Hegg, E. L.; Que, L., Jr. *Eur. J. Biochem.* **1997**, *250*, 625-629.

(13) Que, L., Jr. *Nat. Struct. Biol.* **2000**, *7*, 182-184.

(14) Schofield, C. J.; Zhang, Z. *Curr. Opin. Struct. Biol.* **1999**, *9*, 722-731.

(15) Hanauske-Abel, H. M.; Popowicz, A. M. *Current Medicinal Chemistry* **2003**, *10*, 1005-1019.

(16) Hausinger, R. P. *Crit. Rev. Biochem. Mol. Biol.* **2004**, *39*, 21-68.

(17) Price, J. C.; Barr, E. W.; Tirupati, B.; Bollinger, J. M., Jr.; Krebs, C. *Biochemistry* **2003**, *42*, 7497-7508.

(18) Riggs-Gelasco, P. J.; Price, J. C.; Guyer, R. B.; Brehm, J. H.; Barr, E. W.; Bollinger, J. M., Jr.; Krebs, C. *J. Am. Chem. Soc.* **2004**, *126*, 8108-8109.

(19) Proshlyakov, D. A.; Henshaw, T. F.; Monterosso, G. R.; Ryle, M. J.; Hausinger, R. P. *J. Am. Chem. Soc.* **2004**, *126*, 1022-1023.

(20) Solomon, E. I.; Brunold, T. C.; Davis, M. I.; Kemsley, J. N.; Lee, S.-K.; Lehnert, N.; Neese, F.; Skulan, A. J.; Yang, Y.-S.; Zhou, J. *Chem. Rev.* **2000**, *100*, 235-349.

(21) Krebs, C.; Galonić Fujimori, D.; Walsh, C. T.; Bollinger, J. M., Jr. *Acc. Chem. Res.* **2007**, *40*, 484-492.

(22) Price, J. C.; Barr, E. W.; Glass, T. E.; Krebs, C.; Bollinger, J. M., Jr. *J. Am. Chem. Soc.* **2003**, *125*, 13008-13009.

(23) Hoffart, L. M.; Barr, E. W.; Guyer, R. B.; Bollinger, J. M., Jr.; Krebs, C. *Proc. Natl. Acad. Sci. USA* **2006**, *103*, 14738-14743.

(24) Galonic, D. P.; Barr, E. W.; Walsh, C. T.; Bollinger, J. M., Jr.; Krebs, C. *Nature Chem. Biol.* **2007**, *3*, 113-116.

(25) Wackett, L. P. *Enzyme and Microbial Technology* **2002**, *31*, 577-587.

(26) Gibson, D. T.; Parales, R. E. *Curr. Opin. Biotechnol.* **2000**, *11*, 236-243.

(27) Lau, P. C. K.; De Lozenzo, V. *Environ. Sci. Biotechnol.* **1999**, 124A-128A.

(28) Timmins, K. N.; Pieper, D. H. *Trends Biotechnol.* **1999**, *17*, 201-204.

(29) *Microbial Degradation of Organic Compounds*; Gibson, D. T., Ed.; Marcel Dekker: New York, 1984.

(30) Boyd, D. R.; Sheldrake, G. N. *Nat. Prod. Rep.* **1998**, *15*, 309-324.

(31) Resnick, S. M.; Gibson, D. T. *J. Indust. Microbiol.* **1996**, *17*, 438-457.

(32) Lee, K.; Gibson, D. T. *J. Bacteriol.* **1996**, *289*, 3353-3356.

(33) Lange, C. C.; Wackett, L. P. *J. Bacteriol.* **1997**, *179*, 3858-3865.

(34) Kauppi, B.; Lee, K.; Carredano, E.; Parales, R. E.; Gibson, D. T.; Eklund, H.; Ramaswamy, S. *Structure* **1998**, *6*, 571-586.

(35) Friemann, R.; Lee, K.; Brown, E. N.; Gibson, D. T.; Eklund, H.; Ramaswamy, S. *Acta Cryst.* **2009**, *D65*, 24-33.

(36) Friemann, R.; Ivkovic-Jensen, M. M.; Lessner, D. J.; Yu, C.-L.; Gibson, D. T.; Parales, R. E.; Eklund, H.; Ramaswamy, S. *J. Mol. Biol.* **2005**, *348*, 1139-1151.

(37) Carredano, E.; Karlsson, A.; Kauppi, B.; Choudhury, D.; Parales, R. E.; Parales, J. V.; Lee, K.; Gibson, D. T.; Eklund, H.; Ramaswamy, S. *J. Mol. Biol.* **2000**, *296*, 701-712.

(38) Karlsson, A.; Parales, J. V.; Parales, R. E.; Gibson, D. T.; Eklund, H.; Ramaswamy, S. *Science* **2003**, *299*, 1039-1042.

(39) Ohta, T.; Chakrabarty, S.; Lipscomb, J. D.; Solomon, E. I. *J. Am. Chem. Soc.* **2008**, *130*, 1601-1610.

(40) Wolfe, M. D.; Parales, J. V.; Gibson, D. T.; Lipscomb, J. D. *J. Biol. Chem.* **2001**, *276*, 1945-1953.

(41) Wolfe, M. D.; Lipscomb, J. D. *J. Biol. Chem.* **2003**, *278*, 829-835.

(42) Neibergall, M. B.; Stubna, A.; Mekmouche, Y.; Munck, E.; Lipscomb, J. D. *Biochemistry* **2007**, *46*, 8004-8016.

(43) Chakrabarty, S.; Austin, R. N.; Deng, D.; Groves, J. T.; Lipscomb, J. D. *J. Am. Chem. Soc.* **2007**, *129*, 3514-3515.

(44) Bassan, A.; Blomberg, M. R. A.; Siegbahn, P. E. M. *J. Biol. Inorg. Chem.* **2004**, *9*, 439-452.

(45) Bouvier, F.; Suire, C.; Mutterer, J.; Camara, B. *Plant Cell* **2003**, *15*, 47-62.

(46) Giuliano, G.; Al-Babili, S.; von Lintig, J. *Trends Plant Sci.* **2003**, *8*, 145-149.

(47) Camara, B.; Bouvier, F. *Arch. Biochem. Biophys.* **2004**, *430*, 16-21.

(48) Kloer, D. P.; Schulz, G. E. *Cell. Mol. Life Sci.* **2006**, *63*, 2291-2303.

(49) Borowski, T.; Blomberg, M. R. A.; Siegbahn, P. E. M. *Chem. Eur. J.* **2008**, *14*, 2264-2276.

(50) Anilkumar, G.; Bitterlich, B.; Gelalcha, F. G.; Tse, M. K.; Beller, M. *Chem. Commun.* **2007**, 289-291.

(51) Bitterlich, B.; Anilkumar, G.; Gelalcha, F. G.; Spilker, B.; Grotevendt, A.; Jackstell, R.; Tse, M. K.; Beller, M. *Chem. Asian J.* **2007**, *2*, 521-529.

(52) Bitterlich, B.; Schroder, K.; Tse, M. K.; Beller, M. *Eur. J. Org. Chem.* **2008**, 4867-4870.

(53) Gelalcha, F. G.; Anilkumar, G.; Tse, M. K.; Brückner, A.; Beller, M. *Chem. Eur. J.* **2008**, *14*, 7687-7698.

(54) Gelalcha, F. G.; Bitterlich, B.; Anilkumar, A.; Tse, M. K.; Beller, M. *Angew. Chem. Int. Ed.* **2007**, *46*, 7293-7296.

(55) Enthaler, S.; Schroder, K.; Inoue, S.; Eckhardt, B.; Junge, K.; Beller, M.; Drieβ, M. *Eur. J. Org. Chem.* **2010**, 4893-4901.

(56) Schroder, K.; Enthaler, S.; Join, B.; Junge, K.; Beller, M. *Adv. Synth. Catal.* **2010**, *352*, 1771-1778.

(57) Schroder, K.; Tong, X.; Bitterlich, B.; Tse, M. K.; Gelalcha, F. G.; Bruckner, A.; Beller, M. *Tet. Lett.* **2007**, *48*, 6339-6342.

(58) Schroder, K.; Enthaler, S.; Bitterlich, B.; Schulz, T.; Spannenberg, A.; Tse, M. K.; Junge, K.; Beller, M. *Chem. Eur. J.* **2009**, *15*, 5471-5481.

(59) Schroder, K.; Junge, K.; Spannenberg, A.; Beller, M. *Catalysis Today* **2010**, *157*, 364-370.

(60) Schroder, K.; Join, B.; Amali, A. J.; Junge, K.; Ribas, X.; Costas, M.; Beller, M. *Angew. Chem. Int. Ed.* **2011**, *50*, 1425-1429.

(61) Gosiewska, S.; Lutz, M.; Spek, A. L.; Gebbink, R. J. M. K. *Inorg. Chim. Acta* **2007**, *360*, 405-417.

(62) Taktak, S.; Ye, W.; Herrera, A. M.; Rybak-Akimova, E. V. *Inorg. Chem.* **2007**, *46*, 2929-2942.

(63) Yeung, H.-L.; Sham, K.-C.; Tsang, C.-S.; Lau, T.-C.; Kwong, H.-L. *Chem. Commun.* **2008**, 3801-3803.

(64) Mas-Ballesté, R.; Que, L., Jr. *J. Am. Chem. Soc.* **2007**, *129*, 15964-15972.

(65) Oldenburg, P. D.; Que, L., Jr. *Catalysis Today* **2006**, *117*, 15-21.

(66) Chen, K.; Costas, M.; Kim, J.; Tipton, A. K.; Que, L., Jr. *J. Am. Chem. Soc.* **2002**, *124*, 3026-3035.

(67) Company, A.; Feng, Y.; Güell, M.; Ribas, X.; Luis, J. M.; Que, L., Jr.; Costas, M. *Chem. Eur. J.* **2009**, *15*, 3356-3362.

(68) Company, A.; Gomez, L.; Fontrodona, X.; Ribas, X.; Costas, M. *Chem. Eur. J.* **2008**, *14*, 5727-5731.

(69) Oldenburg, P. D.; Ke, C.-Y.; Tipton, A. A.; Shteinman, A. A.; Que, L., Jr. *Angew. Chem. Int. Ed.* **2006**, *45*, 7975-7978.

(70) Bruijnincx, P. C. A.; Buurmans, I. L. C.; Gosiewska, S.; Moelands, M. A. H.; Lutz, M.; Spek, A. L.; Koten, G. v.; Klein Gebbink, R. J. M. *Chem. Eur. J.* **2008**, *14*, 1228-1237.

(71) Chow, T. W.; Wong, E. L.; Guo, Z.; Liu, Y.; Huang, J.; Che, C.-M. *J. Am. Chem. Soc.* **2010**, *132*, 13229-13230.

(72) Suzuki, K.; Oldenburg, P. D.; Que, L., Jr. *Angew. Chem. Int. Ed.* **2008**, *47*, 1887-1889.

(73) Johnson, R. A.; Sharpless, K. B. In *Catalytic Asymmetric Synthesis*; 2nd ed.; Ojima, I., Ed.; Wiley-VCH: New York, 2000, p 357-398.

(74) Dupau, P.; Epple, R.; Thomas, A. A.; Fokin, V. V.; Sharpless, K. B. *Adv. Synth. Catal.* **2002**, *344*, 421-433.

(75) Zaitsev, A. B.; Adolfsson, H. *Synthesis* **2006**, *11*, 1725-1756.

(76) Mehltretter, G. M.; Bhor, S.; Klawonn, M.; Döbler, C.; Sundermeier, U.; Eckert, M.; Militzer, H.-C.; Beller, M. *Synthesis* **2003**, *2*, 295-301.

(77) Tse, M. K.; Schroder, K.; Beller, M. In *Modern Oxidation Methods*; 2nd ed.; Bäckvall, J.-E., Ed.; Wiley-VCH: 2010, p 1-36.

(78) Jonsson, S. Y.; Färnegårdh, K.; Bäckvall, J.-E. *J. Am. Chem. Soc.* **2001**, *123*, 1365-1371.

(79) Bergstad, K.; Jonsson, S. Y.; Bäckvall, J.-E. *J. Am. Chem. Soc.* **1999**, *121*, 10424-10425.

(80) Döbler, C.; Mehltretter, G.; Beller, M. *Angew. Chem. Int. Ed., Engl.* **1999**, *38*, 3026-3028.

(81) Döbler, C.; Mehltretter, G. M.; Sundermeier, U.; Beller, M. *J. Am. Chem. Soc.* **2000**, *122*, 10289-10297.

(82) Döbler, C.; Mehltretter, G. M.; Sundermeier, U.; Beller, M. *J. Organomet. Chem* **2001**, *621*, 70-76.

(83) Plietker, B. *Synthesis* **2005**, *15*, 2453-2472.

(84) Notaro, G.; Piccialli, V.; Sica, D.; Smaldone, D. *Tetrahedron* **1994**, *50*, 4835-4852.

(85) Shing, T. K. M.; Tai, V. W.-F.; Tam, E. K. W. *Angew. Chem. Int. Ed.* **1994**, *33*, 2312-2313.

(86) Shing, T. K. M.; Tam, E. K. W.; Tai, V. W.-F.; Chung, I. H. F.; Jiang, Q. *Chem. Eur. J.* **1996**, *2*, 50-57.

(87) Shing, T. K. M.; Tam, E. K. W. *Tetrahedron Letters* **1999**, *40*, 2179-2180.

(88) Plietker, B.; Niggemann, M. *Org. Lett.* **2003**, *5*, 3353-3356.

(89) Plietker, B.; Niggemann, M.; Pollrich, A. *Org. Biomol. Chem.* **2004**, *2*, 1116-1124.

(90) Plietker, B.; Niggemann, M. *Org. Biomol. Chem.* **2004**, *2*, 2403.

(91) Plietker, B.; Niggemann, M. *J. Org. Chem* **2005**, *70*, 2402-2405.

(92) Yip, W.-P.; Yu, W.-Y.; Zhu, N.; Che, C.-M. *J. Am. Chem. Soc.* **2005**, *127*, 14239-14249.

(93) Yip, W.-P.; Ho, C.-M.; Zhu, N.; Lau, T.-C.; Che, C.-M. *Chem. Asian J.* **2008**, *3*, 70-77.

(94) Brinksma, J.; Schmieder, L.; van Vliet, G.; Boaron, R.; Hage, R.; De Vos, D. E.; Alstersb, P. L.; Feringa, B. L. *Tet. Lett.* **2002**, *43*, 2619-2622.

(95) de Boer, J. W.; Brinksma, J.; Browne, W. R.; Meetsma, A.; Alsters, P. L.; Hage, R.; Feringa, B. L. *J. Am. Chem. Soc.* **2005**, *127*, 7990-7991.

(96) de Boer, J. W.; Browne, W. R.; Brinksma, J.; Alsters, P. L.; Hage, R.; Feringa, B. L. *Inorg. Chem.* **2007**, *46*, 6353-6372.

(97) de Boer, J. W.; Browne, W. R.; Harutyunyan, S. R.; Bini, L.; Tiemersma-Wegman, T. D.; Alsters, P. L.; Hage, R.; Feringa, B. L. *Chem. Commun.* **2008**, 3747-3749.

(98) Saisaha, P.; Pijper, D.; van Summeren, R. P.; Hoen, R.; Smit, C.; de Boer, J. W.; Hage, R.; Alsters, P. L.; Feringa, B. L.; Browne, W. R. *Org. Biomol. Chem.* **2010**, *8*, 4444-4450.

(99) Oldenburg, P. D.; Shteinman, A. A.; Que, L., Jr. *J. Am. Chem. Soc.* **2005**, *127*, 15672-15673.

(100) Gibson, D. T.; Resnick, S. M.; Lee, K.; Brand, J. M.; Torok, D. S.; Wackett, L. P.; Schocken, M. J.; Haigler, B. E. *J. Bacteriol.* **1995**, *177*, 2615-2621.

(101) Chen, K.; Que, L., Jr. *Angew. Chem. Int. Ed.* **1999**, *38*, 2227-2229.

(102) Costas, M.; Tipton, A. K.; Chen, K.; Jo, D.-H.; Que, L., Jr. *J. Am. Chem. Soc.* **2001**, *123*, 6722-6723.

(103) Hagen, K. S. *Inorg. Chem.* **2000**, *39*, 5867-5869.

(104) Oldenburg, P. D.; Feng, Y.; Pryjomska-Ray, I.; Ness, D.; Que, L. J. *J. Am. Chem. Soc.* **2010**, *132*, 17713-17723.

(105) Renz, M.; Hemmert, C.; Meunier, B. *Eur. J. Org. Chem.* **1998**, 1271-1273.

(106) Xue, G.; Fiedler, A. T.; Martinho, M.; Münck, E.; Que, L., Jr. *Proc. Natl. Acad. Sci. USA* **2008**, *105*, 20615-20620.

(107) Arnold, P. J.; Davies, S. C.; Dilworth, J. R.; Durrant, M. C.; Griffiths, D. V.; Hughes, D. L.; Richards, R. L.; Sharpe, P. C. *J. Chem. Soc., Dalton Trans.* **2001**, 736-746.

(108) Mąkosza, M.; Paszewski, M. *Synthesis* **2002**, *15*, 2203-2206.

(109) V5.054 ed.; Bruker Analytical X-ray Systems: Madison, WI, 2001.

(110) Blessing, R. *Acta Cryst.* **1995**, *A51*, 33-38.

(111) V6.45 ed.; Bruker Analytical X-Ray Systems: Madison, WI, 2003.

(112) Burla, M. C.; Camalli, M.; Carrozzini, B.; Cascarano, G. L.; Giacovazzo, C.; Polidori, G.; Spagna, R. *J. Appl. Cryst.* **2003**, *36*, 1103.

(113) V6.14 ed.; Bruker Analytical X-Ray Systems: Madison, WI, 2000.

(114) Ensing, B.; Buda, F.; Blöchl, P.; Baerends, E. J. *Angew. Chem. Int. Ed., Engl.* **2001**, *40*, 2893-2895.

(115) Buda, F.; Ensing, B.; Gribnau, M. C. M.; Baerends, E. J. *Chem. Eur. J.* **2001**, *7*, 2775-2783.

(116) Comba, P.; Rajaraman, G.; Rohwer, H. *Inorg. Chem.* **2007**, *46*, 3826-3838.

(117) Feng, Y.; Ke, C.-y.; Xue, G.; Que, L., Jr. *Chem. Commun.* **2009**, 50-52.

(118) Guajardo, R. J.; Hudson, S. E.; Brown, S. J.; Mascharak, P. K. *J. Am. Chem. Soc.* **1993**, *115*, 7971-7977.

(119) Kojima, T.; Leising, R. A.; Yan, S.; Que, L., Jr. *J. Am. Chem. Soc.* **1993**, *115*, 11328-11335.

(120) Martinho, M.; Banse, F.; Bartoli, J.-F.; Mattioli, T. A.; Battioni, P.; Horner, O.; Bourcier, S.; Girerd, J.-J. *Inorg. Chem.* **2005**, *44*, 9592 - 9596.

(121) Mukherjee, A.; Martinho, M.; Bominaar, E. L.; M□ünck, E.; Que, L., Jr. *Angew. Chem. Int. Ed.* **2009**, *48*, 1780-1783.

(122) Nam, W.; Ho, R. Y. N.; Valentine, J. S. *J. Am. Chem. Soc.* **1991**, *113*, 7052-7054.

(123) Kaizer, J.; Klinker, E. J.; Oh, N. Y.; Rohde, J.-U.; Song, W. J.; Stubna, A.; Kim, J.; Münck, E.; Nam, W.; Que, L., Jr. *J. Am. Chem. Soc.* **2004**, *126*, 472-473.

(124) Sastri, C. V.; Lee, J.; Oh, K.; Lee, Y. J.; Lee, J.; Jackson, T. A.; Ray, K.; Hirao, H.; Shin, W.; Halfen, J. A.; Kim, J.; Que, L., Jr.; Shaik, S.; Nam, W. *Proc. Natl. Acad. Sci. USA* **2007**, *104*, 19181-19186.

(125) Klinker, E. J.; Shaik, S.; Hirao, H.; Que, L., Jr *Angew. Chem. Int. Ed.* **2009**, *48*, 1291-1295.

(126) Fielder, A. T.; Que, L., Jr. *Inorg. Chem.* **2009**, *48*, 11038–11047.

(127) Yin, G.; Danby, A. M.; Kitko, D.; Carter, J. D.; Scheper, W. M.; Busch, D. H. *J. Am. Chem. Soc.* **2007**, *129*, 1512-1513.

(128) Yin, G.; Danby, A. M.; Kitko, D.; Carter, J. D.; Scheper, W. M.; Busch, D. H. *J. Am. Chem. Soc.* **2008**, *130*, 16245-16253.

(129) Chattopadhyay, S.; Geiger, R. A.; Yin, G.; Busch, D. H.; Jackson, T. A. *Inorganic Chemistry* **2010**, *49*, 7530-7535.

(130) Zhu, S.; Brennessel, W. W.; Harrison, R. G.; Que., L., Jr. *Inorg. Chim. Acta* **2002**, *337*, 32-38.

(131) Groves, J. T. In *Cytochrome P450: Structure, Mechanism, and Biochemistry*; 3rd ed.; Ortiz de Montellano, P. R., Ed.; Kluwer Academic/Plenum Publishers: New York, 2005, p 1-43.

(132) Nam, W.; Ryu, Y. O.; Song, W. J. *J. Biol. Inorg. Chem.* **2004**, *9*, 654-660.

(133) Abu-Omar, M. M.; Loaiza, A.; Hontzeas, N. *Chem. Rev.* **2005**, *105*, 2227-2252.

(134) Ferraro, D. J.; Gakhar, L.; Ramaswamy, S. *Biochem. Biophys. Res. Commun.* **2005**, *338*, 175-190.

(135) Sheldon, R. A. *Chem. Commun.* **2008**, 3352-3365.

(136) Beach, E. S.; Cui, Z.; Anastas, P. T. *Energy Environ. Sci.* **2009**, *2*, 1038-1049.

(137) Beck, A.; Weibert, B.; Burzlaff, N. I. *Eur. J. Inorg. Chem.* **2001**, 521-527.

(138) Beck, A.; Barth, A.; Hu1bner, E.; Burzlaff, N. *Inorg. Chem.* **2003**, *42*, 7182-7188.

(139) Canty, A. J.; Minchin, N. J. *Aust. J. Chem* **1986**, *39*, 1063-9.

(140) Chen, P.; Solomon, E. I. *J. Am. Chem . Soc.* **2004**, *126*, 4991-5000.

(141) Rohde, J.-U.; In, J.-H.; Lim, M. H.; Brennessel, W. W.; Bukowski, M. R.; Stubna, A.; Münck, E.; Nam, W.; Que, L., Jr. *Science* **2003**, *299*, 1037-1039.

(142) Weisman, G. R.; Rogers, M. E.; Wong, E. H.; Jasinski, J. P.; Paight, E. S. *J. Am. Chem. Soc.* **1990**, *112*, 8604-8605.

(143) Hubin, T. J.; McCormick, J. M.; Collinson, S. R.; Buchalova, M.; Perkins, C. M.; Alcock, N. W.; Kahol, P. K.; Raghunathan, A.; Busch, D. H. *J. Am. Chem. Soc.* **2000**, *122*, 2512-2522.

(144) Barefield, E. K. *Coord. Chem. Rev.* **2010**, *254*, 1607-1627.

(145) Yin, G.; McCormick, J. M.; Buchalova, M.; Danby, A. M.; Rodgers, K.; Day, V. W.; Smith, K.; Perkins, C. M.; Kitko, D.; Carter, J. D.; Scheper, W. M.; Busch, D. H. *Inorg. Chem.* **2006**, *45*, 8052-8061.

(146) McDonald, A. R.; Bukowski, M. R.; Farquhar, E. R.; Jackson, T. A.; Koehntop, K. D.; Seo, M. S.; De Hont, R. F.; Stubna, A.; Halfen, J. A.; Munck, E.; Nam, W.; Que, L. J. *J. Am. Chem. Soc.* **2010**, *132*, 17118-17129.

(147) Zang, Y.; Kim, J.; Dong, Y.; Wilkinson, E. C.; Appelman, E. H.; Que, L., Jr. *J. Am. Chem. Soc.* **1997**, *119*, 4197-4205.

(148) White, M. C.; Doyle, A. G.; Jacobsen, E. N. *J. Am. Chem. Soc.* **2001**, *123*, 7194-7195.

(149) Mas-Ballesté, R.; Fujita, M.; Hemmila, C.; Que, L., Jr. *J. Mol. Catal.* **2006**, *251*, 49-53.

(150) Fujita, M.; Costas, M.; Que, L., Jr. *J. Am. Chem. Soc.* **2003**, *125*, 9912-9913.

(151) Quiñonero, D.; Morokuma, K.; Musaev, D. G.; Mas-Balleste, R.; Que, L., Jr. *J. Am. Chem. Soc.* **2005**, *127*, 6548-6549.

(152) Bassan, A.; Blomberg, M. R. A.; Siegbahn, P. E. M.; Que, L., Jr. *J. Am. Chem. Soc.* **2002**, *124*, 11056-11063.

(153) Bassan, A.; Blomberg, M. R. A.; Siegbahn, P. E. M.; Que, L., Jr. *Chem. Eur. J.* **2005**, *11*, 692-705.

(154) Wende, P.; Bernhardt, F.-H.; Pfleger, K. *Eur. J. Biochem.* **1989**, *181*, 189-197.

(155) Beil, S.; Happe, B.; Timmis, K. N.; Pieper, D. H. *Eur. J. Biochem.* **1997**, *247*, 190-199.

(156) Costas, M.; Que, L., Jr. *Angew. Chem. Int. Ed.* **2002**, *41*, 2179-2181.

(157) Mas-Balleste, R.; Costas, M.; van den Berg, T.; Que, L. J. *Chemistry - A European Journal* **2006**, *12*, 7489-7500.

(158) Chen, K.; Que, L., Jr. *Chem. Commun.* **1999**, 1375-1376.

(159) Bryliakov, K. P.; Duban, E. A.; Talsi, E. P. *Eur. J. Inorg. Chem.* **2005**, 72-76.

(160) Hong, S.; Lee, Y.-M.; Cho, K.-B.; Sundaravel, K.; Cho, J.; Kim, M. J.; Shin, W.; Nam, W. *J. Am. Chem. Soc.* **2011**.

(161) Parales, R. E. *J. Ind. Microbiol. Biotechnol.* **2003**, *30*, 271-278.

(162) Que, L., Jr.; Tolman, W. B. *Nature* **2008**, *455*, 333-340.

(163) Klopstra, M.; Roelfes, G.; Hage, R.; Kellogg, R. M.; Feringa, B. L. *Eur. J. Inorg. Chem.* **2004**, 846-856.

(164) de Visser, S. P.; Shaik, S. *J. Am. Chem. Soc.* **2003**, *125*, 7413-7424.

(165) Jensen, M. P.; Lange, S. J.; Mehn, M. P.; Que, E. L.; Que, L., Jr. *J. Am. Chem. Soc.* **2003**, *125*, 2113-2128.

(166) Kang, M.-J.; Song, W. J.; Han, A.-R.; Choi, Y. S.; Jang, H. G.; Nam, W. *J. Org. Chem.* **2007**, *72*, 6301-6304.

(167) de Visser, S. P.; Oh, K.; Han, A.-R.; Nam, W. *Inorg. Chem.* **2007**, *46*, 4632-4641.

(168) Mas-Ballesté, R.; Costas, M.; Berg, T. v. d.; Que, L. J. *Chem. Eur. J.* **2006**, *12*, 7489-7500.

(169) Chen, K.; Que, L., Jr. *J. Am. Chem. Soc.* **2001**, *123*, 6327-6337.